Developing novel mucoadhesive chitosan based formulations for drug delivery to the urinary bladder

Oluwadamilola Miriam Kolawole

Submitted as partial fulfillment for the degree of Doctor of Philosophy

School of Pharmacy

February 2019

Acknowledgements

Oluwadamilola Kolawole

February 2019

Declaration of original authorship

'Declaration: I confirm that this is my own work and the use of all material from other sources has been properly and fully acknowledged.'

Oluwadamilola Kolawole

February 2019

Abstract

My PhD project aims to develop novel chitosan derivatives (with superior mucoadhesiveness) for transmucosal application. The intravesical route was chosen as the exemplar transmucosal mode of drug delivery due to the limited therapeutic efficiency of conventional bladder cancer formulations. Drug carriers with improved mucoadhesive properties may prolong drug residence in the bladder. First, three chitosan grades were used to prepare chitosan/β-glycerophosphate *in situ* gelling mixtures and from these grades, the high molecular weight graded chitosan (HCHI) was chosen for chemical derivatisation based on its superior gelation, mucoadhesive and drug release potential. HCHI was conjugated with varying amounts of methacrylate or phenylboronate groups in order to evaluate the influence of the type and amount of conjugated hydrophobic pendant group on their physicochemical and mucoadhesive properties. The boronated and methacrylated chitosans were characterised using ^{1}H NMR and FT- IR. There was good correlation in the extent of hydrophobic modification for methacrylated and boronated chitosans using ^{1}H NMR and ninhydrin test. Methacrylated and boronated chitosan exhibited comparable resistance to pH influence on their solubility. The degree of methacrylate or boronate conjugation had a significant influence on the mucoadhesiveness of the drug carriers studied using a urine flow-through technique/fluorescent microscopy as well as a texture analyser, on porcine bladder *in vitro*. Boronate groups conferred superior mucoadhesive behaviour on chitosan relative to methacrylate groups. Methacrylated chitosan displayed a similar safety profile to the parent chitosan based on MTT assay on UMUC3 bladder cancer cells. The biocompatibility studies of boronated chitosan will be carried out in future studies using bladder cell lines despite the fact that several *in vitro* and *in vivo* studies have established the safety of phenylboronic molecules. Methacrylation and boronation of chitosan has been identified as efficient strategies to generate more mucoadhesive drug carriers which could prolong drug residence time in the bladder thereby improving therapeutic outcomes of bladder cancer patients. These novel polymers were easily synthesised requiring minimal equipment suitable for industrial scale-up. These excipients could be used to formulate affordable transmucosal dosage forms with superior mucoadhesiveness for a variety of biomedical applications.

List of publications

Kolawole O.M., Lau W-M., Mostafid H., Khutoryanskiy V.V. (2017). Intravesical Drug Delivery for Treatment of Bladder Cancer (mini-review). The United Kingdom and Ireland Controlled Release Society Newsletter, 29-33.

Kolawole O. M., Lau W-M., Mostafid H., Khutoryanskiy V.V. (2017). Advances in intravesical drug delivery systems to treat bladder cancer (A Review). International Journal of Pharmaceutics 532 (1), 105-117.

Kolawole O. M., Lau W-M., Khutoryanskiy V.V. (2018). Methacrylated chitosan as a polymer with enhanced mucoadhesive properties for transmucosal drug delivery. International Journal of Pharmaceutics 550 (1-2), 123-129.

Kolawole O. M., Lau W-M., Khutoryanskiy V.V. (2019). Chitosan/β-glycerophosphate based *in situ* gelling systems for intravesical delivery of mitomycin-C. International Journal of Pharmaceutics X, doi.org/10.1016/j.ijpx.2019.100007.

List of conferences

Pharmacy PhD Showcase 2016, University of Reading, 14th April 2016 - Poster

United Kingdom & Ireland Controlled Release Society Symposium, University of Cardiff, Cardiff, UK, 22-23rd April 2016 – Poster

M4 Colloids Symposium, University of Bath, Bath, UK, 20th July 2016 – Poster

Postgraduate Symposium on Nanoscience and Nanotechnology, University of Birmingham, Birmingham, UK, 13th December 2016 – Poster

Pharmacy PhD Showcase 2017, University of Reading, Reading, UK, 31st March 2017 – Talk

United Kingdom & Ireland Controlled Release Society Symposium, University of Strathclyde, Glasgow, UK, 30-31st May 2017 – Poster

M4 Colloids Symposium, University of Cardiff, Cardiff, UK, 26th July 2017 – Talk

Materials Research Exchange - Exhibition, Business Design Centre, London, UK, 12-13th March 2018 – Delegate

Pharmacy PhD Showcase 2018, University of Reading, Reading, UK, 10th April 2018 – Talk

United Kingdom & Ireland Controlled Release Society Symposium, Queen's University, Belfast, Northern Ireland, UK, 4-5th June 2018 – Poster

Doctoral Research Conference, Reading University, Reading, UK, 20th June 2018 – Three minutes thesis competition (Finalist)

7th European Chemical Society Congress, Arena Convention Centre, Liverpool, UK, 26-30 August 2018 - Poster

5th Royal Society of Chemistry Early Career Symposium, Arena Convention Centre, Liverpool, UK, 30-31 August 2018 - Poster

Table of contents

List of figures

List of tables

Abbreviations

ANOVA	analysis of variance
ATEA	2-(acetylthio) ethylacrylate
CHIGP	General name for LCHIGP, MCHIGP and HCHIGP
DSG-PEG	1,2-distearoyl-sn-glycerol, methoxyPEG 2000
DTX-Pam-NH$_2$	docetaxel loaded amine functionalised polyacrylamide
EDTA	ethylenediaminetetraacetic acid
EDC	N-(3-dimethylaminopropyl)-N'-ethyl carbodiimide hydrochloride
Fe$_3$O$_4$	magnetite
FITC-dextran	fluorescein isothiocyanate covalently bound dextran
GEM-C$_{18}$	stearoyl gemcitabine
HE	hematoxylin and eosin
HEMA	2-hydroxyethylmethacrylate
IC$_{50}$	inhibitory concentration of material required to reduce cell growth by 50%
LC-MS/MS	liquid chromatography used alongside two types of mass spectrometry
MEM	modified Eagle's growth medium
MTT	3-(4,5-dimethylthiazol-2-yl)-2,5-diphenyltetrazolium bromide
NHS	N-hydroxysuccinimide
ns	no statistical differences between data sets
PDI	polydispersity index
Ref	Reference
TEM	transmission electron microscopy
TNM	tumour-lymph nodes-metastasis tumour grading system
WST-1	(2-(4-iodophenyl)-3-(4-nitrophenyl)-5-(2,4-disulfophenyl)-2H-tetrazolium sodium salt
XTT	2,3-Bis-(2-Methoxy-4-Nitro-5-Aulfophenyl)-2H-Tetrazolium-5-carboxanilide
2θ	diffraction angle
λ	wavelength
δ	slope of the concentration versus absorbance graph

1. Introduction: Advances in intravesical drug delivery systems to treat bladder cancer

This chapter describes the pathophysiology, prevalence and staging of bladder cancer, and discusses several formulation strategies used to improve drug residence within the bladder. Various *in vitro* and *in vivo* models recently employed for intravesical drug delivery studies were discussed. Some of the challenges that have prevented the clinical use of some promising formulations are identified.

This chapter was published as:

1.1. Introduction

Bladder cancer (BC) is the most predominant malignancy affecting the urinary tract, characterised by proliferation of abnormal cells in the urothelial lining of the urinary bladder. It is commonly divided into non-muscle invasive bladder cancer (NMIBC) which make up 80% of cases at presentation and muscle invasive bladder cancer (MIBC) where the cancer extends into the underlying smooth muscles. The latter makes up 15% of cases at presentation with the remaining 5% presenting with metastases [1]. Intravesical therapy is only effective in NMIBC and is never used in MIBC. Haematuria is the commonest symptom in 85% patients but other clinical presentations may include urinary urgency and painful urination [2].

Bladder cancer is ranked 7th and 9th in terms of cancer incidence in the United Kingdom and worldwide, respectively [1,3] as well as being ranked fifth based on prevalent cancer types among European men [4]. Bladder cancer is more likely to recur than other forms of cancer including those of the breast, prostate, lung and bowel [1,4]. In 2015 in the UK, 6169 new cases were diagnosed in men versus 2331 new cases in women [5] and it is projected that by 2035 there will be 7771 BC related deaths per year out of 10386 cases of bladder cancer [6]. Also, bladder cancer annual diagnosis in the UK is about 10000 and 50% of such patients die eventually due to disease progression and/or treatment failure [7]. Bladder cancer is statistically twice as prevalent in the white population than in the black population [8]; however in terms of mortality, with five-year survival rate, it is considerably higher in the white community (80%) in comparison with the black community (64%) [3]. The greatest risk factor for bladder cancer is smoking and the risk is 2 to 6 folds higher for smokers than non-smokers, and smoking is responsible for almost 31% and 14% of bladder cancer deaths in males and females, respectively [3]. In Africa, 50% of bladder cancer patients have a previous history of infection with the water-borne parasite, *Schistosoma haematobium*, whereas the incidence of such bladder cancer cases worldwide is only 3% [9].

Non-muscle invasive bladder cancer, also called superficial bladder cancer is the most prevalent form of bladder cancer at first diagnosis. It progresses to non-muscle invasive bladder cancer in about 15% of patients with a poor prognosis despite transurethral resection of the bladder tumour and Bacillus Calmette-Guérin (BCG) immunotherapy [10] and therefore frequent cystoscopic surveillance of the bladder is necessary following initial therapy [3]. Bladder cancer has the highest cost of therapy of any cancer over the lifetime of the affected individual due to the associated cost of surveillance and treatment [9,11,12]. Therefore improved bladder cancer therapeutic delivery systems have been investigated over the last

two decades (Fig. 1.1) in an attempt to reduce the clinical and economic burden of this disease.
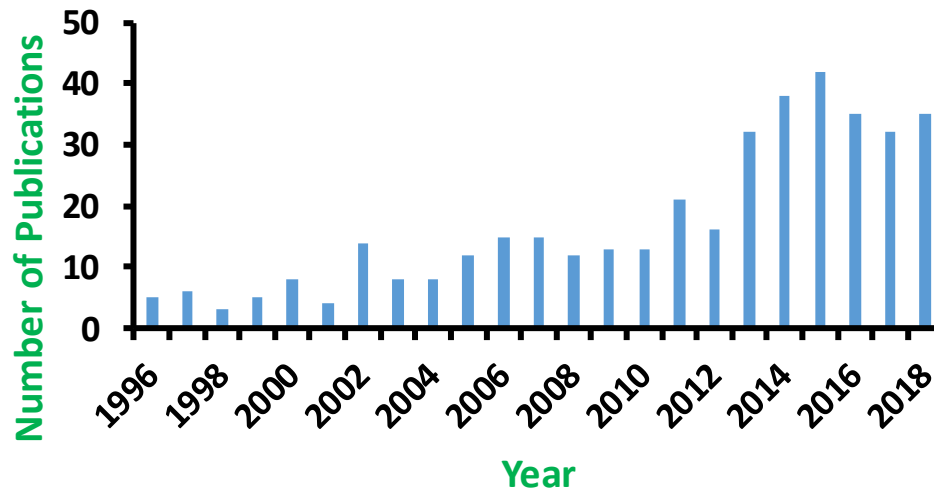
Fig. 1.1. Number of publications reporting bladder cancer therapeutic delivery systems (1996-2018).

Source: Web of Knowledge, now Web of Science (search terms: bladder cancer, delivery systems).

Bladder cancer drug delivery systems are typically presented as liquid formulations and they are administered orally, systemically or locally. The degradative hepatic enzymes and gastric acid lowers oral bioavailability of bladder cancer therapeutic formulations while systemic therapy is less efficient due to the poorly vascularised urothelium [13,14]. Increasing systemic drug dose with the aim of improving local drug concentration within the bladder leads to elevated adverse drug reactions and non-selective toxic effects on healthy tissues [14].

Intravesical drug delivery (IDD) is the instillation of one or multiple therapeutic agents through a catheter, directly into the bladder. IDD provides site-specific drug delivery with minimal toxicity [14]; and this local drug delivery could reduce tumour recurrence and progression [15] because localised therapy improves therapeutic drug concentrations in the bladder which destroys residual urothelial cancerous cells [2,16,17]. Due to cellular and physiological limitations posed by the urothelium as well as the presence of urine, it is not sufficient to simply administer cytotoxic formulations intravesically; there is a need for careful design of drug delivery systems that would be able to circumvent these barriers.

Some good reviews have been published that considered a variety of nanoparticles and nanotechnology for bladder cancer therapy and/or diagnosis [14,18,19] but some of the nanoparticulate systems discussed were developed over a decade ago and recent studies were not discussed fully in some of the articles. Also, formulation strategies that require adjunct equipment such as electromotive device assisted therapy and hyperthermia has not been widely embraced by urologists because of their complex delivery modalities [11]. Thus they were not covered within the scope of this chapter.

This chapter, therefore, will discuss briefly the pathophysiology, prevalence and staging of bladder cancer and will focus on advanced formulations investigated for bladder cancer management that have not been covered previously. Also, *in vitro* and *in vivo* models that are currently used for intravesical drug delivery studies will be discussed. The reviewed advanced drug carriers are categorised into four groups based on non-particulate, particulate, composite systems of hydrogels and particles and liposomal drug carriers.

1.2. Bladder Physiology

1.2.1. Structure of the bladder

In order to carry out its urine storage and voiding functions, the bladder (Fig. 1.2) can change volume although it remains almost spherical in shape [14]. The bladder wall is comprised of four layers: the urothelium, lamina propria, detrusor muscle, and serous (adventitia) layers, with a rich supply of blood vessels, sensory/motor neurons and lymph vessels embedded in these layers [17]. The urothelium acts as the bladder permeability barrier and comprises of intermediate, germinal basal and superficial cell layers, with the latest cell layer comprising of umbrella cells knitted together by tight junctions and enveloped by uroplakin plaques and mucin. These components prevent diffusion of pathogenic and toxic substances into the systemic circulation; their detailed functions have been discussed in a previously published research article [14]. The urothelium, which covers the entire interior surface area of the bladder, prevents the influx of the waste materials present in the urine, into the systemic circulation. The mucin layer adhered to the luminal side of the urothelial layer, comprises of hydrophilic glycosaminoglycans which covers the umbrella cells which limits the adherence of foreign particles or potential chemotherapeutic solutions from penetrating into underlying tight junctions or cell membranes [20]. This also means that, systemic therapeutic agents for NMIBC treatment cannot diffuse efficiently into the bladder [20]. In addition, regulatory information emanating from the bladder lumen is transmitted by the urothelium to the

surrounding tissues (myofibroblasts and musculature) via different neurotransmitters including adenosine triphosphate, adenosine and acetylcholine [21].
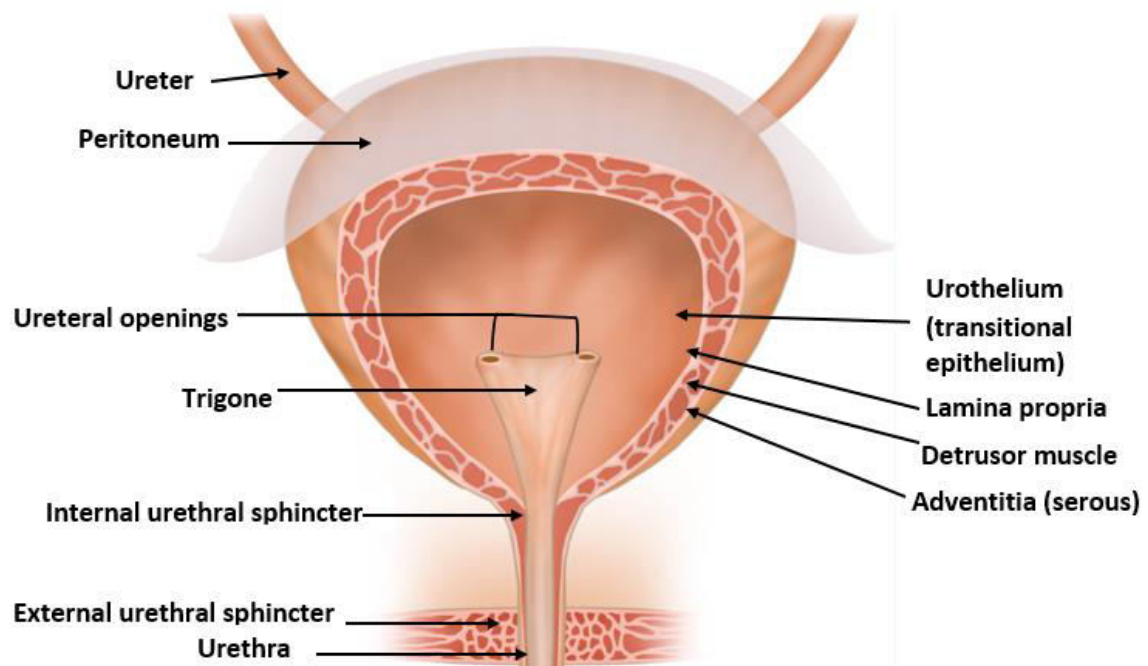
Fig. 1.2. Schematic diagram showing various segments of the bladder. This image was designed and kindly provided by Ms Stephanie Bull.

1.2.2. Urine volume and composition

Urine is a hypertonic solution with its concentration of electrolytes and pH remarkably different from that of the blood. It exhibits a tonicity of about 600 mOsm/L but this value may vary depending on fluid intake of an individual which concentrates or dilutes the urine. Its pH ranges from 4.5 to 8 depending on metabolic conditions and dietary preferences [22].The volume of urine in a human bladder is dependent on the sex, race and ethnicity of an individual but in the adult it averages around 350-450 mL when full [23] although the first sensation of urination occurs at around 150 to 200 mL of urine [14]. Urine voiding activity is regulated by the myovesical plexus (made up of interstitial cells and nerve ganglia) within the bladder wall which determines the functional behaviour of the bladder wall, producing a specific sensation when sufficient urine is present in the bladder and sends a voiding signal to

the detrusor muscle which relaxes or contracts appropriately in order to regulate the extent and frequency of voiding [21].

1.3.   Bladder Cancer

1.3.1.   Genetic / molecular expressions in bladder cancer

Some of the genetic materials that are expressed in bladder cancer can be used as molecular targets to design effective therapies. For example, survivin which is detectable in the urine of bladder cancer patients [24] has been implicated in bladder cancer as it improves the survival rate of cancerous cells by preventing cell death [25]. Bladder cancer patients also are known to express particular membrane glycoproteins, mucins (MUC1 and MUC3) associated with bladder malignancies which promotes cancer cell mobility and survival [26].

The natural immune system of the bladder is achieved through uroplakins, a group of proteins found at the apex of the umbrella cell membrane, namely UPIa, UPIb, UPII, and UPIII. They induce bacterial death when infected. They also perform barrier functions along with tight junctions, where they prevent drug diffusion across the urine/bladder tissue interface as a result of their high density packing [27–29]. Changes in the glycosylation of uroplakins especially UPIII may depict advanced stages of bladder cancer, in addition to clinical conditions such as urinary tract infections and interstitial cystitis [30].

Lewis X glycoantygen, sialyl-Tn (carbohydrate) and its degrading enzyme (sialyltransferase) are expressed on the urothelium and are markers for bladder cancer [30]. Metabolomics of urine samples from bladder cancer and non-bladder cancer subjects' revealed that biomarkers (lipid-metabolic products) such as arachidonite, palmitoyl sphingomyelin, lactate, adenosine and succinate are found in bladder cancer patients only [31]. Chemokine ligand 1 (CXCL1), which modulates interaction between stroma and urothelium, in order to accelerate tumour progression and metastasis, is also expressed in urine samples of bladder cancer patients [32].

1.3.2. Stages of bladder cancer

About 90% of bladder cancer cases are transitional cell carcinomas while squamous cell carcinomas occur in 3-7% patients and around 2% have adenocarcinomas [33]. Usually, the urothelial layer of the bladder is initially affected by most bladder cancer types. The nearby lamina propria and muscular layer becomes involved as the tumour progresses. Afterwards, the lymph nodes or pelvic organs are also affected. The metastatic stage arises when cancerous cells divide and spread to distant organs such as lungs, liver and bone marrow [33].

Table 1.1

Bladder cancer stages. Information taken from [34]

Category	Stage	Description, including tumor coverage
Ta, N0, M0	Stage 0a	Non-invasive papillary carcinoma – hollow centre of the bladder
Tis, N0, M0	Stage 0is	Flat, non-invasive carcinoma (carcinoma *in situ*) – inner bladder lining
T1,N0, M0	Stage I	Invasive – connective tissues beyond the urothelial lining
T2a or T2b, N0, M0	Stage II	Invasive – inner half (T2a); outer half (T2b) of the muscular region
T3a, T3b, T4a, N0, M0	Stage III	Invasive – fatty tissue region visible with microscope (T3a); readily visible (T3b); spread to prostate, uterus and/or vagina (T4a)
T4b, N0, M0, N1-N3, M1	Stage IV	Invasive / metastatic – Pelvic or abdominal wall (T4b); single pelvic lymph node (N1); ≥ 2 lymph nodes (N2); iliac arterial lymph nodes (N3); beyond the bladder to distant sites like bones, liver or lungs

Note: N0 and M0 denotes that lymph nodes and distant sites (metastatic tumours) were not affected, respectively.

The tumour stage defines the extent of disease progression [35]; and the tumour node metastasis staging system developed by International Society of Urological Pathology in 1997 for bladder cancer classification is still being used by World Health Organisation [36]. The American Joint Committee on Cancer TNM tumour grading system categorises bladder cancer based on their growth into the bladder wall (T), spread to neighbouring lymph nodes (N) and metastases (M). Information from these categories is then used to evaluate the overall stage of the disease from stage 0 to IV (Table 1.1).

Eble et al. graded bladder cancers based on cell morphology into tumour grade G1, G2 and G3, with G1 being the most well differentiated, while G3 is the least differentiated bladder cancer having the greatest risk of progression [37]. Recently, WHO proposed a new grading classification for bladder cancer based on improved knowledge of its pathology and genetics (Fig. 1.3), where "urothelial dysplasia" and "urothelial proliferation of uncertain malignant potential" were included as well defined forms of non-invasive urothelial lesions [36].
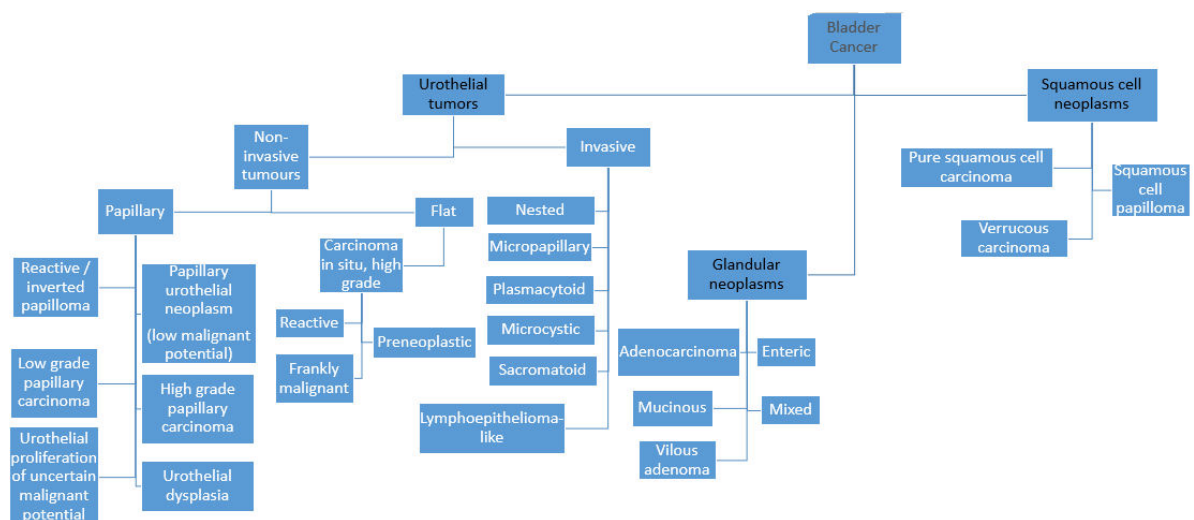
Fig. 1.3. The 2016 WHO Classification of Bladder Cancer (details extracted and presented in a different format) [36]

1.4. Management of bladder cancer

Bladder cancer treatment is dependent on the stage and severity of disease [33]. The UK National Institute for Health and Care Excellence (NICE) has produced guidelines regarding the diagnosis and treatment of bladder cancer. It recommends that both cystoscopy and urine cytology is needed in order to diagnose bladder cancer as cystoscopy alone may miss some tumours such as carcinoma *in situ* [38]. The extent of bladder cancer progression is identified using computer tomography or magnetic resonance imaging techniques. NMIBC is initially treated with transurethral resection of bladder tumours followed by a single dose of intravesical chemotherapy such as Mitomycin-C, doxorubicin, epirubicin and thiotepa to reduce recurrence rate [38,39]. Patients with a low risk of disease recurrence post-surgery may be followed up with cystoscopic surveillance alone, whilst those in the intermediate and high risk categories are treated with induction intravesical chemotherapy (mitomycin-C) or Bacillus Calmette Guérin (BCG) immunotherapy for at least 6 weeks, in addition to the perioperative chemotherapy to ensure recurrence-free survival [39]. The BCG therapy triggers an immune response that ensures future recognition of bladder cancer cells, and this treatment has been proven to prevent cancer progression in about 85% of bladder cancer cases [39].

1.5. Drugs and drug carriers for Intravesical drug delivery

Currently, the chemotherapeutic agents used for bladder cancer treatment are doxorubicin, gemcitabine, epirubicin [40], mitomycin-C, thiotepa, paclitaxel and cisplatin [2], BCG and interferon-α [41,42]. The effectiveness of bladder cancer therapeutic dosage forms depends on their ability to overcome the urothelium as well as the loaded drug having suitable physicochemical properties such as molecular weight ($\geq$ 200 Da), water or lipid solubility, organic/aqueous phase partition coefficient (log P) of -0.4 to -0.2 or -7.5 to -8.0, and minimal ionisation between pH 6 and 7 [14]. Drugs intended for intravesical bladder cancer treatment should have molecular weight above 200 Da to promote permeation into underlying malignant urothelial tissues and avoid systemic uptake; soluble enough in water since the bladder environment is aqueous in nature but they must have some degree of lipophilicity which enhances drug transport across urothelial malignant tissues. Drugs exhibiting a negative logarithm of organic phase to aqueous phase partition coefficient (logP) implies that the drugs are more hydrophilic in nature, which is critical for their solubilisation in the aqueous bladder environment; and such drugs should not be ionised readily between pH 6 and 7, which is the

typical pH in the bladder environment to prevent drug degradation before availability at the target sites [42].

The surface charge of drug carriers influences their cellular uptake, for example, positively charged nanoparticles are taken up by cells and readily absorbed into tissues in preference to anionic or neutral nanoparticles due to electrostatic interaction between oppositely charged dosage form and cell membranes [43–45]. Possibly, the uptake of such drug cargos may be prevented by poor interaction with biorecognitive moieties on cell surfaces such as wheat germ agglutinin (WGA) that facilitate cellular internalisation [21] as well as electrostatic repulsion between negatively charged carriers and bladder mucosa.

1.5.1. Conventional formulations

The primary function of the bladder is to store and void urine. This physiological role leads to the dilution and wash-out of conventional dosage forms for bladder cancer treatment, which are made of simple solutions to aid syringeability through the catthether during intravesical therapy. For instance, the commercial dosage form of mitomycin-C (Kyowa®, Galashiels), a choice drug for the intravesical treatment of superficial bladder cancer, is presented as 2 mg, 10 mg, 20 mg and 40 mg powder for solution, formulated with sodium chloride to improve the aqueous solubility of the drug [46]. The current formulation lack polymeric excipients, making it less resistant to urine dilution and wash-out, resulting in less than optimal effectiveness of treatment, contributing to high disease recurrence rate and treatment costs [47]. As a result, the National Health Service in England spends £65 million yearly for bladder cancer management and treatment [48].

Mucoadhesive gels could potentially extend the residence time of drug formulations in the bladder. The surgical implantation of drug loaded gels into bladder cancer patients is expensive and inconvenient to them [49]. Therefore, local drug delivery by drug instillation via a catheter was adopted which permits easy bladder accessibility and avoids surgery [42]. The usual volume of drug formulation instilled intravesically is approximately 50 mL [50] and micturition is prevented for at least 1-2 h post intravesical drug administration, for effective drug transport into the underlying cancerous tissues [51]. Nevertheless, the instilled drug becomes diluted due to residual urine which is often present in the human urinary bladder and/or is washed out prematurely [52]. These limitations mean frequent catheter insertion, decreased dosing interval, eventual irritation of the urethral lining and possible urinary tract infection are possible complications of intravesical drug delivery [53]. In addition, conventional

drug carriers such as microspheres [54,55] and gelatin nanoparticles [56] display poor drug loading and uncontrolled drug release profiles.

1.5.2. Advanced formulations

Hydrophilic drugs are readily soluble in the aqueous urine medium of the bladder but their permeability and cellular uptake is limited due to the lipophilic nature of the urothelial tissues. Thus, chemical enhancers such as dimethyl sulfoxide have been used to improve the cellular uptake of bladder cancer chemotherapeutics such as doxorubicin and cisplatin into malignant bladder tissues [57]. However, their use is now less favourable because of unwanted side-effects such as frequent and painful urination [14]. Hydrophobic drugs such as paclitaxel formulated with dimethyl sulfoxide for improved solubility and urothelial permeability are associated with painful sensation after intravesical instillation [58].

Therefore, novel drug carriers were developed to improve the aqueous solubility of lipophilic drugs, urothelial permeability of hydrophilic drugs, urothelial adhesion of drug carriers as well as drug uptake/permeation into malignant tissues for prolonged periods of time. They include amphiphilic copolymer based solubilised systems [59], surface modified particulate systems [53,60–66], composite particulate and hydrogel systems [50,67–69] and liposomal systems [70,71] (Table 1.2).

1.5.2.1. Amphiphilic copolymer based solubilised systems

Solubilised systems are isotropic solutions of a substance in a state of thermodynamic stability generated by dispersing the sparingly soluble substance in an amphiphilic material [72]. Cremophor is conventionally used to improve the solubility of paclitaxel in the physiological fluid but its use is limited by adverse effects as well as reduced drug permeation across the mucosal lining due to drug entrapment in polymeric micelles, preventing their release and bioavailability [73]. On the other hand, the amphiphilic copolymeric delivery system, poly (2-methacryloyloxyethyl phosphorylcholine-co-n-butyl) methacrylate (PMB30W) has been proven to be non-toxic with improved paclitaxel solubility and uptake into mammalian cell lines during *in vitro* studies [74,75].

PTX-MBA (novel drug carrier) was formulated by solubilising paclitaxel in PMB30W in order to improve its aqueous solubility, safety and antitumour activity [59]. *In vitro* studies using MBT-2 bladder cancer cells to compare cytotoxicity of PMB30W (1% w/v) and ethanolic cremophor (1:1; v/v) to bladder cancer cells showed that PMB30W displayed no toxic effect to the cells

while dose associated toxicity was reported with ethanolic cremophor after 72 h of instillation. This was confirmed by the lactate dehydrogenase (LDH) activity assay, detecting 0% and 65% LDH release for PMB30W and ethanolic cremophor, respectively, in the same study [59].

Class	Agent	Material	Dosage form	Ref.

Table 1.2. Overview of intravesical formulations explored for bladder cancer therapy

Amphiphilic copolymer based solubilised systems	Paclitaxel	Poly (2-methacryloyloxyethyl phosphorylcholine-co-n-butylmethacrylate) diblock copolymer (30 mol% methacryloyloxyethyl phosphorylcholine hydrophilic unit: 70 mol% hydrophobic butyl methacrylic anhydride unit)	Ionotropic solution	[59]
Surface modified particulate systems	Belinostat	PGON, PLGA	Nanoparticles	[61]
	Doxorubicin	B-cyclodextrin, mesoporous silica	Nanoparticles	[64]
	Mitomycin-C	Poly (L-lysine)-coated and chitosan coated poly(ϵ)caprolactone	Nanoparticles	[60,63]
	Survivin SiRNA	Chitosan, PLGA	Nanoparticles	[53]
	Stearoyl Gemcitabine	Wheat Germ Agglutinin, PLGA	Microparticles	[62]
	Doxorubicin	Copolymer of 2-(acetylthio)ethylacrylate and 2-hydroxyethylmethacrylate	Thiolated Microgels	[65]
	Docetaxel	Amine-functionalised polyacrylamide	Nanogels	[66]
	10-hydroxycamptothecin	Poly (L-lysine)-poly (L-phenylalanine-co-L-cysteine)	Nanogels	[76]
Composite particulate and hydrogel systems	Adriamycin	Poloxamer 407 (triblock copolymer), sodium hydrogen carbonate, HPMC, Human Serum Albumin	Floating hydrogel-nanoparticulate system	[69]
	Bacillus Calmette-Guérin	Chitosan, β-glycerophosphate, magnetite	Mucoadhesive nanoparticle-*in situ* gelling system	[68]
	Deguelin	DOTAP, monomethoxy poly (ethylene glycol)-poly (ϵ-caprolactone) NP + Pluronic F127 hydrogel	Mucoadhesive nanoparticle-*in situ* gelling system	[67]
	Gemcitabine HCl	Chitosan-thioglycolic acid conjugate based NPs + chitosan gel / Poloxamer gel	Thiolated Mucoadhesive nanoparticle-*in situ* gelling system	[50]
Liposomal systems	Paclitaxel	Soya phosphatidylcholine, gellan gum	Liposomes/ion-triggered gelling system	[70]
	Fluorescein sodium	Soybean L-alpha-phosphatidylcholine, MPEG$_{2000}$-DSPE, PEG$_{2000}$-DSPE-Mal	PEG- & Maleimide-liposomes	[71]

The ability of an orthotopic bladder cancer mouse model (mouse implanted with MBT-2 bladder cancer cells) to mimic the human bladder cancer environment has been confirmed in some studies [77,78]. During *ex vivo* studies, orthotopic model of bladder cancer was established through transurethral implantation of MBT-2 BC cells into mice. Then, these mice were treated with various formulations (50 µL of 2 mg/mL PBS, PTX-MBA and PTX-CrEL) at predetermined time intervals and killed after 22 days to determine the degree of tumour growth or regression. It was shown that PTX-MBA (novel formulation) improved tumour regression (more than 2 folds) in comparison with PTX-CrEL (conventional drug carrier) [59]. Some of the mice were sacrificed 30 min post intravesical drug instillation and the degree of drug uptake into tumour tissues quantified using liquid chromatography/tandem mass spectrometer, was shown to be remarkably lower in PTX-CrEL than in the PTX-MBA group of mice (4.905 ± 2.412 µg/g vs 7.719 ± 3.274 µg/g). This revealed improved selectivity of the novel paclitaxel carrier for malignant tissues [59]. However, studies related to the resistance of the delivery system to urine dilution or wash-out were not evaluated and periodic urine voiding and residual urine in the bladder may have affected product performance. Drug release studies were not carried out, thus the pattern of drug release is unknown. This makes it difficult to ascertain that the drug will be released in a controlled manner, which is a critical parameter for improved bladder cancer formulations that would reduce dosing frequency.

1.5.2.2. Surface modified particulate systems

1.5.2.2.1.   Lectin modified particulate systems

Glycans and lectins are biological entities that are sensitive and responsive to bacterial and malignant invasion by destroying them through endocytosis, where they interact and adhere onto mannose receptors on cell surfaces [79–81]. It is anticipated that lectins will be useful for malignant conditions associated with the bladder because they attach to the distal portion of *Escherichia coli* (E. coli) pili and destroy the E. coli in bacteria urinary infections [82]. The urothelial cellular uptake of plant lectins, like wheat germ agglutinin (36 kDa), in pigs and humans, suggested that biologics may be delivered intravesically, as lectins are readily recognised by the glycol-proteins and lipids of the urothelium and facilitate cellular uptake of a bioconjugate [83].

Neutsch and co-workers surface-functionalised fluorescently labelled bovine serum albumin with wheat germ agglutinin (WGA) units and this modification influenced the urothelial cell (SV-HUC-1) adhesive and invasive potential of the fluorescent WGA conjugated bovine serum albumin bioconjugate (fBSA/WGA) [84]. Their cytoadhesive features were greatest when the

total number of targeting ligands was three and such features did not increase further for bioconjugates with 4-6 WGA units [84]. This lectin-modulated interaction was critical for internalisation of the drug carrier (> 175 kDa) within less than 60 min, with more than 40% of drug taken up via endocytosis. The unchanged extent of cell adhesive properties with increased WGA units ($\geq$ 3) may be due to some of their recognitive domains being sterically hindered from binding to glycosylated urothelial cell membranes [84]. Neutsch's group have also suggested the mechanism of WGA metabolism after fluorescently labelled bovine serum albumin release, to have taken place via lysosome degradation [84].

Nanoparticles are structures in the nanometer scale and these nanocarriers can be formulated from lipids, synthetic and biopolymeric polymers, proteins, metals, inorganic and organometallic compounds [85]. Nanoparticles generated from biopolymers, lipids, proteins and some synthetic polymers such as polyesters (PLGA) are biodegradable and drug release from them can be modulated while those prepared using inorganic compounds such as polystyrene are non-biodegradable [86].

Poly(lactic-co-glycolic acid) (PLGA) is a FDA approved copolymer widely used for the delivery of drugs, proteins, DNA, RNA and peptides due to its biodegradability and biocompatibility [87]. Stearoyl gemcitabine loaded PLGA microparticles surface modified with wheat germ agglutinin or human serum albumin, WGA-GEM-C_{18}-PLGA MPs or HSA-GEM-C_{18}-PLGA MPs, were explored for intravesical drug delivery [62]. *In vitro* studies using cancerous and non-malignant cell monolayers showed that the WGA-GEM-C_{18}-PLGA microparticles had better cellular uptake, internalisation and cytostatic action than HSA-GEM-C_{18}-PLGA and unmodified microparticles within 3 min of instillation due to the biorecognitive properties of wheat germ agglutinin, which enables wheat germ agglutinin conjugated drug carriers to be readily taken up into the urothelial tissues via endocytosis. The wheat germ agglutinin modified PLGA microparticles also had a two-fold greater affinity towards malignant cell lines than healthy cells. The fluorescently labelled drug loaded WGA and HSA modified microparticles required a contact time of 30 min and 120 min, respectively, to impart cytotoxic activity on low grade cancerous cell lines using fluorescence microscopy [62]. WGA-GEM-C_{18}-PLGA microparticles were more resistant to wash-off by artificial urine, which allowed for superior retention of cytostatic effect (78 $\pm$ 12%) compared to free prodrug but the degree of cell inhibitory potential of the free drug in the presence of urine was not defined [62]. There was no significant difference in the sustained release effect (after 120 min) for the three formulations

(WGA-, HSA- modified and unmodified PLGA microparticles), which could be attributed to the inability of the study design to simulate wash out features of the urinary bladder.

The WGA-modified microparticles also had low drug release of 13.2 ± 1.8% after 5 days with most of the drug retained within the particle matrix. Nevertheless, studies of bromodeoxyuridine antimetabolic activity suggested that wheat germ agglutinin based particles require a lower dose than free drug for achieving a particular degree of prolonged action [62]. Also, a cell proliferation assay suggested better antiproliferative properties for drug loaded surface modified particles than free drug [62]. Overall, the optimisation and translation of this formulation strategy to the clinic may be limited by the relatively high cost of manufacturing in terms of time and materials required for isolation and purification of the bioconjugate of interest. The bioconjugate size may be heterogenous resulting in immunogenic and adverse reactions. However, Neutsch's group did not envisage such formulation constraint.

Recently, Apfelthaler et al. evaluated a bioconjugate, wheat germ agglutinin conjugated to fluorescein cadaverine labelled poly (L) glutamic acid (WGA/FC-PGA), for a bladder cancer theranostic application [88]. Poly (glutamic acid) may improve the solubility of the hydrophobic agents while wheat germ agglutinin favours the selective uptake of bioconjugate into malignant bladder tissues by interacting selectively with the glycocalyx components (N-acetyl-D-glucosamine and sialic acid) of bladder cancer cells [89]. Flourescein cadaverine helps to track transport of the drug carrier into the cancerous cell endosome and/or lysosome. They confirmed earlier findings by Neutsch's group [62] that the presence of biorecognitive moieties such as wheat germ agglutinin was critical for improved cellular uptake and internalisation of bioconjugates into BC cells. Flow cytometry was used to evaluate the cell-binding ability of the delivery system, WGA/FC-PGA. Size exclusion chromatography was used to purify the synthesised bioconjugate and isolate biorecognitive fractions. Conjugate A (160 kDa) fraction, obtained with 60 to 80 mL eluent, displayed superior cell binding efficiency relative to conjugates B-D due to the presence of more WGA units conjugated to the fluorescein cadaverine labelled poly (L) glutamic acid system. Five fluorescein cadaverine molecules per poly (L) glutamic acid were critical for adequate traceability of the bioconjugate as it exhibited greater cell-induced relative fluorescence intensity than bioconjugate with 30 fluorescein cadaverine per poly (L) glutamic acid. Conjugate A was found to be cytoadhesive at 4°C but become cytoinvasive at 37°C via active transport. On the other hand, conjugates C and D eluted around 90 mL and lacked both cell adhesive and uptake properties [88].

There was no hydrophobic agent delivered within the scope of this study, though the authors acknowledged that their future studies will explore optimal drug loading that will not compromise the cell binding and uptake features of the bioconjugate. They noted that there is a need for conjugate A (the most promising bioconjugate) to replicate similar cytoadhesive and cytoinvasive profile when hydrophobic theradiagnostic agents are loaded.

1.5.2.2.2. Mucoadhesive delivery systems

There are various theories that govern the adhesion of drug delivery systems onto the mucosal surfaces (Figure 1.4), namely wetting, electronic, adsorption, diffusion, fracture, and mechanical [90,91]: (1) The wetting theory relates to the liquid polymer's ability to spread onto the mucus layer of mucosal tissues; (2) electronic mode relies on electron transfer between the mucoadhesive polymer and the mucosal mucus, resulting in electrostatic attraction between surfaces of opposite charges; (3) with adsorption theory, polymers and mucus interact via hydrogen bonds and van der waals forces, hydrophobic effects (amphiphilic polymers) and chemisorption (covalent bond between polymer and mucin); (4) diffusion theory exploits the penetration of the polymer into the mucus gel while the mucin diffuses into the dosage form generating interpenetrating layers; (5) fracture theory relates to the difficulty of separation of the drug carrier from the mucosal surface, which is used to calculate the fracture strength of adhesive bonds involving solid and rigid mucoadhesives; and (5) the mechanical theory pertains to surface roughness of rough and porous delivery systems where increased contact area with mucosal surfaces results in improved mucoadhesiveness [91].
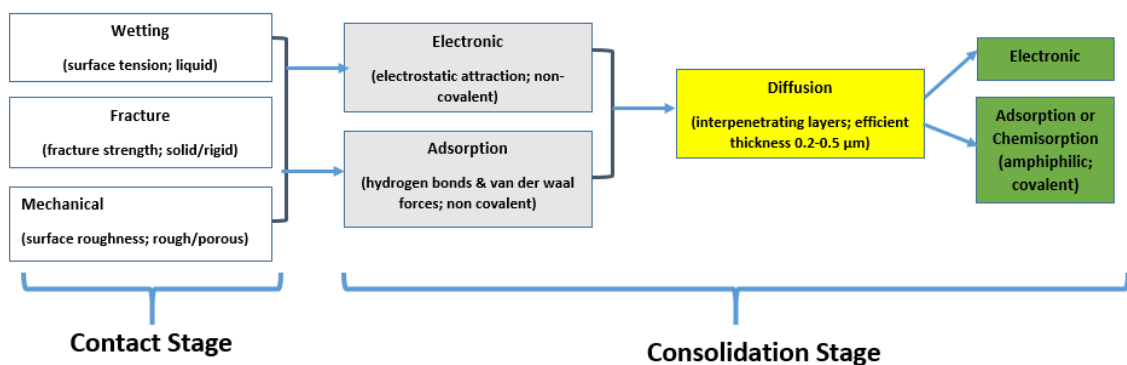
Fig. 1.4. Schematic representation of the interrelationship between various mucoadhesion theories.

Since these theories cannot explain the mechanism of mucoadhesion in isolation, some researchers have described the mechanism of mucoadhesion occurring through two main stages, first is the contact stage where the polymeric liquid dosage form is wetted and swells. The second stage is the consolidation stage where the polymeric material interacts with the mucosal mucus via electronic or adsorption (non-covalent) interaction. Then, interpenetrating layers are formed between the polymer chains and the mucosal membrane dictated by the molecular weight, hydrodynamic size and mobility of the mucoadhesive material. The mucoadhesiveness of the material is sustained via non-covalent or covalent bond formation between the entangled polymer chains and the mucosal membrane [90,91].

A mucoadhesive formulation is an attractive drug delivery system for bladder cancer treatment because the interaction and retention of the dosage form on the bladder mucosal surfaces is critical for drug penetration into malignant tissues and resultant therapeutic action. They are preferred to lectin functionalised PLGA microparticles because their use is less associated with immunogenic reaction resulting from the inefficient purification of some bioconjugates such as wheat germ agglutinin functionalised PLGA microparticles.

Over the last decade, researchers have intensified efforts towards investigating materials with ability to adhere readily to mucosal surfaces because they can prolong the contact time between dosage form and diseased site, which is desirable for intravesical formulations [50,56,65,91]. Examples of such mucoadhesive polymers are presented as Appendix 1 and they differ in terms of their source as well as biodegradability. Due to their successful applications for other transmucosal routes of administration such as buccal, ocular and vaginal [92], mucoadhesive systems have also been explored for intravesical delivery to enhance drug bioavailability and duration of action [64,65,67,68,93].

1.5.2.2.2.1. Cationic particulate systems

Cationic drug carriers adhere onto negatively charged bladder mucosa via electrostatic interaction. Poly (L-lactide-co-glycolide) nanoparticles have been widely used for biomedical applications because of their biocompatibility, biodegradability, ease of modification with polymers and peptides [94,95], ability to protect encapsulated biologics or therapeutics from degradation during transit, as well as possibility for controlled release of loaded drugs [96–98]. Poly (guanidinium oxanorbornene) (PGON) is a non-toxic synthetic polymer which is comprised of cationic guanidinium groups and acts similarly like a peptide based cell permeation enhancer [99]. Martin et al. explored surface functionalisation of PLGA

nanoparticles with a urothelial cell penetrating polymer such as poly (guanidinium oxanorbornene) to improve aqueous solubility, urothelial cellular uptake, internalisation, cytotoxic effect, and duration of action of lipophilic drugs such as belinostat, an histone deacetylase inhibitor [61]. Belinostat promotes hyperacetylation with intrinsic IC_{50} in bladder and prostate cancer cells within the range of 1 to 10 µM; and inhibits bladder cancer progression to its metastatic and aggressive forms [100,101].

All PLGA nanoparticles were 14-160 nm but PGON-modified PLGA nanoparticles had superior drug loading relative to the unmodified and biotinylated chitosan conjugated nanoparticles by 3.3- and 6.8-folds, respectively [61]. *Ex vivo* studies of fluorescently labelled NP-Belinostat-PGON using human ureter as well as *in vivo* studies with mouse bladder suggested that the uptake of belinostat loaded PGON modified PLGA nanoparticles was ten times greater than that of the unmodified nanoparticles [61]. PGON, the cell permeation enhancer, improved urothelial uptake of nanoparticles by interaction with a negatively charged urothelial surface coated with glycosaminoglycan, or opening tight junctions of the urothelium. This facilitated drug transport across the urothelial membrane into underlying tissues [61].

The *in vivo* cytotoxic effect of PGON-modified PLGA nanoparticles was tested using a xenograft murine model generated from the UM-UC-3R human bladder cancer cell line. Tumour growth was not significant after 11 days of treatment for belinostat loaded PGON modified PLGA nanoparticles, whereas the volume of tumours treated with unmodified PLGA nanoparticles and drug-free PGON-modified PLGA nanoparticles increased by at least two folds relative to tumours treated with belinostat loaded PGON modified PLGA nanoparticles. After 21 days, the volume of tumours treated with unmodified drug loaded PLGA nanoparticles and blank PGON modified PLGA nanoparticles had increased by 77% and 71%, respectively, relative to belinostat loaded PGON modified PLGA nanoparticles treated tumours [61]. The burst release profile of the novel drug carrier was evident by Histone H4 hyperacetylation occurring in RT-4 (less-invasive) and T-24 (highly invasive with metastatic tendency) cell lines within 30 min following the instillation of NP-Belinostat-PGON, and the protein expression was sustained for 3 days [61]. Thus, a lower dose of the belinostat loaded PGON modified PLGA nanoparticles may be used to achieve the same therapeutic index observed with free belinostat [61]. Though the degree of tumour regression by the PGON surface decorated PLGA nanoparticles may correlate with their extent of cellular uptake and drug release, the authors have not quantified the amount of belinostat that was taken up for the modified and unmodified nanoparticles.

This information would be useful for determining dosage regimen for bladder cancer treatment using this drug carrier.

In a later study, Martin et al. showed that PLGA nanoparticles functionalised with low molecular weight chitosan 2.5 or 20 kDa (CHI2.5-PLGA or CHI20-PLGA) were able to adhere onto urothelial surface and enhance the uptake of larger therapeutic agents like survivin siRNA [53]. Survivin siRNA expression within urothelial cancerous cells enhanced destruction of survivin mRNA responsible for preventing death of cancerous cells. *In vitro* release studies showed the encapsulation efficiency of the nanoparticles modified with chitosan was superior compared to unmodified nanoparticles (70 vs 60%). CHI2.5-PLGA nanoparticles demonstrated a superior burst release profile relative to CHI20-PLGA nanoparticles. Also the CHI20 decorated carrier displayed 10-fold lower siRNA release than CHI2.5-PLGA nanoparticles over 13 days, inferring that delivery systems conjugated with chitosan of greater molecular weight (20 kDa) could be less beneficial if a fast onset of siRNA release and antitumour activity is desirable. During *ex vivo* studies, CHI20-PLGA and CHI2.5-PLGA nanoparticles displayed improved cellular uptake into UM-UC-3 BC cells in comparison with control PLGA nanoparticles, in the magnitude of 5-10 fold and 4-9 fold, respectively, within 120 min of incubation [53]. During *in vivo* mice studies, bladder uptake was up to 14-fold and 9-fold greater for CHI20-PLGA and CHI2.5-PLGA nanoparticles, respectively, compared to the control formulations [53]. Though siRNA was readily taken up into urothelial malignant cells and tissues for PLGA nanoparticles conjugated with chitosan (20 kDa), the CHI20-PLGA nanoparticles entrapped greater amounts of siRNA, in addition to forming bulkier surface groups, which prevented their release and bioactivity [53]. Thus CHI2.5-PLGA NPs may be desirable for therapy where fast onset of action is needed followed by a sustained release profile over a period of time. Moreover, the amount of drug taken up into bladder tissues was sufficient to reduce mRNA expression and promote tumour regression. The varied physicochemical interaction between the surface of carriers and the urothelial membrane is responsible for the different degree of tumor regression, sustained release, and duration of action observed. Their findings indicated that chitosan chain length used for surface modification of PLGA nanoparticles influenced the carrier's drug loading, release and cellular uptake behaviour.

Poly-ε-caprolactone (PCL) nanoparticles have been explored for intravesical drug delivery because of their biocompatibility, hydrophobicity (to support passive drug uptake) and cost-effectiveness [102]. Erdogar's group investigated the physicochemical and *in vitro* drug

release properties of chitosan (CHI-PCL) and poly-L-lysine (PLL-PCL) coated poly-Ɛ-caprolactone nanoparticles in comparison with uncoated chitosan nanoparticles [60]. The three types of nanoparticles had a mean diameter less than 400 nm before and after coating with chitosan or poly-L-lysine and a zeta potential of 10-35 mV. The extent of mitomycin-C release in pH 6.0 phosphate buffer release medium over 6 h for chitosan nanoparticles, PLL-coated and chitosan-coated poly-Ɛ-caprolactone nanoparticles was 89%, 92% and 91% after 15 min, respectively, suggesting that all the nanoparticulate formulations exhibited similar burst drug release profiles. The drug release pattern of the cationic nanoparticles at 6 h time point was not evaluated as the drug was prone to degradation after 6h, moreover, there is little additional information that may be obtained at that time point. The bladder retention of mitomycin-C loaded chitosan, chitosan and poly-L-lysine coated poly-Ɛ-caprolactone nanoparticles as well as a commercial product containing mitomycin-C was investigated in rats by instilling formulations (500 µL) and urine samples were collected 2, 4 and 6 h post instillation of the drug formulations, centrifuged and drug eliminated into urine quantified using HPLC. All the cationic nanoparticulate mitomycin-C formulations were retained in the bladder for longer period of time relative to the commercial dosage form, with the chitosan coated poly-Ɛ-caprolactone nanoparticles exhibiting the longest residence time in the bladder followed by chitosan nanoparticles while the poly-L-lysine coated nanoparticles were the least retained in the bladder. The amount of drug excreted into the urine after 6 h: 29.8 µg (CHI-PCL nanoparticles) versus 41.5 µg (chitosan nanoparticles) versus 42.3 µg (PLL-PCL nanoparticles). The antitumour properties of the drug carriers were evaluated in a later study in tumour-induced rat model, with the largest number of rats alive in the groups treated with drug loaded chitosan coated poly-Ɛ-caprolactone nanoparticles relative to that of chitosan nanoparticles and poly-L-lysine-coated poly-Ɛ-caprolactone nanoparticles, inferring that the bladder retention of the cationic nanoparticles facilitated their antitumour efficacy. In addition, there was no systemic uptake of all the studied mitomycin-C solution and nanoparticulate formulations based on HPLC analysis of the blood samples collected from rats after they had received intravesical instillation of drug formulations [63], inferring that mitomycin-C based dosage forms may pose minimal side effects.

1.5.2.2.2.   Thiolated particulate systems

Some hydrophilic polymers such as chitosan are intrinsically mucoadhesive due to its cationic amino-groups which promotes interaction with mucin [103–105]. Nevertheless, functional groups such as thiols [106,107], acrylates [108,109], maleimide [110] and catechols [111] have been explored to chemically modify polymers in order to improve their mucoadhesion.

Irmukhametova et al. reported the synthesis of thiolated nanoparticles using self-condensation of 3-mercaptopropyltrimethoxysilane [112], which were subsequently used by Mun et al. to study retention on porcine bladder surface [113]. Thiol-ene click chemistry involving interactions between pentaerythritol tetraacrylate and tetrakis (3-mercapto-propionate) were employed by Štorha and co-workers to produce thiolated nanoparticles [114] that were shown to be adhesive to porcine bladder mucosa. However, these nanoparticles [112,114] have not been explored for formulation of anticancer agents for intravesical bladder cancer therapy.

Zhang and co-workers generated thiol-functionalised cyclodextrin based mesoporous silica nanoparticles (NPs) for potential bladder cancer treatment and reported that they possess superior mucoadhesion compared to hydroxyl and amino-functionalised nanoparticles during mucin-nanoparticles interaction studies [64]. *In vitro* MTT cytotoxic testing on UMUC3 bladder cancer cells showed that the IC_{50} for doxorubicin loaded thiolated nanoparticles and free doxorubicin were 3.92 ± 1.06 µg mL^{-1} and 0.45 ± 0.05 µg mL^{-1}, respectively [64]. The gradual release of doxorubicin from the nanoparticulate formulation into the endosomes/lysosomes of the BC cells may be responsible for the IC_{50} of about 3.92 ± 1.06 µg mL^{-1} reported for doxorubicin loaded thiol-functionalised cyclodextrin based mesoporous silica nanoparticles (Dox-MSNPs-CD-NH$_2$-SH). However, IC_{50} values for doxorubicin loaded hydroxyl-functionalised cyclodextrin based mesoporous silica nanoparticles, [Dox-MSNPs-CD-(OH)] and doxorubicin loaded amine-functionalised cyclodextrin based mesoporous silica nanoparticles [Dox-MSNPs-CD-(NH$_2$)] also evaluated in the study, were not provided. Thus there were no means of establishing the cytotoxic superiority of doxorubicin loaded thiolated drug carriers over amino- and hydroxylated nanoparticles. *In vitro* drug release studies revealed that doxorubicin was released faster (63%) from thiolated nanoparticles deposited onto porcine bladder tissues incubated in simulated urine conditions (pH 6.1) than PBS based release medium (pH 7.4), with drug release of 13% after 48 h due to the relatively acidic pH of the simulated urine (pH 6.1) favourable for the protonation of the unreacted amino groups of the β-cyclodextrin – (NH$_2$)$_7$ on the nanoparticles to ammonium groups; coulombic repulsion between the positively charged amine-derivatised β-cyclodextrin rings around the mesopores of the nanoparticles, which cause them to open up and release the encapsulated doxorubicin [64]. This finding was valuable as the drug carrier will facilitate drug release within the physiological environment of the bladder.

Cook et al. co-polymerised a thiol-bearing monomer, 2-(acetylthio) ethylacrylate with 2-hydroxyethylmethacrylate using ethylene glycol dimethacrylate as a cross-linker (Fig. 1.5) to generate 635-977 nm thiolated microgels [65]. These microgels were found to exhibit high doxorubicin encapsulation efficiency (75-86%), good colloidal stability, excellent bladder mucoadhesion as well as sustained drug release over 300 min. Doxorubicin was released from the insoluble matrix through Fickian diffusion established from the Higuchi drug release model.
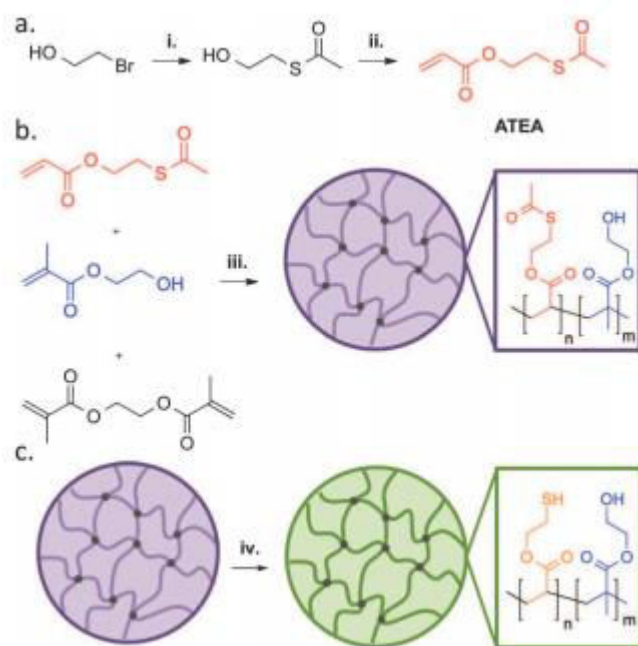
Fig. 1.5. Synthesis of thiolated microgels: (a) Synthetic route to ATEA, a protected thiomonomer. (b) Polymerisation to form ATEA: HEMA copolymer microgels, displaying the pendant functionalities present. (c) Deprotection of ATEA using sodium thiomethoxide to yield thiol-bearing microgels. (i) Potassium thioacetate, acetone, 24 h. (ii) Acryloyl chloride, trimethylamine, DCM, reflux, 24 h. (iii) Ammonium persulfate, ethylene glycol dimethacrylate, water, 70°C, 6 h. (iv) Sodium thiomethoxide, methanol, 30 min. This figure is reproduced from [65]. Reproduced with permission from the Royal Society of Chemistry.

Furthermore, the retention of doxorubicin loaded microgels on the bladder tissues was modulated by variation of the molar proportions of both monomers (ATEA & HEMA) to

generate microgels with desirable thiol content. For example, microgels with the greatest and least degree of thiolation were achieved by 80 mol% and 30 mol% ATEA, respectively [65]. The former resisted wash off by artificial urine during *ex vivo* porcine bladder mucoadhesion studies compared with the latter. This may be associated with the greater amount of thiol groups forming covalent disulphide bridges with the cysteine-rich regions of urothelial mucins as mucosal adherence was independent of surface charge or polarity of carrier. The 30 mol% and 80 mol% ATEA/HEMA based microgels had capacity for loading up to 2.5 mg mL^{-1} and 2.7 mg mL^{-1} doxorubicin, respectively [65], which was greater than the therapeutic doses of doxorubicin (1-2 mg mL^{-1}; 25-100 mL solution) [115,116]. However, future *in vivo* studies are desirable to facilitate further development of these drug carriers.

Cationic amine-functionalised polyacrylamide based nanogels were investigated for intravesical delivery of docetaxel [66] due to their safety, mucoadhesive properties and sustained release potential. They were prepared as a lyophilised solid readily dispersible in water or phosphate buffered saline. These materials had high drug loading (> 90%) with an initial burst release within 9 h and a sustained release over 9 days when formulations were put in a dialysis membrane and drug release evaluated in artificial urine over predetermined time intervals [66]. Docetaxel loaded functionalised carrier displayed superior inhibition towards UMUC3 cells relative to T24 cells, with IC$_{50}$ of 5.6 ng/mL vs 535.6 ng/mL over 4 h and the difference became more pronounced with an exposure time of 72 h, with a calculated IC$_{50}$ of 1.6 ng/mL and 11.6 ng/mL, respectively. Also, the cellular uptake of fluorescently labelled DTX-Pam-NH$_2$ nanogels into UMUC3 cells at 37°C was more pronounced than into T24 cells in a concentration dependent manner. This finding was also confirmed in *ex vivo* studies using porcine bladder tissues, where persistent green fluorescence on bladder tissues suggested the adhesion of the fluorescent carrier onto bladder urothelium. The treatment of intact bladder urothelium with the novel formulation also confirmed its safety when analysed using scanning electron microscopy as it induced only mild disruption of the urothelial tissues [66]. However, the preparation of nanogels was time-consuming as the preparation took about a week. Also, the amine functionalised surface may not have superior mucoadhesive features because its mode of interaction with the bladder mucosa would be via electrostatic attraction rather than covalent bonding which is stronger [106].

Recently, Mun et al. developed a new method for evaluating the retention of thiolated and PEGylated silica nanoparticles on porcine bladder epithelium during *ex vivo* studies as drug containing or blank formulations are being washed off using artificial urine [113]. The

parameter "Wash Out$_{50}$" represented the volume of biological fluid (such as artificial urine) required to detach 50% of the adhered particulate carrier from mucosal tissues. The *in vitro* studies also identified chitosan with superior WO$_{50}$ value and mucoadhesive property relative to thiolated nanoparticles and dextran (89 mL vs 36 mL vs 7 mL). The mucoadhesiveness of thiolated silica nanoparticles was decreased with surface decoration with poly(ethylene glycol) (PEG) and porcine bladder mucoadhesion reduced with increase in PEG molecular weight (5000 vs 750 Da) resulting in WO$_{50}$ of 8 mL and 29 mL, respectively [113].

Nanogels are nanoparticles composed of a hydrogel network. Guo et al. studied 10-hydroxycamptothecin loaded cationic cross-linked polypeptide (poly (L-lysine)-poly (L-phenylalanine-co-L-cysteine) nanogels (HCPT/NG) for intravesical delivery [117]. The poly (L-lysine) segment of the peptide is positively charged and interacts favourably with negatively-charged bladder mucosa while the poly (L-phenylalanine-co-L-cysteine) mimics cell penetrating peptides by promoting drug uptake into bladder cancer cells [117]. The drug carrier had a particle size in a nano-range (≈ 65 nm); was positively charged (16.3 ± 1.4 mV) as well as displayed good drug loading capacity and efficiency of 30.6 and 88.2% (w/w), respectively. Based on confocal laser scanning microscopic and microplate reading method of analysis, the novel drug carrier, HCPT/NG was taken up into bladder cancer cells via endocytosis and drug was efficiently delivered into T24 cell nuclei within 6 h, while the free drug formulation remained in the cytoplasmic region [76]. During *in vitro* studies, T24 bladder cancer cells were treated with free drug, HCPT and drug loaded nanogel formulation, HCPT/NG for 24 h and the cytotoxic effect of the formulations was investigated using MTT assay. The drug loaded nanogels showed greater cytotoxic effect than the free drug (IC$_{50}$ values of 2.7 mg/L vs 7.9 mg/L) [76].

With the *in vivo* studies using orthotopic bladder cancer model, the drug loaded novel formulation, HCPT/NG demonstrated remarkably improved antitumour activity using flow cytometric cell analysis, with cell death occurring predominantly in the nanogel treated regions relative to that treated with free drug. In addition, the drug loaded nanogel exhibited superior tumour necrotic region (46.3 ± 2.2%) relative to the cells exposed to free drug, up to 3.8-fold increase. The *in vivo* biodistribution of the drug carriers was studied: six hours post treatment with drug loaded nanogel or free drug solution, the mice were sacrificed and their bladder and other major organs were excised, homogenised and evaluated by HPLC. The drug loaded nanogel, HCPT/NG was preferentially retained in the bladder and rarely in other organs, displaying 3.2-fold greater drug concentration in the bladder than that of the free

drug-treated mice. This finding also correlates with the improved safety of the drug carrier due to targeted drug delivery, further confirmed by the insignificant changes in body weight of the mice throughout the studies [76]. This drug carrier appears promising for the treatment of superficial bladder cancer. However, *in vitro* drug release and *in vivo* mucoadhesive profile of the free drug HCPT or drug loaded nanogel, HCPT/NG were evaluated using phosphate buffered saline. It will be more physiologically relevant if artificial urine was used.

1.5.2.3. Composite system of nanoparticles and hydrogels

Composite systems of nanoparticles and hydrogels were explored to combine the benefits of both formulations including improved drug loading, release, mucoadhesion and urothelial uptake. Hydrogels are three-dimensional hydrophilic or amphiphilic polymer networks, prepared by physical or chemical crosslinking of polymers. These materials exhibit excellent ability to retain water or biological fluids [118,119]. They are soft, flexible and biocompatible; this makes them readily fabricated as building blocks for soft tissues [120–122]. The physically cross-linked hydrogels are more readily eliminated after drug release and uptake into the urothelial tissues, than hydrogels prepared using covalently bonded polymers. However, a balance is required between prolonged duration of action and biodegradability so that covalently linked hydrogels do not cause any harm to the body.

In situ gelling systems are liquid formulations with flowing tendency at room temperature and forms gels at physiological environment in response to various stimuli such as pH, enzymes or temperature. In recent years, temperature has become the commonly explored stimuli for such formulations where sol-gel transition takes place at 37°C (within the body) because temperature is the easiest stimulus to manipulate in order to generate environmentally responsive hydrogels [123–125]. It is desirable that dosage forms intended for mucosal delivery (including the intravesical route) have gelation temperature within the range of 30°C to 36°C [126]. Over the last decade, biomedical researchers have explored these systems for drug/biomolecule delivery [127–129] and tissue engineering [130] because they are readily manufactured, exclude use of organic solvents, administered in a minimally invasive mode, and provide sustained release [131]. In addition, their liquid consistency also allows their easy mixing with therapeutic agents before administration to a patient [132]. Thus, they have been employed for intravesical drug delivery, serving as drug reservoir, from where drug is released steadily over extended period of time.

1.5.2.3.1.   Floating composite systems of NPs and hydrogels

Adriamycin, an anthracycline antibiotic, is useful for reducing bladder cancer recurrence [133] when administered intravesically after transurethral resection of the bladder tumour but its application was limited because it causes irritation and scarring of the bladder; additional problem with this drug is its rapid release [134]. Floating strategies were used for oral formulations to improve residence time of drugs in the gastrointestinal tract [135–137]. Thus composite nanoparticle-hydrogel delivery system, with *in situ* gelling and floating potential within the bladder, was designed to serve as a drug depot to release adriamycin gradually and prevent urinary obstruction associated with the high viscosity of conventional non-floatable mucoadhesive poloxamer based hydrogels [69]. The safety of adriamycin has also been improved by formulating it as human serum albumin based nanoparticles (103 nm) that are loaded into Poloxamer 407 (P407) and hydroxypropyl methyl cellulose (HPMC) based thermosensitive gel [69]. The P407 facilitated gelation through micellar packing and entanglements [138,139] while HPMC enabled attachment of the nanoparticles to the bladder wall and prolonged erosion of the gel which ensured sustained drug release. One of the components of this formulation (sodium hydrogen carbonate) enables the drug carrier to float in urine environment. It produces carbon dioxide microbubbles in acidic medium which enables the hydrogel system to float, thereby preventing urinary obstruction [69]. Nanoparticles with adriamycin formulated using P407 and HPMC were reported to undergo sol-gel transition within the shortest time possible, achieving gelation temperature of 10°C and gelation time of 2 min when evaluated at 37°C, in comparison with other evaluated carriers (nanoparticles-adriamycin or non-floating hydrogel), with gelation temperature of 12 to 18°C and gelation time of 2-5 min at 37°C. Nevertheless, all these formulations may be refridgerated to improve syringeability during intravesical drug administration as they will form gel at room temperature.

The amount of drug released into the urine of rats as well as the amount retained in their bladder following intravesical administration of a suspension of adriamycin nanoparticles and adriamycin loaded composite nanoparticles-hydrogel system facilitated a controlled drug release with 81.87% drug released over 10 h compared to the adriamycin nanoparticles, with loaded drug released instantly [69]. The *in vitro* and *in vivo* drug release studies did not correlate well due to the disparity in the volume of the evaluation medium as well as hydrogel volume used. This is because the *in vivo* studies had to use hydrogel volume of 0.1 mL that can be accommodated in rat's bladder (volume of ≤ 1 mL), while the *in vitro* studies used 400 mL release medium and hydrogel volume of 12 mL applicable to humans. However, to achieve this

excellent retentive effect, urine needed to be acidified for the formulation to float. This may be less acceptable due to potential irritation of the bladder caused by low pH [69]. Thus floating *in situ* gelling drug carrier with sustained release profile at pH 6-7 (intrinsic pH of the bladder environment) would be worth investigating in the future.

1.5.2.3.2. Non-floating, mucoadhesive composite systems of polymeric nanoparticles and hydrogels

Some authors investigated delivery systems that form non-floatable gels *in situ* but made of materials that do not potentially obstruct urine elimination as they are flexible and steadily dissolve in urine over time, though mucoadhesive for sufficient length of time to allow for drug uptake into urothelial membranes.

Chitosan formulated with β-glycerophosphate disodium salt is an example of physically cross-linked temperature-responsive gelling system (Fig. 1.6) that has been evaluated by some researchers [44,140–142]. They suggested molecular mechanism for the gelation process in terms of increased electrostatic repulsion between chitosan macromolecules as well as interactions between positively charged chitosan molecules and negatively charged β-glycerophosphate which stabilises the resultant hydrogel system below physiological temperature as well as increased chitosan intermolecular hydrophobic interactions prevalent around 37°C expelling water molecules and generating less hydrated gel network [143,144]. It was suggested by Supper and co-workers [131] that these molecular interactions have not explained the influence of temperature on the gelation process while some authors [145,146] have established the role of polyol moiety of gelling material in the thermo-sensitivity of chitosan- β-glycerophosphate *in situ* gelling systems.
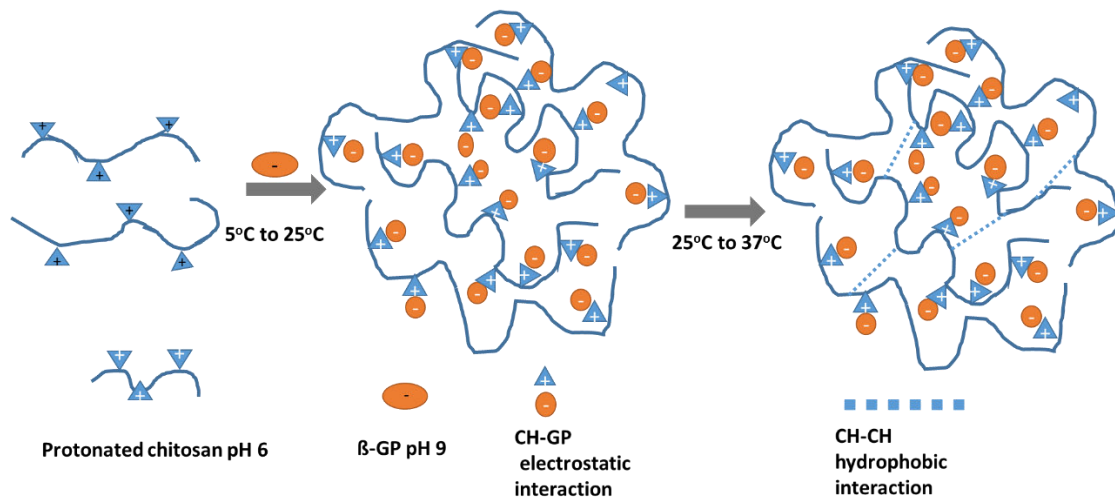
Fig. 1.6. Schematic diagram showing *in situ* gelation process of chitosan/ß-glycerophosphate mixture at 37°C, with the electrostatic interaction between the amine groups of chitosan and phosphate groups of β-glycerophosphate ensuring that drug carrier remain liquid below 25°C; with increased temperature at 37°C, chitosan intermolecular hydrophobic interactions become more pronounced as hydrating water molecules around chitosan macromolecules are expelled, generating less hydrated gel network.

Therapeutic agents have been delivered locally and systemically using thermoresponsive chitosan- β-glycerophosphate (CHIGP) *in situ* gelling system [44,141,142,147,148]. Common features for all these studies is that the release of the loaded drugs such as ellagic acid [44], insulin [141], meglumine antimoniate [147], venlafaxine hydrochloride [148] and cisplatin [142] was sustained over the release study period. In addition, their gelation time and temperature was dependent on the concentration and volume ratio of chitosan and β-glycerophosphate. Despite the promising efficacy and drug release properties of CHIGP *in situ* gelling systems, they have not been explored for intravesical drug delivery.

Magnetic delivery system was studied for the adjuvant treatment of superficial bladder cancer. Bacillus Calmette Guérin (BCG) powder and magnetite nanoparticles were incorporated into CHIGP solution. The nanoparticulate component targeted the carrier to bladder tissues under the influence of magnetic field. The resultant Fe_3O_4-BCG-CHIGP system formed gel *in situ* and resisted urine wash-off [68]. BCG loaded magnetic gel dosage form stimulated greater Th1 immune reaction with increased expression of interleukin-2 (IL-2, 149.3 ± 8.06 pg/mL) and interferon γ (IFN-γ, 373.47 ± 40.53 pg/mL) in the urine and superior antitumour activity (tumour volume of 0.53 ± 0.27 mm^3) compared to conventional BCG solution with "IL-2" of 98.84 ± 7.03 pg/mL; IFN-γ of 220.28 ± 54.19 pg/mL and tumour volume

of 1.82 ± 0.48 mm^3. The duration of BCG residence within the bladder tissues was also extended beyond one month, evident by the CD4+ lymphocyte levels detected in submucosal regions: 3913 ± 467 lymphocytes were recorded for magnetic BCG nanoparticle-hydrogel carrier compared to 2578 ± 269 lymphocytes when BCG solution was used.

Chitosan has an intrinsic mucoadhesive property and may be responsible for improved antitumour immune reaction exhibited by the magnetic carrier in the bladder [68]. In addition, tight junctions of the urothelial membrane are loosened up due to their interaction with chitosan, thereby increasing and sustaining local drug concentration [149]. *In vitro* release studies were not carried out by Zhang's group [68] due to the lack of reliable techniques used for detection and quantification of BCG. Moreover, the BCG radiolabelling technique explored by Shen et al. was not helpful [150]. So, initial burst release profile was suggested based on persistent cytokine expression in rat urine up to 48 h during *in vivo* studies. The burst release profile of BCG may result in adverse reactions such as induction of immune reactions. So, further studies should be carried out to ascertain if the delivery system is appropriate for BCG. Moreover, alternative method of BCG quantification may be helpful for dosage determination.

Deguelin has been employed for chemotherapy of lung, breast and colon cancer due to its antiangiogenic potential [151–153]. However, its clinical use is limited because of its hydrophobicity as well as potential toxic effects on the heart, lungs and nerves associated with high drug dose [151]. N-[1-(2, 3-Dioleoyloxy) propyl]- N, N, N-trimethylammonium chloride (DOTAP) has cationic hydrophilic head and hydrophobic chain and nanoparticles formulated using this amphiphilic material are able to solubilise lipophilic drugs and enhance urothelial uptake so that the dose required for therapy is reduced, minimising toxic effects. This justifies their acceptance by FDA for the gene-based treatment of lung cancer [154–156].

Men et al. reported the improved deguelin's aqueous solubility and residence time in the bladder using the formulations composed of amphiphilic N-[1-(2,3-dioleoyloxy)propyl]-N, N, N-trimethylammonium chloride (DOTAP) surface modified monomethoxyl poly (ethylene glycol)-poly (ℇ-caprolactone) (MPEG-PCL) based nanoparticles and thermosensitive *in situ* gelling Pluronic F127, and biological properties compared with that of unmodified MPEG-PCL nanoparticles [67]. Pluronic F127 hydrogel improved urothelial uptake and tissue absorption of deguelin while cationic DOTAP-modified MPEG-PCL nanoparticulate component facilitated sustained drug release [157]. Deguelin loaded nanoparticles had encapsulation efficiency of 98.2% but rate of loading drug into these nanoparticles was low (4.9%). *In vitro* drug release studies were performed using dialysis membrane maintained in a water-bath containing PBS

(pH 7.4) and 0.5% w/w Tween 80. This formulation formed gel readily at 25°C *in vitro* and fluorescent gel was observed in mice within 10 min of intravesical administration which sustained for 2 h [67]. *In vitro* cellular uptake studies using DOTAP modified *in situ* gelling formulation and unmodified nanoparticles loaded with fluorescent coumarin-6 (with similar hydrophobic nature to deguelin) showed that the DOTAP modified nanoparticles were more readily taken up by T24 bladder cancer cells than the unmodified nanoparticles. *In vivo* studies using mice confirmed cellular uptake of fluorescent model drug loaded formulation based on fluorescence observed within sections of bladder tissues. MTT assay also confirmed that the deguelin loaded DOTAP modified nanoparticle-hydrogel system exhibited cytotoxic effect on T24 bladder cancer cells at a lower IC$_{50}$ values than that of the unmodified nanoparticles and free drug. The tolerability of deguelin was improved with the intravesical administration of the novel drug loaded formulation because similar drug amount (2 mg kg^{-1}) given intravenously to mice, killed them. Thus the novel deguelin based dosage form may be safer, effective without causing urethral blockage due to its gradual elimination from the bladder [67]. However, the anti-angiogenic properties of the novel drug carrier was not carried out, though that of the free drug was investigated with transgenic zebrafish model using fluorescence microscopy, with the intersegmental embryo vessels developing abnormally or did not grow relative to control embryo. It will be valuable to undertake this study to ascertain the superior antitumour efficacy of the new intravesical delivery system relative to the free drug.

Şenyiğit et al. have employed chitosan-thioglycolic acid conjugate to prepare nanoparticles and incorporated them into 2% chitosan gel or *in situ* gel forming poloxamer (mixture of 20% poloxamer 407 and 10% poloxamer 188) for improved intravesical delivery of gemcitabine hydrochloride [50]. Gemcitabine-HCl loaded thiolated chitosan nanoparticles had greater drug loading than deguelin loaded DOTAP-modified MPEG-PCL nanoparticles evaluated by Men et al. [67] (9.4% vs 4.9%) but the latter had greater encapsulation efficiency than the former (98.2% vs 19.2%). This finding may be associated with the differences in the physicochemical properties of the formulation. Composite system of chitosan gel and chitosan-thioglycolic acid conjugate based nanoparticles was more resistant to dilution by artificial urine (Tyrode solution) than composite system of *in situ* gel forming poloxamer gel and chitosan-thioglycolic acid conjugate based nanoparticles at 37°C based on rheological frequency sweep data (Storage modulus 15Pa vs 6 Pa). *In vitro* drug release studies also suggested that the rate of drug release following dispersal of nanoparticles into chitosan gel and Poloxamer gel decreased by a magnitude of 1.5 and 2.6, respectively as well as release rate of 33.4 ± 5.0% vs 19.6 ± 1.6% in 4 h [50]. During bioadhesion test using bovine bladder mucosa, chitosan gel

based delivery system also had improved bioadhesive properties (in terms of its force of detachment from the bladder tissues) compared to Poloxamer gel based carrier (1.003 ± 0.048 N.mm vs 0.378 ± 0.022 N. mm).

The incorporation of the drug carriers with Tyrode solution resulted in a 51% and 80% reduction in bioadhesive properties, respectively [50]. Greater percentage of the drug permeated the bladder mucosa for the chitosan gel based carrier compared to Poloxamer gel (33.16 ± 5.11% vs 18.78 ± 1.97%) during *ex vivo* studies. Thus chitosan gel based drug carrier may be a potential intravesical delivery system for Gemtacibine hydrochloride in order to improve drug efficacy and residence time within the bladder. This investigation was intended to mimic the behaviour of the proposed formulation within the urine containing environment. However, the gelation time reported for poloxamer gel-Tyrode solution and poloxamer gel based drug carrier-Tyrode solution (457 ± 4 s vs 483 ± 2 s) at 37°C was quite unexpectedly low for formulations with gelation temperature of 51.7 ± 1.0^{o}C and 53.7 ± 1.9^{o}C, respectively.

1.5.2.4. Liposomal systems

Liposomes comprise of synthetic or natural phospholipids which assemble to form bilayers surrounding an aqueous core. They can encapsulate both hydrophilic and hydrophobic drugs as well as DNA plasmids, and are taken up into the cells through endocytosis [158,159].

Liposomes were not usually explored for intravesical drug delivery because of their instability in human urine. Recently, Nakamura's group modified cationic liposomal surfaces with cholesteryl-PEG to overcome their urine aggregation and promote uptake into urothelial tissues [160]. N- (carbonyl-methoxypolyethyleneglycol 200)-1,2-distearoyl-sn-glycero-3-phosphoethanolamine-PEG-based formulations were the most resistant to aggregation in the presence of human urine relative to 1,2-distearoyl-sn-glycerol, methoxyPEG 2000 and cholesterol-PEG. This finding was due to the superior flexible conformation of N-(carbonyl-methoxypolyethylene glycol 200)-1, 2-distearoyl-sn-glycero-3-phosphoethanolamine-PEG (DSPE-PEG) in comparison to 1, 2-distearoyl-sn-glycerol, methoxyPEG 2000 (DSG-PEG) and cholesterol-PEG. Also, the rich density of negative charge on DSPE-PEG shields the cationic liposomes thereby enhancing stability in the urine.

Additionally, fluorescently labelled liposomal suspension in human urine was incorporated into MB49 cells and these cells were evaluated by flow cytometry. The surface functionalisation of the cationic liposomes with PEG ensures that the drug carrier is taken up into MB49 murine cells uniformly. Surprisingly, 2 or 5 mol% Chol-PEG functionalised cationic liposomes were taken up into the cells more efficiently compared to unmodified and other PEG modified liposomes. This result was in contrast to their stability behaviour in human urine as more rigid conformation of cholesterol-PEG based carrier supported their uptake into MB49 cells [160]. Thus lipid based carriers incorporating both DSPE and cholesterol-PEG may be formulated for improved stability in human urine as well as cellular uptake into cancerous urothelial tissues.

GuhaSarkar et al. explored paclitaxel loaded composite liposomes in gellan hydrogel (PTX-LP-Gel) for intravesical delivery [70]. Paclitaxel was encapsulated efficiently into the drug carrier (91.2 ±0.7%) because of the affinity of the hydrophobic drug towards lipid bilayers. Apart from being mucoadhesive, gellan is a temperature and ion-responsive polysaccharide, so it becomes physically cross-linked in the presence of urine, resulting in prolonged retention of the drug carrier onto the urothelial surface. Gellan (0.1%) was identified as the optimum concentration for syringeability through the catheter. The liposomal component (124 nm, PDI 0.22, surface charge -16.8 mV) enhances urothelial cell permeation as a result of merging with the lipid content of the cell membranes. Based on cryo-TEM results, the size of the drug loaded liposome was increased with paclitaxel encapsulation to ~200 nm. The novel drug carrier, PTX-LP-Gel exhibited a sustained drug release profile over 50 h (17.8 ±3.0% of loaded drug) due to the smart matrix of the hydrogel; though porous structure facilitates controlled drug and/or liposome diffusion out of the hydrogel. Cellular uptake studies using confocal laser scanning microscopy confirmed superior NBT-II and T24 cell internalisation of loaded rhodamine-6G, relative to the control cell group. Also, cytotoxic testing of the novel drug carrier using NBT-II and T24 cell lines suggested that they retained their cytotoxic effect with IC_{50} values of 55.7 ± 13.0 nM and 1.9 ± 0.5 μM, respectively. The composite system of liposomes and gellan hydrogels was not detected in non-target organs during *in vivo* retention studies and the amount detected in the rat bladder 7 days post instillation was remarkably greater than that of the commercial product, Taxol (1.71 ± 0.86 μg/g vs 0.02 ± 0.01 μg/g).

The safety of the novel drug carrier, LP-Gel was confirmed based on scanning electron and atomic force microscopic images depicting intact urothelium, with residence of the gel formulation for up to 24 h. This work revealed that the limited mucoadhesiveness associated

with conventional liposomes can be overcome by incorporation of liposomes within gellan gel. Moreover, toxic effect of cross-linkers (such as glutaraldehyde and 1-ethyl-3-(3-dimethylaminopropyl) carbodiimide hydrochloride) used with mucoadhesive polymers, to improve mucoadhesiveness of liposomes, will be avoided [70]. Overall, this work generated safe, injectable, mucoadhesive, ion-triggered *in situ* gelling carrier, resistant to pH changes in the bladder with a sustained release profile.

Recently, our group reported that maleimide-terminated PEGylated liposomes (PEG-Mal), with diameter 86±1 nm and PDI of 0.22 exhibited superior urothelial mucoadhesiveness relative to PEGylated liposomes and conventional liposomes (WO_{50} values 48 mL vs 24 mL vs 15 mL) due to its stronger interaction with the thiol content of membrane mucins via covalent linkages [71]. However, PEGylated liposomes displayed greater bladder mucosal epithelial penetration than PEG-Mal liposomes ($p < 0.05$), which may be due to the strong adhesive property of the latter slightly retarding their mucosal penetration [71]. *In vitro* model drug release studies also showed that PEG-Mal liposomes facilitated controlled release of the model drug (fluorescein sodium) with 95-100% released after 8 h relative to same amount of the model drug released in 4 h with the PEGylated liposomes [71]. This study indicated the influence of PEG and maleimide functionalisation on the urothelial mucosal adhesion and penetration as well as drug release pattern. However, the use of fluorescein sodium to mimic drugs may be less reliable. Thus, future studies will explore loading bladder cancer chemotherapeutic agents in order to ascertain that similar biological properties were exhibited by the liposomal formulations.

1.6.   *In vitro – in vivo* models to study intravesical drug delivery

Various *in vitro* and *in vivo* models have been used to study drug delivery systems intended for intravesical administration. Different types of bladder cancer cells have been employed for cell viability studies. Murine sources include MBT-2 [59], MB49 [160], and NBT-II [70], while T-24, RT-4, UM-UC-3, 5637 and HT-1376 are human cell lines [53,62,64,66,67,70,76]. They differ in terms of their invasive and metastatic tendencies. SV-HUC-1 are non-malignant human bladder cell lines studied to evaluate the biocompatibility of drug carriers [62]. These cells are often maintained in appropriate medium containing 5% carbon dioxide at 37°C for optimal growth [53,59,61,62,64,66,67].

During *in vitro* studies, cell viability in the presence of potential drug carriers have been evaluated using different methods such as lactate dehydrogenase assay [59],

bromodeoxyuridine, XTT assay [62], MTT assay [64,66,67,76], WST-1 assay [61] and sulphorhodamine-B colorimetry [70]. During LDH assay, the damage of the intravesical carriers to cell membrane was measured in terms of specific enzymes or antibodies release into the cytosol when carriers were mixed with malignant cells. Bromodeoxyuridine assay relies on the incorporation of bromodeoxyuridine (synthetic nucleoside and analog of thymidine) into newly synthesised DNA of replicating cells which substitutes thymidine and denature cells. This process is detectable by expression of antibodies after the cells have been exposed to acid or heat [161]. With MTT assay, some reducing enzymes that are present in the mitochondria of viable cells reduce the MTT reagent (tetrazolium salt) resulting in a coloured formazan product which is solubilised in an appropriate solvent such as dimethyl sulfoxide and the absorbance of the formazan solution is read using spectrophotometric method, which correlates with the number of metabolically active cells in the culture. The XTT and WST-1 assay operates under similar principle as MTT assay except that the resultant formazan product is water soluble, thus does not require to be solubilised prior to spectrophotometric analysis [162]. Another technique, sulphorhodamine-B colorimetry requires that sulphorhodamine binds to the protein constituents of the cells in a stoichiometric manner so that the amount of dye extracted from the stained cells is directly proportional to the cell mass [163]. Some researchers did not carry out *in vitro* cell viability or cytotoxicity testing of their formulations [50,65,69]. However, *in vitro* drug release [50,65] and floating tendency [69] of their formulations in the presence of artificial urine were evaluated.

There are detailed protocols available for the preparation of artificial urine for *in vitro* cell based studies, which is representative of the components of the human urine but they are varied in composition and concentration of their constituents, which imparts on their pH (6.2-7.8), specific gravity (1.008-1.02 g/mL) and osmolality value (430-861 mOsm/kg) [164–170]. Examples of constituents include urea, uric acid, creatinine, trisodium citrate, sodium chloride, potassium chloride, ammonium chloride, calcium chloride dihydrate, magnesium sulphate heptahydrate, sodium bicarbonate, disodium oxalate, sodium sulphate, sodium dihydrogen phosphate and disodium hydrogen phosphate [164–170]. The artificial urine with pH, specific gravity and osmolality of 6.2, 1.01 g/mL and 446 mOsm/kg, respectively, was appropriate for various biomedical applications [170].

Martin et al. evaluated the uptake of fluorescent carriers suspended in artificial urine instilled into healthy human ureter using *ex vivo* binding assay [61]. The *in vitro* cytotoxicity of free drug, blank nanoparticles, drug loaded modified and unmodified PLGA nanoparticles, on T-24

cells (metastatic, invasive high grade BC), RT-4 cells and UM-UC-3 cells (papillary, well differentiated, non-invasive) were studied using WST-1 assay and IC_{50} values determined [61]. These values may help to establish the dose of formulation that would be toxic to urothelial cells.

During *in vivo* studies, mice were induced with human bladder cancer (orthotopic model) by transurethral implantation [59] or subcutaneous injection [53,61] of bladder cancer cells like UM-UC-3 cells as well as oral intake of water containing 0.05% (w/v) N-butyl-N-(4-hydroxybutyl)-nitrosamine for 20 weeks [76]. Predetermined concentration of carriers were instilled and the degree of tumour regression determined from the weight of the bladder tumour after sacrificing mice [53,59,61]. The actual drug taken up may be evaluated based on LC-MS/MS analysis of extracts from bladder tumour homogenate [59]. Other authors quantified *in vivo* retention of drug carriers in terms of observable fluorescence within the bladder using fluorescence microscopy [53,62,66] or acid-fast staining and/or HE staining [68]. Men et al. also used mice but did not test the antitumour efficacy of their formulations on orthotopic mice models [67]. They simply tested the drug uptake into bladder tissues from the delivery system using flow cytometry. Nevertheless, they evaluated the cytotoxic effects of free deguelin, drug nanoparticles and drug loaded hydrogel-nanoparticle composite formulations on T-24 cells using MTT assay while the anti-angiogenic potential of deguelin was assessed using transgenic zebrafish model [67].

Similar number of injections (six) were administered to mice and rats based malignant models but dose and dosing interval of the drug carriers differ probably due to the pharmacological profile of various chemotherapeutic agents used [59,61,68]. Therefore, it would be difficult to compare degree of tumour regression across studies. Moreover, some studies were less detailed in terms of the original volume of tumour [59]. Thus it is not easy to ascertain the degree of tumour regression by the final volume of tumour observed.

Wistar rats are typically used for *in vivo* studies, so Lin et al. used these rats to assess the urine wash-off resistance and sustained release profile of Poloxamer-based floating and non-floating carriers [69]. Zhang et al. [68] used similar rats to evaluate urothelial cellular uptake of chitosan/β-glycerophosphate/Fe_3O_4-magnetic hydrogel-nanoparticles system. The immunological response of rat bladder to the intravesical instillation of BCG-based carriers was quantified by urinary analysis of cytokines and tissue histochemical analysis of CD4+ T cells [68]. GuhaSarkar's group evaluated the *in vivo* retention of rhodamine and paclitaxel loaded liposomes and liposome-gel systems using healthy female and male rats [70]. However,

the antitumour effect of the drug loaded formulations was not investigated in rats, in addition to their retention in the bladder.

On the other hand, *in vivo* testing of formulations was not carried out in some studies reported [50,62,64–66]. However, *ex vivo* mucoadhesive studies of some formulations were conducted using porcine [64–66] or bovine [50] bladder tissues. They quantified the mucoadhesiveness of their drug carriers differently using confocal laser scanning microscope [64,66], fluorescence stereomicroscope [65] and TA-XT Plus texture analyser [50]. Recently, our group evaluated urothelial mucosal retention and penetration as well as drug release properties of liposomal dosage forms using fluorescein sodium as a model drug [71].

1.7. Clinical trials

TCGel®, a polymeric thermoresponsive hydrogel containing Pluronic F-127 (27%), PEG-400 (1.1%), HPMC (0.3%), and double distilled water (71.6%) was developed by Theracoat Ltd (Israel). It exhibited improved safety and residence within the bladder cavity between 6 and 8 h and was gradually eliminated during urine voiding, in comparison to simple mitomycin-C solution during preclinical evaluation [171]. Thus it was assessed for intravesical application by mixing TCGel® with 40 mg mitomycin-C (standard dose prior to surgery) and pharmacological effect compared with same amount of mitomycin-C mixed with water, in an ongoing trial for management of low risk recurrent NMIBC [172]. In the US, there is a clinical trial investigating mitomycin-C therapy in combination with radiofrequency induced hyperthermia for non-muscle invasive Carcinoma *in situ* bladder cancer therapy [173]. Another trial explores an improved method of delivering mitomycin-C for the treatment of low grade upper urinary urothelial carcinoma using MitoGel™ which is a thermosensitive sustained release poloxamer

based mitomycin-C formulation that may be used for chemoablation to preserve the bladder in low risk upper tract urothelial cancer, developed by UroGen Pharma Ltd (New York) [174].

1.8. Conclusions

The intravesical route is the most viable means of improving drug delivery for bladder cancer treatment, especially at the early stages of the disease, due to the limitations of delivery via the oral and systemic routes. However, intravesical drug delivery has a few disadvantages such as drug dilution by urine and drug wash-out during micturition, particularly when conventional formulations made of a simple solution of the chemotherapeutic agent are used. Moreover, the urothelium limits permeation of potentially useful therapeutic agents for bladder cancer treatment while carrying out its regulatory role. This results in frequent dosing or catheter retention within the urethral tract that leads to bladder irritation and infection.

Drug carriers reviewed are mostly of polymeric nature with potential to treat superficial bladder cancer and prevent disease progression to its metastatic and advanced forms. Moreover, the composite nanoparticulate and *in situ* gelling formulations are able to combine benefits of both delivery systems to generate dosage forms, with improved safety, efficacy and sustained release profile.

There are variations in the design of the *in vitro* and *in vivo* studies as well as evaluation of data generated from such studies. Some studies were not detailed enough to allow for comparison of cytotoxic or mucoadhesive profiles. Also, some authors did not carry out particular *in vitro* and *ex vivo* studies conducted by others, making it difficult to establish dosage regimen for such formulations.

The issue of formulation design (modulation of formulation properties to generate a uniform thin gel layer *in situ*, with adequate strength and sustained drug release) for higher capacity of human bladder, identified by GuhaSarkar et al. [14] still persist, as it is still difficult to upscale the dosage of drug carriers in animals, for human use. This has prevented promising formulations from being tested in human bladder during clinical trials. However, their findings have suggested that solubilisation of lipophilic drugs in amphiphilic systems; surface modification of particulate systems and incorporation of such particulate systems into *in situ* gelling formulations would generate advanced carriers with superior drug loading, safety, *in situ* gelling, mucoadhesive/floating and selective bladder cancer cell penetrating features that would improve the cytotoxic profile of the incorporated therapeutics. Drug carriers that would

explore combination of delivery strategies would be desirable in order to prevent bladder cancer recurrence and progression.

Promising safety and cytotoxicity data generated from some of the studies offer hope that single drug loaded carriers may be investigated instead of multiple drugs based delivery systems widely explored in ongoing clinical trials for bladder cancer treatment. The harmonisation of the acceptable and realistic protocols for *in vitro* and *in vivo* models for studying intravesical delivery systems may accelerate the translation of some of the formulations, currently being developed, into the clinic. Therapeutic outcomes of patients would also be improved with promising disease prognosis.

1.9. Aims and Objectives of the work

1.9.1. Aims of the work

The aims of this project were:

- To investigate the *in situ* gelling properties of chitosan/β-glycerophosphate delivery systems using three chitosan grades.
- To investigate the mucoadhesive properties of two types of chitosan derivatives in comparison with the parent chitosan.

My working hypothesis is that chitosan solution mixed with β-glycerophosphate solution in the appropriate concentration and volume ratio will generate a drug carrier that gel at physiological temperature (37°C) and could be retained in the bladder for extended period of time. The second hypothesis is that methacrylation or boronation of chitosan will improve its

mucoadhesiveness relative to unmodified chitosan, also beneficial for improved residence of drug carriers in the bladder.

1.9.2. Objectives of the work

The objectives of this project were:

- To develop three chitosan/β-glycerophosphate delivery systems using different chitosan grades (in terms of molecular weight), with chitosan solutions as control.
- To evaluate their syringeability (texture analyser), gelation (vial inversion/rheology), mucoadhesiveness (flow through technique/fluorescence microscopy and tensile test) and drug release profile (HPLC).
- To evaluate cytotoxicity and cellular uptake potential of drug loaded CHIGP systems.

- To synthesise two types of methacrylated chitosan as well as three types of boronated chitosan that differ in terms of their degree of chemical modification.
- To characterise them in terms of their modification with methacrylate or boronate groups using NMR, FT-IR and ninhydrin test.
- To evaluate pH influence on the solubility of polymer solutions/dispersions (UV-Vis spectroscopy), mucoadhesiveness (flow-through technique/ fluorescence microscopy and tensile test), and safety (MTT assay).
- To develop and characterise drug loaded methacrylated and boronated nanoparticles in terms of their particle size and zeta potential (DLS), drug loading/encapsulation efficiency (HPLC) and cytotoxic effect (MTT assay) and uptake into UMUC3 cells (flow cytometry).

References

1. Cheung G, Sahai A, Billia M, Dasgupta P, Khan MS. Recent advances in the diagnosis and treatment of bladder cancer. BMC Med. 2013;11(1):13.

2. Kaufman DS, Shipley WU, Feldman AS. Bladder cancer. Lancet. 2009;374(9685):239–49.

3. Torre LA, Bray F, Siegel RL, Ferlay J, Lortet-tieulent J, Jemal A. Global Cancer Statistics, 2012. CA Cancer J Clin. 2015;65(2):87–108.

4. Aziz A, Shariat SF, Roghmann F, Brookman-May S, Stief CG, Rink M, Chun FK, Fisch M, Novotny V, Froehner M, Wirth MP, Schnabel MJ, Fritsche HM, Burger M, Pycha A, Brisuda A, Babjuk M, Vallo S, Haferkamp A, Roigas J, Noldus J, Stredele R, Volkmer B, Bastian PJ, Xylinas E, May M. Prediction of cancer-specific survival after radical cystectomy in pT4a urothelial carcinoma of the bladder: Development of a tool for clinical decision-making. BJU Int. 2016;117(2):272–9.

5. Cancer Research UK. Cancer Registration Statistics, England: 2015 [Internet]. Statistical Bulletin. 2017 [cited 2016 Aug 10]. Available from:

https://www.ons.gov.uk/peoplepopulationandcommunity/healthandsocialcare/conditi
onsanddiseases/bulletins/cancerregistrationstatisticsengland/2014.

6.   Cancer Research UK. Bladder cancer mortality statistics: Projections of mortality for
        bladder cancer [Internet]. Cancer Statistics Newsletter. 2016. Available from:
        http://www.cancerresearchuk.org/health-professional/cancer-statistics/statistics-by-
        cancer-type/bladder-cancer/mortality#heading-Three.

7.   NICE. National Institute for Health and Care Excellence Costing report for Bladder
        Cancer: Implementing the NICE guideline on bladder cancer [Internet]. NICE guidelines.
        2015. Available from: https://www.nice.org.uk/guidance/ng2/resources/costing-
        report-pdf-3780397.

8.   Schinkel JK, Shao S, Zahm SH, McGlynn KA, Shriver CD, Zhu K. Overall and recurrence-
        free survival among black and white bladder cancer patients in an equal-access health
        system. Cancer Epidemiol. 2016;42:154–8.

9.   Sievert KD, Amend B, Nagele U, Schilling D, Bedke J, Horstmann M, Hennenlotter J,
        Kruck S, Stenzl A. Economic aspects of bladder cancer: What are the benefits and costs?
        World J Urol. 2009;27(3):295–300.

10.   Williams SK, Hoenig DM, Ghavamian R, Soloway M. Intravesical therapy for bladder
        cancer. Expert Opin Pharmacother. 2010;11(6):947–58.

11.   Barocas DA, Globe DR, Colayco DC, Onyenwenyi A, Bruno AS, Bramley TJ, Spear RJ.
        Surveillance and treatment of non-muscle-invasive bladder cancer in the USA. Adv Urol.
        2012;2012:19–24.

12.   Yeung C, Dinh T, Lee J. The Health Economics of Bladder Cancer: An Updated Review of
        the Published Literature. Pharmacoeconomics. 2014;32(11):1093–104.

13.   Elstad NL, Fowers KD. OncoGel (ReGel/paclitaxel)--clinical applications for a novel
        paclitaxel delivery system. Adv Drug Deliv Rev. 2009;61(10):785–94.

14.   GuhaSarkar S, Banerjee R. Intravesical drug delivery: Challenges, current status,
        opportunities and novel strategies. J Control Release. 2010;148(2):147–59.

15. van Rhijn BWG, Burger M, Lotan Y, Solsona E, Stief CG, Sylvester RJ, Witjes JA, Zlotta AR. Recurrence and progression of disease in non-muscle-invasive bladder cancer: from epidemiology to treatment strategy. Eur Urol. 2009;56(3):430–42.

16. Kaufman DS. Challenges in the treatment of bladder cancer. Ann Oncol. 2006;17(Supplement 5):v106-12.

17. Konety BR, Joyce GF, Wise M. Bladder and upper tract urothelial cancer. J Urol. 2007;177(5):1636–45.

18. Chen CH, Chan TM, Wu YJ, Chen JJ. Review: Application of nanoparticles in urothelial cancer of the urinary bladder. J Med Biol Eng. 2015;35(4):419–27.

19. Tomlinson B, Lin T, Dall'Era M, Pan C-X. Nanotechnology in bladder cancer: current state of development and clinical practice. Nanomedicine. 2015;10(7):1189–201.

20. Soler R, Bruschini H, Martins JR, Dreyfuss JL, Camara NO, Alves MT, Leite KR, Truzzi JC, Nader HB, Srougi M, Ortiz V. Urinary glycosaminoglycans as biomarker for urothelial injury: is it possible to discriminate damage from recovery? Urology. 2008;72(4):937–42.

21. Khandelwal P, Abraham SN, Apodaca G. Cell biology and physiology of the uroepithelium. Am J Physiol Renal Physiol. 2009;297(6):F1477-501.

22. Lewis SA. Everything you wanted to know about the bladder epithelium but were afraid to ask. Am J Physiol Renal Physiol. 2000;278(6):F867-74.

23. Gray M. Traces: Making sense of urodynamics testing - Part 9: Evaluation of detrusor response to bladder filling. Urol Nurs. 2012;32(1):21–8, 18.

24. Smith SD, Wheeler MA, Plescia J, Colberg JW, Weiss RM AD. Urine detection of survivin and diagnosis of bladder cancer. JAMA. 2001;285(3):324–8.

25. Swana HS, Grossman D, Anthony JN, Weiss RM AD. Tumor Content of the Antiapoptosis Molecule Survivin and Recurrence of Bladder Cancer. N Engl J Med. 1999;341(6):452–3.

26.   Cardillo MR, Castagna G, Memeo L, De Bernardinis E, Di Silverio F. Epidermal growth factor receptor, MUC-1 and MUC-2 in bladder cancer. J Exp Clin Cancer Res. 2000;19(2):225–33.

27.   Wu XR, Lin JH, Walz T, Häner M, Yu J, Aebi U, Sun TT. Mammalian uroplakins: A a group of highly conserved urothelial differentiation-related membrane proteins. J Biol Chem. 1994;269:13716–24.

28.   Yu J, Lin JH, Wu XR, Sun TT. Uroplakins Ia and Ib, two major differentiation products of bladder epithelium, belong to a family of four transmembrane domain (4TM) proteins. J Cell Biol. 1994;125(1):171–82.

29.   Kong X-T, Deng F-M, Hu P, Liang F-X, Zhou G, Auerbach AB, Genieser N, Nelson PK, Robbins ES, Shapiro E, Kachar B, Sun T-T. Roles of uroplakins in plaque formation, umbrella cell enlargement, and urinary tract diseases. J Cell Biol. 2004;167(6):1195–204.

30.   Kątnik-Prastowska I, Lis J, Matejuk A. Glycosylation of uroplakins. Implications for bladder physiopathology. Glycoconj J. 2014;31(9):623–36.

31.   Wittmann BM, Stirdivant SM, Mitchell MW, Wulff JE, McDunn JE, Li Z, Dennis-Barrie A, Neri BP, Milburn M V., Lotan Y, Wolfert RL. Bladder Cancer Biomarker Discovery Using Global Metabolomic Profiling of Urine. PLoS One. 2014;9(12):e115870.

32.   Burnier A, Shimizu Y, Dai Y, Nakashima M, Matsui Y, Ogawa O, Rosser CJ, Furuya H. CXCL1 is elevated in the urine of bladder cancer patients. Springerplus. 2015;4(1):610.

33.   Sharma P. Cancer Immunology - Bladder Cancer [Internet]. National Cancer Research. 2014 [cited 2015 Feb 11]. Available from: http://www.cancerresearch.org/cancer-immunotherapy/impacting-all-cancers/bladder-cancer.

34.   Team TACS medical and editorial content. Bladder Cancer Stages [Internet]. American Cancer Society. 2016 [cited 2017 Aug 3]. Available from: https://www.cancer.org/cancer/bladder-cancer/detection-diagnosis-staging/staging.html.

35.   Bischoff CJ, Clark PE. Bladder cancer. CurrOpinOncol. 2009;21(3):272–7.

36.   Moch H, Cubilla AL, Humphrey PA, Reuter VE, Ulbright TM. The 2016 WHO

Classification of Tumours of the Urinary System and Male Genital Organs—Part A: Renal, Penile, and Testicular Tumours. Eur Urol. 2016;1–14.

37.   Eble JN, Sauter G EJ. Pathology and Genetics of Tumours of the Urinary System and Male Genital Organs. BJU Int. 2004;94(4):675.

38.   NICE. National Institute for Health and care Excellence guidelines: Bladder cancer diagnosis and management [Internet]. NICE guidelines. 2015 [cited 2016 Aug 11]. Available from: https://www.nice.org.uk/guidance/ng2/chapter/1-Recommendations.

39.   Lerner SP, Au JL. Risk-adapted use of intravesical chemotherapy. BJU Int. 2008;102(9 Pt B):1247–53.

40.   Paranychianakis GS, Dauaher HH. Intravesical 4'-epidoxorubicin (Epirubicin) versus bacillus Calmetter-Guerin: a controlled prospective study on the prophylaxis of superficial bladder cancer. Cancer. 1993;72:1749–55.

41.   Stricker P, Goldstein D, Golovsky D, Nash P, Ehsman S, Rumma J, Mammen G. Bacillus Calmette-Guerin plus intravesical interferon alpha-2b in patients with superficial bladder cancer. Urology. 1996;48:957–62.

42.   Shen Z, Shen T, Wientjes MG, O'Donnell M a., Au JLS. Intravesical treatments of bladder cancer: Review. Pharm Res. 2008;25(7):1500–10.

43.   Kim W-Y, Chang DJ, Hennessy B, Kang HJ, Yoo J, Han S-H, Kim Y-S, Park H-J, Geo S-Y, Mills G, Kim K-W, Hong WK, Suh Y-G, Lee H-Y. A Novel Derivative of the Natural Agent Deguelin for Cancer Chemoprevention and Therapy. Cancer Prev Res. 2008;1(7):577–87.

44.   Kim S, Nishimoto SK, Bumgardner JD, Haggard WO, Gaber MW, Yang Y. A chitosan/β-glycerophosphate thermo-sensitive gel for the delivery of ellagic acid for the treatment of brain cancer. Biomaterials. 2010;31(14):4157–66.

45.   He C, Hu Y, Yin L, Tang C, Yin C. Effects of particle size and surface charge on cellular uptake and biodistribution of polymeric nanoparticles. Biomaterials. 2010;31(13):3657–66.

46.   Kirin K. Summary of Product Characteristics: Mitomycin-C [Internet]. emc. 1992 [cited 2018 Oct 23]. Available from: https://www.medicines.org.uk/emc/product/4262.

47. Svatek RS, Hollenbeck BK, Holmäng S, Lee R, Kim SP, Stenzl A, Lotan Y. The economics of bladder cancer: Costs and considerations of caring for this disease. Eur Urol. 2014;66(2):253–62.

48. Action Bladder Cancer UK. The Facts About Bladder Cancer [Internet]. Bladder Cancer Facts. 2018 [cited 2018 Nov 12]. Available from: http://www.actionbladdercanceruk.org/the-facts-about-bladder-cancer/.

49. Singh NK, Lee DS. In situ gelling pH- and temperature-sensitive biodegradable block copolymer hydrogels for drug delivery. J Control Release. 2014;193:214–27.

50. Senyiğit ZA, Karavvana SY, Ilem-Özdemir D, Çalişkan Ç, Waldner C, Şen S B-SA. Design and evaluation of an intravesical delivery system for superficial bladder cancer : preparation of gemcitabine HCl-loaded chitosan – thioglycolic acid nanoparticles and comparison of chitosan / poloxamer gels as carriers. Int J Nanomedicine. 2015;10:6493–507.

51. Tyagi P, Wu PC, Chancellor M, Yoshimura N, Huang L. Recent advances in intravesical drug/gene delivery. Mol Pharm. 2006;3(4):369–79.

52. Grabnar I, Bogataj M, Beliˇ A, Logar V, Karba R, Mrhar A. Kinetic model of drug distribution in the urinary bladder wall following intravesical instillation. Int J Pharm. 2006;322:52–9.

53. Martin DT, Steinbach JM, Liu J, Shimizu S, Kaimakliotis HZ, Wheeler M a, Hittelman AB, Mark Saltzman W, Weiss RM. Surface-Modified Nanoparticles Enhance Transurothelial Penetration and Delivery of Survivin siRNA in Treating Bladder Cancer. Mol Cancer Ther. 2014;13(1):71–81.

54. Bogataj M, Mrhar A, Korošec L. Influence of physicochemical and biological parameters on drug release from microspheres adhered on vesical and intestinal mucosa. Int J Pharm. 1999;177(2):211–20.

55. Le Visage C, Rioux-Leclercq N, Haller M, Breton P, Malavaud B, Leong K. Efficacy of paclitaxel released from bio-adhesive polymer microspheres on model superficial bladder cancer. J Urol. 2004;171(3):1324–9.

56. Lu Z, Yeh TK, Tsai M, Au JLS, Wientjes MG. Paclitaxel-loaded gelatin nanoparticles for

intravesical bladder cancer therapy. Clin Cancer Res. 2004;10(22):7677–84.

57.   Giannantoni A, Di Stasi SM, Chancellor MB, Costantini E, Porena M. New Frontiers in Intravesical Therapies and Drug Delivery. Eur Urol. 2006;50(6):1183–93.

58.   Parkin J, Shea C, Sant GR. Intravesical dimethyl sulfoxide (DMSO) for interstitial cystitis--a practical approach. Urology. 1997;49(5A Suppl):105–7.

59.   Tamura K, Kikuchi E, Konno T, Ishihara K, Matsumoto K, Miyajima A, Oya M. Therapeutic effect of intravesical administration of paclitaxel solubilized with poly(2-methacryloyloxyethyl phosphorylcholine-co-n-butyl methacrylate) in an orthotopic bladder cancer model. BMC Cancer. 2015;15(1):317.

60.   Erdoğar N, Iskit AB, Mungan NA, Bilensoy E. 2012. Prolonged retention and in vivo evaluation of cationic nanoparticles loaded with Mitomycin C designed for intravesical chemotherapy of bladder tumours. J Microencapsul. 2012;29(6):576–82.

61.   Martin DT, Hoimes CJ, Kaimakliotis HZ, Cheng CJ, Zhang K, Liu J, Wheeler MA, Kelly WK, Tew GN, Saltzman WM, Weiss RM. Nanoparticles for urothelium penetration and delivery of the histone deacetylase inhibitor belinostat for treatment of bladder cancer. Nanomedicine. 2013;9(8):1124–34.

62.   Neutsch L, Wirth E-M, Spijker S, Pichl C, Kählig H, Gabor F, Wirth M. Synergistic targeting/prodrug strategies for intravesical drug delivery--lectin-modified PLGA microparticles enhance cytotoxicity of stearoyl gemcitabine by contact-dependent transfer. J Control Release. 2013;169(1–2):62–72.

63.   Erdoğar N, Iskit AB, Eroglu H, Sargon MF, Mungan NA, Bilensoy E. Cationic core-shell nanoparticles for intravesical chemotherapy in tumor-induced rat model: Safety and efficacy. Int J Pharm. 2014;471(1–2):1–9.

64.   Zhang Q, Neoh KG, Xu L, Lu S, Kang ET, Mahendran R, Chiong E. Functionalized mesoporous silica nanoparticles with mucoadhesive and sustained drug release properties for potential bladder cancer therapy. Langmuir. 2014;30(21):6151–61.

65. Cook MT, Schmidt SA, Lee E, Samprasit W, Opanasopit P, Khutoryanskiy V V. Synthesis of mucoadhesive thiol-bearing microgels from 2-(acetylthio)ethylacrylate and 2-hydroxyethylmethacrylate: novel drug delivery systems for chemotherapeutic agents to the bladder. J Mater Chem B. 2015;3(32):6599–604.

66. Lu S, Neoh KG, Kang ET, Mahendran R, Chiong E. Mucoadhesive polyacrylamide nanogel as a potential hydrophobic drug carrier for intravesical bladder cancer therapy. Eur J Pharm Sci. 2015;72:57–68.

67. Men K, Liu W, Li L, Duan X, Wang P, Gou M, Wei X, Gao X, Wang B, Du Y, Huang M, Chen L, Qian Z, Wei Y. Delivering instilled hydrophobic drug to the bladder by a cationic nanoparticle and thermo-sensitive hydrogel composite system. Nanoscale. 2012;4:6425.

68. Zhang D, Sun P, Li P, Xue A, Zhang X, Zhang H, Jin X. A magnetic chitosan hydrogel for sustained and prolonged delivery of Bacillus Calmette-Guérin in the treatment of bladder cancer. Biomaterials. 2013;34(38):10258–66.

69. Lin T, Wu J, Zhao X, Lian H, Yuan A, Tang X, Zhao S, Guo H, Hu Y. In situ floating hydrogel for intravesical delivery of adriamycin without blocking urinary tract. J Pharm Sci. 2014;103:927–36.

70. GuhaSarkar S, More P, Banerjee R. Urothelium-adherent, ion-triggered liposome-in-gel system as a platform for intravesical drug delivery. J Control Release. 2017;245:147–56.

71. Kaldybekov DB, Tonglairoum P, Opanasopit P, Khutoryanskiy V V. Mucoadhesive maleimide-functionalised liposomes for drug delivery to urinary bladder. Eur J Pharm Sci. 2018;111:83–90.

72. Tadros T. Encyclopedia of Colloid and Interface Science. In: Tadros T, editor. Berlin, Heidelberg: Springer Berlin Heidelberg; 2013. p. 1046–7.

73. Knemeyer I, Wientjes MG, Au JL. Cremophor reduces paclitaxel penetration into bladder wall during intravesical treatment. Cancer Chemother Pharmacol. 1999;44(3):241–8.

74. Wada M, Jinno H, Ueda M, Ikeda T, Kitajima M, Konno T, Watanabe J, Ishihara K.

Efficacy of an MPC-BMA co-polymer as a nanotransporter for paclitaxel. Anticancer Res. 2007;27(3B):1431–5.

75. Goda T, Goto Y, Ishihara K. Cell-penetrating macromolecules: Direct penetration of amphipathic phospholipid polymers across plasma membrane of living cells. Biomaterials. 2010;31(8):2380–7.

76. Guo H, Xu W, Chen J, Yan L, Ding J, Hou Y, Chen X. Positively charged polypeptide nanogel enhances mucoadhesion and penetrability of 10-hydroxycamptothecin in orthotopic bladder carcinoma. J Control Release. 2017;259:136–48.

77. Kikuchi E, Menendez S, Ozu C, Ohori M, Cordon-cardo C, Logg CR, Kasahara N, Bochner BH. Highly Efficient Gene Delivery for Bladder Cancers by Intravesically Administered Replication-Competent Retroviral Vectors Cancer Therapy : Preclinical Highly Efficient Gene Delivery for Bladder Cancers by Intravesically Administered Replication-Competent. Clin Cancer Res. 2007;13(15):4511–9.

78. Matsushima M, Horinaga M, Fukuyama R, Yanaihara H, Kikuchi E, Kawachi M, Iida M, Nakahira Y, Oya M, Asakura H. Enhanced antitumor effect of combination intravesical mitomycin C and bacillus Calmette-Guerin therapy in an orthotopic bladder cancer model. Oncol Lett. 2011;2(1):13–9.

79. Haltner E, Easson JH, Lehr CM. Lectins and bacterial invasion factors for controlling endo- and transcytosis of bioadhesive drug carrier systems. Eur J Pharm Biopharm. 1997;44(1):3–13.

80. Yi SM, Harson RE, Zabner J, Welsh MJ. Lectin binding and endocytosis at the apical surface of human airway epithelia. Gene Ther. 2001;8(24):1826–32.

81. Bies C, Lehr C-M, Woodley JF. Lectin-mediated drug targeting: history and applications. Adv Drug Deliv Rev. 2004;56(4):425–35.

82. Dhakal BK, Kulesus RR, Mulvey M a. Mechanisms and consequences of bladder cell invasion by uropathogenic Escherichia coli. Eur J Clin Invest. 2008;38 Suppl 2:2–11.

83. Neutsch L, Plattner VE, Polster-Wildhofen S, Zidar A, Chott A, Borchard G, Zechner O, Gabor F, Wirth M. Lectin mediated biorecognition as a novel strategy for targeted delivery to bladder cancer. J Urol. 2011;186(4):1481–8.

84. Neutsch L, Eggenreich B, Herwig E, Marchetti-Deschmann M, Allmaier G, Gabor F, Wirth M. Lectin bioconjugates trigger urothelial cytoinvasion - A glycotargeted approach for improved intravesical drug delivery. Eur J Pharm Biopharm. 2012;82:367–75.

85. Silva GA. Introduction to nanotechnology and its applications to medicine. Surg Neurol. 2004;61(3):216–20.

86. Cho K, Wang X, Nie S, Chen Z, Shin DM. Therapeutic nanoparticles for drug delivery in cancer. Clin Cancer Res. 2008;14(5):1310–6.

87. Jain RA. The manufacturing techniques of various drug loaded biodegradable poly(lactide-co-glycolide) (PLGA) devices. Biomaterials. 2000;21(23):2475–90.

88. Apfelthaler C, Anzengruber M, Gabor F, Wirth M. Poly – (L) – glutamic acid drug delivery system for the intravesical therapy of bladder cancer using WGA as targeting moiety. Eur J Pharm Biopharm. 2017;115:131–9.

89. Wright CS, Kellogg GE. Differences in hydropathic properties of ligand binding at four independent sites in wheat germ agglutinin-oligosaccharide crystal complexes. Protein Sci. 1996;5(8):1466–76.

90. Smart JD. The basics and underlying mechanisms of mucoadhesion. Adv Drug Deliv Rev. 2005;57(11):1556–68.

91. Khutoryanskiy V V. Advances in Mucoadhesion and Mucoadhesive Polymers. Macromol Biosci. 2011;11(6):748–64.

92. Bonengel S, Bernkop-Schnürch A. Thiomers--from bench to market. J Control Release. 2014;195:120–9.

93. Barthelmes J, Dünnhaupt S, Unterhofer S, Perera G, Schlocker W B-SA. Thiolated particles as effective intravesical drug delivery systems for treatment of bladder related diseases. Nanomedicine (Lond). 2013;8(1):65–75.

94. Fahmy TM, Samstein RM, Harness CC, Saltzman WM. Surface modification of biodegradable polyesters with fatty acid conjugates for improved drug targeting. Biomaterials. 2005;26(28):5727–36.

95. Cheng CJ, Saltzman WM. Enhanced siRNA delivery into cells by exploiting the synergy between targeting ligands and cell-penetrating peptides. Biomaterials. 2011;32(26):6194–203.

96. Khan A, Benboubetra M, Sayyed PZ, Ng KW, Fox S, Beck G, Benter IF, Akhtar S. Sustained polymeric delivery of gene silencing antisense ODNs, siRNA, DNAzymes and ribozymes: in vitro and in vivo studies. J Drug Target. 2004;12(6):393–404.

97. Anthony T, Fong P, Goyal A, Saltzman WM, Moss RL, Breuer C. Development of a parathyroid hormone-controlled release system as a potential surgical treatment for hypoparathyroidism. J Pediatr Surg. 2005;40(1):81–5.

98. Cu Y, Booth CJ, Saltzman WM. In vivo distribution of surface-modified PLGA nanoparticles following intravaginal delivery. J Control Release. 2011;156(2):258–64.

99. Hennig A, Gabriel GJ, Tew GN, Matile S. Stimuli-responsive polyguanidino-oxanorbornene membrane transporters as multicomponent sensors in complex matrices. J Am Chem Soc. 2008;130(31):10338–44.

100. Buckley MT, Yoon J, Yee H, Chiriboga L, Liebes L, Ara G, Qian X, Bajorin DF, Sun T-T, Wu X-R, Osman I. The histone deacetylase inhibitor belinostat (PXD101) suppresses bladder cancer cell growth in vitro and in vivo. J Transl Med. 2007;5:49.

101. Qian X, Ara G, Mills E, LaRochelle WJ, Lichenstein HS, Jeffers M. Activity of the histone deacetylase inhibitor belinostat (PXD101) in preclinical models of prostate cancer. Int J Cancer. 2008;122(6):1400–10.

102. Haas J, Ravi Kumar MN V, Borchard G, Bakowsky U, Lehr C-M. Preparation and characterization of chitosan and trimethyl-chitosanmodified poly-(ε-caprolactone) nanoparticles as DNA carriers. AAPS PharmSciTech. 2005;6(1):E22–30.

103. Sogias IA, Williams AC, Khutoryanskiy V V. Why is chitosan mucoadhesive? Biomacromolecules. 2008;9(7):1837–42.

104. Van der Lubben IM, Verhoef JC, Borchard G, Junginger HE. Chitosan and its derivatives

in mucosal drug and vaccine delivery. Eur J Pharm Sci. 2001;14(3):201–7.

105. Barthelmes J, Perera G, Hombach J, Dünnhaupt S B-SA. Development of a mucoadhesive nanoparticulate drug delivery system for a targeted drug release in the bladder. Int J Pharm. 2011;416(1):339–45.

106. Bernkop-Schnürch A, Greimel A. Thiomers: The next generation of mucoadhesive polymers. Am J Drug Deliv. 2005;3:141–54.

107. Barthelmes et al. Thiomer nanoparticles: stabilization via covalent cross-linking. Drug Deliv. 2011;18:613–9.

108. Davidovich-Pinhas M, Bianco-Peled H. Physical and structural characteristics of acrylated poly(ethylene glycol)-alginate conjugates. Acta Biomater. 2011;7(7):2817–25.

109. Brannigan RP, Khutoryanskiy V V. Synthesis and evaluation of mucoadhesive acryloyl-quaternized PDMAEMA nanogels for ocular drug delivery. Colloids Surfaces B Biointerfaces. 2017;155:538–43.

110. Tonglairoum P, Brannigan RP, Opanasopit P, Khutoryanskiy V V. Maleimide-bearing nanogels as novel mucoadhesive materials for drug delivery. J Mater Chem B. 2016;4(40):6581–7.

111. Xu J, Soliman GM, Barralet J, Cerruti M. Mollusk glue inspired mucoadhesives for biomedical applications. Langmuir. 2012;28(39):14010–7.

112. Irmukhametova GS, Mun G a., Khutoryanskiy V V. Thiolated mucoadhesive and PEGylated nonmucoadhesive organosilica nanoparticles from 3-mercaptopropyltrimethoxysilane. Langmuir. 2011;27:9551–6.

113. Mun EA, Williams AC, Khutoryanskiy V V. Adhesion of thiolated silica nanoparticles to urinary bladder mucosa: Effects of PEGylation, thiol content and particle size. Int J Pharm. 2016;512(1):32–8.

114. Štorha A, Mun E a., Khutoryanskiy V V. Synthesis of thiolated and acrylated nanoparticles using thiol-ene click chemistry: towards novel mucoadhesive materials for drug delivery. RSC Adv. 2013;3(30):12275.

115. Amling CL. Diagnosis and management of superficial bladder cancer. Curr Probl Cancer.

2001;25(4):219–78.

116. Lamm DL, McGee WR, Hale K. Bladder cancer: current optimal intravesical treatment. Urol Nurs. 2005;25(5):323–6, 331–2.

117. Shin MC, Zhang J, Min KA, Lee K, Byun Y, David AE, He H, Yang VC. Cell-penetrating peptides: Achievements and challenges in application for cancer treatment.Journal of Biomedical Materials Research - Part A. 2014;102:575–87.

118. Kopeček J. Hydrogel biomaterials: A smart future? Biomaterials. 2007;28(34):5185–92.

119. Yu L, Ding J. Injectable hydrogels as unique biomedical materials. Chem Soc Rev. 2008;37(8):1473–81.

120. Khetan S, Guvendiren M, Legant WR, Cohen DM, Chen CS, Burdick J a. Degradation-mediated cellular traction directs stem cell fate in covalently crosslinked three-dimensional hydrogels. Nat Mater. 2013;12(5):458–65.

121. Oommen OP, Wang S, Kisiel M, Sloff M, Hilborn J, Varghese OP. Smart design of stable extracellular matrix mimetic hydrogel: Synthesis, characterization, and in vitro and in vivo evaluation for tissue engineering. Adv Funct Mater. 2013;23(10):1273–80.

122. Rice JJ, Martino MM, De Laporte L, Tortelli F, Briquez PS, Hubbell JA. Engineering the Regenerative Microenvironment with Biomaterials. Adv Healthc Mater. 2013;2(1):57–71.

123. Kim MR, Park TG. Temperature-responsive and degradable hyaluronic acid/Pluronic composite hydrogels for controlled release of human growth hormone. J Control Release. 2002;80(1–3):69–77.

124. He C, Kim SW, Lee DS. In situ gelling stimuli-sensitive block copolymer hydrogels for drug delivery. J Control Release. 2008;127(3):189–207.

125. Narendra KS, Lee DS. In situ gelling pH- temperature-sensitive biodegradable block copolymer hydrogels for drug delivery. J Control Release. 2014;193:214–27.

126. Choi HG, Oh YK, Kim CK. In situ gelling and mucoadhesive liquid suppository containing

acetaminophen: Enhanced bioavailability. Int J Pharm. 1998;165(1):23–32.

127.   Taylor MJ, Tanna S, Sahota T. In vivo study of a polymeric glucose-sensitive insulin delivery system using a rat model. J Pharm Sci. 2010;99(10):4215–27.

128.   Gong C, Qi T, Wei X, Qu Y, Wu Q, Luo F, Qian Z. Thermosensitive Polymeric Hydrogels As Drug Delivery Systems. Curr Med Chem. 2012;20(1):79–94.

129.   Wang W, Zhang P, Shan W, Gao J, Liang W. A novel chitosan-based thermosensitive hydrogel containing doxorubicin liposomes for topical cancer therapy. J Biomater Sci Polym Ed. 2013;24(14):1649–59.

130.   Niranjan R, Koushik C, Saravanan S, Moorthi A, Vairamani M, Selvamurugan N. A novel injectable temperature-sensitive zinc doped chitosan/β-glycerophosphate hydrogel for bone tissue engineering. Int J Biol Macromol. 2013;54:24–9.

131.   Supper S, Anton N, Seidel N, Riemenschnitter M, Schoch C, Vandamme T. Rheological study of chitosan/polyol-phosphate systems: Influence of the polyol part on the thermo-induced gelation mechanism. Langmuir. 2013;29(32):10229–37.

132.   Nguyen MK, Lee DS. Injectable biodegradable hydrogels. Vol. 10, Macromolecular Bioscience. 2010. p. 563–79.

133.   Dalbagni G. The management of superficial bladder cancer. Nat Clin Pract Urol. 2007;4(5):254–60.

134.   Eto H, Oka Y, Ueno K, Nakamura I, Yoshimura K, Arakawa S, Kamidono S, Obe S, Ogawa T, Hamami G. Comparison of the prophylactic usefulness of epirubicin and doxorubicin in the treatment of superficial bladder cancer by intravesical instillation: a multicenter randomized trial. Kobe University Urological Oncology Group. Cancer Chemother Pharmacol. 1994;35 Suppl(1):S46-51.

135.   Singh BN, Kim KH. Floating drug delivery systems: An approach to oral controlled drug delivery via gastric retention. J Control Release. 2000;63(3):235–59.

136.   Pawar VK, Kansal S, Garg G, Awasthi R, Singodia D, Kulkarni GT. Gastroretentive dosage forms: A review with special emphasis on floating drug delivery systems. Drug Deliv.

2011;18(2):97–110.

137. Prajapati VD, Jani GK, Khutliwala T a., Zala BS. Raft forming system - An upcoming approach of gastroretentive drug delivery system. J Control Release. 2013;168(2):151–65.

138. Mortensen K. Structural Study on the Micelle Formation of PEO-PPO-PEO triblock copolymer in aqueous solutions. Macromolecules. 1993;26:805–12.

139. Alexandridis and Hatton. Poly(ethylene oxide)poly(propylene oxide)poly(ethylene oxide) block copolymer surfactants in aqueous solutions and at interfaces: thermodynamics, structure, dynamics, and modeling. Colloids Surfaces A Physicochem Eng Asp. 1995;96(1–2):1–46.

140. Kim B, Han G, Toley BJ, Kim CK, Rotello VM, Forbes NS. Tuning payload delivery in tumour cylindroids using gold nanoparticles. Nat Nanotechnol. 2010;5(6):465–72.

141. Khodaverdi E, Tafaghodi M, Ganji F, Abnoos K, Naghizadeh H. In Vitro Insulin Release from Thermosensitive Chitosan Hydrogel. AAPS PharmSciTech. 2012;13(2):460–6.

142. Abdel-Bar HM, Abdel-Reheem AY, Osman R, Awad GAS, Mortada N. Defining cisplatin incorporation properties in thermosensitive injectable biodegradable hydrogel for sustained delivery and enhanced cytotoxicity. Int J Pharm. 2014;477(1–2):623–30.

143. Lavertu M, Filion D, Buschmann MD. Heat-induced transfer of protons from chitosan to glycerol phosphate produces chitosan precipitation and gelation. Biomacromolecules. 2008;9(2):640–50.

144. Qiu X, Yang Y, Wang L, Lu S, Shao Z, Chen X. Synergistic interactions during thermosensitive chitosan-β-glycerophosphate hydrogel formation. RSC Adv. 2011;1(2):282.

145. Schuetz YB, Gurny R, Jordan O. A novel thermoresponsive hydrogel based on chitosan. Eur J Pharm Biopharm. 2008;68(1):19–25.

146. Patois E, Osorio-Da Cruz S, Tille JC, Walpoth B, Gurny R, Jordan O. Novel thermosensitive chitosan hydrogels: In vivo evaluation. J Biomed Mater Res - Part A.

2009;91(2):324–30.

147. Aliaghaie M, Mirzadeh H, Dashtimoghadam E, Taranejoo S. Investigation of gelation mechanism of an injectable hydrogel based on chitosan by rheological measurements for a drug delivery application. Soft Matter. 2012;8(27):7128.

148. Peng Y, Li J, Li J, Fei Y, Dong J, Pan W. Optimization of thermosensitive chitosan hydrogels for the sustained delivery of venlafaxine hydrochloride. Int J Pharm. 2013;441(1–2):482–90.

149. Rosenthal R, Günzel D, Finger C, Krug SM, Richter JF, Schulzke JD, Fromm M, Amasheh S. The effect of chitosan on transcellular and paracellular mechanisms in the intestinal epithelial barrier. Biomaterials. 2012;33(9):2791–800.

150. Shen ZJ, Wang Y, Ding GQ, Pan CW, Zheng RM. Study on enhancement of fibronectin-mediated bacillus Calmette-Guerin attachment to urinary bladder wall in rabbits. World J Urol. 2007;25(5):525–9.

151. Lee HY, Oh SH, Woo JK, Kim WY, Van Pelt CS, Price RE, Cody D, Tran H, Pezzuto JM, Moriarty RM, Hong WK. Chemopreventive effects of deguelin, a novel Akt inhibitor, on tobacco-induced lung tumorigenesis. J Natl Cancer Inst. 2005;97(22):1695–9.

152. Oh SH, Woo JK, Yazici YD, Myers JN, Kim WY, Jin Q, Hong SS, Park HJ, Suh YG, Kim KW, Hong WK, Lee HY. Structural basis for depletion of heat shock protein 90 client proteins by deguelin. J Natl Cancer Inst. 2007;99(12):949–61.

153. Peng X, Karna P, Regan RMO, Liu X, Naithani R, Moriarty RM, Wood WC, Lee H, Yang L. Down-Regulation of Inhibitor of Apoptosis Proteins by Deguelin Selectively Induces Apoptosis in Breast Cancer Cells. Mol Pharmacol. 2007;71(1):101–11.

154. Gopalan B, Ito I, Branch CD, Stephens C, Roth J a, Ramesh R. Nanoparticle based systemic gene therapy for lung cancer: molecular mechanisms and strategies to suppress nanoparticle-mediated inflammatory response. Technol Cancer Res Treat. 2004;3(6):647–57.

155. Simberg D, Weisman S, Talmon Y, Barenholz Y. DOTAP (and other cationic lipids): chemistry, biophysics, and transfection. Crit Rev Ther Drug Carrier Syst. 2004;21(4):257–317.

156. Díez S, Navarro G, de ILarduya CT. In vivo targeted gene delivery by cationic nanoparticles for treatment of hepatocellular carcinoma. J Gene Med. 2009;11(1):38–45.

157. Kabanov A V., Lemieux P, Vinogradov S, Alakhov V. Pluronic block copolymers: Novel functional molecules for gene therapy. Adv Drug Deliv Rev. 2002;54(2):223–33.

158. Cortesi R, Nastruzzi C. Liposomes, micelles and microemulsions as new delivery systems for cytotoxic alkaloids. Pharm Sci Technol Today. 1999;2(7):288–98.

159. Alexis F, Rhee JW, Richie JP, Radovic-Moreno AF, Langer R, Farokhzad OC. New frontiers in nanotechnology for cancer treatment. Urol Oncol Semin Orig Investig. 2008;26(1):74–85.

160. Nakamura T, Noma Y, Sakurai Y, Harashima H. Modifying Cationic Liposomes with Cholesteryl-PEG Prevents Their Aggregation in Human Urine and Enhances Cellular Uptake by Bladder Cancer Cells. Biol Pharm Bull. 2017;40(2):234–7.

161. Lehner B, Sandner B, Marschallinger J, Lehner C, Furtner T, Couillard-Despres S, Rivera FJ, Brockhoff G, Bauer HC, Weidner N, Aigner L. The dark side of BrdU in neural stem cell biology: Detrimental effects on cell cycle, differentiation and survival. Cell Tissue Res. 2011;345(3):313–28.

162. Aslantürk ÖS. In Vitro Cytotoxicity and Cell Viability Assays: Principles, Advantages, and Disadvantages. Genotoxicity - A Predict Risk to Our Actual World. 2018;1–18.

163. Vanicha V KK. Sulforhodamine B colorimetry assay for cytotoxicity screening. Nat Protoc. 2006;1(3):1112–6.

164. Brown P, Ackermann D, Finlayson B. Calcium oxalate dihydrate (weddellite) precipitation. J Cryst Growth. 1989;98(3):285–92.

165. Brooks T, Keevil CW. A simple artificial urine for the growth of urinary pathogens. Lett Appl Microbiol. 1997;24(3):203–6.

166. Opalko FJ, Adair JH, Khan SR. Heterogeneous nucleation of calcium oxalate trihydrate in artificial urine by constant composition. J Cryst Growth. 1997;181(4):410–7.

167. Grases F, Llobera A. Experimental model to study sedimentary kidney stones. Micron.

1998;29(2–3):105–11.

168. Mayrovitz HN, Sims N. Biophysical effects of water and synthetic urine on skin. Adv Skin Wound Care. 2001;14(6):302–8.

169. Christmas KG, Gower LB, Khan SR, El-Shall H. Aggregation and Dispersion Characteristics of Calcium Oxalate Monohydrate: Effect of Urinary Species. J Colloid Interface Sci. 2002;256(1):168–74.

170. Chutipongtanate S, Thongboonkerd V. Systematic comparisons of artificial urine formulas for in vitro cellular study. Anal Biochem. 2010;402(1):110–2.

171. Zacchè MM, Srikrishna S, Cardozo L. Novel targeted bladder drug-delivery systems: A review. Res Reports Urol. 2015;7:169–78.

172. TheraCoat Ltd. Pre-TURBT TC-3 Gel Intravesical Instillation in NMIBC (OPTIMA) [Internet]. 2015 [cited 2016 Jan 11]. p. 1–4. Available from: https://clinicaltrials.gov/ct2/show/NCT01803295?term=NCT01803295&rank=1

173. Institute UNC. Mitomycin C Intravesical Chemotherapy in Conjunction with Synergo® Radiofrequency-Induced Hyperthermia for Treatment of Carcinoma in Situ Non-muscle Invasive Bladder Cancer patients Unresponsive to Bacillus Calmette-Guérin, With or Without Papilary Tumors [Internet]. NCI-Supported Clinical Trials. 2018 [cited 2018 Oct 20]. Available from: https://www.cancer.gov/about-cancer/treatment/clinical-trials/search/v?id=NCI-2018-01714&r=1.

174. Institute UNC. The OLYMPUS Study-Optimized Delivery of Mitomycin for Primary UTUC Study [Internet]. NCI-Supported Clinical Trials. 2018 [cited 2018 Oct 21]. Available from: https://www.cancer.gov/about-cancer/treatment/clinical-trials/search/v?id=NCI-2017-00020&r=1

2. Chitosan / β-glycerophosphate *in situ* gelling mucoadhesive systems for intravesical delivery of mitomycin-C

Out of all the drug delivery systems described in Chapter 1, chitosan/β-glycerophosphate *in situ* gelling systems will be investigated because of the biocompatibility of chitosan and β-glycerophosphate as well as mucoadhesive, and drug permeation enhancing properties of chitosan. Also, mixture of chitosan and β-glycerophosphate in the appropriate concentration and volume ratio generate drug carriers that could improve drug residence in the bladder and promote patient compliance to dosage regimen due to a reduction in dosing frequency. Mitomycin-C was chosen as the model drug because it is drug of choice for the treatment of superficial bladder cancer.

2.1. Introduction

Bladder cancer has been identified as a major clinical issue with prevalence and mortality rate escalating globally [1] and there is increasing research in this area to improve drug delivery [2,3]. Oral and other systemic route of administrations are not employed for bladder cancer treatment, especially at the early stages of the disease because therapeutic drug concentrations cannot be achieved in the bladder due to the hostile environment of the stomach, hepatic metabolism as well as drug transport to non-target organs [4]. Consequently, drugs are instilled via the catheter directly into the bladder, referred to as intravesical drug delivery, to increase local drug availability. The local route of administration has been explored further for bladder cancer treatment because it minimises systemic toxicity and facilitates targeted drug delivery to urothelial malignant tissues [2,4].

Polymers exhibiting the ability to adhere to mucosal tissues in the bladder are typically referred as mucoadhesive dosage forms. These dosage forms are commonly prepared using polymers that interact with glycoprotein components of mucin through non-covalent bonding such as hydrogen bonds, chain entanglements and electrostatic interactions [5–7]. They are particularly desirable for drug delivery to the bladder because they may be able to overcome some inherent limitations of intravesical administration such as substantial drug dilution and wash-out during urine formation and elimination.

Chitosan, (1,4)-2-amino-2-deoxy-β-D-glucan, is a natural polymer generated by the partial deacetylation of chitin under basic or enzymatic conditions [8]. Chitosan is a mucoadhesive polymeric excipient that has been approved by the national food regulatory authorities in Japan and Korea as a food additive; in the European Union as an excipient for nasal drug delivery and vaccine delivery, and the FDA has approved chitosan containing medical devices and antimicrobial wound dressings for non-systemic use. However, the FDA does not currently permit the use of chitosan as constituents of food, drug products or biopharmaceutical delivery systems due to its structural heterogeneity, large batch variations and possible allergic reactions as a result of its crustacean source[9]. Nevertheless, chitosan is still one of the most researched mucoadhesive polymer for transmucosal drug delivery due to its good biocompatibility and versatility to generate a wide range of drug carriers [10]. It is commercially available as various grades depending on molecular weight and degree of deacetylation, with the highly deacetylated forms preferred because they can be readily functionalised for a variety of biomedical applications [11]. The continued interest in chitosan over the last two decades for drug delivery and tissue engineering is due to its biocompatible, biodegradable, mucoadhesive,

and cell permeation properties [10,11]. Tyagi et al reported that chitosan exhibited properties desirable for the formulation of intravesical dosage forms: effective and extended mucoadhesion as well as non-interference with bladder physiology [12].

Glycerophosphate is presented as its sodium salt which is hydrolysed in the body to inorganic phosphate and glycerol [13]. It has been approved by the Medicines and Healthcare products Regulatory Agency as a phosphate supplement in intravenous nutrition for adult patients marketed by Fresenius Kabi, which is a concentrate containing 21.6% sodium glycerophosphate for infusion [14].

The possibility of chitosan solution forming *in situ* gelling systems with physical cross-linking was first reported by Chenite et al. (2000), where chitosan solution (pH ~ 6) formed a gel in the presence of β-glycerophosphate at about 37°C [15]. Chitosan/β-glycerophosphate mixtures were reported to be safe, biodegradable and thermosensitive with relatively easy drug loading that allow its release at the point of administration; plus their preparation does not require expensive equipment [16,17]. They also display sustained gel stability for 90 days when stored at -80°C [18].

Various researchers have investigated one or two grades of chitosan or its derivatives with αβ- or β-glycerophosphate and reported improved efficacy and sustained drug release of various therapeutics [18–25]. Zhang and co-workers have mixed Bacillus Calmette Guérin (BCG) with ferric oxide (Fe_3O_4) nanoparticles and incorporated the nanoparticulate formulation into chitosan/β-glycerophosphate *in situ* gelling systems to generate composite system for intravesical bladder cancer treatment [26]. To the best of our knowledge, chitosan/β-glycerophosphate *in situ* gelling systems have not been explored for intravesical drug delivery. Moreover, the wash-out influence of artificial urine on the retention of *in situ* gelling drug carriers has not been studied. The drug-loaded *in situ* gelling formulations may form a mucoadhesive gel layer across a wide surface area of the bladder mucosa allowing for therapeutic concentrations of the drug to diffuse across urothelial cancerous tissues for extended period of time.

Mitomycin-C is the drug for superficial / non-invasive bladder cancer therapy, used preferably immediately or ≤ 24 h after transurethral resection of bladder tumour to reduce recurrence rate [27,28]. Mitomycin-C is generally administered at a concentration of 1-2mg/mL for superficial bladder cancer treatment [29]. According to a randomised controlled trial, 1 mg/mL mitomycin-

C formulation (20-40mL) resulted in recurrence reduction of 23.5% in bladder cancer patients [30]. So, mitomycin-C at 1 mg/mL was selected for the current study.

Bilensoy and co-workers explored cationic chitosan- and poly-L-lysine-coated poly-Ɛ-caprolactone (PCL) nanoparticles for improved intravesical delivery of mitomycin-C [31–33]. They reported that bladder tumour induced rats treated with chitosan-coated PCL nanoparticles displayed superior antitumour efficacy (evident with more rats alive up to 83 days) relative to other groups treated with poly-L-lysine-coated PCL nanoparticles and uncoated chitosan nanoparticles *in vivo* [33]. Their findings suggested that chitosan coated drug carriers may be efficient for improved drug localisation and accumulation in bladder tissues.

Despite the potential of *in situ* gelling systems to facilitate controlled drug release [34], they have not been explored as delivery systems for mitomycin-C in enhancing the therapeutic outcome of bladder cancer. This current work sought to explore chitosan based *in situ* gelling systems to improve the residence time of mitomycin-C in the bladder. We present the first report on the formulation of chitosan/β-glycerophosphate gels using three grades of chitosan for intravesical drug delivery, with chitosan molecular weight modulating gelation, mucoadhesive and drug release profile of the CHIGP formulations.

2.2. Materials and methods

2.2.1. Materials

Low (LCHI), medium (MCHI) and high molecular weight (HCHI) grades of chitosan, β-glycerophosphate (β-GP), FITC-dextran (3-5 kDa), dextran (5 kDa), fluorescein sodium, trifluoroacetic acid, urea, uric acid, magnesium sulphate heptahydrate, sodium hydrogen phosphate, creatinine, sodium bicarbonate, sodium sulphate, disodium oxalate and trisodium citrate acid were purchased from Sigma-Aldrich (UK); disodium phosphate, sodium chloride, potassium chloride, ammonium chloride, and calcium chloride dihydrate, mitomycin-C, HPLC grade methanol, acetonitrile, water and other chemical reagents were from Fischer Scientific/Chemicals (UK) and used as received without further purification. Dialysis membranes with molecular weight cut off 12-14 kDa were supplied by Medicell International (UK). Freshly excised porcine urinary bladders were provided by PC Turner Abattoir (Farnborough, Hampshire, UK).

2.2.2. Characterisation of three chitosan grades

The molecular weights of the three grades of chitosan were determined by gel permeation chromatography using an Agilent PL Aquagel-OH (mixed H8 μm) as column with 0.1 M sodium nitrate as a solvent system (pH 2.1) at a flow rate of 0.5 mL/min at 30°C, which separates chitosan based on size. For the purpose of ^{1}H NMR analysis, approximately 20 mg of LCHI, MCHI and HCHI were dissolved in 3 mL deuterium oxide (D_2O) acidified with 30 μL trifluoroacetic acid for 12 h at room temperature and the ^{1}H NMR spectra were recorded using a 400 MHz ULTRASHIELD PLUS™ B-ACS 60 spectrometer (Bruker, UK). The degrees of acetylation of chitosan samples were evaluated based on the integration pattern of the N-acetyl protons (δ = 1.6 ppm) relative to the other protons (δ = 3.0-3.6 ppm). An exemplar ^{1}H NMR spectrum is provided in Fig. 2.1.

The acetylation level evaluates the amount of reacted chitosan amine groups. it was calculated using the following equation [35]:

Degree of acetylation (DA) (%) = (I_{CH3}/3) / (I_{H2-H6} / 6) x 100 %   (1),

where the integral intensity of N-acetyl protons is denoted as I_{CH3} and I_{H2-H6} depicted the integral intensities of H-2, -3, -4, -5 and H-6 of the deacetylated glucosamine ring of chitosan.
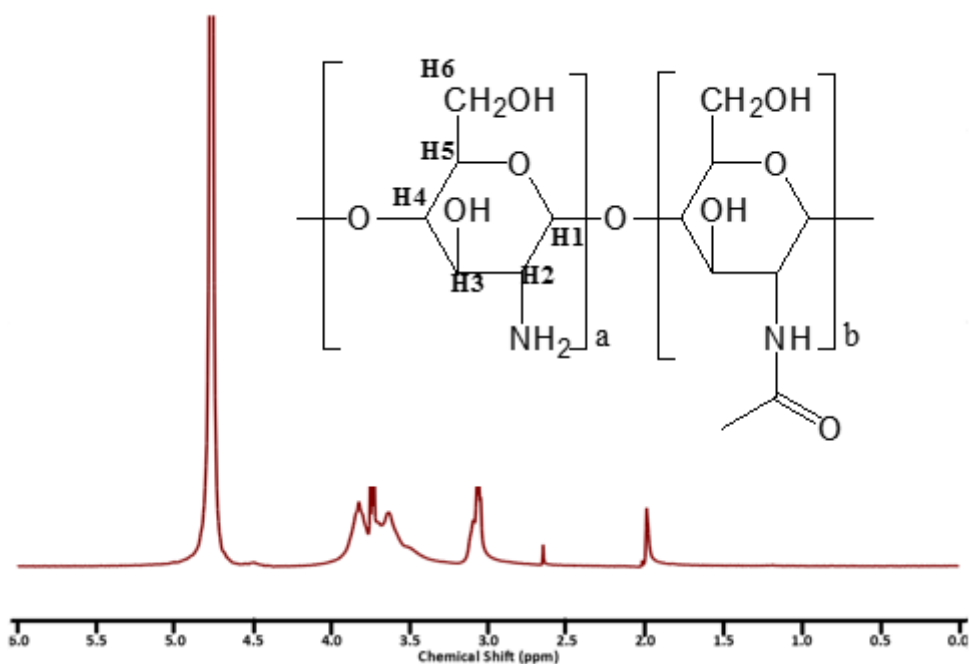
Fig. 2.1. ^{1}H NMR spectra of chitosan recorded in D_2O acidified with 1% trifluoroacetic acid. Protons for the acetylated segment of chitosan was detected at around 2 ppm while that of the deacetylated glucosamine H2-H6 protons were evident at 3.0-3.8 ppm.

The amount of free amine groups (%) available for functionalisation or interaction with β-glycerophosphate to generate *in situ* gelling systems can then be determined by deduction of the obtained degree of acetylation values from 100%.

2.2.3. Preparation of CHI and CHIGP formulations

1% w/v LCHI in 12% w/v β-GP (LCHIGP), 1% w/v MCHI in 12% w/v β-GP (MCHIGP) and 1% w/v HCHI in 12% w/v β-GP (HCHIGP) formulations were prepared according to a previously reported procedure with modification [22]. Briefly, 1% w/v of chitosan solutions were prepared in 0.1 M acetic acid (buffered to pH 4 using 1 M potassium hydroxide) for 12 h at room temperature. The β-glycerophosphate solutions (48% w/v, 2 mL) were added to chitosan solutions (6 mL) in a dropwise manner under ice-cold conditions, giving a final β-GP concentration of 12% w/v and chitosan to β-GP volume ratio of 3:1. LCHI, MCHI and HCHI (1% w/v) solution in 0.1M acetic acid (pH 4) was also prepared for comparison.

2.2.4. Characterisation of CHI and CHIGP formulations

2.2.4.1. pH determination

The pH of CHI and CHIGP solutions was measured using a calibrated pH meter (SevenEasy Mettler-Toledo). Data was expressed as mean ± S.D (n=3).

2.2.4.2. Zeta potential measurement

The zeta potential of the formulations was evaluated based on our previously reported method [36]. Briefly, folded DTS-1070 capillary cells (Malvern, UK) were filled with 1 % w/v chitosan solutions or CHIGP formulations (sol form) and their zeta-potential values were determined at 25 and 37°C using the Zetasizer Nano-ZS (Malvern Instruments, UK). The samples were studied after 1 in 20 dilution to 0.05% w/v chitosan: 0.6% w/v β-glycerophosphate using ultrapure water. The instrument was set to operate at an absorbance of 0.01 and a refractive index of 1.59, which is the refractive index of aqueous chitosan solution. Measurements were conducted in triplicates with 50 sub-runs per reading.

2.2.4.3. Syringeability through the catheter experiment

The ability of the chitosan or CHIGP solution to pass through a catheter via a syringe was evaluated using a TA-XT Plus Texture Analyser (Stable Micro Systems, UK) operated at the compression mode. Male SpeediCath® 28414 CH 14/4.7 mm catheter (Coloplast A/S, Denmark) was used in this study. The experiment was carried out using a previously reported method with slight modification [37]. Briefly, the samples were packed into 2 mL plastic syringes connected to a catheter. The syringe was vertically secured while the probe was lowered until it had an initial contact with the syringe plunger. Then, the probe was lowered at a constant speed of 2 mm/s for 25 mm (Fig. 2.2). The work done to expel the syringe contents (work of compression) at 25°C was assessed as a function of the area under the force-distance curve recorded during the plunger compression (n=3). Sodium chloride (0.9% w/v) which is typically used in the urology clinic to prepare mitomycin-C solution for intravesical administration served as the control.
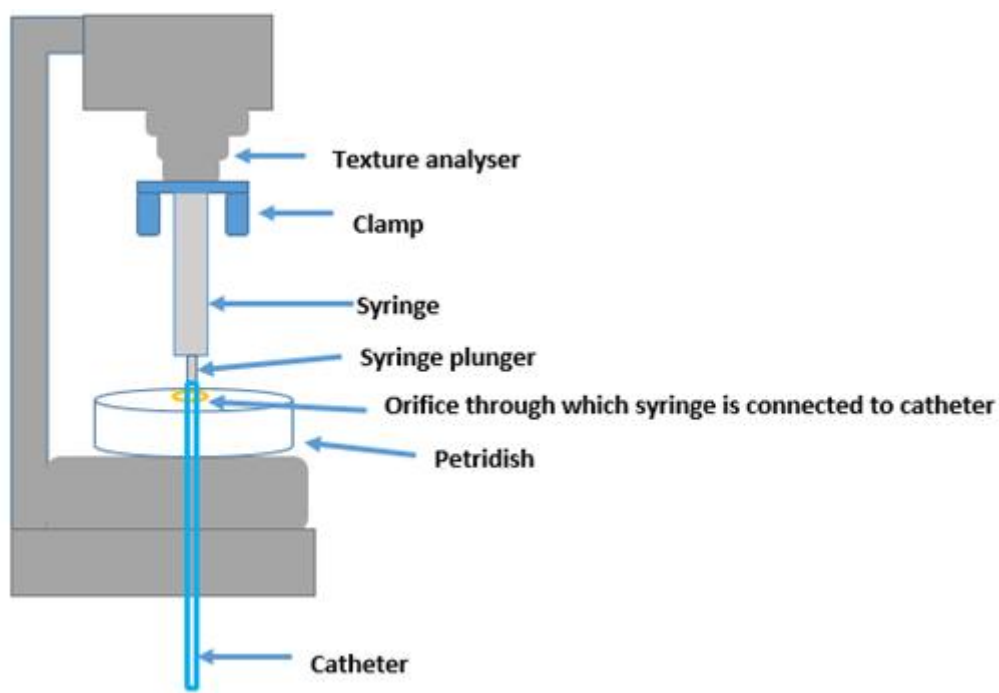
Fig. 2.2. Schematic representation of the texture analyser used to perform syringeability studies.

2.2.4.4. Gelation studies using a vial inversion method

The gelation time of the formulations was evaluated at 37°C using a modified version of a vial inversion method reported earlier [22] to determine the ease of gelation of the formulations within the bladder environment. Briefly, 3 mL LCHIGP, MCHIGP, HCHIGP samples were incubated in glass vials in a temperature-controlled water bath (Grant Instruments, Ltd, Cambridge) at 37°C. The vials were inverted at predetermined time intervals to evaluate the flow of the samples by visual examination. The gelation time was identified as the point where the formulations stopped flowing.

2.2.4.5. Rheology

Apart from evaluating the sol-gel transition temperature and gelation time of viscoelastic materials, rheological techniques also provide information on gel strength. The viscoelastic properties of the formulations were evaluated using an AR-2000ex rheometer (TA Instruments, UK) operated in the oscillatory mode using 40 mm parallel plate and a trim gap of 0.4 mm. The samples were steadily deposited onto the lower plate of the rheometer and the chosen trim gap was applied to reduce sample shearing, with the solvent trap in place during sample analysis to prevent sample loss. In order to determine the linear viscoelastic region of the samples at 25°C, a "strain sweep" was carried out where the magnitude of strain applied on the samples was steadily increased from 0.05 to 10%, at a constant frequency of 1 Hz. The strain where the

storage / elastic modulus (G') and loss / viscous modulus (G") was unchanged and independent of the prevalent frequency, was chosen for the frequency sweep studies.

2.2.4.5.1. Gel strength determination: Frequency sweep analysis

Based on the strain sweep analysis, 1% strain was chosen for the "frequency sweep" conducted at 25°C with samples scanned from frequency of 0.01 to 10 Hz to confirm optimal frequency for the rheological experiment. In order to evaluate the gel strength of the formulations, a "frequency sweep" was carried out at 37°C over the frequency range of 0.01-10 Hz, applying 1% strain. The gel strength of the samples was evaluated based on the ratio of their storage modulus (G') to loss modulus (G") at a frequency of 0.1 Hz. The higher the G'/G" value, the stronger the gel and vice versa, which implies that stronger gels are generated from samples whose elastic properties (G') are considerably greater than their viscous nature (G") [38].

2.2.4.5.2. Gelation temperature determination: Temperature ramp test

The gelation temperature of the samples was evaluated using a temperature ramp test with samples heated from 20 to 50°C at 1°C/min, frequency and strain of 1 Hz and 1%, respectively. The sol-gel transition temperature was the temperature where a rapid increase in the magnitude of G' relative to G" occurs as the samples are subjected to increasing temperature via the rheometer plate. The tangent of the loss modulus to storage modulus was also evaluated over the studied temperature range. LCHIGP, MCHIGP and HCHIGP samples were also evaluated for their storage modulus values at 37°C during the temperature ramp test as this rheological parameter depicted their elastic properties at physiological temperature which impacts their gelation potential.

2.2.4.5.3. Gelation time determination: Time sweep analysis

The gelation time of the samples was evaluated by carrying out a time sweep experiment, with samples maintained at 37°C for 30 min, applying a respective strain and frequency of 1% and 1 Hz. The gelation time is identified as the time where there is a sharp increase in the G' value relative to that of G" when samples are maintained at 37°C for predetermined length of time. The tangent of the ratio of the loss modulus to storage modulus over 30 min was also investigated. As some samples displayed similar gelation time during time sweep analysis with different gelation times recorded during the vial inversion method, the G' values of the CHIGP systems (which correlates with their elastic properties) after 30 min of maintaining them at 37°C were also evaluated.

2.2.5. Retention on porcine bladder: urine wash-out experiment

The artificial urine used for *ex vivo* porcine retention and drug release studies was prepared according to a previously reported method [39]. Briefly, the following compounds were dissolved in 2 L ultrapure water (18.2 MΩ): urea (24.27 g), uric acid (0.34 g), magnesium sulphate heptahydrate (1.00 g), sodium hydrogen phosphate (1.00 g), disodium phosphate (0.11 g), creatinine (0.90 g), sodium bicarbonate (0.34 g), sodium sulphate (2.58 g), disodium oxalate (0.03 g), trisodium citrate (2.97 g), sodium chloride (6.34 g), potassium chloride (4.50 g), ammonium chloride (1.61 g), and calcium chloride dihydrate (0.89 g). The resultant artificial urine had a final pH of 6.2±0.2.

The LCHIGP, MCHIGP, HCHIGP (containing 1% w/v CHI and 12% β-glycerophosphate) were mixed with 0.1% w/v fluorescein sodium solution in the ratio of 9:1 prior to the urine wash-out experiment. FITC-dextran 0.4% w/v served as the negative control while LCHI, MCHI and HCHI solutions (1 % w/v) were the positive controls.

The mucosal retention of fluorescein sodium on porcine urinary bladder mucosa, in the presence of chitosan and CHIGP samples was investigated using a fluorescent MZ10F microscope (Leica Microsystems, UK) coupled with an "ET GFP" filter and a Zeiss Imager with exposure time of 70 ms (A1/AxioCam MRm, 1296 x 966 pixels; 0.8 x magnification), according to a slightly modified method earlier developed by our group [40]. The study was carried out using freshly excised porcine urinary bladders (stored on ice during transport from the abattoir to the laboratory), refrigerated (4°C) and used within 24 h. Contact with the mucosal side of the bladder tissue was avoided during excision of the required bladder sections (about 1.5 x 2.5 cm) and rinsed with artificial urine solution (~ 3 mL) prior to tissue imaging. The bladder tissue was placed on a 75 mm x 25 mm glass slide and maintained in an incubator at 37°C during urine wash-out (Fig. 2.3). Microscopic images were recorded on each tissue section before and after applying ~ 50 µL of sample as well as after each of the five washing cycles with 10 mL artificial urine/cycle at 2 mL/min.
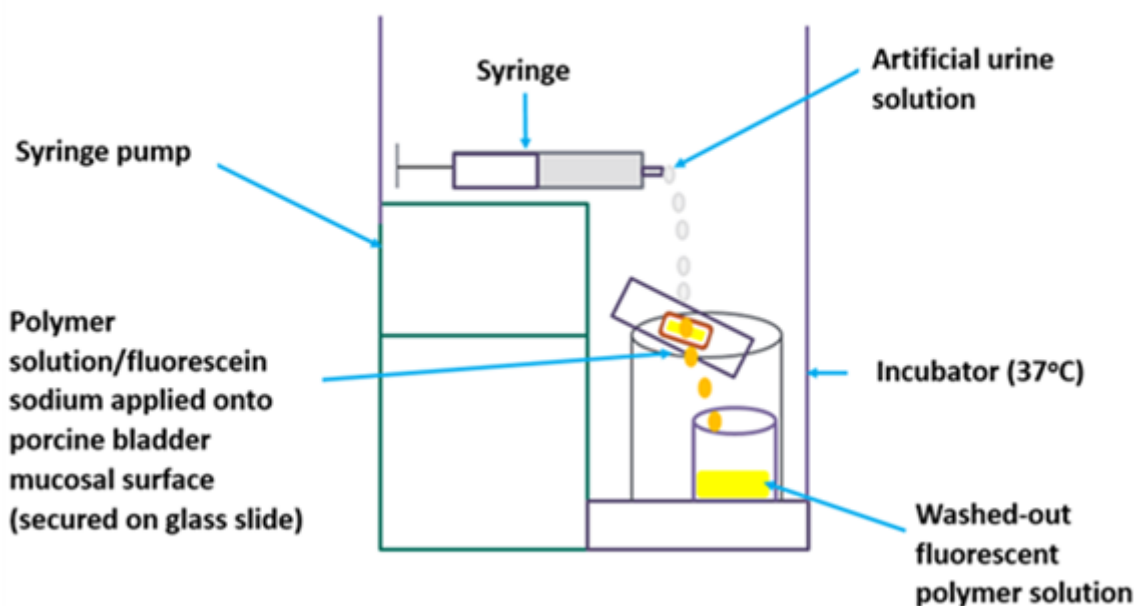
Fig. 2.3. Schematic set up for retention studies using porcine bladder tissues and artificial urine.

Image J software (Java 8, National Institute of Health, USA) was employed to evaluate the microscopic images, generating mean fluorescence values as a function of urine volume used for the wash-out. The normalised fluorescence intensity during each urine wash-out cycle is obtained by subtracting the background fluorescence intensity from the raw fluorescence intensity at the wash-out cycle of interest. The value "1" was used to depict the fluorescence intensity from the tissue before artificial urine wash-out. "WO_{50}" is defined as the volume of biologically relevant fluid (simulated urine) required to wash out 50 % of the fluorescent formulation from mucosal surface[40]. The WO_{50} values were determined using the polynomial fit of the wash-out graphs of the samples, which represents the volume of artificial urine needed to wash out 50% of the chitosan solutions and CHIGP formulations.

2.2.6. Mucoadhesive properties of the formulations

The TA-XT Plus Texture Analyser (Stable Micro Systems Ltd, UK) coupled with a 5 kg load cell was used as an additional technique to study the mucoadhesive properties of the formulations. Chitosan solutions (0.4% w/v) served as the positive controls while the negative control was dextran solution (0.4% w/v). Porcine bladder tissues were secured at the base of a cylindrical container. The bottom of the cylindrical container had a circular cut-out region (20 mm in diameter) exposing the mucosal surface of the bladder tissue. This container was screwed onto the probe of the texture analyser through a hole drilled on the lid of the container. Another bladder tissue was placed on a Petri dish and coupled onto the lower platform of the texture analyser, exposing bladder mucosal surface (20 mm in diameter) as shown in Fig. 2.4.
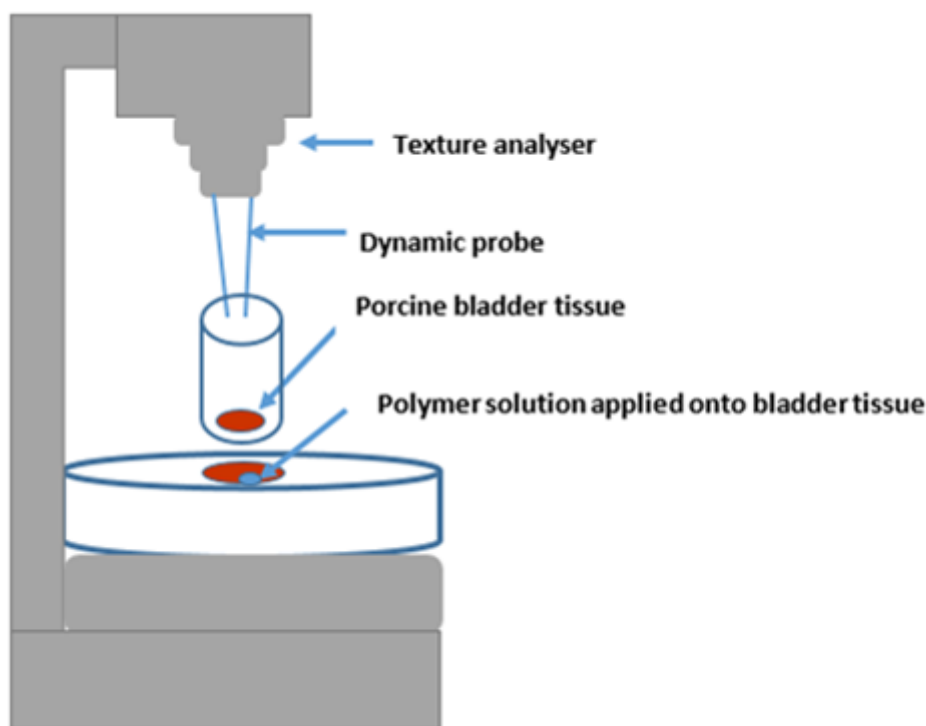
Fig. 2.4. Schematic representation of texture analyser demonstrating bioadhesion evaluation.

The tests were performed using an earlier reported equipment settings [41] with slight modification: pre-speed test 1.0 mm/s; test speed 0.1 mm/s; post-test speed 0.1 mm/s; applied force 0.05 N; contact time 120 s; trigger type auto; trigger force 0.1 N; and return distance of 10.0 mm. Bladder tissues were incubated at 37°C for 5 min prior to the study and the samples (0.4 mL) were applied onto the exposed area of the bladder tissue secured onto the lower platform of the texture analyser. The probe was then lowered such that the blank tissue comes in contact with the formulation applied onto the tissue secured on the lower platform for 2 min

after which the parameters of interest (detachment force and total work of adhesion) were determined as shown in Fig. 2.5. The Texture Analyser software (T.A. Exponent, Stable Micro Systems, UK) was used to record the force versus distance curves. The maximum force needed to detach tissue from formulation indicated the adhesive strength of the samples while the total work of adhesion was evaluated from the area under the force versus distance curve [41,42].
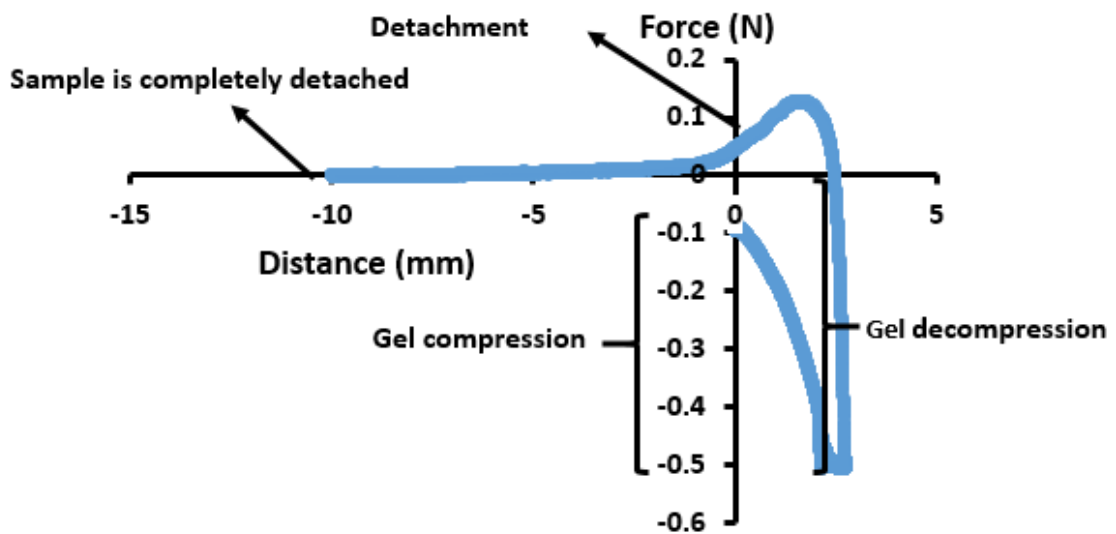
Fig. 2.5. Typical pattern of the detachment of hydrogels from porcine bladder mucosa during the mucoadhesion studies carried out using the texture analyser (Stable Micro Systems Ltd, UK).

2.2.7. Mitomycin-C *in vitro* release experiment

2.2.7.1. Preparation of mitomycin-C loaded CHI and CHIGP formulations

Mitomycin-C-loaded CHIGP formulations were prepared by dissolving 2mg mitomycin-C in 1%w/v chitosan solutions (1.5 mL) and vortexed for one minute before β-GP solution (48 % w/v, 0.5 mL) was added dropwise under ice-cold conditions and stirred for a further 30 min, producing a final β-glycerophosphate concentration of 12% w/v and drug concentration of 1 mg/mL (generating MMC/LCHIGP, MMC/MCHIGP, MMC/HCHIGP). This method was used because earlier chitosan studies reported that CHIGP formulations where β-glycerophosphate solution was added to the drug containing chitosan formulations exhibited superior sustained release profile relative to formulations, where drug was incorporated into the CHIGP mixture [24,43]. MMC-loaded LCHI, MCHI and HCHI samples were prepared as described above without

addition of β-glycerophosphate. Mitomycin-C solution (2 mL, 1 mg/mL) was prepared by dissolution of the drug in water for 30 min under ice-cold conditions.

2.2.7.2. Mitomycin-C *in vitro* release efficiency

In vitro drug release studies were carried out using a modified method used by Senyiğit et al. (2015) [44]. Briefly, 2 mL mitomycin-C solution, mitomycin-C loaded CHI and CHIGP formulations were loaded in dialysis membrane bags (12-14 kDa MWCO) and allowed to gel in a water bath at 37°C for 1 h. Mitomycin-C solution was not maintained in the water bath for 1 h as it had no possibility of forming a gel and the samples was simply transferred into the dialysis bag. The dialysis bags with the drug solution and gelled samples were placed in a stoppered 100 mL glass bottle containing 40 mL of artificial urine (pH 6.2 ± 0.2), maintained in a shaker water bath at 37°C (60 rpm). At predetermined time intervals (0, 0.5, 1, 2, 4, 6, and 24 hours), 1 mL of artificial urine was taken and replenished with same amount of fresh artificial urine. Drug content was analysed using previously reported HPLC-UV method with slight modification [45]. The HPLC instrument was coupled with the quaternary pump and VWD UV detector (Agilent, Germany) operated at 365 nm. The aliquot samples (10 μL) were injected into the reverse phase C_{18} column, 150 mm x 4.6 mm, 5 μM (Dionex™, Thermo Scientific, UK) maintained at 25°C. The mobile phase consisted of 83.5% of 25 mM sodium phosphate (pH 5.4) and 16.5% of methanol/acetonitrile (1:1), which was run in an isocratic mode at a flow rate of 1.5 mL/min, with run time of 15 min.

Mitomycin-C eluted at ≈ 10 min, depicted in Fig. 2.6. The standard curve of mitomycin-C was generated by analysing eight standard solutions of known concentrations (Appendix 2).
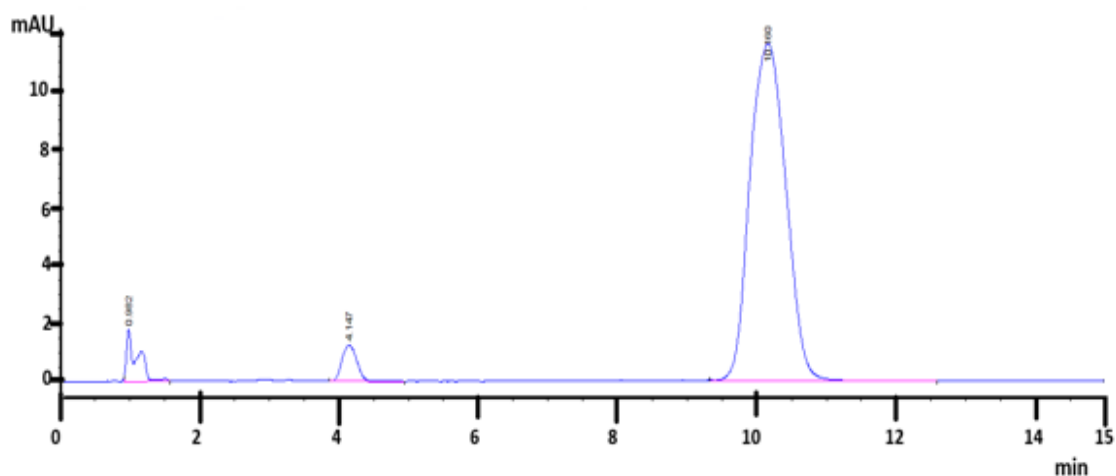
Fig. 2.6. Exemplar HPLC-UV chromatogram of mitomycin-C loaded CHI and chitosan/β-glycerophosphate systems, with mitomycin-C eluting at about 10 min and salt constituents of the artificial urine eluting at 0.9, 1.2 and 4 min.

2.2.8. Statistical analysis

All studies were carried out in triplicate, data expressed as mean ± SD and statistical differences were determined using t-test and One-Way ANOVA/ post-hoc Bonferroni test with GraphPad Prism (version 5.04, USA) with $p < 0.05$ implying statistical significance.

2.3. Results and discussion
2.3.1. Characterisation of chitosan and chitosan/β-glycerophosphate formulations

According to the gel permeation chromatography data, the low (LCHI), medium (MCHI) and high (HCHI) molecular weight chitosan grades were 62, 124 and 370 kDa, respectively, with polydispersity indices (PDI) of 3.43, 3.54 and 6.98, respectively, which matches manufacturer specifications. The gel permeation data is provided as Appendix 3. The degrees of deacetylation were 82 ± 1%, 72 ± 2%, and 71 ± 2%, respectively, which are in good agreement with those used by previous researchers to formulate CHIGP *in situ* gelling systems [25,46].

The focus of this study was to develop and characterise thermoresponsive and mucoadhesive formulations using chitosan/β-glycerophosphate mixtures. LCHIGP, MCHIGP and HCHIGP were formulated to contain 1% w/v chitosan, 12% w/v β-glycerophosphate and chitosan to β-glycerophosphate volume ratio of 3:1. The LCHI, MCHI and HCHI solutions had pH of about 4

and remained transparent liquid samples above 37°C. On the other hand, CHIGP formulations formed transparent solutions (pH 7.1-7.3) below 37°C, which is similar to the pH in the bladder environment, and turned into cloudy gels at 37 °C (Fig. 2.7). Chitosan/β-glycerophosphate mixtures are transparent below physiological temperature due to electrostatic attraction between negatively charged phosphate groups of β-glycerophosphate and positively charged ammonium groups of chitosan as well as hydrogen bonding between chitosan repeating units [47]. Alcohol groups of glycerophosphate provide additional hydration due to hydrogen bonding with water molecules, thereby preventing gel formation below physiological temperature [48]. An increase in temperature up to 37°C results in partial dissociation of hydrogen bonds with water molecules, leading to the formation of less hydrated gel.
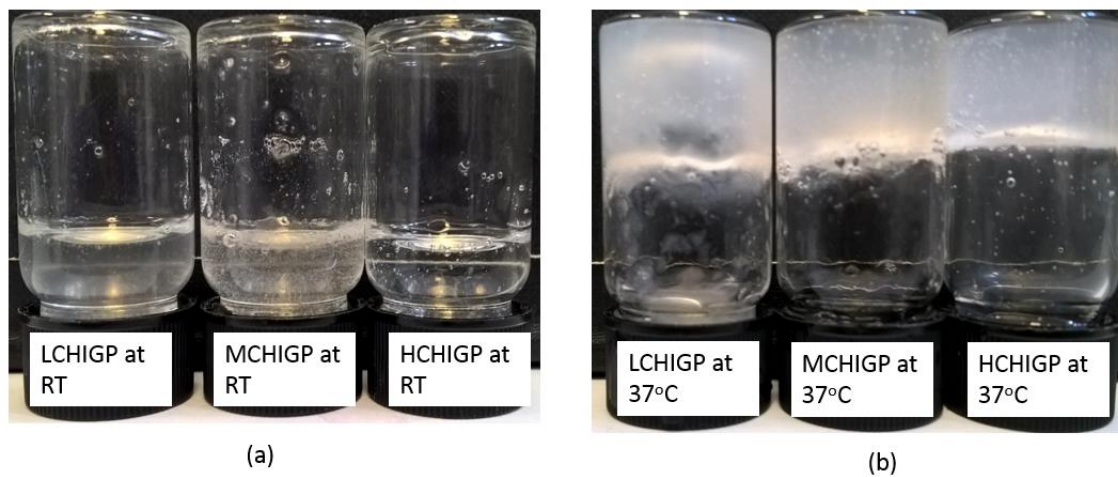
Fig.2.7. Exemplar images of chitosan/ß-glycerophosphate formulations at (a) room temperature and (b) 37°C.

All chitosan/β-glycerophosphate mixtures showed fast in situ gelation as detected using the vial inversion method. MCHIGP and HCHIGP formulations formed a physical gel within 7 ± 2 min and 5 ± 1 min, respectively, while LCHIGP mixture formed a very weak gel at 15 ± 5 min that eventually collapsed upon further incubation at 37°C (Fig. 2.7).

Despite the fact that LCHI had the greatest extent of deacetylation and a favourable pH of about 7 (Table 2.1), its gelation was not sustained. Chitosan intermolecular interactions occur via entanglements, which becomes more pronounced with increased chitosan molecular weight [21]. One of the reasons for weak gel formation for LCHIGP is the reduced degree of entanglements in LCHIGP due to its lower chitosan molecular weight, resulting in lower viscosity at increased temperature [21]. This finding is in contrast to the study by Khodaverdi et al. (2012) [22], who reported fast onset of gelation with highly deacetylated chitosan as a result of their

assessment of medium weight chitosan. This finding proved that the molecular weight of chitosan played a more remarkable influence on their gelling properties than the degree of deacetylation of chitosan used in preparing the *in situ* gelling formulations.

2.3.2. Rheological studies of gelation

This study was carried out to understand the structural and dynamic features of chitosan/ß-glycerophosphate formulations. During rheological analysis, samples were directly in contact with the heated rheometer plate at the temperature of interest, which simulated the physiological conditions of the bladder. A strain of 1% and frequency of 1 Hz was selected for the current rheological study as the storage modulus (G') and loss modulus (G") of the samples remained constant upon application of that magnitude of strain and frequency to the samples.

Frequency dependent rheological profiles of 1 % w/v pure chitosan solutions are characteristic of viscous liquids, where G' is lower than G" at all studied frequency ranges. This behaviour was evident with all studied chitosan samples (LCHI, MCHI and HCHI) as G" (viscous property) remained greater than G' (elastic nature) at 25 and 37°C during frequency sweep analysis, inferring the absence of gelation (data not shown). This data is in good agreement with the report by Supper et al (2013) [23], where G' was lower than G" during frequency sweep studies carried out with 1.5 % w/v chitosan solutions at 20, 30 and 40°C. During frequency sweep of 1% w/v of LCHI, MCHI and HCHI solutions from 0.1 Hz to 10 Hz, they all exhibited rheological profile where their loss modulus G" values were greater than storage modulus G' values, though differed in terms of the magnitude of storage and loss modulus (Appendix 4).

Gels typically display solid-like mechanical profiles, where the storage modulus (G') is greater than the loss modulus (G") throughout the evaluated frequency ranges. LCHIGP, MCHIGP and HCHIGP displayed gel-like behaviour at the onset of all rheological analysis (Fig. 2.8). This behaviour is desirable as it supports the rapid gelation of the samples at physiological temperature. Moreover, drug incorporation into the CHIGP formulations as well as urine presence in the bladder will potentially increase their gelation temperature and time.
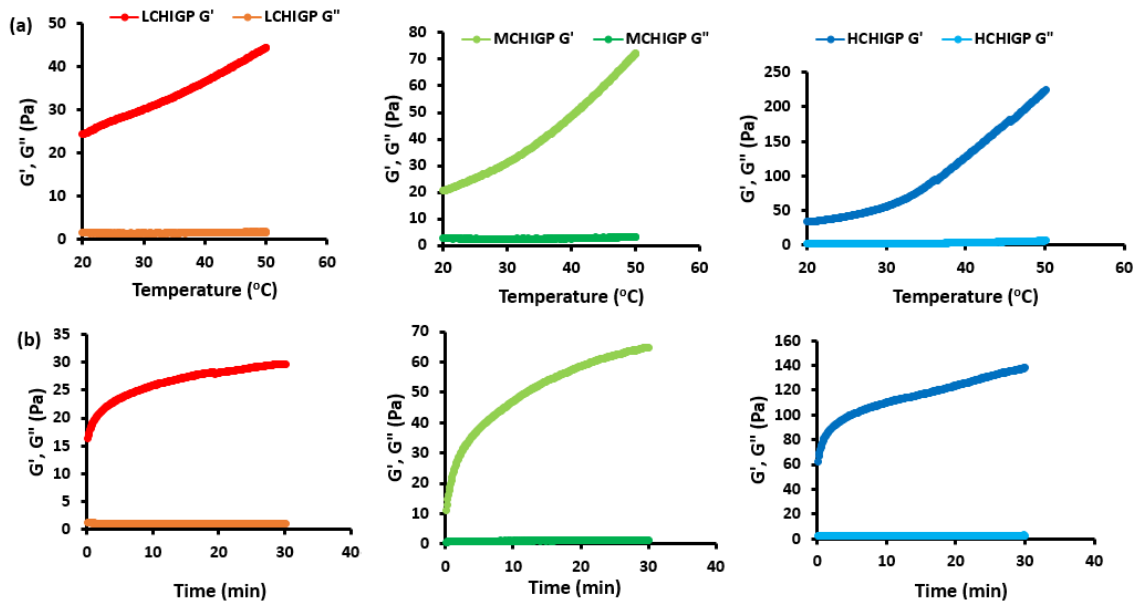
Fig. 2.8. Exemplar rheological profiles of LCHIGP (red), MCHIGP (green) and HCHIGP (blue) showing (a) the temperature-dependent changes in viscoelastic properties at ramp rate 1°C/min; (b) time-dependent viscoelastic changes of samples maintained at 37°C for 30 min, with G' persistently greater than G" for all studied samples, though differ in terms of the magnitude of their G' values.

With frequency sweep analysis at 37°C, the greater the similarity in the values of G' and G", the weaker the gel. On the other hand, stronger gels exhibit rheological profiles, where the elastic modulus (G') is greater than the viscous modulus (G") [38]. HCHI based formulations displayed superior gel strength (in terms of their G'/G" values at frequency of 0.1 Hz during frequency sweep at 37°C) relative to MCHI and LCHI based samples (Table 2.1). There was a statistically significant difference between the gel strength of LCHIGP and MCHIGP as well as between LCHIGP and HCHIGP ($p < 0.05$), but the gel strength of MCHIGP and HCHIGP was similar ($p > 0.05$). This finding indicated that both MCHIGP and HCHIGP formulations may be potentially less susceptible to rapid erosion by the urine in the bladder.

Table 2.1

Rheological properties of Chitosan/ß-glycerophosphate samples

Samples	pH	Frequency sweep, 37°C	Temperature ramp (20-50°C, 1°C/min)			Time sweep for 30 min at 37°C (Pa)		
		G'/G" ratio at 0.1 Hz	Gelation temp (°C)	G' at 37°C (Pa)	Tan δ at 37°C	Gelation time (min)	G' after 30 min at 37°C (Pa)	Tan δ after 30 min at 37°C
LCHIGP	7.4±0.2	12.9±1.8	30.4±0.3	38.5±3.5	0.04±0.01	1.6±0.3	30.2±0.3	0.03±0.01
MCHIGP	7.5±0.2	15.8±0.1	29.8±0.2	41.1±2.2	0.03±0.01	1.4±0.3	59.7±7.1	0.02±0.03
HCHIGP	7.3±0.2	16.7±0.2	29.6±0.1	95.8±5.5	0.03±0.01	1.0±0.1	138.0±7.9	0.02±0.02

* Higher G'/G" values at 0.1 Hz (frequency sweep at 37°C) infer stronger gels; storage modulus (G') values at 37°C during temperature ramp test, G' after 30 min during the time sweep test also depict elastic property and correlate with their ease of gelation. Loss factor or tan δ was calculated as tangent of G"/G' ratio, when these values are closest to zero this indicates greater ease of gelation, n = 3 (mean±SD).

The temperature ramp analysis was conducted from 20 to 50°C because this range was sufficient to study the transition of the drug carrier from the sol (≤ 25°C) to the gel state (25-37°C). Formulations intended for intravesical delivery ideally should have a gelation temperature of 30 to 36°C [49]. This ensures that such drug carriers remain liquid at room temperature during injection through the catheter and only transform into a gel within the bladder. *In situ* gelling systems with gelation temperature above 37°C are not suitable for intravesical administration as they could be readily washed out of the bladder during urine voiding since they will remain liquid at physiological temperature.

For predominantly viscous materials, G" is initially lower than G' during temperature ramp test but as temperature increases, G" increases at a faster rate than G' and the sol-gel transition temperature is attained at the point of G" and G' intersection [50]. Alternatively, gelation temperature is identified as the temperature where there was a greater growth rate of G' (elastic property) relative to the G" (viscous property) without samples necessarily displaying cross-over of G' and G" [20]. This method of evaluating gelation temperatures may be explored for CHIGP formulations with medium viscosity showing a rheological profile with storage modulus G' greater than the loss modulus G" at the onset of the "temperature ramp" test with no possibility of G' and G" intersection at any studied temperature (Fig. 2.8a). Moreover, some

researchers have acknowledged that G'/G" cross-over point during temperature ramp test may not depict the actual gelation temperature of the material [21,51].

The temperature ramp and time sweep tests for chitosan solutions were not carried out as the delivery system was not *in situ* gelling in nature. Our current study revealed that the temperature ramp profiles of some formulations may imply that they have similar gelation temperatures, which may not necessarily correlate with their ease of gelation using a different method of evaluating their thermogelation such as vial inversion studies at 37°C. The gelation temperatures of LCHIGP, MCHIGP and HCHIGP formulations determined as a function of the temperature at which there was a rapid increase in G' during temperature ramp test were 30.4±0.3°C, 29.8±0.2°C, and 29.6±0.1°C, respectively (p >0.05). LCHIGP, MCHIGP and HCHIGP displayed similar gelation temperature based on the temperature at which there was a rapid change in their tan δ values (Figure 2.9). So, there was the need to define the elastic potential of our CHIGP formulations based on their G' and tan (delta) values at physiological temperature of 37°C (Table 2.1). HCHIGP displayed significant greater extent of elastic features (95.8±5.5 Pa) relative to MCHIGP (41.1±2.2 Pa) and LCHIGP (38.5±3.5 Pa) (p<0.05). Similarly, tan δ values of MCHIGP and HCHIGP were smaller than that of LCHIGP, inferring that chitosan molecular weight has substantial effect on the ease of gelation of CHIGP *in situ* gelling systems despite the fact that MCHIGP and HCHIGP displayed similar tan (delta) values during temperature ramp and time sweep test.

Based on rheological time sweep at 37°C for 30 min (Fig. 2.9b), the gelation times of LCHIGP, MCHIGP and HCHIGP were found to be 1.6, 1.4 and 1.0 min, respectively, with HCHIGP forming gel most readily. As there was no significant differences in their gelation time based on their sharp increase in G' relative to G" as well as their tan δ values at any particular time, G' values of the gels as well as their tan δ values were determined after maintaining the samples at 37°C for 30 min. HCHIGP displayed a 2.3-fold and 4.3-fold increase in elastic features, relative to MCHIGP and LCHIGP, respectively. This result suggested that chitosan molecular weight influenced the gelation potential and gel strength of the formulations with β-glycerophosphate.

The gelation time for MCHIGP and HCHIGP formulations determined using rheological method is in good agreement with that of vial inversion data. In contrast, the results observed for LCHIGP differs as it formed gel less readily and the gel reversed to its sol state upon prolonged incubation at 37°C (Fig. 2.7) whereas temperature ramp and time sweep studies indicated that it displayed similar gelation temperature and time with that of MCHIGP and HCHIGP formulations. Nevertheless, gel strength evaluation confirmed that LCHIGP was the weakest gel.

It can be concluded that the elastic modulus (G') measured at 37°C may be a useful method for evaluating the gelation potential of CHIGP formulations, in addition to the already established techniques used in rheology to determine gelation temperature and time: (1) G'/G" intersection evaluated during temperature ramp and time sweep test; (2) temperature and time where there is a rapid increase in G' relative to G".

It should be noted that all these rheological experiments were performed with the samples that were not diluted with urine. Following the intravesical administration of these *in situ* gelling formulations, a dilution with urine is expected. This could potentially affect the gelation time. The effect of dilution of these formulations with urine was evaluated in a later section, describing retention on the bladder mucosa.
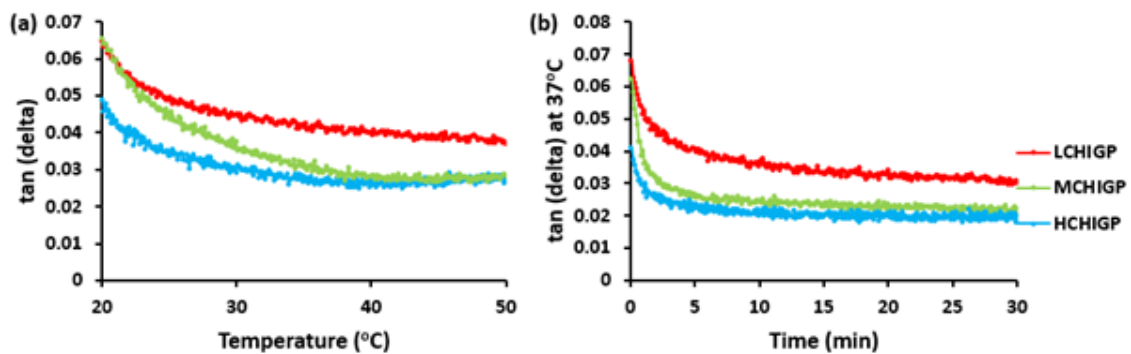
Fig. 2.9. Tan (delta) rheological profiles for temperature-dependent (a) and time-dependent (b) changes of LCHIGP (red), MCHIGP (green) and HCHIGP (blue), with HCHIGP gels displaying the tan delta values closest to zero, inferring that they exhibited the greatest elasticand gel properties.

2.3.3. Syringeability through the urethral catheter

Syringeability is a critical parameter for evaluating the efficiency of intravesical dosage forms. A formulation that could flow through the catheter readily to quickly reach the bladder is one of the desirable attributes for intravesical delivery. Since administration of intravesical formulations is usually carried out at ambient temperature, the syringeability test of our samples was conducted using a texture analyser at 25°C.
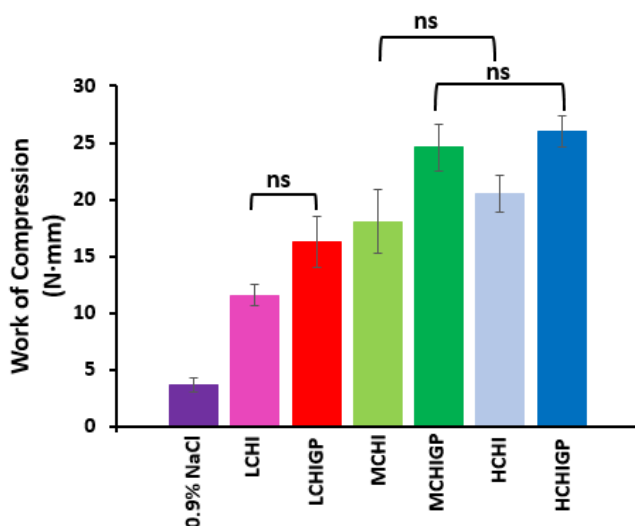
Fig. 2.10. Syringeability of chitosan and chitosan/ß-glycerophosphate formulations evaluated as the work done to expel samples from 2mL plastic syringes into the urethral catheter. Experiment was conducted at 25°C using the texture analyser (Stable Micro Systems Ltd, UK), mean±SD, n = 3. Syringeability is inversely proportional to the work of compression; there was significant statistical difference in the work of compression values between all groups of samples ($p < 0.05$) except those designated with "ns". Sodium chloride (0.9%) served as the control.

Figure 2.10 shows the values of work required to release chitosan and CHIGP formulations from the syringe through a catheter, which is inversely proportional to syringeability of these formulations. The values for the work of compression of 0.9% NaCl, LCHI, MCHI, HCHI, LCHIGP, MCHIGP, HCHIGP were 3.75±0.62 N·mm, 11.60±0.94 N·mm, 18.07±2.80 N·mm, 20.54±1.63 N·mm, 16.29±2.24 N·mm, 24.62±2.05 N·mm, 26.03±1.38 N·mm. Sodium chloride (0.9% w/v), which is typically used to dissolve mitomycin-C for intravesical application displayed the lowest work of compression amongst all studied samples, implying that it was the most syringeable. There was statistically significant difference between the work of compression of 0.9% sodium chloride solution and all the other studied samples ($p < 0.05$). This may be related to a gradual growth in chitosan molecular weight of 62 kDa, 124 kDa and 370 kDa for LCHI, MCHI and HCHI, respectively, as greater molecular weight of macromolecules results in higher solution viscosity

and better resistance to flow. Also, the decreased syringeability may become less remarkable with further increase in chitosan molecular weight evident with MCHI and HCHI based samples. It should be noted that all values of the work of compression determined for the CHI and CHIGP systems (14-26 N·mm) were lower than the syringeability of chitosan and poloxamer gel based formulations reported in the study of Senyiğit et al (30-130 N·mm), indicating that our formulations are also syringeable.

2.3.4. Retention study on bladder tissues

The ability of polymeric dispersions to flow and adhere onto mucosal membranes is dependent on the surface energy between the drug carrier and mucosal surface. *In situ* gelling systems possess lower surface energy than that of the mucosal surfaces and readily spread over them, thereby maximising the contact area and optimising adhesion [52]. Thus such systems are desirable to promote urothelial mucoadhesion and resistance to urine wash-out.

Ex vivo porcine urinary bladder retention studies were performed with fluorescein sodium as a model compound formulated using both chitosan solutions and their mixtures with ß-glycerophosphate. FITC-dextran (3-5 kDa) was also used in these experiments as a negative control due to the well-known poor adhesiveness of this oligomeric polysaccharide to mucosal tissues [53].

Based on the polynomial fit of the mucosal fluorescence retention versus urine volume graph (Fig. 2.11), the WO_{50} values for FITC-dextran, LCHI, MCHI, HCHI, LCHIGP, MCHIGP and HCHIGP were 7±1, 8±1, 9±1, 14±3, 6±1, 8±1, and 9±1 mL, respectively.
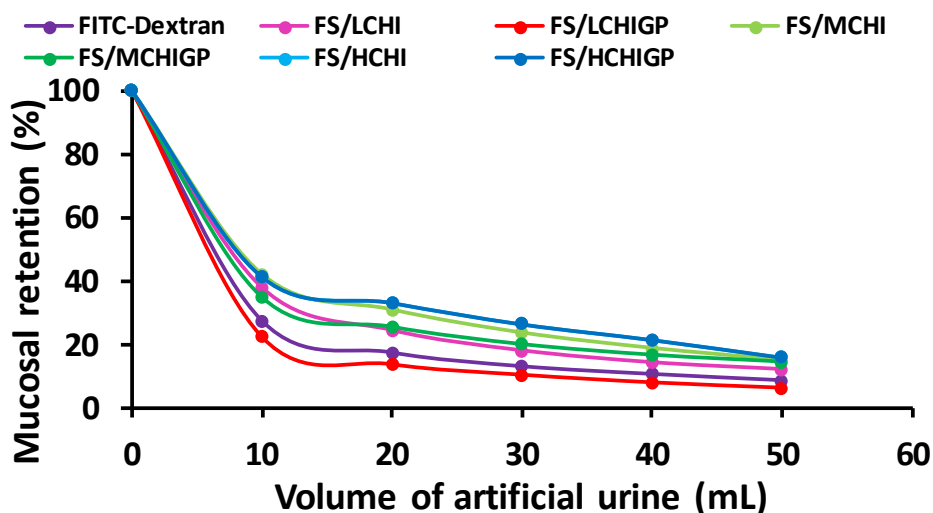
Fig. 2.11. The mucosal fluorescence retention profile of FITC-dextran, chitosan and chitosan/β-glycerophosphate systems on porcine bladder tissues evaluated using imageJ software and WO_{50} values calculated based on the polynomial fit of the graphs; n=3, error bars not shown to prevent overlap.

Figure 2.12 presents the results of these wash off experiments in the form of fluorescent images. The relative fluorescence intensity values were used to calculate the wash out$_{50}$ values (WO_{50}) of the formulations. It is clearly seen that FITC-dextran was removed from the surface of bladder mucosa with the first 10 mL of simulated urine, which is consistent with our previous findings [36,40,54]. Formulations composed of chitosans and fluorescein sodium demonstrated excellent retention performance on the bladder surface with HCHI displaying superior resistance to urine wash out compared to its lower molecular weight analogues (p<0.05). The formulations containing ß-glycerophosphate displayed reduced mucoadhesive properties relative to their respective chitosan solutions (Fig. 2.12). For example, WO_{50} value for HCHI (14 mL) is significantly higher compared to its HCHIGP formulation (9 mL). This was a surprising result as one would have expected the combination of excellent mucoadhesive properties of chitosan with formation of a gel *in situ* would provide a synergistic or enhanced retention effect on mucosa [55]. However, this is not the case.

There was no significant difference between the fluorescence retention profiles of FITC-dextran and FS/LCHI, FS/LCHIGP, FS/MCHIGP and FS/HCHIGP after washing out with 10 mL of artificial urine ($p > 0.05$), but the mucoadhesiveness of FS/MCHI and FS/HCHI was more than that of FITC-dextran depicted by fluorescence intensity (Fig. 2.12a & b) ($p < 0.05$). With 20 mL artificial urine washing, the fluorescence retention of FS/HCHIGP was greater than that of FITC-dextran ($p < 0.05$). The significant difference between the mucoadhesiveness of FITC-Dextran and MCHIGP was evident after 4 washing cycles with 40 mL artificial urine ($p < 0.05$). The mucoadhesive properties of FS/LCHI and FS/LCHIGP were similar to that of FITC-dextran after washing with 50 mL artificial urine (Fig. 2.12a & b).
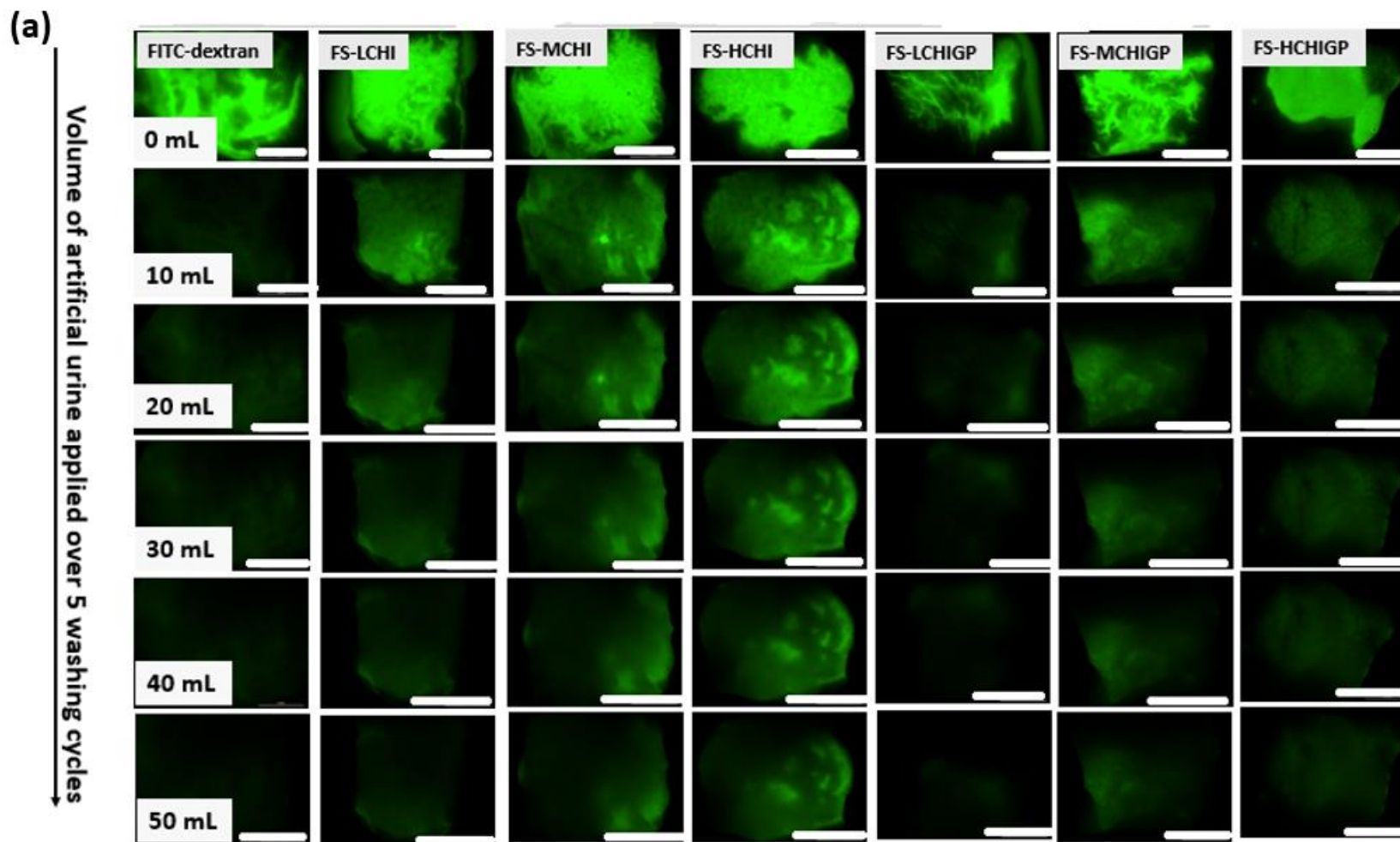
Fig. 2.12a. Retention study of fluorescein sodium (FS) formulations and FITC-dextran as a negative control: (a) Exemplar microphotographs showing wash-out from porcine urinary bladder tissue with artificial urine solution over 5 washing cycles, scale bar is 2 mm

83
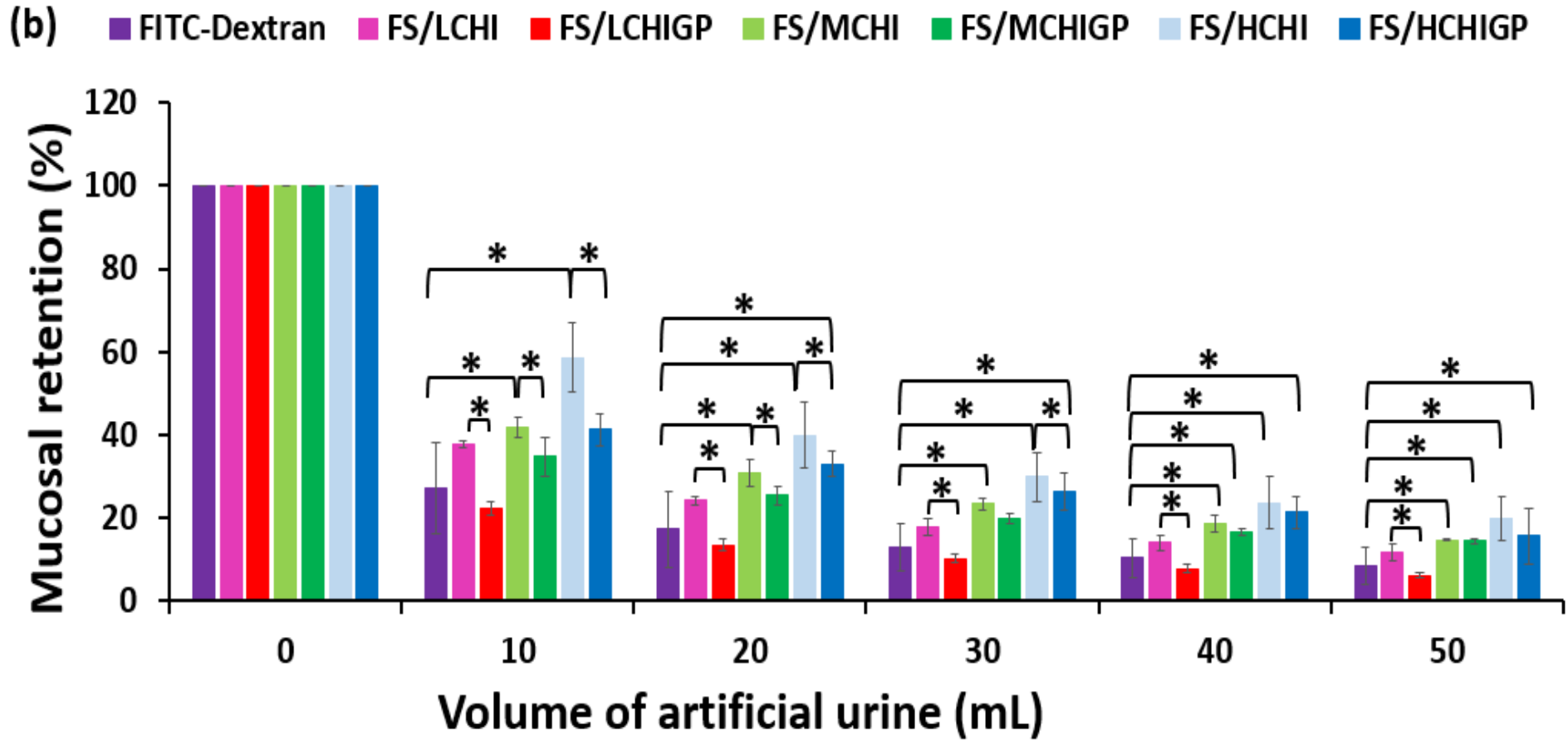
Fig. 2.12b. Retention study of fluorescein sodium (FS) formulations and FITC-dextran as a negative control: Mucosal retention on porcine urinary bladder tissues. Result presented as mean ± standard deviation, n = 3; Asterisk (*) depicts statistically significant differences between samples (p < 0.05).

FS/LCHI, FS/LCHIGP and FS/MCHIGP displayed similar WO_{50} values with FITC-dextran (p > 0.05). On the other hand, FS/MCHI, FS/HCHI and FS/HCHIGP were more mucoadhesive than FITC-dextran based on their WO_{50} values (Fig. 2.13). This finding demonstrated that high molecular weight chitosan may be the most efficient grade to formulate CHIGP delivery systems for intravesical administration.
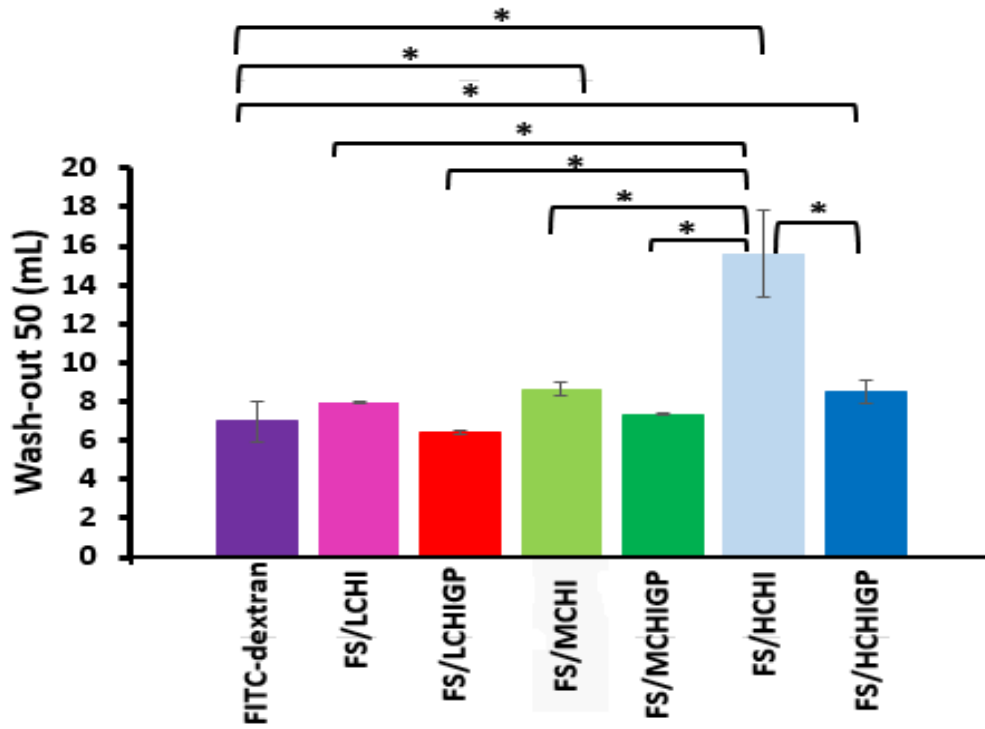
Fig. 2.13. Artificial urine wash-out-50 (WO_{50}) values determined for different formulations. Results presented as mean ± standard deviation, n = 3; Asterisk (*) depicts statistically significant differences between samples (p < 0.05).

2.3.5. Mucoadhesive properties tested using tensile method

The tensile method was used to probe the mucoadhesive properties of the formulations further [5]. As it was expected, dextran as the non-mucoadhesive control displayed the lowest force of detachment and total work of adhesion values (Fig. 2.14). Pure chitosan samples had a greater mucoadhesive performance compared to CHIGP formulations. For example, the values of maximal detachment force and total work of adhesion determined for HCHI (0.41±0.02 N and 0.56±0.13 N·mm, respectively) were significantly greater (p<0.05) than the respective values for HCHIGP (0.13±0.01 N and 0.35±0.02 N·mm, respectively).
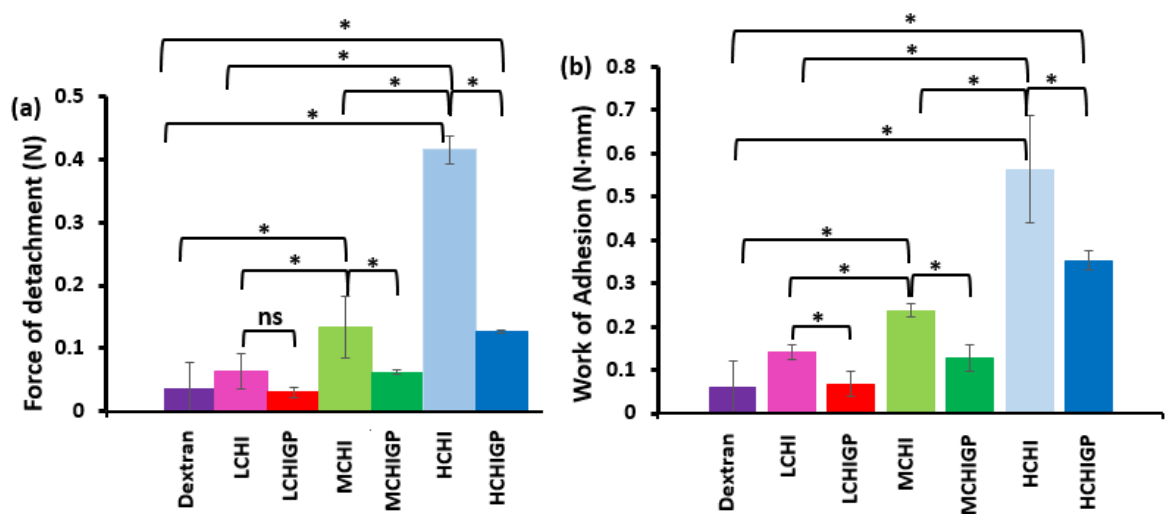
Fig.2.14. Adhesion of CHI (1% w/v) and CHIGP samples to porcine bladder mucosa using tensile method: (a) force of detachment values, (b) work of adhesion values. Result presented as mean ± standard deviation, n = 3; Asterisk (*) implies statistically significant difference between data sets (p<0.05).

The detachment characteristics of all formulations correlate well with their resistance to urine wash-out: the use of both methods indicates greater mucoadhesiveness of chitosan samples compared to their mixtures with ß-glycerophosphate.

To get a further insight into the reasons why chitosan solutions alone show superior retention and mucoadhesive properties compared to the formulations of chitosan with ß-glycerophosphate, additional experiments were performed by determining zeta potential of all samples at 25°C and 37°C (Table 2.2). The chitosan formulations displayed relatively high positive values of zeta potential (ZP) due to the cationic nature of chitosan associated with the presence of free amino groups that facilitates electrostatic interactions with the negatively charged bladder mucosal surfaces [36]. For the formulations with β-glycerophosphate, ZP values

significantly decreased (p < 0.05) in comparison. This trend was observed both at 25°C and 37°C. A significant reduction in ZP values is related to partial neutralisation of cationic chitosan macromolecules with anionic β-glycerophosphate, which is in good agreement with the literature data [56].

Table 2.2

Zeta potential values of chitosan solutions (CHI) and chitosan/ß-glycerophosphate mixtures (CHIGP) at 25°C and 37°C.

Chitosan Samples	Zeta potential, 25°C (mV)		Zeta potential, 37°C (mV)	
	CHI	CHIGP	CHI	CHIGP
Low	43.9±2.7	1.5±0.1	46.0±1.6	1.1±0.2
Medium	50.1±7.8	1.9±0.1	50.0±2.7	1.2±0.2
High	56.6±2.3	2.3±0.1	51.8±0.3	1.6±0.2

It is well established that excellent mucoadhesive properties of chitosan are related to the interactions of its macromolecules with negatively charged mucin [7]. The nature of these interactions is predominantly electrostatic; however, the contribution of hydrogen bonding and hydrophobic effects cannot be completely disregarded [35]. A reduction in the positive values of zeta potential observed in the case of CHIGP formulations compared to chitosan alone may well be the main reason for their decreased interactions with bladder mucosal surfaces. A second factor that could possibly contribute to weakening of mucoadhesive performance is the physical cross-linking of chitosan macromolecules caused by their interactions with β-glycerophosphate. This cross-linking could restrict diffusion of chitosan macromolecules and prevent them from formation of an interpenetrating layer with mucins present on the mucosal surface. According to the diffusion theory of mucoadhesion related to the penetration of the polymeric dosage form into the mucus gel as well as diffusion of mucin into the dosage form generating interpenetration layers, this could reduce the mucoadhesive properties of these formulations [5].

2.3.6. Mitomycin-C *in vitro* release

Dialysis technique using semi-permeable membrane is an established method for drug release studies in intravesical drug delivery [44,57]Mitomycin-C (MMC) was chosen for the current study as a drug that is typically used intravesically to treat superficial / non-invasive bladder cancer.
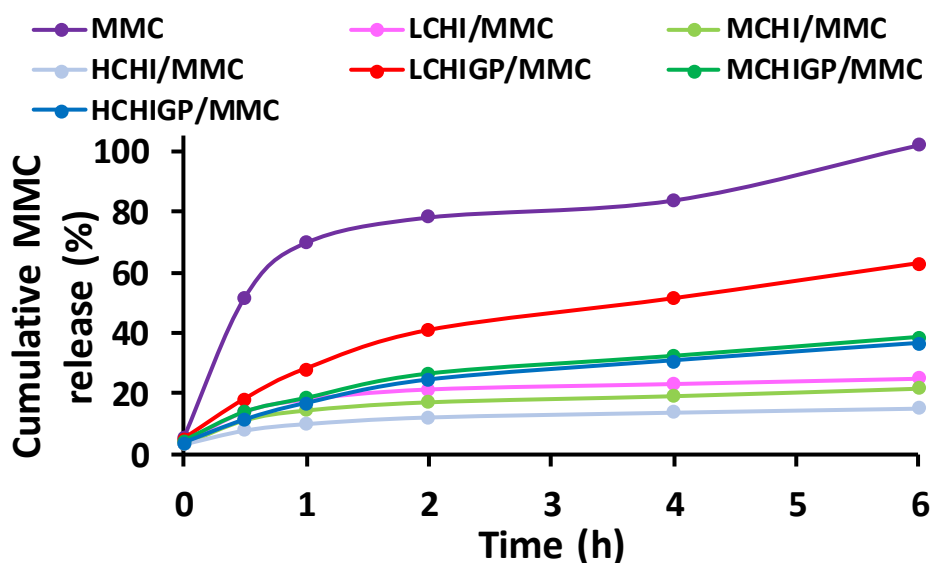
Fig. 2.15. *In vitro* release profiles of mitomycin-C from free drug solution, chitosan solutions and CHIGP formulations in pH 6.2 artificial urine. Results are presented as mean values (n = 3); error bars are not shown to avoid overlapping for some samples.

Figure 2.15 shows the release profiles from drug solution, CHI, and CHIGP formulations. Within the first 30 min, the release of mitomycin-C from the free drug solution, LCHI, MCHI, HCHI, LCHIGP, MCHIGP and HCHIGP samples was 52±21, 14±2, 11±2, 8±1, 18±2, 14±1 and 11±1%, respectively. Expectedly, drug release from free mitomycin-C solution was greatest after 30 min, which was more significant than that of the CHI and CHIGP formulations ($p < 0.05$). After 6 h, the drug release profile for free drug solution was 100% and it was statistically similar to that of LCHIGP ($p > 0.05$), inferring that *in situ* gelling systems based on low molecular weight chitosan had the least ability to sustain drug release amongst the CHIGP samples. As expected, the release from the free drug solution was faster compared to polymer-containing formulations, which is consistent with the literature on release studies involving small molecules (see [43] as an example). There was no significant difference in the drug release pattern of the pure chitosan formulations (LCHI, MCHI and HCHI), as compared at 0.5 h and 6 h ($p > 0.05$). This behaviour is

not ideal for intravesical dosage forms where it is desirable for a substantial amount of the therapeutic dose to be available after transurethral resection of the tumours, for superficial bladder cancer management. In contrast, there was some influence of chitosan molecular weight on the drug release from CHIGP samples. For example, a cumulative release of 63±23%, 39±20% and 37±17% of the drug was observed over 6 h release period for the LCHIGP, MCHIGP and HCHIGP samples, respectively. This finding is in good agreement with the report by Zhou et al (2008) [43], where high molecular weight chitosan based gels (CS-αβ-GP) exhibited slower adriamycin release compared to low molecular weight chitosan polysaccharide based formulations (50% vs 70%) over 24 h. There was statistically significant difference in the cumulative amount of drug released from MCHIGP and HCHIGP compared to the free drug solution ($p<0.05$). The drug release behaviour of the samples beyond 6 h was not studied because mitomycin-C degraded with prolonged exposure to artificial urine [45]. The drug degradation is due to the hydrolysis of its labile ester bond in the aqueous medium. Nevertheless, drug degradation in the physiological fluid may be avoided as its release and diffusion across underlying diseased tissues will take place quickly.

MMC/LCHIGP displayed 1.6-fold and 1.7-fold increase in the amount of mitomycin-C released, relative to MCHIGP and HCHIGP, respectively, after 6 h release period, inferring that LCHIGP favoured an overall rapid drug release relative to MCHIGP and HCHIGP. The amount of MMC released from chitosan decorated poly-Ɛ-caprolactone nanoparticles evaluated by Bilensoy et al., (2009) [44] was 80% over a 6 h release period using phosphate buffer pH 6.0. In a subsequent report, *in vitro* studies were carried out by the same group using a different release medium of citrate buffer but having similar pH 6.0 [32], and 89%, 92% and 91% of MMC were respectively released in 15 min from chitosan, poly-L-lysine-coated and chitosan coated poly-Ɛ-caprolactone nanoparticles, inferring that the type of release medium used modulates the release profile of the nanoparticles rather than their pH values. Moreover, the use of physiologically relevant release medium like simulated urine used in the current study is valuable to generate reliable drug release data. These drug carriers exhibited fast drug release, which will necessitate frequent dosing which is not convenient for bladder cancer patients as their therapy is carried out in the hospital. In contrast, our MMC/MCHIGP and MMC/HCHIGP favoured sustained drug release as 39 and 37% of the drug were respectively released in 6 h from these formulations. This may prolong dosing interval and minimise bladder cancer recurrence. On the other hand, MMC/LCHIGP, with 63% of drug released within 6 h, displayed a comparable release profile with the best chitosan based formulations (chitosan coated PCL nanoparticles) reported by Bilensoy et al., (2009) [44].

2.4. Conclusions

In situ gelling systems composed of chitosan of three molecular weights and β-glycerophosphate were formulated in this work and studies for their potential applicability for intravesical delivery of mitomycin-C to treat bladder cancer were carried out. These formulations were evaluated for their ability to form gels *in situ*, rheological properties, syringeability, retention on and adhesion to the urinary bladder mucosa as well as the drug release *in vitro*.

The molecular weight of chitosan was found to modulate syringeability, gelation, mucoadhesive properties and drug release profiles of the formulations. Chitosan with the highest molecular weight (370 kDa) combined with β-glycerophosphate displayed superior resistance to urine wash-out compared to the formulations with lower molecular weights; it also provided controlled release of mitomycin-C over a 6 h period.

This work showed that the mucoadhesive properties of chitosan are reduced by its formulation with β-glycerophosphate. This is related to the reduction in positive values of zeta potential for these formulations compared to chitosan alone. So, in terms of the retention of the formulations in the bladder, the use of *in situ* gelling dosage forms composed of chitosan and β-glycerophosphate did not show any superior mucoadhesive benefit over simple solutions of chitosan without gelation properties. However, the drug release pattern from chitosan solutions demonstrated that the local availability of mitomycin-C in the bladder may be limited as a maximum of 15.1 to 24.9% of the drug was released over the study period. Thus, HCHIGP still demonstrated superior urothelial mucoadhesive properties relative to LCHIGP and MCHIGP. Future work will explore chemical modification of chitosan prior to formulating with β-glycerophosphate to develop *in situ* gelling systems with improved mucoadhesiveness.

References

1.	Torre LA, Bray F, Siegel RL, Ferlay J, Lortet-tieulent J, Jemal A. Global Cancer Statistics, 2012. CA Cancer J Clin. 2015;65(2):87–108.

2.	Kolawole OM, Lau WM, Mostafid H, Khutoryanskiy V V. Advances in intravesical drug delivery systems to treat bladder cancer. Int J Pharm. 2017;532(1):105–17.

3.	Hu B, Yan Y, Tong F, Xu L, Zhu J, Xu G, Shen R. Lumbrokinase/paclitaxel nanoparticle complex: Potential therapeutic applications in bladder cancer. Int J Nanomedicine. 2018;13:3625–40.

4.	GuhaSarkar S, Banerjee R. Intravesical drug delivery: Challenges, current status, opportunities and novel strategies. J Control Release. 2010;148(2):147–59.

5.	Khutoryanskiy V V. Advances in Mucoadhesion and Mucoadhesive Polymers. Macromol Biosci. 2011;11(6):748–64.

6.	Davidovich-Pinhas, M., Bianco-Peled H. Methods to study mucoadhesive dosage forms. In: Khutoryanskiy, V. V. (Ed.). In: Khutoryanskiy V V., editor. Mucoadhesive Materials and Drug Delivery Systems. John Wiley & Sons; 2014. p. 175–96.

7.	Khutoryanskiy V V. Mucoadhesive Materials and Drug Delivery Systems. John Wiley & Sons; 2014. 33 p.

8.	Ravi Kumar MNV. A review of chitin and chitosan applications. React Funct Polym. 2000;46(1):1–27.

9.	Dornish, M., Kaplan, D.S., Arepalli SR. Regulatory status of chitosan and derivatives. In: Sarmento, B., das Neves J, editor. Chitosan-Based Systems for Biopharmaceuticals: Delivery, Targeting and Polymer Therapeutics. Chichester, UK: John Wiley and Sons, Ltd; 2012. p. 463–78.

10.	Bernkop-Schnürch A, Dünnhaupt S. Chitosan-based drug delivery systems. Eur J Pharm Biopharm. 2012;81(3):463–9.

11.	Jayakumar R, Menon D, Manzoor K, Nair S V., Tamura H. Biomedical applications of chitin and chitosan based nanomaterials - A short review. Carbohydr Polym. 2010;82(2):227–32.

12. Tyagi P, Tyagi S, Kaufman J, Huang L, de Miguel F. Local drug delivery to bladder using technology innovations. Urol Clin North Am. 2006;33(4):519–30, x.

13. U.S. National Library of Medicine. Sodium Glycerophosphate PubChem CID 14754 [Internet]. Open Chemistry Database. 2005 [cited 2018 Oct 23]. Available from: https://pubchem.ncbi.nlm.nih.gov/compound/14754#section=Top

14. MHRA. Sodium Glycerophosphate 21.6% Concentrate for solution for Infusion [Internet]. Summary of Product Characteristics. 2016 [cited 2018 Oct 23]. p. 1–6. Available from: http://www.mhra.gov.uk/home/groups/spcpil/documents/spcpil/con1491542495748. pdf.

15. Chenite A, Chaput C, Wang D, Combes C, Buschmann M., Hoemann C., Leroux J., Atkinson B., Binette F, Selmani A. Novel injectable neutral solutions of chitosan form biodegradable gels in situ. Biomaterials. 2000;21(21):2155–61.

16. Kean T, Thanou M. Biodegradation, biodistribution and toxicity of chitosan. Adv Drug Deliv Rev. 2010;62(1):3–11.

17. Hastings CL, Kelly HM, Murphy MJ, Barry FP, O'Brien FJ, Duffy GP. Development of a thermoresponsive chitosan gel combined with human mesenchymal stem cells and desferrioxamine as a multimodal pro-angiogenic therapeutic for the treatment of critical limb ischaemia. J Control Release. 2012;161(1):73–80.

18. Peng Y, Li J, Li J, Fei Y, Dong J, Pan W. Optimization of thermosensitive chitosan hydrogels for the sustained delivery of venlafaxine hydrochloride. Int J Pharm. 2013;441(1–2):482–90.

19. Zheng L, Ao Q, Han H, Zhang X, Gong Y. Evaluation of the chitosan/glycerol-beta-phosphate disodium salt hydrogel application in peripheral nerve regeneration. Biomed Mater. 2010;5(3):35003.

20. Kim S, Nishimoto SK, Bumgardner JD, Haggard WO, Gaber MW, Yang Y. A chitosan/β-glycerophosphate thermo-sensitive gel for the delivery of ellagic acid for the treatment of brain cancer. Biomaterials. 2010;31(14):4157–66.

21.   Aliaghaie M, Mirzadeh H, Dashtimoghadam E, Taranejoo S. Investigation of gelation mechanism of an injectable hydrogel based on chitosan by rheological measurements for a drug delivery application. Soft Matter. 2012;8(27):7128.

22.   Khodaverdi E, Tafaghodi M, Ganji F, Abnoos K, Naghizadeh H. In Vitro Insulin Release from Thermosensitive Chitosan Hydrogel. AAPS PharmSciTech. 2012;13(2):460–6.

23.   Supper S, Anton N, Seidel N, Riemenschnitter M, Schoch C, Vandamme T. Rheological study of chitosan/polyol-phosphate systems: Influence of the polyol part on the thermo-induced gelation mechanism. Langmuir. 2013;29(32):10229–37.

24.   Abdel-Bar HM, Abdel-Reheem AY, Osman R, Awad GAS, Mortada N. Defining cisplatin incorporation properties in thermosensitive injectable biodegradable hydrogel for sustained delivery and enhanced cytotoxicity. Int J Pharm. 2014;477(1–2):623–30.

25.   Zhou HY, Jiang LJ, Cao PP, Li JB, Chen XG. Glycerophosphate-based chitosan thermosensitive hydrogels and their biomedical applications. Carbohydr Polym. 2015;117:524–36.

26.   Zhang D, Sun P, Li P, Xue A, Zhang X, Zhang H, Jin X. A magnetic chitosan hydrogel for sustained and prolonged delivery of Bacillus Calmette-Guérin in the treatment of bladder cancer. Biomaterials. 2013;34(38):10258–66.

27.   Mostafid AH, Rajkumar RGN, Stewart AB, Singh R. Immediate administration of intravesical mitomycin C after tumour resection for superficial bladder cancer. BJU Int. 2006;97(3):509–12.

28.   NICE. NICE Guidelines, Bladder cancer: diagnosis and management. NICE guidelines. 2015 [cited 2018 Oct 23]. Available from: www.nice.org.uk/guidance/ng2/chapter/recommendations#diagnosing-and-staging-bladder-cancer-2.

29.   Kirin K. Summary of Product Characteristics: Mitomycin-C [Internet]. emc. 1992 [cited 2018 Oct 23]. Available from: https://www.medicines.org.uk/emc/product/4262.

30. Au JL, Badalament RA, Wientjes MG, Young DC, Warner JA, Venema PL, Pollifrone DL, Harbrecht JD, Chin JL, Lerner SP, Miles BJ. Methods to Improve Efficacy of Intravesical Mitomycin C : Results of a Randomized Phase III Trial. J Natl Cancer Inst. 2001;93(8):597–604.

31. Bilensoy E, Sarisozen C, Esendağli G, Doğan AL, Aktaş Y, Şen M, Mungan NA. Intravesical cationic nanoparticles of chitosan and polycaprolactone for the delivery of Mitomycin C to bladder tumors. Int J Pharm. 2009;371:170–6.

32. Erdoğar N, Iskit AB, Mungan NA, Bilensoy E. 2012. Prolonged retention and in vivo evaluation of cationic nanoparticles loaded with Mitomycin C designed for intravesical chemotherapy of bladder tumours. J Microencapsul. 2012;29(6):576–82.

33. Erdoğar N, Iskit AB, Eroglu H, Sargon MF, Mungan NA, Bilensoy E. Cationic core-shell nanoparticles for intravesical chemotherapy in tumor-induced rat model: Safety and efficacy. Int J Pharm. 2014;471(1–2):1–9.

34. Packhaeuser CB, Schnieders J, Oster CG, Kissel T. In situ forming parenteral drug delivery systems: An overview. Eur J Pharm Biopharm. 2004;58(2):445–55.

35. Sogias IA, Williams AC, Khutoryanskiy V V. Why is chitosan mucoadhesive? Biomacromolecules. 2008;9(7):1837–42.

36. Kolawole OM, Lau WM, Khutoryanskiy V V. Methacrylated chitosan as a polymer with enhanced mucoadhesive properties for transmucosal drug delivery. Int J Pharm. 2018;550(1–2):123–9.

37. Jones DS, Woolfson AD, Brown AF, Coulter WA, McClelland C, Irwin CR. Design, characterisation and preliminary clinical evaluation of a novel mucoadhesive topical formulation containing tetracycline for the treatment of periodontal disease. J Control Release. 2000;67(2–3):357–68.

38. Ström A, Schuster E, Goh SM. Rheological characterization of acid pectin samples in the absence and presence of monovalent ions. Carbohydr Polym. 2014;113:336.

39. Chutipongtanate S, Thongboonkerd V. Systematic comparisons of artificial urine formulas for in vitro cellular study. Anal Biochem. 2010;402(1):110–2.

40.   Mun EA, Williams AC, Khutoryanskiy V V. Adhesion of thiolated silica nanoparticles to urinary bladder mucosa: Effects of PEGylation, thiol content and particle size. Int J Pharm. 2016;512(1):32–8.

41.   Caló E, Barros JMSD, Fernández-Gutiérrez M, San Román J, Ballamy L, Khutoryanskiy V V. Antimicrobial hydrogels based on autoclaved poly(vinyl alcohol) and poly(methyl vinyl ether-: Alt -maleic anhydride) mixtures for wound care applications. RSC Adv. 2016;6(60):55211–9.

42.   Boateng JS, Pawar H V., Tetteh J. Polyox and carrageenan based composite film dressing containing anti-microbial and anti-inflammatory drugs for effective wound healing. Int J Pharm. 2013;441(1–2):181–91.

43.   Zhou HY, Chen XG, Kong M, Liu CS, Cha DS, Kennedy JF. Effect of molecular weight and degree of chitosan deacetylation on the preparation and characteristics of chitosan thermosensitive hydrogel as a delivery system. Carbohydr Polym. 2008;73(2):265–73.

44.   Senyiğit ZA, Karavvana SY, Ilem-Özdemir D, Çalişkan Ç, Waldner C, Şen S B-SA. Design and evaluation of an intravesical delivery system for superficial bladder cancer : preparation of gemcitabine HCl-loaded chitosan – thioglycolic acid nanoparticles and comparison of chitosan / poloxamer gels as carriers. Int J Nanomedicine. 2015;10:6493–507.

45.   Myers AL, Zhang YP, Kawedia JD, Zhou X, Sobocinski SM, Metcalfe MJ, Kramer MA, Dinney CPN, Kamat AM. Solubilization and Stability of Mitomycin C Solutions Prepared for Intravesical Administration. Drugs R D. 2017;17(2):297–304.

46.   Supper S, Anton N, Seidel N, Riemenschnitter M, Curdy C, Vandamme T. Thermosensitive chitosan/glycerophosphate-based hydrogel and its derivatives in pharmaceutical and biomedical applications. Expert Opin Drug Deliv. 2014;11(2):249–67.

47.   Chenite A, Buschmann M, Wang D, Chaput C, Kandani N. Rheological characterisation of thermogelling chitosan / glycerol-phosphate solutions. Carbohydr Polym. 2001;46:39–47.

48. Ruel-Gariépy E, Chenite A, Chaput C, Guirguis S, Leroux JC. Characterization of thermosensitive chitosan gels for the sustained delivery of drugs. Int J Pharm. 2000;203(1–2):89–98.

49. Choi HG, Oh YK, Kim CK. In situ gelling and mucoadhesive liquid suppository containing acetaminophen: Enhanced bioavailability. Int J Pharm. 1998;165(1):23–32.

50. Lin K-Y. Nonsolvent-Induced Gelation and Its Effect on Membrane Morphology. Macromolecules. 2002;35(17):6697–706.

51. Madbouly SA, Ougizawa T. Thermal Cross - Linking of Poly (Vinyl Methyl Ether). II . Rheological Behavior at the Gel Point Thermal Cross-Linking of Poly (Vinyl Methyl. J Macromol Sci (Part B). 2004;43(3):655–70.

52. Smart JD. The basics and underlying mechanisms of mucoadhesion. Adv Drug Deliv Rev. 2005;57(11):1556–68.

53. Štorha A, Mun E a., Khutoryanskiy V V. Synthesis of thiolated and acrylated nanoparticles using thiol-ene click chemistry: towards novel mucoadhesive materials for drug delivery. RSC Adv. 2013;3(30):12275.

54. Kaldybekov DB, Tonglairoum P, Opanasopit P, Khutoryanskiy V V. Mucoadhesive maleimide-functionalised liposomes for drug delivery to urinary bladder. Eur J Pharm Sci. 2018;111:83–90.

55. Zahir-Jouzdani F, Wolf JD, Atyabi F, Bernkop-Schnürch A. In situ gelling and mucoadhesive polymers: why do they need each other? Expert Opin Drug Deliv. 2018;15(10):1007–19.

56. Owczarz P, Ziółkowski P, Modrzejewska Z, Kuberski S, Dziubiński M. Rheo-kinetic study of sol-gel phase transition of chitosan colloidal systems. Polymers (Basel). 2018;10(1):47–60.

57. GuhaSarkar S, More P, Banerjee R. Urothelium-adherent, ion-triggered liposome-in-gel system as a platform for intravesical drug delivery. J Control Release. 2017;245:147–56.

3. Methacrylated chitosan as a polymer with enhanced mucoadhesive properties for transmucosal drug delivery

Despite the limited mucoadhesiveness of CHIGP *in situ* gelling systems (WO$_{50}$ values 6-9 mL), HCHIGP (prepared using high molecular weight chitosan) was the most promising in terms of ease of gelation, sustained drug release and mucoadhesiveness. Therefore, high molecular weight chitosan was chemically modified with methacrylate groups to improve its mucoadhesiveness.

This chapter was published as:

Kolawole, O.M., Lau, W-M., Khutoryanskiy, V.V., 2018. Methacrylated chitosan as a polymer with enhanced mucoadhesive properties for transmucosal drug delivery. Int. J. Pharm. 550 (1-2), 123-129.

3.1. Introduction

Ability of water-soluble polymers to adhere to mucosal surfaces, defined as mucoadhesion, has been exploited in the design of mucoadhesive drug delivery systems in the last decades. Various studies have reported the use of mucoadhesive polymers to improve drug delivery in the eye, the nasal cavity, the mouth, the vagina and the urinary bladder [1–8]. Advantages of mucoadhesive delivery systems include improved drug bioavailability, non-invasive nature of dosage form administration and ease of their application, and the possibility of targeting specific organs, etc.

Chitosan is a cationic polysaccharide that has been widely used in the design of dosage forms for transmucosal drug delivery due to its non-toxic nature and excellent mucoadhesive properties [3,6]. Chitosan often exhibits superior mucoadhesive properties compared to many other water-soluble polymers; however, there is still a strong interest to improve its performance through chemical modification [9]. Various dosage forms were developed using chitosan derivatives such as glycol chitosan, trimethyl chitosan, carboxymethyl chitosan, thiolated chitosan, half-acetylated chitosan, glycol chitosan-catechol, methylpyrrolidinone chitosan, and acrylated chitosan and they have all displayed improved retention on mucosal surfaces, thereby extending the duration of action of loaded therapeutics [9].

Over the last few years, acrylate- and maleimide-functionalised materials have been explored for transmucosal drug delivery due to their enhanced mucoadhesiveness [10–17]. This is achieved through the quick formation of covalent bonds between acrylate- or maleimide-groups of a mucoadhesive polymer and thiol-groups present in cysteine-rich domains on mucosal surfaces.

Methacrylate groups are also capable of forming covalent bonds with thiols under physiological conditions, similarly to acrylate groups and maleimide. A few studies exist where methacrylate groups have been conjugated to pharmaceutical materials for drug delivery and tissue engineering. For example, Yu et al. (2007) reported the development of methacrylated chitosan that was subsequently cross-linked by radical polymerisation to prepare biodegradable macroporous scaffolds for cell culture applications [18]. Lin et al. (2013) reported the synthesis of methacrylated gelatin that was then used in mixtures with human endothelial colony-forming cells/mesenchymal stem cells for *in vivo* injection and transdermal photo-crosslinking [19]. However, to our knowledge, the potential of methacrylated polymers as mucoadhesive materials has not been explored yet.

In this study, we developed methacrylated derivatives by reacting chitosan with methacrylic anhydride and evaluated their physicochemical properties, *in vitro* adhesion to porcine urinary bladder mucosa and cytotoxicity in UMUC3 cells to establish their suitability as materials for transmucosal delivery.

3.2. Materials and methods

3.2.1. Materials

High molecular weight chitosan (CHI, 370 kDa; deacetylation degree 70.9 ± 2.2%), methacrylic anhydride (MA), ninhydrin, trifluoroacetic acid, citric acid, fluorescein sodium, FITC-Dextran (3-5 kDa), 3-(4,5-Dimethylthiazol-2-yl)-2,5-diphenyltetrazolium bromide (MTT), deuterated water (D_2O), dextran (5 kDa), foetal bovine serum (FBS) and UMUC3 malignant urothelial cells (Sigma-Aldrich UK); modified Eagle's medium with Earle salts & non-essential amino acids and trypsin-EDTA (Lonza UK); dialysis membrane with molecular weight cut off 12-14 kDa (Medicell International UK); and most chemical reagents (Fischer Scientific UK) were used as received without further purification. Freshly excised porcine urinary bladders were received from PC Turner Abattoir (Farnborough, Hampshire, UK).

3.2.2. Synthesis of methacrylated chitosan

Methacrylated chitosan was synthesised by reacting chitosan with methacrylic anhydride at various molar ratios (Table 3.1) in order to generate two types of products using the method developed in-house with slight modification [20] (See Fig. 3.1).
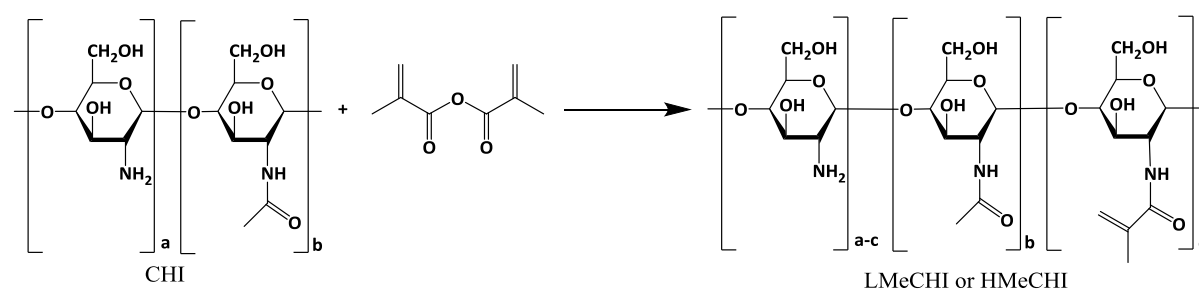
Fig. 3.1. Reaction scheme for the synthesis of methacrylated chitosan: CHI is a parent chitosan and LMeCHI and HMeCHI are chitosans with low and high degrees of methacrylation, respectively; a (deacetylated), b (acetylated), and c (methacrylated) segments of chitosan repeating units.

Briefly, 1.5 % w/v chitosan solution (100 mL) was prepared by dissolving predetermined amount of chitosan in 4% v/v acetic acid at room temperature for 12 h. Different amounts of methacrylic anhydride were added slowly to chitosan solution and the mixture was maintained at 40°C, shaken at 60 rpm for 12 h, protected from light. The products were redispersed in deionised water; purified by dialysis (MWCO 12-14 kDa membrane) against 4.5 L deionised water with six water changes over 72 h. The final products were freeze-dried using a Heto PowerDry LL3000 Freeze Dryer (Thermo Scientific, UK).

Table 3.1

Molar feed ratios for the synthesis of LMeCHI and HMeCHI, with low and high degrees of methacrylation, respectively.

Parameters	LMeCHI	HMeCHI
Concentration, chitosan	1.5 % (w/v)	1.5 % (w/v)
Weight/volume of methacrylic anhydride	1.035 g (1 mL)	6.21 g (6 mL)
Moles of MA per unit mole chitosan	0.79	4.65

3.2.3. Characterisation of methacrylated chitosan

3.2.3.1. ^{1}H Nuclear magnetic resonance spectroscopy (^{1}H NMR)

Solutions of CHI, LMeCHI & HMeCHI (0.6% w/v) were prepared in D$_2$O acidified with 30μL trifluoroacetic acid and allowed to be dissolved overnight at room temperature. The ^{1}H NMR spectra were recorded using a 400 MHz ULTRASHIELD PLUS™ B-ACS 60 spectrometer (Bruker, UK).

3.2.3.2. Fourier Transform-Infrared Spectroscopy (FT-IR)

Solid samples of modified and unmodified chitosan were scanned from 4,000 to 400 cm^{-1}, resolution of 4 cm^{-1}. Data was processed based on the average of six scans per spectrum generated by the Nicolet iS5-iD5 ATR FT-IR spectrometer (Thermo Scientific, UK).

3.2.3.3. Turbidimetric measurements

The influence of pH on the turbidity of polymer samples, was studied according to Sogias et al. (2010) with slight modification. Briefly, polymer solutions were prepared in 0.1 M acetic acid at room temperature with initial pH 3. NaOH solution (0.1 mol·L^{-1}) was added to increase the

pH stepwise and turbidity values of polymer dispersions were measured at 400 nm with JENWAY 7315 UV-Vis spectrophotometer (Bibby Scientific, UK).

3.2.3.4. Zeta potential measurements

Zeta potential values of CHI, LMeCHI and HMeCHI solutions/dispersions were determined in folded DTS-1070 capillary cell using Zetasizer Nano-ZS (Malvern Instruments, UK) at 25°C. Solutions/dispersions of chitosan and derivatives (0.4 % w/v) were diluted 1:20 with ultrapure water prior to analysis. The machine was operated at a refractive index of 1.59 and an absorbance of 0.01. Triplicate readings were recorded with 50 sub-runs per measurement.

3.2.3.5. X-ray Diffractometry

The influence of methacrylation on the crystallinity of chitosan was evaluated using a wide-angle powder D8 Advance diffractometer/LYNXEYE XE detector (Bruker, UK). Solid samples of CHI, LMeCHI and HMeCHI were loaded into a capillary tube, sealed with wax to prevent loss and placed onto the goniometer and aligned under a microscope for diffraction analysis, scanning at diffraction ranges from 5 to 65° with a scan step of 0.02^{o}, generating characteristic diffractograms at the rate of 2.5 scans min $^{-1}$.

3.2.3.6. Ninhydrin test to quantify methacrylate groups

The amount of methacrylate groups conjugated to chitosan was quantified using a previously published method with slight modification [14]. Briefly, 2 % w/v solution of ninhydrin in DMSO was prepared by stirring for 12 h at room temperature in the dark. Unmodified and modified chitosan solutions (0.05 – 0.5% w/v) were prepared by dissolving in 0.1 M acetic acid, stirred for 18 h in the dark at room temperature. 5mL of ninhydrin solution and 1.25 mL of 4M phosphate buffer (pH 5.4 ± 0.2) were mixed with 0.5 mL polymer solution. The resultant mixtures were incubated in a water bath at 85°C (OLS 200, Grant, UK) shaken at 60 rpm for 30 min. Each mixture (1 mL) was analysed using a JENWAY 7315 UV-Vis spectrophotometer (Bibby Scientific, UK) at 500 nm.

3.2.4. *Ex vivo* Porcine mucoadhesion studies

3.2.4.1. Preparation of polymer / fluorescein sodium mixture and artificial urine solution

The polymeric solutions/dispersions of CHI, LMeCHI and HMeCHI were prepared by dissolving polymers in 0.1 M acetic acid and stirred overnight at room temperature. Resultant polymer solutions/dispersions were mixed with 0.1% w/v fluorescein sodium to yield final polymer concentration of 0.4 % w/v (FS/CHI, FS/LMeCHI and FS/HMeCHI, respectively). FITC-dextran

0.4 % (w/v) was dissolved in deionised water overnight under dark conditions at room temperature to serve as negative control.

A protocol developed by Chutipongtanate & Thongboonkerd (2010) [21] was used to prepare artificial urine. Briefly, the compounds (Table 3.2) were stirred in deionised water for 3 h at room temperature, pH adjusted to 6.2 and made up to a final volume of 2 L.

Table 3.2.

Constituents of artificial urine contained in 2 L sample (pH 6.2 ± 0.2)

Compounds	Amount (g)	Amount (mM)	Source
Urea	24.27	200	Sigma Life Science
Uric acid	0.34	1.00	Sigma Life Science
$MgSO4.7H_2O$	1.00	2.00	Sigma Life Science
NaH_2PO4	1.00	3.60	Sigma Life Science
Creatinine	0.90	4.00	Sigma-Aldrich
$NaHCO_3$	0.34	2.00	Sigma-Aldrich
Na_2SO4	2.58	9.00	Sigma-Aldrich
Na_2C_2O4	0.03	0.10	Sigma-Aldrich
$Na_3C_6H_5O_7$	2.97	5.00	Sigma-Aldrich
NaCl	6.34	54.00	Fisher Chemical
Na_2HPO_4	0.10	0.40	Fisher Chemical
KCl	4.50	30.00	Fisher Chemical
NH_4Cl	1.61	15.00	Fisher Scientific
$CaCl_2.2H_2O$	0.89	3.00	Fisher Scientific

3.2.4.2.   Retention on porcine urinary bladder mucosa

Fluorescence microscopy (MZ10F microscope (Leica Microsystems, UK) fitted with an "ET GFP" filter, a Zeiss Imager A1/AxioCam MRm camera; 1296 x 966 pixels; 0.8 x magnification) was used to evaluate the mucosal retention of fluorescein sodium in the presence of the polymeric carriers based on a slightly modified protocol developed in-house [22]. Freshly excised porcine urinary bladders stored on ice were used in this study within 24 h of procurement. The mucosal side of the bladder tissue was preserved during excision of the required section (about 1.5 x 2.5 cm) and rinsed with artificial urine solution (~ 3 mL) prior to blank tissue imaging. The bladder tissue was placed on a 75 mm x 25 mm glass slide and maintained in an incubator at 37^oC during urine wash-out. The following exposure times were used: FITC-dextran (80 ms), FS/CHI (211 ms), FS/LMeCHI and FS/HMeCHI (279 ms). Microscopic images were recorded for each tissue sections before and after applying ~ 100 μL of sample as well as after each of the five washing cycles with 10 mL artificial urine/cycle at 2 mL/min. The studies were carried out in triplicates. Image J software (National Institute of Health, USA) was used to analyse the microscopic images, generating average fluorescence values as a function of urine volume used for the wash-out. In order to normalise the mean fluorescence values, fluorescence values obtained based on blank tissues were deducted from fluorescence values obtained after each wash-out cycle while the value "1" was used to depict the fluorescence intensity from the tissue prior to wash. From the wash-out trends of the polymers, the WO_{50} values were determined using exponential or polynomial fit of the graphs, which depicts the volume of artificial urine needed to wash out 50% of the polymer dispersion.

3.2.5. Bioadhesive test

The TA-XT Plus Texture Analyser (Stable Micro Systems Ltd, UK) coupled to a 5 kg load cell was used as an additional technique to study the adhesion of LMeCHI and HMeCHI samples. Blank chitosan solutions (0.4% w/v) served as the positive control while the negative control was dextran solution (0.4% w/v). The experiment was carried out as previously described in Section 2.3.6. Briefly, porcine bladder tissues were secured at the base of a cylindrical container. The vessel bottom had a circular cut-out region (20 mm diameter) exposing the mucosal surface of the bladder tissue. This container was screwed onto the probe of the texture analyser through a hole drilled on the lid of the container. Another bladder tissue was placed on a petridish and coupled onto the lower platform of the texture analyser, exposing the mucosal surface (20 mm diameter) of another bladder tissue. The tests were performed using an earlier reported equipment settings [23] with slight modification: pre-speed test 1.0

mm/s; test speed 0.1 mm/s; post-test speed 0.1 mm/s; applied force 0.05 N; contact time 120.0 s; trigger type auto; trigger force 0.1 N; and return distance of 10.0 mm. Bladder tissues were maintained in an incubator at $37^{o}C$ for 5 min prior to the study. CHI, dextran, LBCHI, MBCHI and HBCHI samples (0.4 mL) were applied onto the exposed area of the bladder tissue secured onto the lower platform of the texture analyser. The probe was then lowered such that the upper blank bladder tissue comes in contact with the formulation applied onto the bladder tissue secured on the lower platform for 2 min. The Texture Analyser software (T.A. Exponent) was used to record the area under the force versus distance curves (work of adhesion) as well as the force of adhesion/adhesive strength which is the maximum force needed to detach tissue from the polymer solutions/dispersions [23,24].

3.2.6. Cell culture and viability experiment

Human urothelial carcinoma cell line, UMUC3 cells (Sigma-Aldrich, UK) were cultured in MEM supplemented with 10% FBS. The cells were cultured in an incubator maintained at $37^{o}C$ containing 5% CO_2 atmosphere. The MTT assay was used to evaluate cell viability using a previously reported method with slight modification [25]. Briefly, UMUC3 cells were seeded into a 96-well plate at a density of 1×10^4 cells/well. After 24 h, the cells were treated with polymer solution in growth medium (6.25 – 200 µg mL^{-1}) for 4 h. The cells were allowed to grow for a further 72 h. After the incubation period, 20µL of MTT solution (5 mg mL^{-1}) was added to each well. After 4 h, the supernatant was removed and 100 µL DMSO was added. Then, absorbance was read using the microplate reader (Benchmark-BIO-RAD) at 570 nm. Untreated cells were used as positive control and culture medium was used as background control. Each concentration had three triplicates in each experiment and all experiments were done in triplicate. The cell viability was evaluated as a function of viable cells post treatment and total untreated cells. The polymer concentration that yielded half-maximum inhibitory response (IC_{50} value) was determined based on the best linear fit of the cell viability versus polymer concentration graph.

3.2.7. Statistical analysis

All experimental data were carried out in triplicates and data expressed as average ± standard deviation. Data were compared using t-test and one-way ANOVA and post-hoc Bonferroni test with GraphPad Prism 5.04 (GraphPad Software Inc., San Diego, California), with $p < 0.05$ depicting significant statistical difference between data sets.

3.3. Results and discussion

Over the last decade, chitosan has been progressively explored for mucosal delivery of drugs and biotherapeutics due to its biocompatibility, biodegradability, mucoadhesiveness and cell permeation enhancing features [26]. Recently, acrylated chitosan has been proven to have superior intestinal mucoadhesiveness relative to the thiolated analogue [14].

The aim of this study was to synthesise methacrylated chitosan using an efficient single step chemical modification. Two types of methacrylated chitosan derivatives with different degrees of substitution were synthesised and evaluated on their solubility at various pH, mucoadhesiveness and biocompatibility. These derivatives were prepared by reaction of chitosan with methacrylic anhydride.

3.3.1. Methacrylated chitosan derivatives synthesis / physicochemical characterisation

The two methacrylated chitosan derivatives LMeCHI and HMeCHI were synthesised with a yield of 62% and 24%, respectively (Table 3.3). There was no significant difference in their appearance being both off-white colour in nature.

Table 3.3

Synthetic yield, physical properties and degree of methacrylation (using ^{1}H NMR spectroscopy and ninhydrin test) of LMeCHI and HMeCHI

Parameter		LMeCHI	HMeCHI
Synthetic yield		62% (w/w)	24 % (w/w)
Physical appearance		off-white solid	off-white solid
Methacrylation extent	^{1}H NMR	11.2 ± 3.4 %	38.5 ± 3.9%
	Ninhydrin test	34.3 ± 2.0 %	55.4 ± 1.0%

The ^{1}H NMR spectra (Fig. 3.2) show the distinctive peaks for chitosan at δ 2.0 ppm (CH$_3$ from acetylated part of chitosan) as well as, 3.09-3.8 ppm representing protons from the glucosamine ring. With the methacrylated derivatives, additional peaks were evident at 5.6 and 6.2 ppm depicting the alkenyl double bond from the methacrylate moiety conjugated to chitosan. Also, the additional peak at 1.84 ppm appeared in the spectra of the methacrylated chitosan is due to CH$_3$ of methacrylic groups. These spectral data are in good agreement with the report by Yu et al. (2007) [18].

The ratio of mean intensity of the proton peaks of the methacrylate groups (δ = 5.6–6.2 ppm) relative to that of chitosan glucosamine protons (δ = 3.0-3.8 ppm) provides their extent of methacrylation.

$$Methacrylation\ (\%) = \frac{Integral\ of\ methacrylate\ protons\ at\ 5.6\ \&\ 6.2\ ppm\ /2}{Integral\ of\ H2 - H6\ \ protons\ /6} \cdot 100\%$$
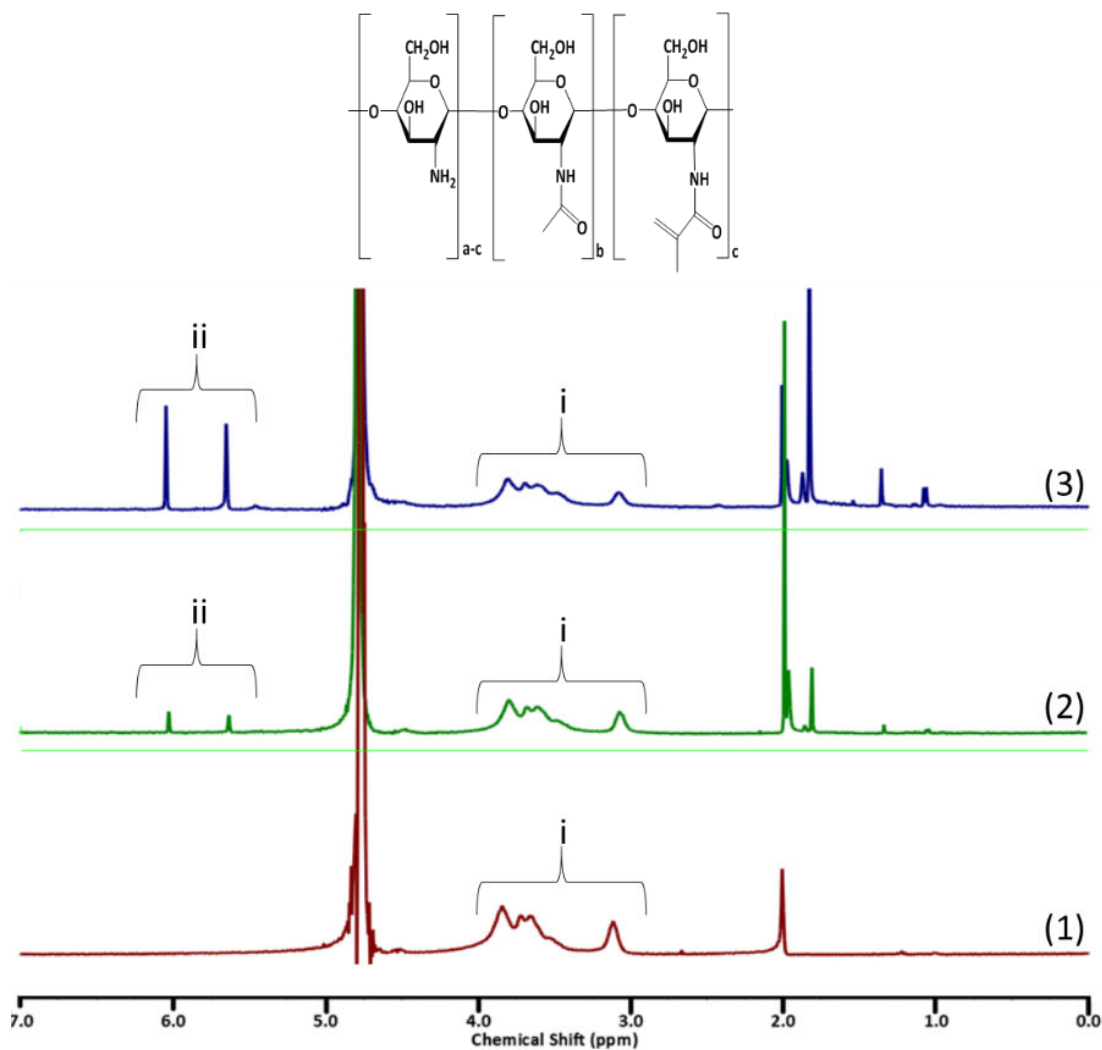
Fig. 3.2. ^{1}H NMR spectra of (1) CHI (2) LMeCHI and (3) HMeCHI recorded in D_2O acidified with 1% trifluoroacetic acid. H2-H6 protons of CHI were detected at (i) 3.0-3.8 ppm and (ii) vinyl groups of methacrylate segment evident around 5.6-6.2 ppm.

3.3.2. Quantification of acrylate groups

In addition to ^{1}H NMR, the ninhydrin test was also used to confirm the degree of methacrylation, where ninhydrin reacts with the unmodified amine groups of chitosan to form a coloured product detectable by UV [27]. The slope of the adsorption versus concentration curve of unconjugated chitosan is represented as α_{CHI}, while that of LMeCHI and HMeCHI are denoted as α_{MeCHI} (unmodified amine groups of the methacrylated products).

Methacrylation percentage can be defined as (1 - α_{MeCHI}/ α_{CHI}) * 100% [14].

Table 3.2 provided data on the extent of methacrylation for LMeCHI and HMeCHI. The degrees of methacrylation for LMeCHI and HMeCHI, calculated from the ninhydrin test (34.3% vs. 55.4%, respectively) were greater than the values calculated using ^{1}H NMR (11.2% vs. 38.5%). This may be due to the differences in experimental design as the ^{1}H NMR spectra of polymers were recorded in D_2O, acidified with 1% trifluoroacetic acid, whereas analysis with ninhydrin was performed with the samples dissolved in 0.1 M acetic acid. Different solvents used in these methods could affect the conformation of polymers and availability of functional groups. Potentially, ^{1}H NMR could underestimate the degree of methacrylation because methacrylate groups could not be on the surface. Nevertheless, the data from both techniques reveal that HMeCHI had a greater degree of methacrylation than LMeCHI.

3.3.3. FT-IR analysis

FT-IR shows characteristic absorption bands for chitosan (Fig. 3.3) at 1026-1151 cm^{-1} (amine C-N stretch). Since both chitosan and methacrylate groups display alkyl C-H stretch (2850 and 2930 cm-[1]), the increase in the intensity of the absorption bands is evident of the methacrylated products. The appearance of a new double bond signal at 1537-1653 cm^{-1} depicted alkenyl C=C stretch, while amide C=O stretch evident at 1635 cm^{-1} in LMeCHI and HMeCHI confirms the methacrylation of chitosan. The FT-IR spectra of LMeCHI is similar to that of HMeCHI, but differs in terms of the intensity, which is related to their extent of methacrylation.
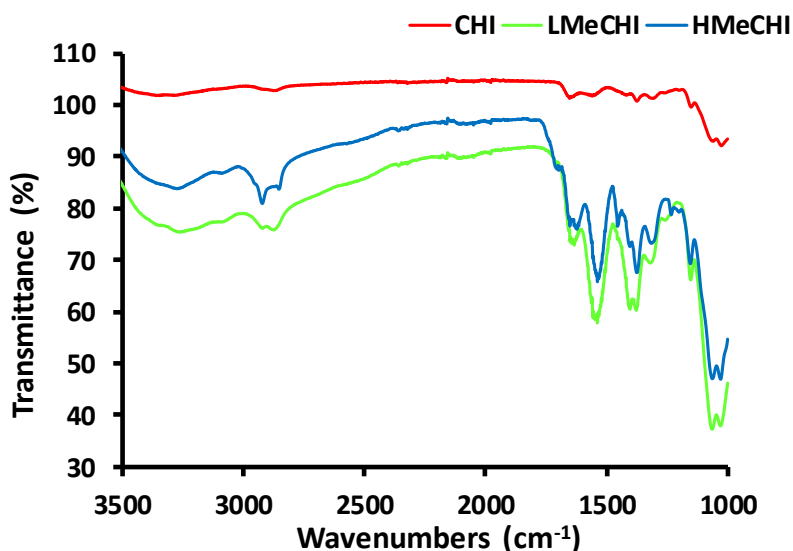
Fig. 3.3. FT-IR spectra of CHI , LMeCHI and HMeCHI with characteristic peak at 1537-1635 cm^{-1} as well as 1653 cm^{-1} for LMeCHI and HMeCHI depicting alkenyl C=C and amide C=O linkage between chitosan and methacrylate groups, respectively.

3.3.4. Turbidimetric measurements

The effect of pH on turbidity of polymers were analysed where unmodified chitosan shows a turbidity-pH profile (Fig. 3.4) in good agreement with our previous report [20]: the solution remains transparent until the pH reaches 6.5; then a further increase in solution pH results in a dramatic increase in turbidity. LMeCHI sample exhibits a pH-dependent solubility similar to unmodified chitosan, with a sharp increase in turbidity observed at pH > 6.5.
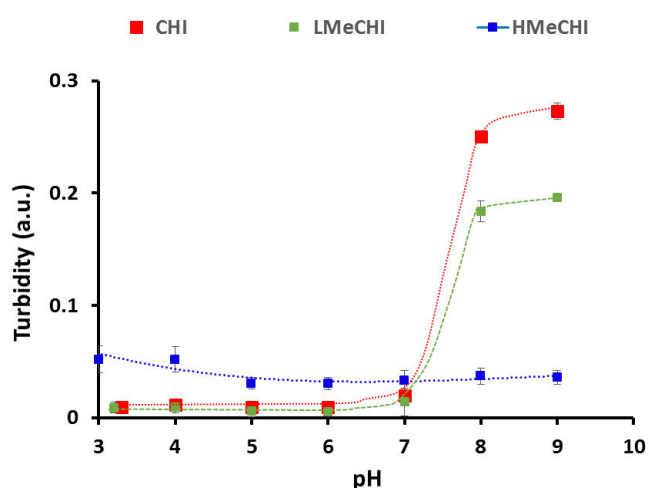
Fig.3.4. Effect of pH on solution turbidity of unmodified chitosan, LMeCHI and HMeCHI. Lines are used as a guide to the eye.

On the other hand, the turbidity profile of HMeCHI is distinctly different, where a slightly turbid colloidal solution was formed at first and maintained in the studied pH range. This is likely to be due to the relatively hydrophobic nature of methacrylate groups that cause aggregation of chitosan macromolecules and formation of micellar structures. The solution of LMeCHI did not show any sign of turbidity at pH < 6.5 possibly because its degree of methacrylation did not reach a certain threshold to become sufficiently hydrophobic to undergo aggregation. The relatively unchanged turbidity of HMeCHI possibly relates to the disruption of the semi-crystalline nature of chitosan caused by introduction of bulky methacrylate groups; a similar effect was reported for half-acetylated chitosan [20]. The physiological implication of this finding is that dosage forms generated from highly methacrylated chitosan may be more resistant to the pH fluctuations in the bladder possible with metabolic and dietary conditions (pH 4.6 to 8), than LMeCHI and unmodified chitosan based delivery systems.

3.3.5. X-ray Diffractometry

The X-ray diffractograms (Fig. 3.5) shows the unmodified chitosan exhibited two major peaks at diffraction angles (2θ) of 10.1 and 20.8^{o}, which correlate with the peaks displayed by chitosan reported in our earlier publications [20,28–30]. X-ray diffractograms of LMeCHI and HMeCHI (Fig. 3.5) reveal a decrease in crystallinity upon methacrylation of chitosan with the disappearance of the peak at 10.1^{o} and broadening of the peak at 20.8^{o}. This suggests that chitosan has been successfully modified and the modification reduced the ability of chitosan macromolecules to form crystalline domains. This is in good agreement with our previous report on reduction of chitosan's crystallinity upon its re-acetylation [20]. The reduced crystallinity of methacrylated chitosan could facilitate improved aqueous solubility of the drug carriers relative to the parent chitosan, which is beneficial for intravesical formulations that are presented as liquid, injectable dosage forms.
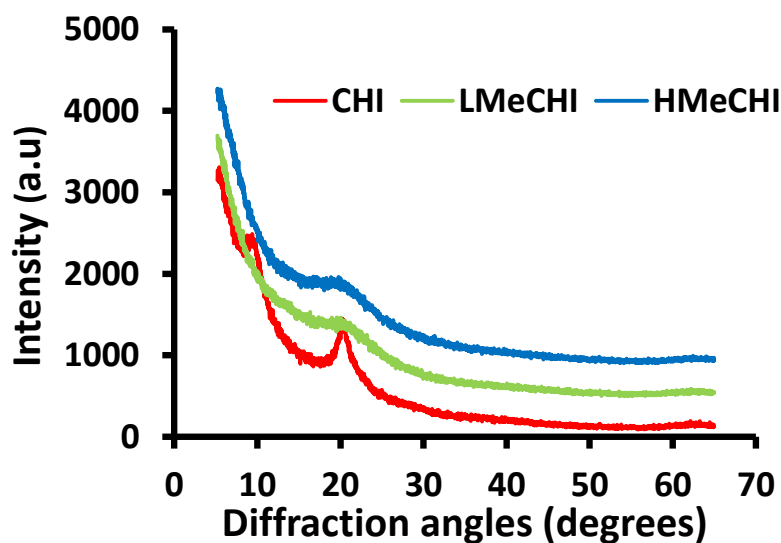
Fig. 3.5. X-ray diffractograms of CHI, LMeCHI and HMeCHI generated at 2.5 scans·min^{-1}, scan angle 5-65°, scan step size of 0.02^{o}, spectra offset for improved clarity.

3.3.6. Mucoadhesion studies

In order to evaluate the mucosal retention, fluorescein sodium was added to the unmodified and methacrylated chitosan solutions prior to the experiment. In the study, the unmodified chitosan, cationic in nature with proven mucoadhesive potential [31], was chosen as the positive control, while dextran with limited mucoadhesiveness [32] served as the negative control.
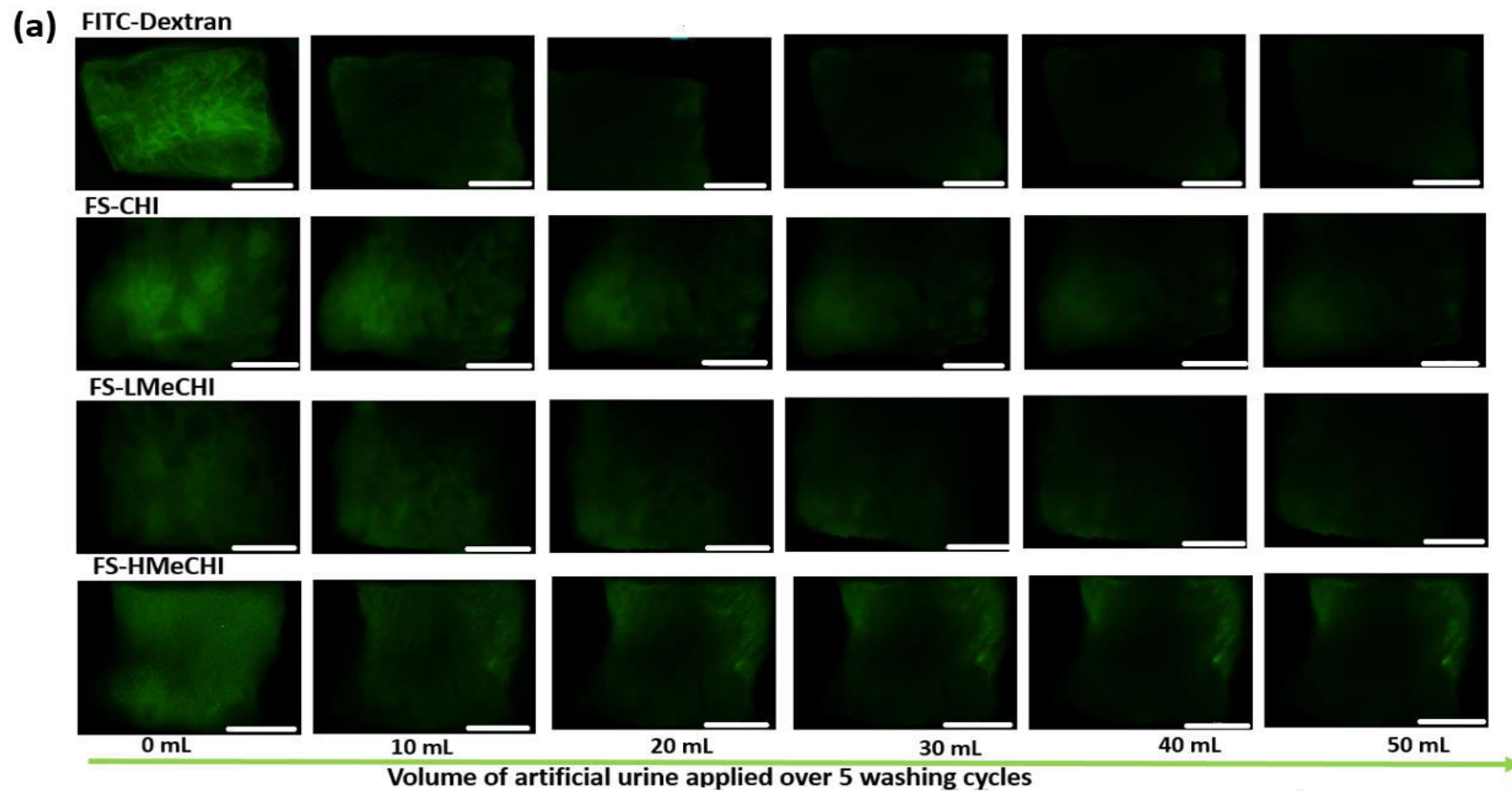
Fig. 3.6 (a) Exemplar microphotographs showing FITC-Dextran, FS/CHI, FS/LMeCHI, and FS/HMeCHI wash-out from porcine urinary bladder with artificial urine solution over 5 washing cycles, scale bar is 2 mm.
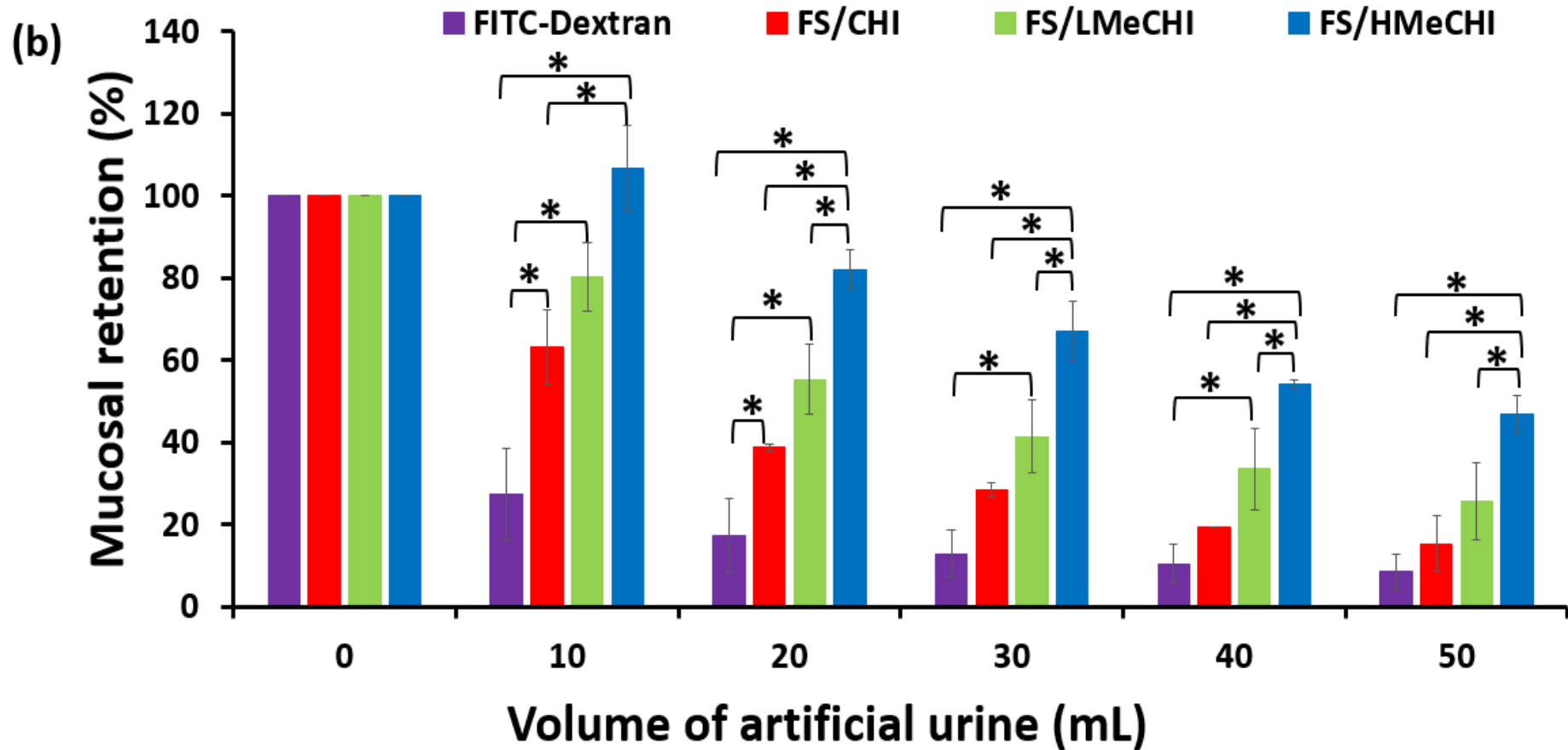
Fig. 3.6 (b) Mucosal retention of fluorescein sodium (FS) from CHI, LMeCHI and HMeCHI on porcine urinary bladder tissue; FITC dextran served as negative control and FS/CHI (unmodified chitosan) as positive control. Result presented as mean ± standard deviation, n = 3, * (Asterisk) depicts significant statistical differences between samples ($p < 0.05$).

The mucosal retention of CHI, LMeCHI and HMeCHI on *ex vivo* bladder tissue was quantified using numerical WO_{50} values [22]. WO_{50} is defined as the volume of artificial urine required to remove 50% of fluorescein sodium from the bladder mucosal surface. FITC-dextran serving as the negative control was the least retained on the porcine bladder mucosa, displays WO_{50} of 7 ± 1 mL based on extrapolation as 10 mL of artificial urine was used for each wash-out cycle (Fig. 3.6) similar to that reported previously [22]. WO_{50} values for FS/CHI, FS/LMeCHI and FS/HMeCHI were 15 ± 4 mL, 24 ± 1 mL and 48 ± 1 mL, respectively, based on the polynomial fit of the mucosal fluorescence retention versus urine volume graph (Fig. 3.7). FITC-dextran was significantly less mucoadhesive than the unmodified chitosan and the methacrylated chitosan after washing out the bladder mucosa with 10 mL of artificial urine. The significantly superior mucoadhesiveness of HMeCHI over LMeCHI became evident after the second washing cycle (20 mL artificial urine). The statistical difference between the mucoadhesiveness of unmodified chitosan and HMeCHI was sustained with bladder mucosa wash out with 50 mL of artificial urine. However, LMeCHI was statistical similar to unmodified chitosan after wash-out with 50 mL artificial urine, probably due to its low degree of methacrylation which is not sufficient to confer superior mucoadhesive property on chitosan. Nevertheless, bladder wash-out with 30 mL artificial urine showed that LMeCHI was significantly more mucoadhesive than FITC-dextran (non-mucoadhesive control) while unmodified chitosan was similar to FITC-dextran after the third washing cycle. Despite these urine wash-out behaviour, the statistical analysis of their WO_{50} values affirms that the methacrylated chitosan was more mucoadhesive than unmodified chitosan and dextran (non-mucoadhesive control). This finding suggested that increased methacrylation confers greater mucoadhesive potential on chitosan. The superior mucoadhesive behaviour of HMeCHI as shown in Fig. 3.6 is likely due to the presence of a higher percentage of unsaturated methacrylate groups that formed covalent bonds with thiols of mucin present on the mucosal surface [14]. Interestingly, HMeCHI displayed a similar WO_{50} value (48 mL) to PEGylated maleimide functionalised liposomes (WO_{50} value 48 mL) evaluated for bladder delivery [16], suggesting that functionalisation of chitosan with methacrylate moieties may facilitate comparable covalent interactions with mucosal glycoproteins, achievable with maleimide derivatisation of liposomes.
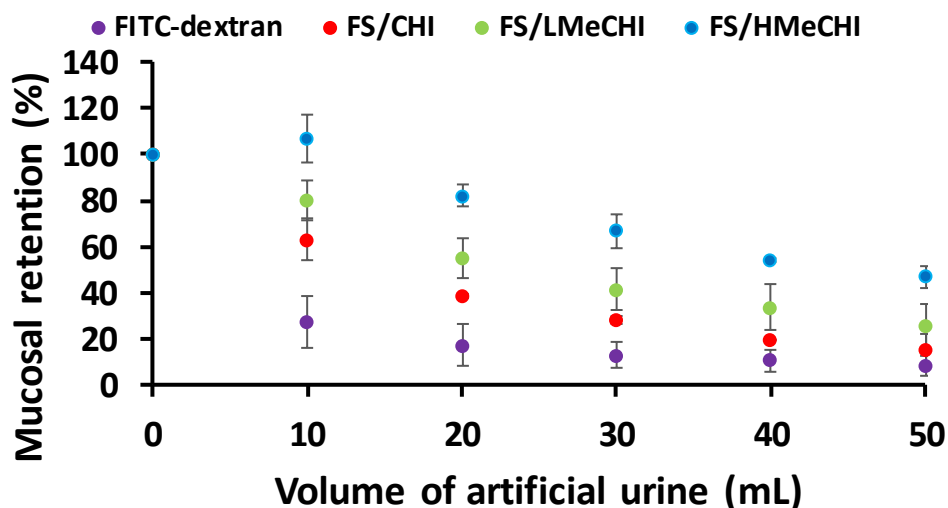
Fig. 3.7. The mucosal fluorescence retention profile of FITC-dextran, unmodified chitosan and methacrylated chitosan on porcine bladder tissues evaluated using ImageJ software and WO_{50} values calculated based on the polynomial fit of the graph; Results presented as mean ± standard deviation; n=3.

The zeta potential of 13.3 ± 3.2, 41.4 ± 7.0 and 54.4 ± 1.9 mV were recorded for 0.02% w/v polymer solutions/dispersions of CHI, LMeCHI and HMeCHI, respectively. The degree of positive charge of these polymers supported their favourable interaction with the negatively charged bladder mucosal surface[4]. Moreover, the methacrylated chitosan may also facilitate loosening of tight junctions which promotes cellular internalisation of the drug carrier [33]. There was significant statistical difference in the mucoadhesive profile of parent chitosan and the highly methacrylated derivative (HMeCHI) after five washing cycles (p < 0.05).

3.3.7. Bioadhesion test

The bioadhesion test provides valuable information about the bioadhesive features of LMeCHI and HMeCHI. The force of adhesion was directly proportional to the work of bioadhesion, suggesting that a material with a greater force of adhesion is likely to have a larger work of bioadhesion.

The force needed to surmount the adhesive bonds between the drug carrier and bladder mucosa is referred to as the force of adhesion/adhesive strength while the work of adhesion is defined by the area under the force-distance curves, which depicts all forces that must be removed in order to separate the bladder tissue from the drug carrier [23,24].

Dextran, the non-mucoadhesive control exhibited the least "force of adhesion" and "work of bioadhesion" as seen in Fig. 3.8. The force of adhesion presented in increasing order: dextran (0.04±0.01 N) < CHI (0.06±0.01 N) < LMeCHI (0.10±0.02 N) < HMeCHI (0.11±0.01 N).
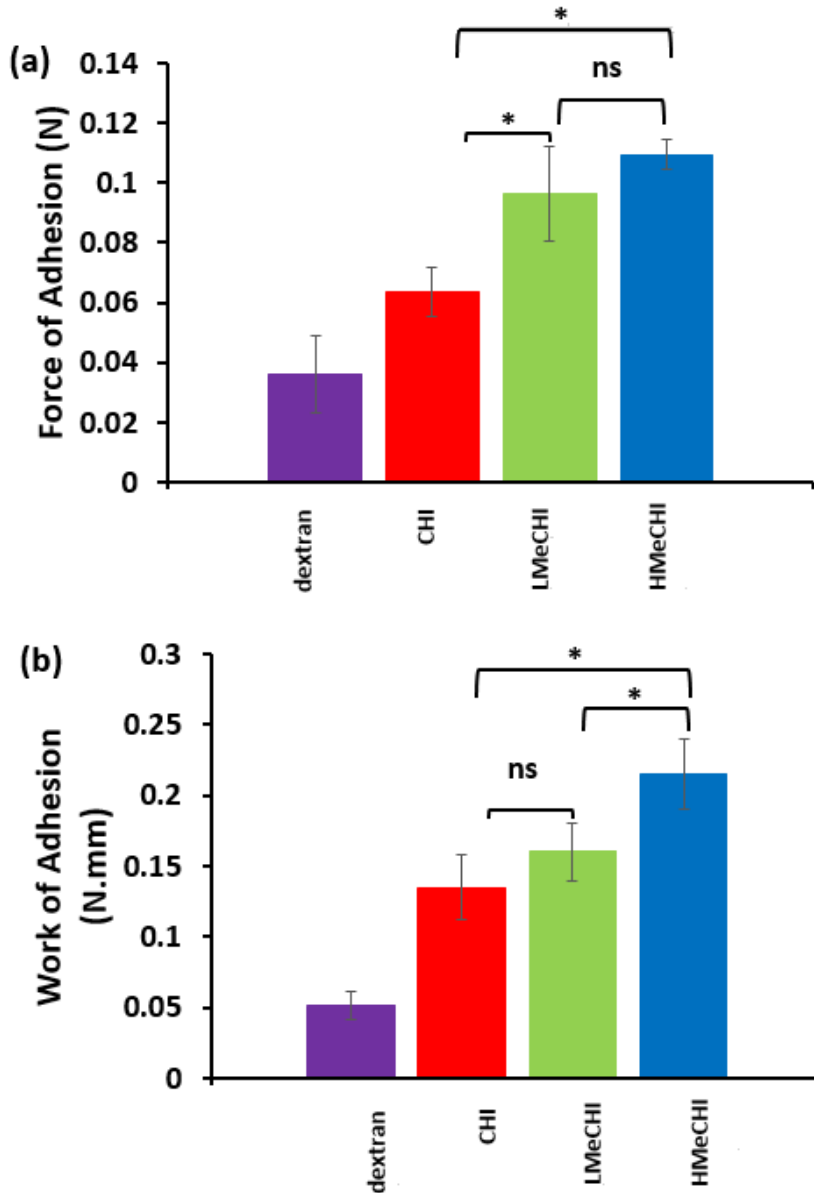
Fig. 3.8. Bioadhesive profile: (a) Force of adhesion; (b) work of adhesion of dextran, CHI, LMeCHI, and HMeCHI; result presented as average ± standard deviation, n = 3, * (Asterisk) depicts significant statistical differences between samples ($p < 0.05$); ns signifies otherwise.

The work of adhesion of CHI was less than that of LMeCHI and HMeCHI (0.14±0.02 N·mm vs 0.16±0.02 N·mm vs 0.22±0.02 N·mm). The adhesive strength of the polymers correlated well with their work of adhesion. In terms of the force of adhesion, there was significant statistical difference between the unmodified chitosan and the methacrylated chitosan (LMeCHI and

HMeCHI) but that of LMeCHI and HMeCHI were statistically similar. As their work of adhesion was a more reliable method of evaluating the bioadhesiveness of materials, unmodified chitosan and LMeCHI behaved similarly in terms of the work of adhesion values. However, parent chitosan was remarkably less bioadhesive than HMeCHI, and LMeCHI displayed inferior bioadhesiveness relative to HMeCHI statistically. These findings inferred that the bioadhesiveness of the polymers was improved with increased extent of methacrylation. Also, there was good agreement in their mucoadhesive profile using the urine-wash-out and tensile test.

3.3.8. Cell viability studies

Distressing symptoms like painful sensation during urination are common in bladder cancer. So, drug carriers intended for bladder cancer therapy should not aggravate the discomfort experienced by patients. UMUC3 human bladder carcinoma cells have been used as an *in vitro* model for studying the cytotoxic and irritation effect of drug delivery systems intended for bladder cancer treatment [34–36]. The selected duration of cell incubation with polymer solution (4 h) was clinically relevant as most drug carriers required such contact time with diseased tissues for effective therapy [37]. The safety of methacrylated gellan gum has been reported [38], but there was no data available for methacrylated chitosan.

MTT assay is a well-established colorimetric assay for investigating the cell metabolic, growth inhibitory or toxic effects of novel intravesical formulations [34,35,39,40]. Cellular enzymes reduce the MTT reagent (tetrazolium salt) to its insoluble purplish formazan, which is then solubilised using appropriate solvent. The absorbance of the coloured solution at wavelength of 500 to 600 nm via spectrophotometer correlates to the amount of viable cells available after cell treatment [41]. This assay is appropriate for our cytotoxicity test because UMUC3 cells are rapidly dividing cancerous cells that exhibit high rates of MTT reduction.
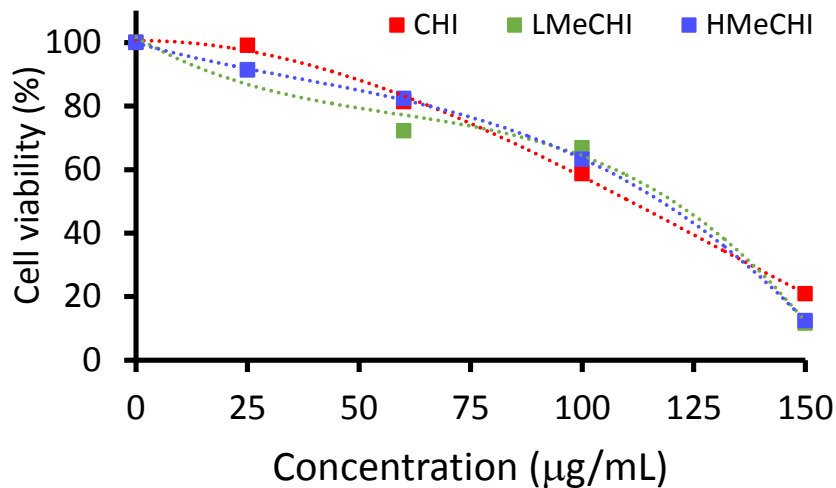
Fig.3.9. UMUC3 cell viability studies using CHI, LMeCHI and HMeCHI. Polymer treatment for 4 h and cell viability studied at 72 h post exposure to polymers. The untreated cells served as the control. Cell viability is normalised against the control; n=3. Lines are used as a guide to the eye. Error bars are not shown on this figure to avoid overcrowding.

The UMUC3 cell cytotoxic effect of the polymers was studied over 72 h (Fig. 3.9). CHI, LMeCHI and HMeCHI displayed IC_{50} values of 108.40 ± 5.81, 96.17 ± 5.27 and 104.16 ± 4.81 µg mL^{-1}, respectively. One-way ANOVA statistical analysis shows that there is no statistically significant differences in the IC_{50} values between all three polymers ($p > 0.05$). This suggests the methacrylated chitosan is as safe as the unmodified chitosan and thus could be exploited further for intravesical drug delivery especially due to its superior mucoadhesive features.

3.4. Conclusions

To our knowledge, this is the first report where the pH-dependent solubility, mucoadhesive properties and safety profile of unmodified and methacrylated chitosan have been compared. Methacrylate groups were grafted onto chitosan through the reaction of its amino-groups with methacrylic anhydride in order to synthesise novel mucoadhesive polymers. The volume ratio of high molecular weight chitosan (CHI) to methacrylic anhydride was varied to generate two types of methacrylated chitosan that differed in terms of their degree of methacrylation (LMeCHI and HMeCHI). ^{1}H NMR and ninhydrin test data analysis confirmed the successful synthesis of the methacrylated products.

Methacrylation of chitosan has been identified as a simple and viable synthetic strategy to generate drug carriers with greater mucoadhesive properties. This novel drug carrier can be used to formulate dosage forms that allows prolonged drug residence time in the bladder thereby improving extent of drug absorption and therapeutic outcomes from bladder cancer treatment. Methacrylated chitosan with enhanced mucoadhesive properties could also be of interest for application in other areas of transmucosal drug delivery. Future research using these mucoadhesive chitosan derivatives may include preparation of formulations with various active pharmaceutical ingredients, studies of their physicochemical characteristics and drug release studies.

References

1. Ludwig A. The use of mucoadhesive polymers in ocular drug delivery. Adv Drug Deliv Rev. 2005;57(11):1595–639.

2. Andrews GP, Laverty TP, Jones DS. Mucoadhesive polymeric platforms for controlled drug delivery. Eur J Pharm Biopharm. 2009;71(3):505–18.

3. Bernkop-Schnürch A, Dünnhaupt S. Chitosan-based drug delivery systems. Eur J Pharm Biopharm. 2012;81(3):463–9.

4. Khutoryanskiy V V. Mucoadhesive Materials and Drug Delivery Systems. John Wiley & Sons 2014: 33.

5. Sosnik A, Das Neves J, Sarmento B. Mucoadhesive polymers in the design of nano-drug delivery systems for administration by non-parenteral routes: A review. Prog Polym Sci. 2014;39(12):2030–75.

6. Casettari L, Illum L. Chitosan in nasal delivery systems for therapeutic drugs. J Control Release 2014;190:189–200.

7. Morales JO, Brayden DJ. Buccal delivery of small molecules and biologics: of mucoadhesive polymers, films, and nanoparticles. Curr Opin Pharmacol. 2017;36:22–8.

8. Kolawole OM, Lau WM, Mostafid H, Khutoryanskiy V V. Advances in intravesical drug delivery systems to treat bladder cancer. Int J Pharm. 2017;532(1):105–17.

9. Ways T, Lau W, Khutoryanskiy V. Chitosan and Its Derivatives for Application in Mucoadhesive Drug Delivery Systems. Polymers (Basel). 2018;10(3):267.

10. Davidovich-Pinhas M, Bianco-Peled H. Alginate-PEGAc: A new mucoadhesive polymer. Acta Biomater. 2011;7(2):625–33.

11. Tonglairoum P, Brannigan RP, Opanasopit P, Khutoryanskiy V V. Maleimide-bearing nanogels as novel mucoadhesive materials for drug delivery. J Mater Chem B. 2016;4(40):6581–7.

12. Eshel-Green T, Bianco-Peled H. Mucoadhesive acrylated block copolymers micelles for the delivery of hydrophobic drugs. Colloids Surfaces B Biointerfaces 2016;139:42–51.

13. Brannigan RP, Khutoryanskiy V V. Synthesis and evaluation of mucoadhesive acryloyl-quaternized PDMAEMA nanogels for ocular drug delivery. Colloids Surfaces B Biointerfaces 2017;155:538–43.

14. Shitrit Y, Bianco-Peled H. Acrylated chitosan for mucoadhesive drug delivery systems. Int J Pharm. 2017;517(1–2):247–55.

15. Shtenberg Y, Goldfeder M, Schroeder A, Bianco-Peled H. Alginate modified with maleimide-terminated PEG as drug carriers with enhanced mucoadhesion. Carbohydr Polym. 2017;175:337–46.

16. Kaldybekov DB, Tonglairoum P, Opanasopit P, Khutoryanskiy V V. Mucoadhesive maleimide-functionalised liposomes for drug delivery to urinary bladder. Eur J Pharm Sci. 2018;111:83–90.

17. Eliyahu, S., Aharon, A., Bianco-Peled H. Acrylated chitosan nanoparticles with enhanced mucoadhesion. Polymers (Basel) 2018;10(2):106.

18. Yu LMY, Kazazian K, Shoichet MS. Peptide surface modification of methacrylamide chitosan for neural tissue engineering applications. J Biomed Mater Res - Part A. 2007;82(1):243–55.

19. Lin RZ, Chen YC, Moreno-Luna R, Khademhosseini A, Melero-Martin JM. Transdermal regulation of vascular network bioengineering using aphotopolymerizable methacrylated gelatin hydrogel. Biomaterials 2013;34(28):6785–96.

20. Sogias IA, Khutoryanskiy V V., Williams AC. Exploring the factors affecting the solubility of chitosan in water. Macromol Chem Phys. 2010;211(4):426–33.

21. Chutipongtanate S, Thongboonkerd V. Systematic comparisons of artificial urine formulas for in vitro cellular study. Anal Biochem. 2010;402(1):110–2.

22. Mun EA, Williams AC, Khutoryanskiy V V. Adhesion of thiolated silica nanoparticles to urinary bladder mucosa: Effects of PEGylation, thiol content and particle size. Int J Pharm. 2016;512(1):32–8.

23. Caló E, Barros JMSD, Fernández-Gutiérrez M, San Román J, Ballamy L, Khutoryanskiy V V. Antimicrobial hydrogels based on autoclaved poly(vinyl alcohol) and poly(methyl vinyl ether-: Alt -maleic anhydride) mixtures for wound care applications. RSC Adv. 2016;6(60):55211–9.

24. Boateng JS, Pawar H V., Tetteh J. Polyox and carrageenan based composite film dressing containing anti-microbial and anti-inflammatory drugs for effective wound healing. Int J Pharm. 2013;441(1–2):181–91.

25. Lau WM, Ng KW, White AW, Heard CM. Therapeutic and cytotoxic effects of the novel antipsoriasis codrug, naproxyl-dithranol, on HaCaT cells. Mol Pharm. 2011;8(6):2398–407.

26. Jayakumar R, Menon D, Manzoor K, Nair S V., Tamura H. Biomedical applications of chitin and chitosan based nanomaterials - A short review. Carbohydr Polym. 2010;82(2):227–32.

27. Yin J, Luo K, Chen X, Khutoryanskiy V V. Miscibility studies of the blends of chitosan with some cellulose ethers. Carbohydr Polym. 2006;63(2):238–44.

28. Luo K, Yin J, Khutoryanskaya O V., Khutoryanskiy V V. Mucoadhesive and elastic films based on blends of chitosan and hydroxyethylcellulose. Macromol Biosci. 2008;8(2):184–92.

29. Gohel V, Vyas P, Chhatpar HS, Zitouni M, Fortin M, Thibeault J-S, Brzezinski R, Muzzarelli RA, Larionova NI, Zubaerova DK, Guranda DT, Pechyonkin MA, Balabushevich NG, Prochazkova S, Vårum KM, Ostgaard K, Wischke C, Borchert HH. Quantitative determination of chitosans by ninhydrin. Carbohydr Polym. 2006;38(2):255–7.

30. Sogias IA, Williams AC, Khutoryanskiy V V. Why is chitosan mucoadhesive? Biomacromolecules 2008;9(7):1837–42.

31. Štorha A, Mun E a., Khutoryanskiy V V. Synthesis of thiolated and acrylated nanoparticles using thiol-ene click chemistry: towards novel mucoadhesive materials for drug delivery. RSC Adv. 2013;3(30):12275.

32. Smith J, Wood E, Dornish M. Effect of chitosan on epithelial cell tight junctions. Pharm Res. 2004;21(1):43–9.

33. Zhang Q, Neoh KG, Xu L, Lu S, Kang ET, Mahendran R, Chiong E. Functionalized mesoporous silica nanoparticles with mucoadhesive and sustained drug release properties for potential bladder cancer therapy. Langmuir 2014;30(21):6151–61.

34. Lu S, Neoh KG, Kang ET, Mahendran R, Chiong E. Mucoadhesive polyacrylamide nanogel as a potential hydrophobic drug carrier for intravesical bladder cancer therapy. Eur J Pharm Sci. 2015;72:57–68.

35. Lu S, Xu L, Kang ET, Mahendran R, Chiong E, Neoh KG. Co-delivery of peptide-modified cisplatin and doxorubicin via mucoadhesive nanocapsules for potential synergistic intravesical chemotherapy of non-muscle-invasive bladder cancer. Eur J Pharm Sci. 2016;84:103–15.

36. Mugabe C, Matsui Y, So AI, Gleave ME, Baker JHE, Minchinton AI, Manisali I, Liggins R, Brooks DE, Burt HM. In vivo evaluation of mucoadhesive nanoparticulate docetaxel for intravesical treatment of non-muscle-invasive bladder cancer. Clin Cancer Res. 2011;17(9):2788–98.

37. Coutinho DF, Sant S V., Shin H, Oliveira JT, Gomes ME, Neves NM, Khademhosseini A, Reis RL. Modified Gellan Gum hydrogels with tunable physical and mechanical properties. Biomaterials 2010;31(29):7494–502.

4. Synthesis and evaluation of boronated chitosan as a mucoadhesive polymer for intravesical drug delivery

Another method of improving the mucoadhesiveness of high molecular weight chitosan was investigated to determine if boronated chitosan could display superior mucoadhesive properties relative to methacrylated chitosan and unmodified chitosan.

4.1. Introduction

Bladder cancer is one of the frequent causes of tumour-associated mortality worldwide and the overall survival tendency for the advanced stage of the disease is only about a year despite the fact that urothelial cancerous tissues respond well to conventional chemotherapeutic agents [1–3]. The local bioavailability and residence time of formulations delivered to the bladder is often reduced as drugs are diluted or washed out of the bladder due to urine filling and excretion. Thus there is a need to develop better mucoadhesive delivery systems that are resistant to urine wash out, thereby prolonging duration of drug action and preventing disease progression.

Chitosan is a biopolymer with well-established biodegradable, biocompatible and mucoadhesive properties [4–6]. It is a polysaccharide consisting of acetylated and deacetylated glucosamine units, with the deacetylated segment that can be modified to be a more mucoadhesive derivative such as chitosan-cysteine [7], chitosan-thioglycolic acid [8], chitosan-4-thio-butyl-amidine [9], chitosan-glutathione [10], chitosan-N-acetylcysteine conjugates [11], chitosan-graft-6-mercaptonicotinic acid [12] and methacrylated chitosan [13].

One of the constituents of the cell membranes are mucin oligosaccharides, which comprise of sialic acid groups that are overexpressed in malignant tissues and organs such as the bladder [14]. So, sialic acid moieties have been explored as therapeutic targets by conjugating polymeric drug carriers with phenylboronic acid groups which bind favourably with sialic acid groups to form reversible covalent complexes [15], thereby facilitating enhanced mucoadhesion and cellular uptake of their therapeutic payload.

Phenylboronic acid decorated polymers have been explored for the delivery of drugs and biotherapeutics because they are biocompatible, mucoadhesive, form stable colloidal systems, with tumour-targeting abilities [16–18]. Transmucosal routes that have been explored include ocular [19–21], nasal [22] and vaginal [23]. The ability of these boronated delivery systems to be responsive to glucose presence makes them valuable for glucose detection [18,24,25] and as glucose sensitive sustained insulin release system [26]. They have also been explored for cancer targeting [27–30] and gene delivery [31,32] due to their favourable interaction with sialic acid moieties.

Liu et al demonstrated that cyclosporine loaded phenylboronic acid conjugated polymeric nanoparticles reduced ocular drug clearance. The boronated nanoparticles displayed good drug encapsulation efficiency (13.7 % w/w), reduction in inflammation after topical application

to dry-eye induced mice, and sustained drug release of up to 5 days showing their potential in reducing dosing interval and improving ocular drug bioavailability [20].

Recently, *in vivo* studies using H22 lung metastasis tumour-bearing mice showed that doxorubicin loaded boronate modified chitosan nanoparticles exhibit greater antitumour activity than carboxymethyl chitosan nanoparticles [33]. 3- and 4-carboxyphenylboronic acid modified chitosan nanoparticles were shown to exhibit superior doxorubicin loading, active tumour targeting, cellular internalisation and target site retention, relative to unmodified nanoparticles [33,34].

Asantewaa et al. studied the correlation between the physicochemical features of various boronic-acid-chitosan conjugates to their glucose adsorption properties [35]. However, to our knowledge, there are no studies investigating how the physicochemical properties of different boronated chitosan affect urothelial mucoadhesiveness as a potential intravesical dosage form for bladder cancer treatment. Thus there is a critical need to establish whether boronated chitosan has sufficient interaction with the urothelial mucosa that is constantly in contact with urine, to prolong drug residence time in the bladder.

In this work, we synthesised boronate-conjugated chitosan derivatives by reaction of chitosan with 4-carboxyphenylboronic acid using EDC and NHS as coupling agents and characterised their physicochemical properties and evaluated *in vitro* adhesion to porcine urinary bladder mucosa to establish their intravesical drug delivery potential. Boronate conjugation of chitosan influenced its mucoadhesiveness with the highly boronated derivative (HBCHI) being statistically more mucoadhesive than LBCHI, MBCHI and unmodified chitosan. Methacrylate groups have proven to improve the mucoadhesiveness of chitosan [13]. This work aims to investigate the mucoadhesive properties of boronated chitosan in comparison to methacrylated chitosan and unmodified chitosan.

4.2. Materials and Methods

4.2.1. Materials

Chitosan (high molecular weight grade, 370 kDa; deacetylation extent 70.9 ± 2.2%), ninhydrin, trifluoroacetic acid, FITC-dextran (3-5 kDa), dextran 5 kDa, deuterium oxide, urea, uric acid, magnesium sulphate heptahydrate, sodium hydrogen phosphate, creatinine, sodium bicarbonate, sodium sulphate, disodium oxalate and trisodium citrate were all purchased from Sigma-Aldrich, UK. 4-carboxyphenylboronic acid (4-CPBA), N-3(dimethylaminopropyl)-N-ethylcarbodiimide hydrochloride (EDC), N-hydroxysuccinimide (NHS), dimethyl sulfoxide (DMSO), disodium hydrogen phosphate, sodium chloride, potassium chloride, ammonium chloride and calcium chloride dihydrate were all purchased from Fisher Scientific, UK. Dialysis membrane with molecular weight cut off 12-14 kDa was obtained from Medicell International, UK. All chemical reagents were used as received without further purification. Freshly excised porcine urinary bladders were procured from PC Turner Abattoir (Farnborough, Hampshire, UK).

4.2.2. Synthesis of boronated chitosan

Three types of boronated chitosan were synthesised by varying the molar amount of 4-CPBA (Table 4.1) using a published method with modification [34].

Briefly, 1.5% w/v chitosan solution (100 mL) was prepared in 4% v/v acetic acid for 12 h at room temperature for complete polymer dissolution. According to Table 4.1, the required amounts of 4-CPBA, EDC and NHS were dissolved in predetermined amounts of DMSO, stirred under dark conditions at room temperature for 30 min. The 4-CPBA/NHS/EDC mixtures were then added slowly to chitosan solution and the resultant chitosan/4-CPBA/NHS/EDC mixture was stirred for 24 h at room temperature, in the dark to prevent degradation of 4-carboxyphenylboronic acid, EDC and NHS. The products were redispersed in deionised water, purified by dialysis in the dark (MWCO 12-14 kDa membrane) against 4.5 L of 7 mM HCl for 24 h (three changes) followed by dialysis against 4.5 L deionised water for 2 days (6 changes) to remove unreacted 4-CPBA. The products were freeze-dried using Heto PowerDry LL3000 Freeze Dryer (Thermo Scientific, UK).

Table 4.1

Materials used for the synthesis of boronated chitosan, with low (LBCHI), medium (MBCHI), and high (HBCHI) degrees of modification.

Parameters	LBCHI	MBCHI	HBCHI
Chitosan (CHI) concentration (% w/v)	1.5	1.5	1.5
4-carboxyphenyl boronic acid (4-CPBA, g)	0.28	0.56	1.11
N-3(dimethylaminopropyl)-N-ethylcarbodiimide hydrochloride (EDC, g)	0.39	0.77	1.54
N-hydroxysuccinimide (NHS, g)	0.23	0.47	0.93
DMSO for 4-CPBA, EDC & NHS dissolution (mL)	5	10	20
Moles of 4-CPBA per unit mole CHI	0.20	0.39	0.79

4.2.3. Characterisation of boronated chitosan

4.2.3.1. ^{1}H NMR spectroscopy

Solutions of CHI, LBCHI MBCHI, and HBCHI (0.6% w/v) were prepared in D_2O acidified with 30 μL trifluoroacetic acid and allowed to be dissolved overnight at room temperature. The ^{1}H NMR spectra were recorded using 400 MHz ULTRASHIELD PLUS™ B-ACS 60 spectrometer (Bruker, UK).
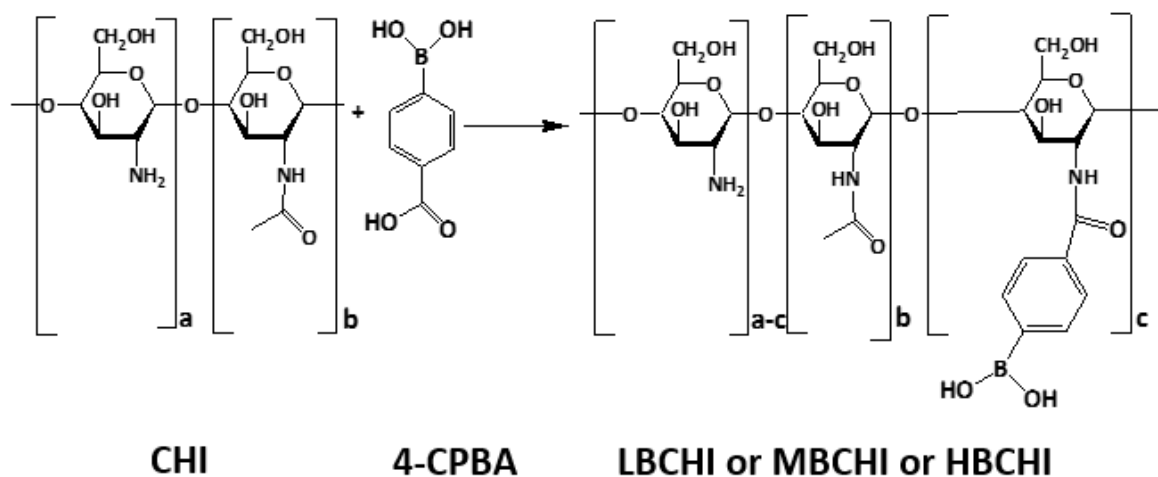
Fig. 4.1. Reaction scheme for the synthesis of boronated chitosan: CHI is a parent chitosan and LBCHI,

MBCHI, and HBCHI are chitosans with low, medium, and high degrees of boronation, respectively; a (deacetylated), b (acetylated), and c (boronated) segments of chitosan repeating units.

.

4.2.3.2. Quantification of the extent of chemical modification

The quantity of boronate groups conjugated to chitosan was calculated using a previously published method with slight modification [36]. Briefly, 2 % w/v solution of ninhydrin in DMSO was prepared by stirring for 12 h, protected from light at room temperature. Unmodified and modified chitosan solutions (0.05 – 0.5% w/v) were prepared by dissolving in 0.1 M acetic acid, stirred for 12 h under dark conditions at room temperature. 5mL of ninhydrin solution and 1.25 mL of 4M phosphate buffer (pH 5.4±0.2) were mixed with 0.5 mL polymer solution. The resultant mixtures were incubated in a water bath at $85^{o}C$ shaken at 60 rpm for 30 min. The degree of chitosan amine substitution was determined using microplate spectrophotometer at 500 nm (Epoch, BioTek Instruments Inc., UK). Mixture of ninhydrin solution and phosphate buffer solution (4M, pH 5.4) (4:1) served as the blank control.

4.2.3.3. Fourier Transform-Infrared spectroscopy (FT-IR)

Solid samples of modified and unmodified chitosan were scanned from 4, 000 to 600 cm^{-1}, resolution of 4 cm^{-1} to identify characteristic functional groups in both chitosan and the boronate moieties that suggested that boronation was successful. Data was processed based on the average of sixteen scans per spectrum generated by FT-IR spectrometer (PerkinElmer Spectrum 100, Thermo Scientific, UK).

4.2.3.4. Turbidimetric analysis

The influence of pH on the turbidity of polymer samples was evaluated based on a method reported by Sogias et al. (2010) with slight modification [37]. Briefly, polymer solutions (0.1% w/v, pH 3) were prepared in 0.1M acetic acid at room temperature. NaOH solution (0.1 $mol·L^{-1}$) was added to increase the pH stepwise from 3 to 9 and 0.1 $mol·L^{-1}$ HCl was used to adjust the pH of the samples if necessary. The turbidity values of polymer dispersions were measured at 400 nm using UV-Vis spectrophotometer (Jenway 7315, Bibby Scientific, UK).

4.2.3.5. X-ray diffraction analysis

In order to investigate the influence of boronation on the crystallinity of chitosan, solid forms of the polymers were studied using an earlier reported method [13]. Briefly, solid samples of

CHI, LBCHI, MBCHI, and HBCHI were loaded into a capillary tube sealed with wax to avoid loss and placed onto the goniometer and aligned under a microscope to be analysed with a wide-angle powder D8 Advance diffractometer/LYNXEYE XE detector (Bruker, UK). Samples were scanned at diffraction ranges from 5 to 65$^\text{o}$C with a scan step of 0.02$^\text{o}$, producing distinctive diffractograms at the rate of 2.5 scans min-^{1}.

4.2.4. *Ex vivo* porcine mucoadhesion studies

4.2.4.1. Preparation of polymer / fluorescein sodium mixtures and artificial urine solutions

The solutions/dispersions of CHI, LBCHI, MBCHI and HBCHI were prepared by dissolving the polymers in 0.1 M acetic acid and stirred overnight in dark conditions at room temperature. Resultant polymer solutions/dispersions were mixed with 0.1% w/v fluorescein sodium (9:1) to yield final fluorescent polymer concentration of 0.4 % w/v (FS/CHI, FS/LBCHI, FS/MBCHI and FS/HBCHI, respectively). FITC-dextran 0.4 % (w/v) in deionised water served as negative control.

Chutipongtanate and Thongboonkerd (2010) method [38] was used to prepare artificial urine. Briefly, urea (24.27 g), uric acid (0.34 g), magnesium sulphate heptahydrate (1.00 g), sodium hydrogen phosphate (1.00 g), disodium hydrogen phosphate (0.11 g), creatinine (0.90 g), sodium bicarbonate (0.34 g), sodium sulphate (2.58 g), disodium oxalate (0.03 g), trisodium citrate (2.97 g), sodium chloride (6.34 g), potassium chloride (4.50 g), ammonium chloride (1.61 g), and calcium chloride dihydrate (0.89 g) were dissolved in 2 L ultrapure water (18.2 MΩ) for 3 h at room temperature. The resultant artificial urine had a final pH of 6.2±0.2.

4.2.4.2. Retention on porcine urinary bladder mucosa

Fluorescence microscopy (MZ10F microscope, Leica Microsystems, UK), coupled to an "ET GFP" filter camera (Zeiss Imager A1/AxioCam MRm camera, 1296 x 966 pixels, 0.8 x magnification) was used to investigate the mucosal retention of model drug fluorescein sodium in the presence of the polymeric carriers based on a slightly modified protocol developed in-house [39]. Freshly excised porcine urinary bladders were stored on ice until use and used within 24 h of procurement. The mucosal side of the bladder tissue was prevented from any possible   damage during excision of the studied mucosal section (about 1.5 x 2.5 cm) and rinsed with artificial urine solution (~ 3 mL) prior to blank tissue imaging. The bladder tissue was placed on a glass slide and maintained in an incubator at 37$^\text{o}$C during urine wash-out. The following exposure times were used: FITC-dextran (80 ms), FS/CHI (211 ms), FS/LBCHI, FS/MBCHI and FS/HBCHI (86 ms). Microscopic images of the tissues were taken

before and after sample application (50µL) as well as after each of the five washing cycles with 10 mL artificial urine/cycle at 2 mL/min. The studies were carried out in triplicates. Image J software (National Institute of Health, USA) was used to analyse the microscopic images, generating average fluorescence values as a function of urine volume used for the wash-out. Fluorescence intensity values were normalised against the blank tissue control. The WO_{50} values (volume of artificial urine required to wash-out 50% of the applied fluorescence sodium/polymer mixture) were determined based on the polynomial fit of the percent mucosal fluorescence retention versus artificial urine volume graphs.

4.2.5. Tensile method

The TA-XT Plus Texture Analyser (Stable Micro Systems Ltd, UK) coupled to a 5 kg load cell was used as an additional technique to study the mucoadhesive properties of the polymer samples. Blank chitosan solutions (0.4% w/v in 0.1 M acetic acid solution) served as the positive control, while the negative control was dextran solution (0.4% w/v in water). The experiment was carried out as described in Section 2.6. Briefly, porcine bladder tissues were secured at the base of a cylindrical container. The vessel bottom had a circular cut-out region (20 mm diameter) exposing the mucosal surface of the bladder tissue. This container was screwed onto the probe of the texture analyser through a hole drilled on the lid of the container. Another bladder tissue was placed on a petridish and coupled onto the lower platform of the texture analyser, exposing the mucosal surface (20 mm diameter) of another bladder tissue. The tests were performed using an earlier reported equipment settings [40] with slight modification: pre-speed test 1.0 mm/s; test speed 0.1 mm/s; post-test speed 0.1 mm/s; applied force 0.05 N; contact time 120.0 s; trigger type auto; trigger force 0.1 N; and return distance of 10.0 mm. Bladder tissues were maintained in an incubator at 37°C for 5 min prior to the study. CHI, dextran, LBCHI, MBCHI and HBCHI samples (0.4 mL) were applied onto the exposed area of the bladder tissue secured onto the lower platform of the texture analyser. The probe was then lowered such that the upper blank bladder tissue comes in contact with the formulation applied onto the bladder tissue secured on the lower platform for 2 min. The Texture Analyser software (T.A. Exponent) was used to record the area under the force versus distance curves (work of adhesion) as well as the force of adhesion/adhesive strength which is the maximum force needed to detach tissue from the polymer solutions/dispersions [40,41].

4.2.6. Statistical analysis

All experimental data were collected in triplicates and data expressed as mean ± standard deviation. Data were compared using t-test and one-way ANOVA/post-hoc Bonferroni test with GraphPad Prism 5.04 (GraphPad Software Inc., San Diego, California), with $p < 0.05$ depicting significant statistical difference between data sets.

4.3. Results and discussion

The potential for chitosan as material for drug delivery and tissue engineering cannot be overemphasized due to its physical and biological properties such as biocompatibility, mucoadhesiveness and permeation enhancing properties [5,42–44]. Chemical modification of chitosan with boronate groups may impact on its safety and urothelial mucoadhesiveness. The biocompatible nature of boronate modified chitosan nanoparticles has been previously established in mouse and mammalian cells [33,34]. Over 90% of human bone marrow neuroblastoma SH-SY5Y cells, human liver cancer HepG2 cells and mouse liver cancer H22 cells remained viable after incubation with chitosan and boronated chitosan based nanoparticles for 48h [34]. Also, boronated dextran based formulations were tested on healthy rabbit eyes and did not trigger any inflammatory response acutely (1 week) and chronically (12 weeks) [20]. These studies suggested that boronated drug carriers are safe. Consequently, cytotoxicity testing was not carried out for the studied boronated chitosan. Moreover, several *in vitro* and *in vivo* studies have established the safety of phenylboronate molecules [17,20,45].

We recently reported that methacrylated chitosan displayed greater mucoadhesive properties than the parent chitosan based on *ex vivo* urine wash-out studies using porcine urinary bladder model, with WO_{50} values of 48 mL and 15 mL, respectively [13]. We hypothesise that conjugation of chitosan with boronate groups may exhibit superior mucoadhesive potential in comparison to methacrylate groups as well as unmodified chitosan. The highly boronated chitosan (HBCHI) was synthesised using similar ratio of reactants as LMeCHI [13] so that they can be compared. With the synthesis of LBCHI and MBCHI, we would be able to investigate what extent of boronate conjugation could affect the urothelial mucoadhesiveness.

4.3.1. Synthesis of boronated chitosan derivatives and physical properties

According to Table 4.1, three types of boronated chitosan were synthesised using EDC/NHS chemistry which is an efficient synthetic method for covalent amide bond formation [46]. The synthetic yields of LBCHI, MBCHI, and HBCHI were 61%, 43%, and 33%, respectively and all

with whitish appearance (Table 4.2). The product yield decreased with greater extent of chitosan modification. This finding correlates well with our previous studies where chitosan with low extent of methacrylation produced a greater yield (62%) than sample with a high extent of methacrylation (24%) [13]. HBCHI had lower yield than LMeCHI (33% vs 62%) despite the fact that both chitosan derivatives were synthesised with the same moles of methacrylic anhydride or 4-carboxyphenyboronic acid per unit mole of chitosan (0.79). This may be due to the differences in the chemical reactivity of methacrylate and boronate groups with chitosan.

Table 4.2

Synthetic yield and degrees of boronation (using ^{1}H NMR spectroscopy and ninhydrin test) of LBCHI, MBCHI, and HBCHI

Parameter		LBCHI	MBCHI	HBCHI
Synthetic yield (% w/w)		61	43	33
Boronation extent (%)	^{1}H NMR	3.9 ± 0.3	5.5 ± 0.1	16.5 ± 0.2
	Ninhydrin test	4.4 ± 1.8	7.4 ± 1.2	10.7 ± 2.2

According to the ^{1}H NMR spectra (Fig. 4.2), the characteristic peaks of chitosan were evident at 2.0 ppm (-CH$_3$ from the acetylated segment of chitosan) as well as 3.09-3.8 ppm (protons from the glucosamine ring). With the boronated chitosan, additional peaks were evident at 7.79-7.96 ppm representative of the phenyl ring protons from the boronate moiety, confirming the successful conjugation of phenylboronate groups to chitosan. Also, the peaks at 2.67-2.8 ppm for the boronated chitosan are the result of the quartet methyne protons of the boronic acid. These spectral data are in good agreement with that reported by Zhang et al [14].
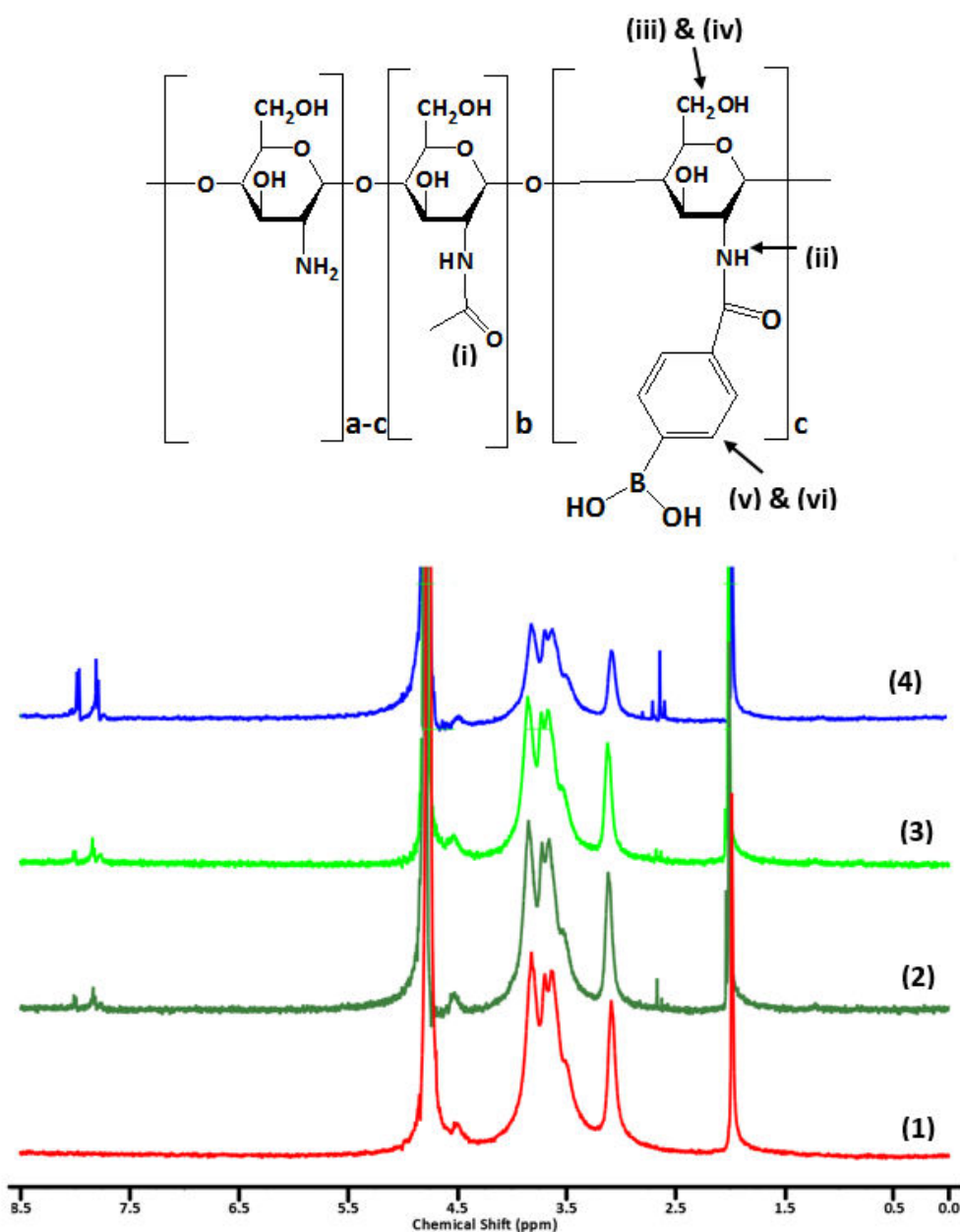
Fig. 4.2. ^{1}H NMR spectra of (1) CHI (2) LBCHI (3) MBCHI and (4) HBCHI recorded in D_2O acidified with 1% trifluoroacetic acid. Methyl protons from the acetylated part of chitosan observed at 2.0 ppm (i), methyne protons from the boronate moiety were evident at 2.67 - 2.8 ppm (ii), H2-H6 protons of CHI were detected at 3.0-4.0 ppm (iii & iv), and benzene ring of the boronate groups detected around 7.8 and 8.0 ppm (v & vi).

Their degree of boronation was calculated from the ratio of mean intensity of the proton peaks of the boronate moieties (δ = 7.8-8.0 ppm) relative to that of the chitosan glucosamine protons (δ = 3.0-4.0 ppm).

$$Boronation\ (\%) = \frac{Integral\ of\ boronate\ protons\ at\ 7.8\ \&\ 8.0\ ppm\ /2}{Integral\ of\ chitosan\ H2-H6\ protons\ /6} \cdot 100\% \qquad (1)$$
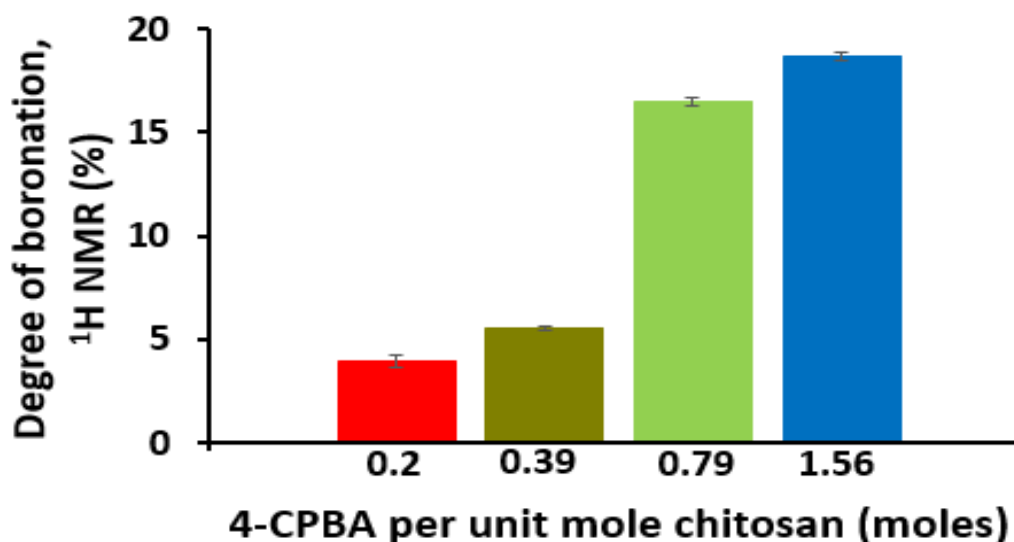
Fig. 4.3. Boronation extent versus molar ratio of 4-CPBA per unit mole of chitosan through ^{1}H NMR analysis (n=3, mean ± standard deviation), with red, dark green, green and blue bar charts depicting CHI, LBCHI, MBCHI and HBCHI, respectively.

Based on ^{1}H NMR data analysis (Fig. 4.3), a two-fold increase in the ratio of 4-CPBA per unit mole of chitosan used for LBCHI to generate MBCHI (Table 4.1) did not show a doubling of boronate conjugation (3.9% vs 5.5%, respectively) despite doubling the amount of boronate groups available to conjugate with the chitosan primary amino group. However, a 3-fold increase in the degree of boronation occurred when doubling the quantity of 4-CPBA in HBCHI against MBCHI with boronation of 5.5% and 16.5%, respectively. This finding may be due to a critical amount of 4-CPBA required to conjugate boronate groups to chitosan amine groups significantly.

4.3.2. Calculation of boronation extent using ninhydrin test

The ninhydrin test was used as an additional means of quantifying the degree of substitution of chitosan amine groups with boronate moieties. The principle of detection is based on the fact that ninhydrin reacts with the unmodified amine groups of chitosan to form a coloured product measurable by UV spectroscopy [47]. The slope of the adsorption versus

concentration curve of unconjugated chitosan is represented as δ_{CHI}, while that of LBCHI, MBCHI, and HBCHI are denoted as δ_{BCHI}. Boronation percentage can be defined as (1-$\delta_{BCHI}/\delta_{CHI}$)* 100% [13,36]. The respective boronation extent for LBCHI, MBCHI, and HBCHI were 4.4%, 7.4%, and 10.7% (Table 4.2). These values were comparable with that calculated using ^{1}H NMR spectroscopy (3.9%, 5.5%, and 16.5%, respectively) and showing the same trend in the degree of boronation with an increase in the molar ratio of 4-CPBA used.

4.3.3. FT-IR analysis

FT-IR spectra (Fig. 4.4) showed pronounced absorption band at 1026-1151 cm^{-1} indicating the amine C-N stretch from chitosan. Since both chitosan and boronate groups exhibit alkyl C-H stretch at 2850 and 2930 cm^{-1}, the increases in the intensity of the absorption bands depicts the formation of the boronated chitosan. The appearance of the new signal at 1311 cm^{-1} indicated $-B(OH)_2$ groups of the boronic acid segment and peaks evident at 713 and 1533 cm^{-1} represented para-substituted benzene ring. The prominent absorption peak at 1636 cm^{-1} in LBCHI, MBCHI and HBCHI confirmed the successful grafting of phenylboronate groups onto chitosan. This finding is in good agreement with the FT-IR spectra of chitosan-boronate conjugate reported in earlier studies [14] where $-B(OH)_2$ groups were evident at 1333.34 cm^{-1}; aromatic C-H bending bands were observed at 712.57 cm^{-1} while that of the benzene ring appeared at 1546.34 cm^{-1}. Also, the absorption peak confirming chitosan boronation (1636 cm^{-1}) is comparable to that of the chitosan-boronate conjugate earlier reported (1643.37 cm^{-1}). The FT-IR spectrum of LBCHI, MBCHI and HBCHI are comparable but vary in terms of the spectral intensity, which is dictated by their degree of boronation.
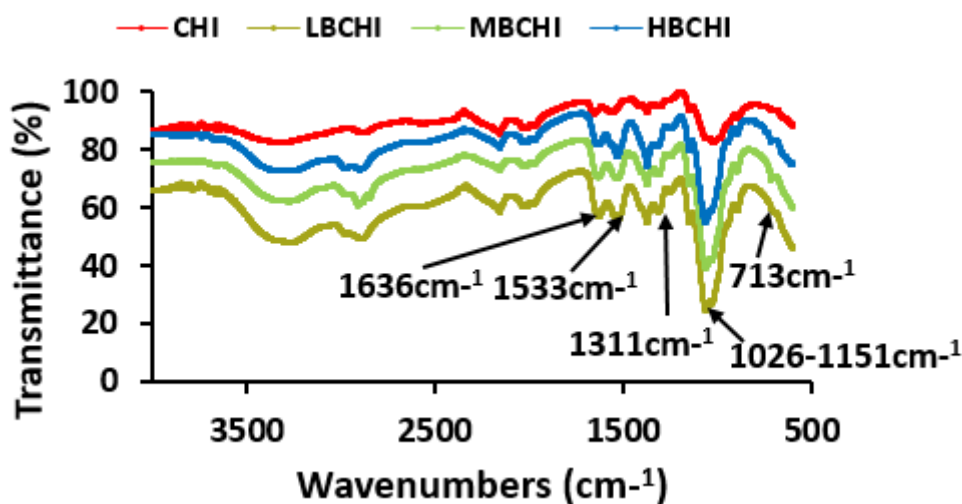
Fig. 4.4. FT-IR spectra of chitosan and boronated chitosan with distinct peak at 1311 cm^{-1} indicative of –B(OH)$_2$ groups; absorption bands at 713 and 1533 cm^{-1} depicted p-substituted benzene and absorption band confirming amide C=O linkage between chitosan and boronate groups evident at 1636 cm^{-1}.

4.3.4. Turbidimetric analysis

The typical pH of the bladder environment is between 6 and 7. However, various factors such as diet and disease states such as bladder cancer can impact urine pH resulting in pH ranges from 4.6 to 8 [48–50]. Moreover, changes in solution turbidity may impact product stability and performance. Thus there is a need to develop drug carriers that will withstand possible pH changes in the bladder.

The modified and unmodified chitosan solutions maintained transparency until pH 6.5, where further increase in pH resulted in a drastic increase in solution turbidity ($p < 0.05$) (Fig. 4.5). This turbidity-pH pattern is in good agreement with our earlier reports [13,37], where the unmodified chitosan and the chitosan with low extent of methacrylation displayed steep increase in degree of turbidity at ≥ pH 6.5 comparable to our boronated chitosans. The influence of boronate conjugation on the turbidity of chitosan solution was pronounced at pH ≥ 7, where the boronated chitosans displayed a lower turbidity than that of the unmodified chitosan ($p < 0.05$). This is because at pH ≥ 7 and higher degree of boronate conjugation, the bulky boronate groups will disrupt the semi-crystalline nature of chitosan, thereby improving its solubility and decreasing the solution turbidity [13,37]. There was significant difference in the turbidity values of the boronated chitosan at pH 9 ($p < 0.05$) (Fig. 4.6).
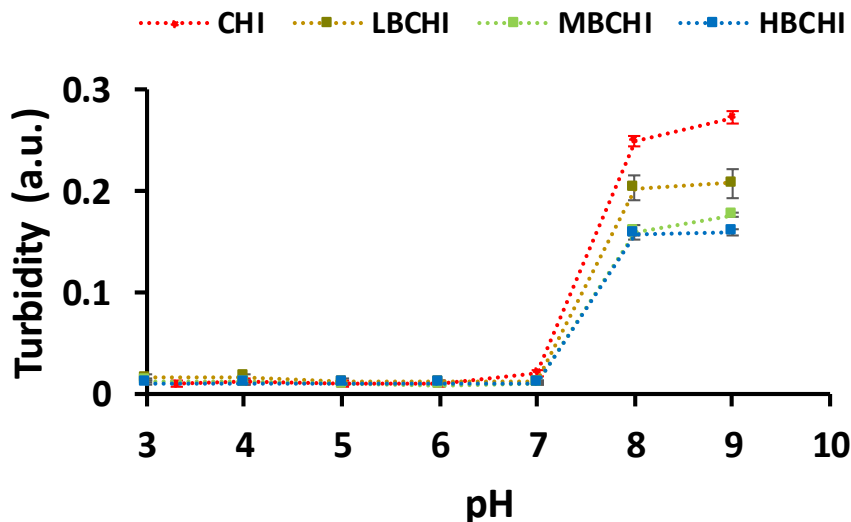
Fig. 4.5. Influence of pH on solution turbidity of unmodified and boronated chitosan (n=3, mean ± standard deviation)

Methacrylated chitosan previously reported from our group (LMeCHI), exhibited comparable pH-turbidity pattern to HBCHI [13] in terms of their turbidity values at pH 7 (0.014 vs. 0.0099) as well as at pH 9 (0.196 vs. 0.16) (p > 0.05). Since LMeCHI and HBCHI were synthesised using similar chitosan to hydrophobic group bearing moiety molar ratio, this finding suggested that methacrylate and boronate groups may have similar pH influence on the solution turbidity of the modified chitosan. This implies that the ability of methacrylated or boronated chitosan to withstand pH fluctuations in the bladder could be improved by increasing the amount of methacrylate or boronate groups conjugated to chitosan.

Also, at pH ≥ 7, the turbidity of all the studied boronated chitosans was more than that of the chitosan with high degree of methacrylation earlier reported [13]. This finding is expected as HMeCHI was synthesised using ten times the molar amount of the hydrophobic group bearing material per unit mole of chitosan used to prepare the most promising boronated chitosan (HBCHI). The physiological implication of these findings is that the ability of boronated chitosan to withstand pH fluctuations in the bladder may be improved by increasing the amount of boronate groups conjugated to chitosan.

4.3.5. X-ray diffraction analysis

Chitosan is a semi-crystalline polymer that displayed two main peaks at diffraction angles of 9.8^{o} and 20.5^{o} (Fig. 4.6). This finding is in good agreement with that of the chitosan peaks previously reported [13,37,51,52]. There was reduction in the crystallinity of chitosan after boronation with the disappearance and broadening of peaks as well as peaks appearing at a diffraction angle different from that of chitosan. The boronated chitosan did not exhibit any peak at a diffraction angle of 9.8^{o}. The distinctive broad peaks for LBCHI, MBCHI and HBCHI were evident at 20.5^{o}, 21.6^{o} and 21.9^{o}, respectively (Fig. 4.7). This finding is in good agreement with that observed with the methacrylated chitosans with loss and broadening of peaks evident at diffraction angles of 8.3^{o} and 22.4^{o}, respectively [13]. The physiological implication of this findings is that boronated chitosan may generate drug solubilised amphiphilic copolymeric systems more readily than the parent chitosan, which is desirable for injectable formulations intended for intravesical application.
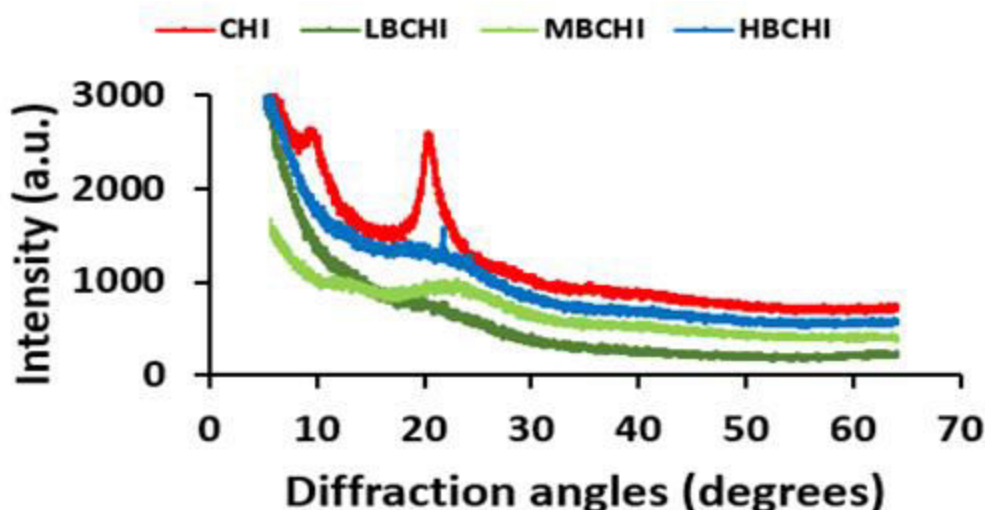
Fig. 4.6. X-ray diffractograms of CHI, LBCHI, MBCHI and HBCHI generated at scan angle 5-65°, 2.5 scans·min^{-1}, scan step of 0.02^{o}, spectra offset for improved clarity.

4.3.6. Urine wash-out studies

Fluorescein sodium (FS), which served as the model drug, was mixed with the unmodified and boronated chitosan prior to the mucoadhesion studies. The unmodified chitosan served as the mucoadhesive positive control [53], while the negative control was FITC-dextran, with limited mucoadhesive property [54]. The *ex vivo* porcine bladder was used to measure the wash-out$_{50}$ values of fluorescein sodium in the presence of the unmodified and boronated chitosan. WO$_{50}$

138

is the volume of artificial urine needed to remove 50% of fluorescein from the bladder mucosal surface [39].

FITC-dextran displayed the least mucosal retention on the porcine bladder mucosa (WO_{50} of 7±2 mL, Fig. 4.8) from extrapolation as 10 mL of artificial urine was used for each wash-out cycle similar to that reported previously [13,39]. FITC-dextran was significantly less mucoadhesive than the boronated chitosan over the five washing cycles (with 50 mL artificial urine) ($p < 0.05$). Also, unmodified chitosan was significantly more mucoadhesive than FITC-dextran ($p < 0.05$).

Typically, cationic polymers like chitosan interact with negatively charged sialic acid groups present on urothelial mucosal surfaces via electrostatic interaction. Phenylboronic acid is composed of phenyl substituent and two hydroxyl groups attached to boron, which enables it form a complex with the diol groups of sialic acid at physiological pH [15]. The presence of counter ions present in the artificial urine used for the wash-out studies may inhibit the favourable interaction of chitosan with sialic acid-rich mucosal surfaces. Chitosan conjugation with boronate groups (HBCHI) resulted in 3.1-fold increase in their WO_{50} values. Based on the polynomial fit of the fluorescence intensity versus urine volume graph, the WO_{50} values of the polymer samples were determined (Fig. 4.7).
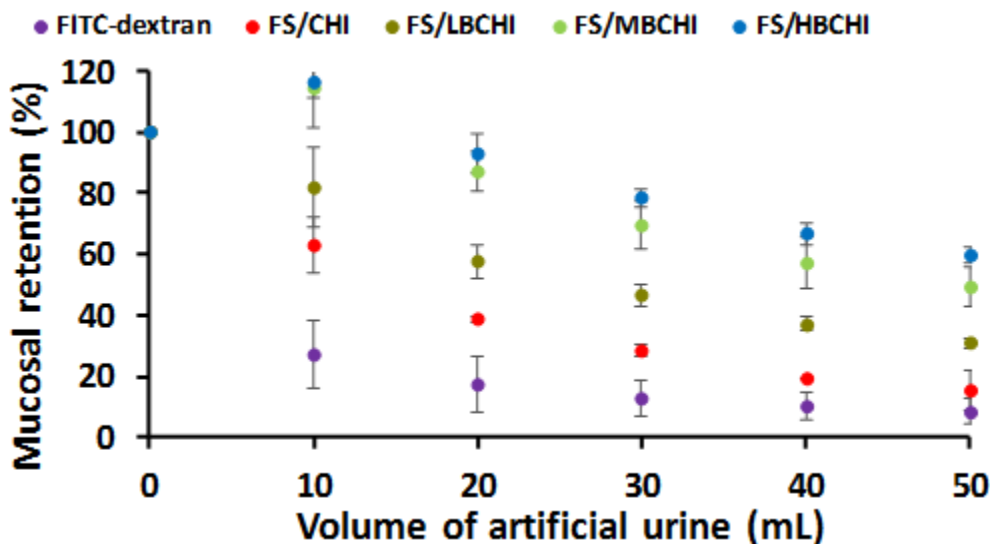
Fig. 4.7. The mucosal fluorescence retention profile of FITC-dextran, unmodified chitosan and boronated chitosan on porcine bladder tissues evaluated using ImageJ software and WO_{50} values calculated based on the polynomial fit of the graphs. Results presented as mean±SD, n=3

The WO_{50} values of FS/CHI, FS/LBCHI, FS/MBCHI and FS/HBCHI were 15±4 mL, 23±3 mL, 48±5 mL and 55±2 mL, respectively. Boronated chitosan may interact with mucosal surfaces through various mechanisms [22] shown in Scheme 4.1: (i) the phenylboronic acid groups could potentially form covalent linkage with sialic acid expressed on cell membranes to form reversible covalent complexes [55,56], (ii) hydrogen bond formation with mucin glycoproteins possible due to its constituent hydroxyl groups [43] and (iii) electrostatic interaction between cationic polymer and negatively charged sialic acid residues [42,53]. Therefore, the greater degree of mucoadhesion as seen in HBCHI could be due to the more boronate groups being available to interact with the mucosal surface (Fig. 4.8 and Fig. 4.9).
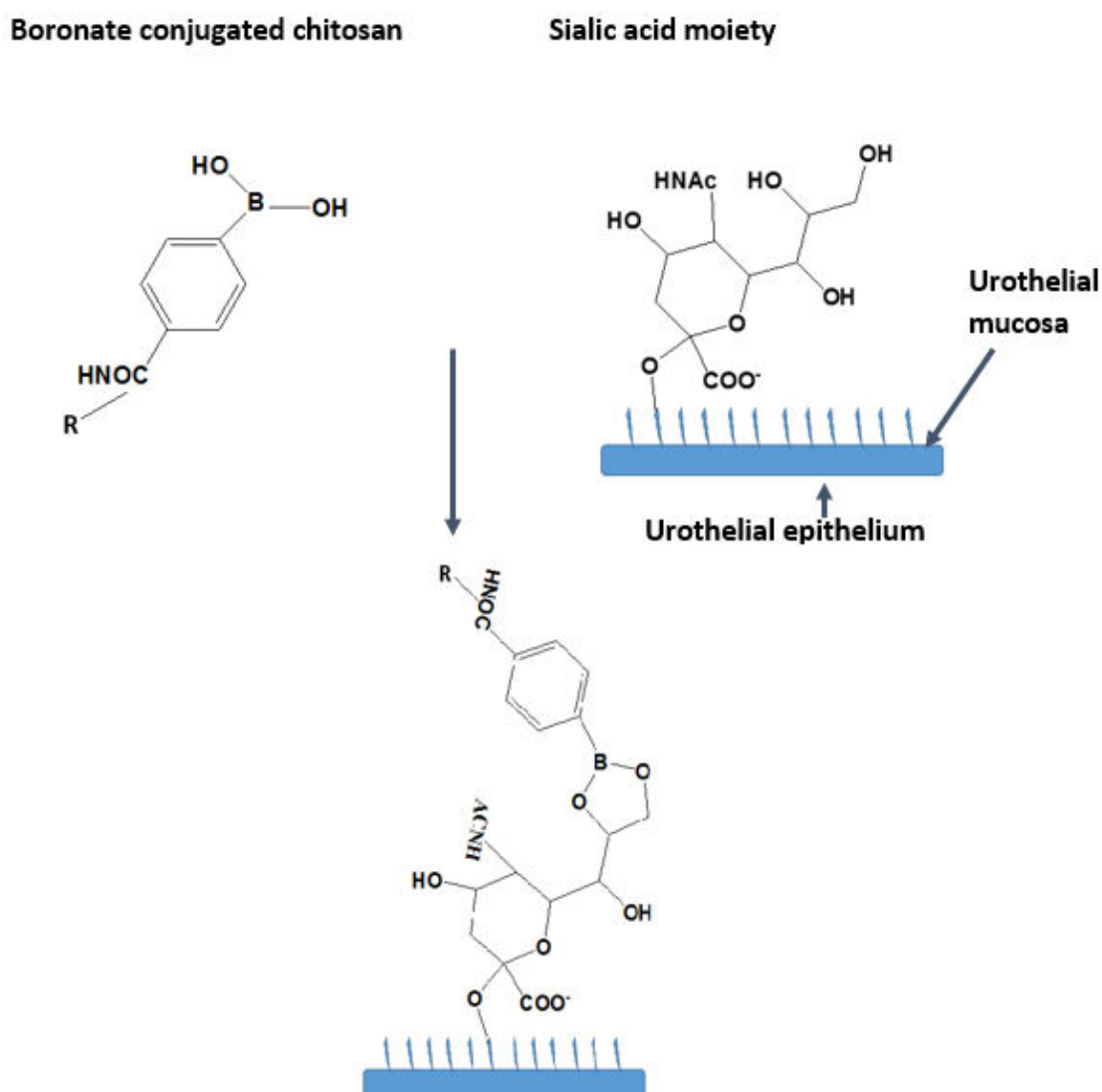
Scheme 4.1. Schematic illustration of the urothelial mucoadhesiveness of boronated chitosan to prevent wash-out during urine voiding, where "R" is the chitosan backbone

Significant difference in the mucoadhesive behaviour of the parent chitosan and the boronated derivatives (LBCHI, MBCHI and HBCHI) can be seen after two urine washing cycles and differences remained significant after five washing cycles ($p < 0.05$). MBCHI and HBCHI were significantly more mucoadhesive than LBCHI after the first washing cycle with 10 mL artificial urine. On the other hand, the mucoadhesive behaviour of MBCHI and HBCHI was not significantly different after 5 washing cycles with 50 mL artificial urine. This finding indicated that the urine wash-out resistance of boronated chitosan may become unchanged after a particular degree of boronation. Figure 4.9 confirmed that FS/CHI and FS/LBCHI displayed comparable mucoadhesiveness in terms of their WO_{50} values (15±4 mL vs 23±3 mL) but that of HBCHI was significantly more mucoadhesive than MBCHI, with WO_{50} values of 48±5 mL and 56±2 mL, respectively. Thus, boronation still had some influence on the mucoadhesiveness of the boronated chitosans, which was most prominent after washing out the bladder mucosa with 30 mL artificial urine.
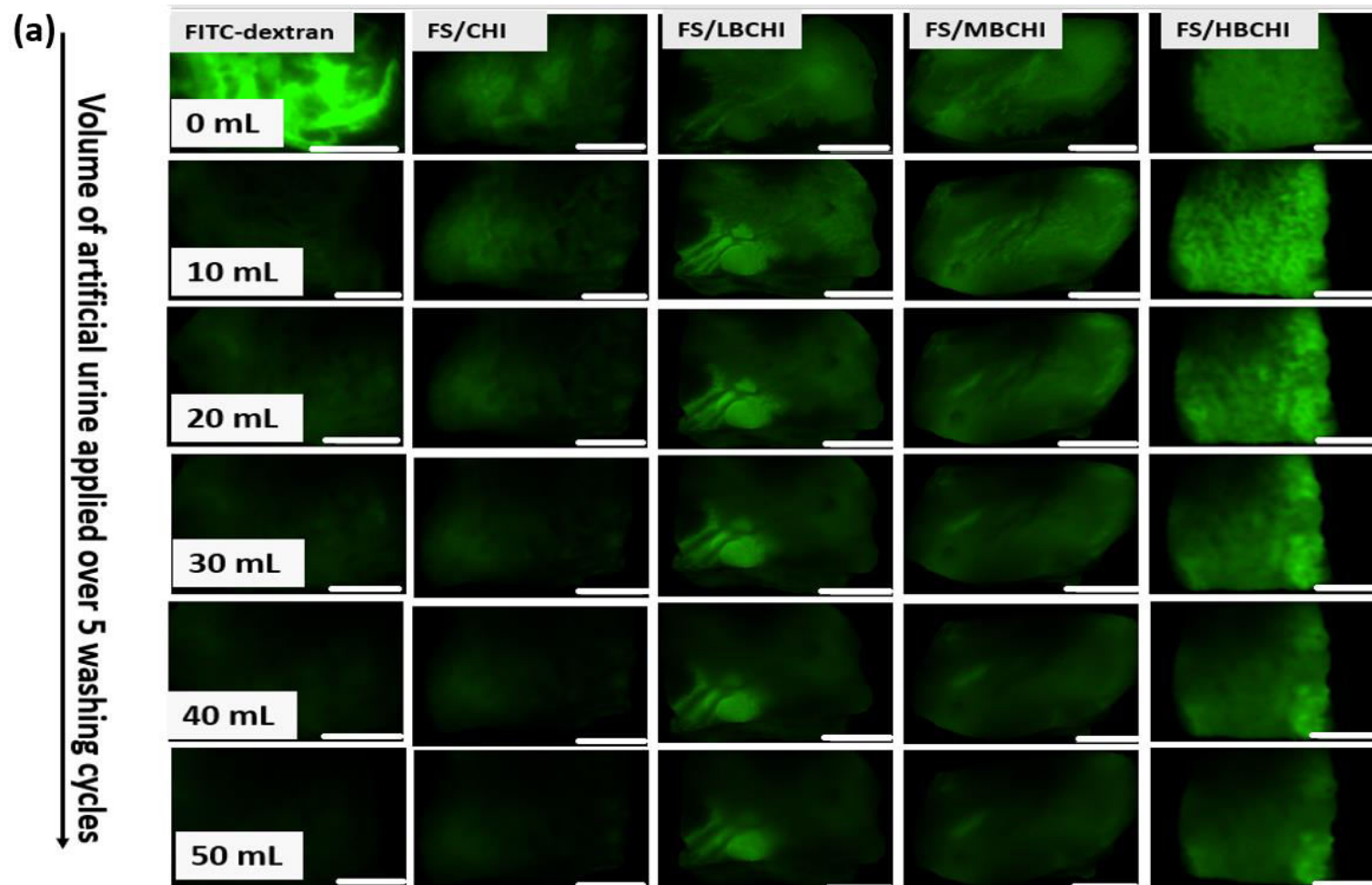
Fig. 4.8a. *Ex vivo* urine wash-out studies using porcine urinary bladder with fluorescently labelled dextran, FS/CHI, FS/LBCHI, FS/MBCHI and FS/HBCHI: Exemplary fluorescent microscopic photos of the urinary bladder over 5 washing cycles, scale bar is 2 mm.
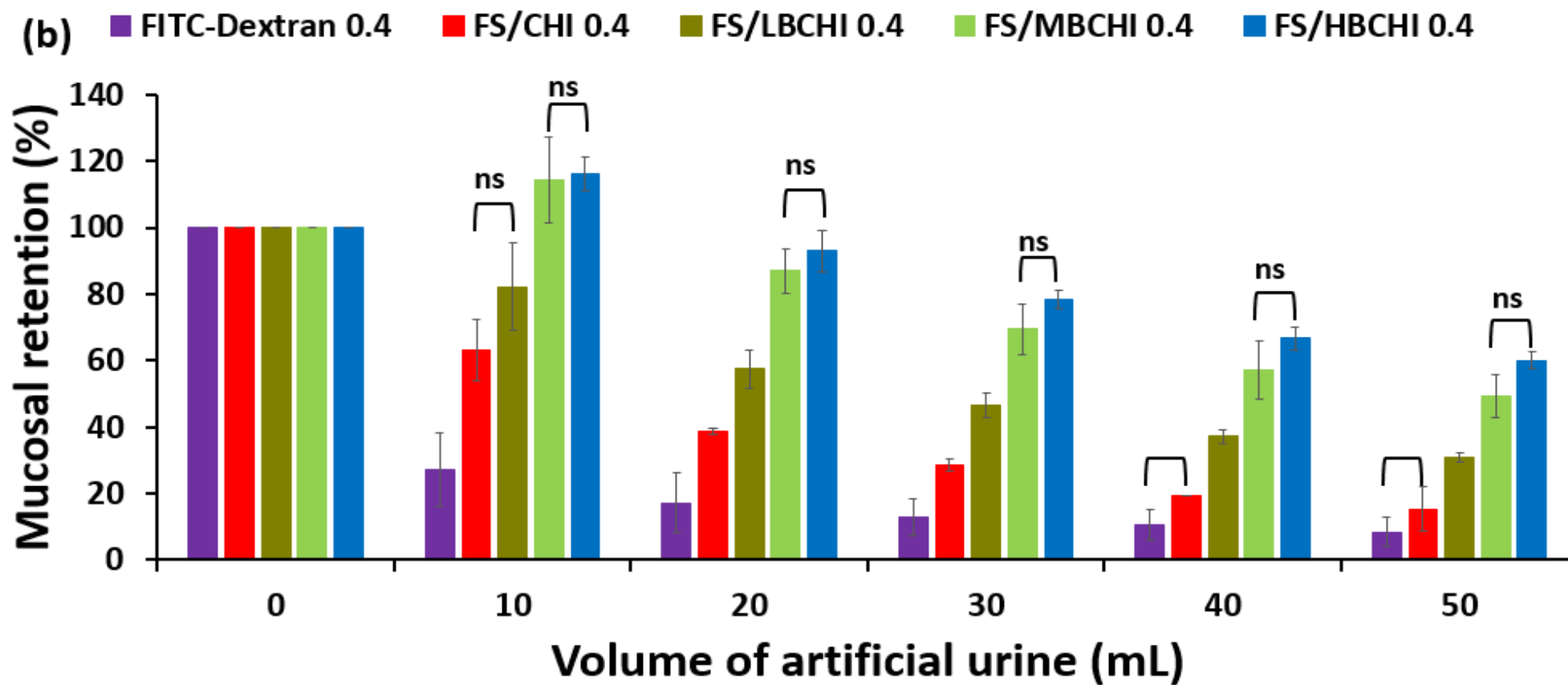
Fig. 4.8 (b) Mucosal retention of the model drug fluorescein sodium mixed with CHI, LBCHI, MBCHI and HBCHI at different washing cycles; FITC-dextran served as negative control and FS/CHI (unmodified chitosan) as a positive control. Results presented as average ± standard deviation, n = 3, all the studied groups of samples displayed statistically significant differences between them ($p < 0.05$) except those depicted by "ns" implying no significant differences between particular groups of samples

Interestingly, HMeCHI early reported by our group which was synthesised using 4.65 moles per unit mole of chitosan displayed similar porcine mucoadhesive profile with MBCHI (WO$_{50}$ values of 48 mL), synthesised using 0.39 moles of 4-CPBA per unit mole of chitosan (Fig. 4.8 and Fig. 4.9). This finding further affirmed that boronate conjugated chitosan was more mucoadhesive than methacrylate derivatised chitosan.
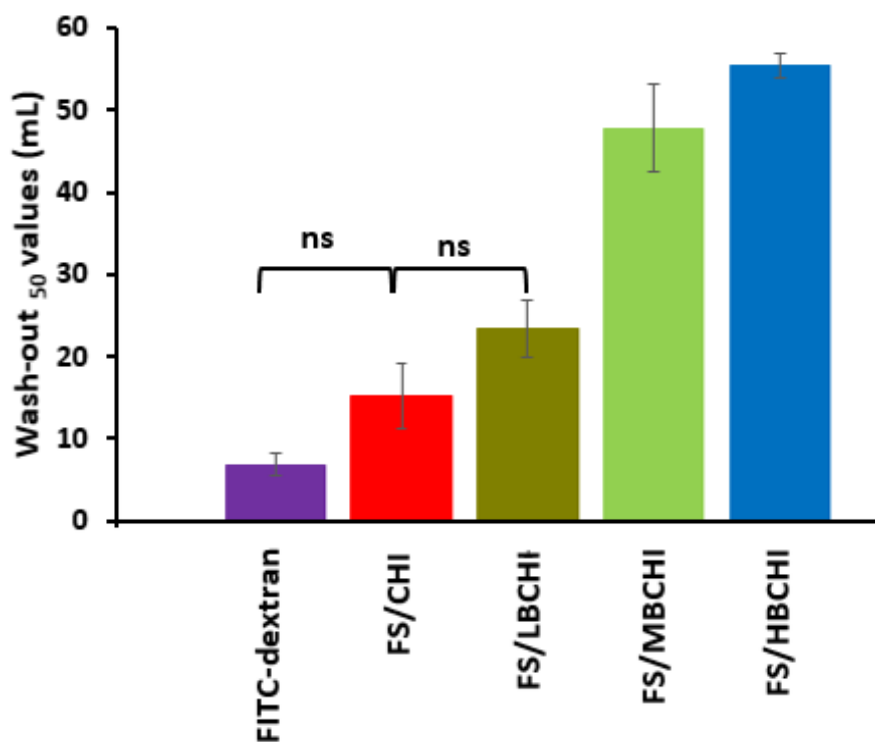
Fig. 4.9. Urine Wash-out$_{50}$ values of FITC-dextran, CHI, LBCHI, MBCHI and HBCHI. Results presented as average ± standard deviation, n = 3; all the studied groups of samples displayed statistically significant differences between them (p < 0.05) except those depicted by "ns" implying no significant differences between particular groups of samples.

4.3.7. Mucoadhesive properties studied using tensile test

The force of detachment or adhesive strength indicates the force required to overcome the adhesive bonds between the drug carrier and bladder mucosa, while the work of adhesion is the area under the force-distance curves.
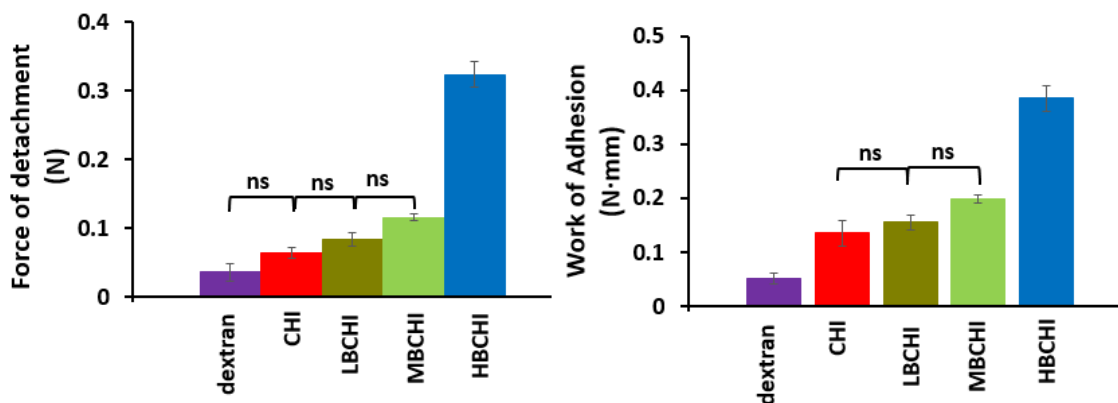
Fig. 4.10. (a) Force of detachment and (b) work of adhesion of dextran, CHI, LBCHI, MBCHI and HBCHI to porcine bladder mucosa measured using tensile test. Results presented as mean ± standard deviation, n = 3; all the studied groups of samples displayed statistically significant differences between them (p < 0.05) except those depicted by "ns" implying no significant differences between particular groups of samples.

Though, dextran and CHI displayed similar force of detachment (Fig. 4.10), the work of adhesion values showed that CHI was statistically more mucoadhesive than dextran. MBCHI and HBCHI were significantly more mucoadhesive compared to the unmodified chitosan with the force of detachment in increasing order from dextran (0.04±0.01 N) < CHI (0.06±0.01 N) < LBCHI (0.08±0.01 N) < MBCHI (0.12±0.01 N) < HBCHI (0.32±0.02 N). CHI vs LBCHI; LBCHI vs MBCHI and MBCHI vs HBCHI displayed comparable forces of detachment and work of adhesion values. The work of adhesion presented in increasing order: CHI (0.14±0.02 N·mm) < LBCHI (0.16±0.02 N·mm) < MBCHI 0.2±0.01 N·mm < HBCHI (0.4 N±0.02 N·mm). Overall, the adhesive strength of the polymers correlated well with their work of adhesion as MBCHI and HBCHI exhibited greater force of detachment and work of adhesion relative to the parent chitosan. These findings inferred that the mucoadhesiveness of the polymers was improved with increased extent of boronation. This is in good agreement with the urine-wash-out test data.

4.4. Conclusions

Boronated chitosans were successfully synthesised. Based on ^{1}H NMR analysis, chitosan conversion to boronated chitosan occurred in a controlled but less predictable manner. This is because an initial two-fold increase in the molar ratio of 4-CPBA per unit mole of chitosan (0.20 vs 0.39) used for the synthesis of boronated chitosan did not result in the doubling of the boronation extent of LBCHI and MBCHI (3.9% and 5.5%, respectively, using ^{1}H NMR analysis) but a further two-fold increase in the CPBA/CHI ratio resulted in about three-fold increase in the degree of boronation with HBCHI displaying 16.5% as its degree of boronation (Table 4.2). There was good correlation in the boronation extent of boronated chitosan using ^{1}H NMR and ninhydrin method of boronate quantification.

Chitosan boronation had a profound influence on the mucoadhesiveness of the new polymers as mucoadhesive properties (in terms of wash-out$_{50}$ profile, force of adhesion/detachment and work of adhesion) was greatest for the highly boronated chitosan. Nevertheless, all the boronated chitosan still exhibited superior mucoadhesiveness (WO$_{50}$ values of 23-55 mL) relative to our previously reported methacrylated chitosans (WO$_{50}$ values of 24-48 mL).

Boronation did not show a significant influence on the solution turbidity of the polymers as the pH of the polymer solutions was progressively increased from 3 to 8. However, all the unmodified and modified chitosan displayed relatively low turbidity at ≤ 6.5, implying that the colloidal stability of all the boronated chitosans could be sustained if the pH of the bladder environment is ≤ 6.5 and they could all be explored for intravesical drug delivery. Nevertheless, boronation influenced their turbidity profile at pH 9, with HBCHI displaying the lowest turbidity in comparison to boronated chitosan and the parent chitosan, inferring that the potential of boronate groups to maintain colloidal stability of boronated chitosan (evident by lowered turbidity) becomes evident at higher pH of 9.

The tensile test corroborated the findings from the wash-out studies indicating mucoadhesiveness was improved with increasing extent of boronation. These boronated chitosan delivery systems could potentially extend the residence time of therapeutic payload on malignant urothelial tissues due to their superior covalent interaction with sialic acid residues on urothelial mucosal surfaces relative to the parent chitosan, thereby limiting the dosing frequency of boronated chitosan based dosage forms used for bladder disease treatment. Future research will explore studying the safety of boronated chitosan as well as

formulating with excipients and loading with drugs for the treatment of bladder diseases to study their drug release and efficacy.

References

1.   Torre LA, Bray F, Siegel RL, Ferlay J, Lortet-tieulent J, Jemal A. Global Cancer Statistics, 2012. CA Cancer J Clin. 2015;65(2):87–108.

2.   Antoni S, Ferlay J, Soerjomataram I, Znaor A, Jemal A, Bray F. Bladder Cancer Incidence and Mortality: A Global Overview and Recent Trends. Eur Urol. 2017;71(1):96–108.

3.   Babjuk M. Trends in Bladder Cancer Incidence and Mortality: Success or Disappointment? Eur Urol. 2017;71(1):109–10.

4.   Jayakumar R, Menon D, Manzoor K, Nair S V., Tamura H. Biomedical applications of chitin and chitosan based nanomaterials - A short review. Carbohydr Polym. 2010;82(2):227–32.

5.   Bernkop-Schnürch A, Dünnhaupt S. Chitosan-based drug delivery systems. Eur J Pharm Biopharm. 2012;81(3):463–9.

6.   Casettari L, Illum L. Chitosan in nasal delivery systems for therapeutic drugs. J Control Release 2014;190:189–200.

7.   Bernkop-Schnürch et al. 1999. Synthesis and in vitro evaluation of chitosan-cysteine conjugates. Sci Pharm. 1999;67:196–208.

8.   Kast CE, Bernkop-Schnürch A. Thiolated polymers - thiomers: Development and in vitro evaluation of chitosan-thioglycolic acid conjugates. Biomaterials 2001;22(17):2345–52.

9.   Bernkop-Schnürch A. Thiolated polymers—thiomers: synthesis and in vitro evaluation of chitosan–2-iminothiolane conjugates. Int J Pharm. 2003;260(2):229–37.

10.   Kafedjiiski K, Föger F, Werle M, Bernkop-Schnürch A. Synthesis and in vitro evaluation of a novel chitosan-glutathione conjugate. Pharm Res. 2005;22(9):1480–8.

11.   Schmitz T, Grabovac V, Palmberger TF, Hoffer MH, Bernkop-Schnürch A. Synthesis and

characterization of a chitosan-N-acetyl cysteine conjugate. Int J Pharm. 2008;347 (1–2):79–85.

12. Millotti G, Samberger C, Frohlich E, Bernkop-schnurch A. Chitosan- graft -6-mercaptonicotinic Acid : Synthesis , Characterization , and Biocompatibility. Biomacromolecules 2009;10:3023–7.

13. Kolawole OM, Lau WM, Khutoryanskiy V V. Methacrylated chitosan as a polymer with enhanced mucoadhesive properties for transmucosal drug delivery. Int J Pharm. 2018;550(1–2):123–9.

14. Zhang D, Yu G, Long Z, Yang G, Wang B. Controllable layer-by-layer assembly of PVA and phenylboronic acid-derivatized chitosan. Carbohydr Polym. 2016;140:228–32.

15. Cambre JN, Sumerlin BS. Biomedical applications of boronic acid polymers. Polymer (Guildf). 2011;52(21):4631–43.

16. Li Y, Xiao W, Xiao K, Berti L, Luo J, Tseng HP, Fung G, Lam KS. Well-defined, reversible boronate crosslinked nanocarriers for targeted drug delivery in response to acidic pH values and cis-diols. Angew Chemie - Int Ed. 2012;51(12):2864–9.

17. Cheng C, Zhang X, Wang Y, Sun L, Li C. Phenylboronic acid-containing block copolymers: Synthesis, self-assembly, and application for intracellular delivery of proteins. New J Chem. 2012;36(6):1413–21.

18. Ma R, Yang H, Li Z, Liu G, Sun X, Liu X, An Y, Shi L. Phenylboronic acid-based complex micelles with enhanced glucose-responsiveness at physiological pH by complexation with glycopolymer. Biomacromolecules. 2012;13(10):3409–17.

19. Liu S, Jones L, Gu FX. Development of Mucoadhesive Drug Delivery System Using Phenylboronic Acid Functionalized Poly(D,L-lactide)-b-Dextran Nanoparticles. Macromol Biosci. 2012;12(12):1622–6.

20. Liu S, Chang CN, Verma MS, Hileeto D, Muntz A, Stahl U, Woods J, Jones LW, Gu FX. Phenylboronic acid modified mucoadhesive nanoparticle drug carriers facilitate weekly treatment of experimentallyinduced dry eye syndrome. Nano Res. 2015;8(2):621–35.

21. Prosperi-Porta G, Kedzior S, Muirhead B, Sheardown H. Phenylboronic-Acid-Based Polymeric Micelles for Mucoadhesive Anterior Segment Ocular Drug Delivery. Biomacromolecules 2016;17(4):1449–57.

22. Zheng C, Guo Q, Wu Z, Sun L, Zhang Z, Li C, Zhang X. Amphiphilic glycopolymer nanoparticles as vehicles for nasal delivery of peptides and proteins. Eur J Pharm Sci. 2013;49(4):474–82.

23. Li C, Liu Z, Yan X, Lu W, Liu Y. Mucin-controlled drug release from mucoadhesive phenylboronic acid-rich nanoparticles. Int J Pharm. 2015;479(1):261–4.

24. Wu W, Shen J, Li Y, Zhu H, Banerjee P, Zhou S. Specific glucose-to-SPR signal transduction at physiological pH by molecularly imprinted responsive hybrid microgels. Biomaterials. 2012;33(29):7115–25.

25. Zhang C, Losego MD, Braun P V. Hydrogel-based glucose sensors: Effects of phenylboronic acid chemical structure on response. Chem Mater. 2013;25(15):3239–50.

26. Wu W, Mitra N, Yan ECY, Zhou S. Multifunctional Hybrid Nanogel for and Self-Regulated Insulin Release at Physiological pH. ACS Nano. 2010;4(8):4831–9.

27. Wang X, Zhen X, Wang J, Zhang J, Wu W, Jiang X. Doxorubicin delivery to 3D multicellular spheroids and tumors based on boronic acid-rich chitosan nanoparticles. Biomaterials 2013;34(19):4667–79.

28. Wang J, Zhang Z, Wang X, Wu W, Jiang X. Size- and pathotropism-driven targeting and washout-resistant effects of boronic acid-rich protein nanoparticles for liver cancer regression. J Control Release 2013;168(1):1–9.

29. Wang J, Wu W, Zhang Y, Wang X, Qian H, Liu B, Jiang X. The combined effects of size and surface chemistry on the accumulation of boronic acid-rich protein nanoparticles in tumors. Biomaterials 2014;35(2):866–78.

30. Lee SY, Lee H, In I, Park SY. PH/redox/photo responsive polymeric micelle via boronate ester and disulfide bonds with spiropyran-based photochromic polymer for cell imaging and anticancer drug delivery. Eur Polym J. 2014;57:1–10.

31. Piest M, Ankoné M, Engbersen JFJ. Carbohydrate-interactive pDNA and siRNA gene vectors based on boronic acid functionalized poly(amido amine)s. J Control Release 2013;169(3):266–75.

32. Ji M, Li P, Sheng N, Liu L, Pan H, Wang C, Cai L, Ma Y. Sialic Acid-Targeted Nanovectors with Phenylboronic Acid-Grafted Polyethylenimine Robustly Enhance siRNA-Based Cancer Therapy. ACS Appl Mater Interfaces 2016;8(15):9565–76.

33. Wang X, Wei B, Cheng X, Wang J, Tang R. 3-Carboxyphenylboronic acid-modified carboxymethyl chitosan nanoparticles for improved tumor targeting and inhibitory. Eur J Pharm Biopharm. 2017;113:168–77.

34. Wang X, Tang H, Wang C, Zhang J, Wu W, Jiang X. Phenylboronic acid-mediated tumor targeting of chitosan nanoparticles. Theranostics 2016;6(9):1378–92.

35. Asantewaa Y, Aylott J, Burley JC, Billa N, Roberts CJ. Correlating physicochemical properties of boronic acid-chitosan conjugates to glucose adsorption sensitivity. Pharmaceutics 2013;5(1):69–80.

36. Shitrit Y, Bianco-Peled H. Acrylated chitosan for mucoadhesive drug delivery systems. Int J Pharm. 2017;517(1–2):247–55.

37. Sogias IA, Khutoryanskiy V V., Williams AC. Exploring the factors affecting the solubility of chitosan in water. Macromol Chem Phys. 2010;211(4):426–33.

38. Chutipongtanate S, Thongboonkerd V. Systematic comparisons of artificial urine formulas for in vitro cellular study. Anal Biochem. 2010;402(1):110–2.

39. Mun EA, Williams AC, Khutoryanskiy V V. Adhesion of thiolated silica nanoparticles to urinary bladder mucosa: Effects of PEGylation, thiol content and particle size. Int J Pharm. 2016;512(1):32–8.

40. Caló E, Barros JMSD, Fernández-Gutiérrez M, San Román J, Ballamy L, Khutoryanskiy V V. Antimicrobial hydrogels based on autoclaved poly(vinyl alcohol) and poly(methyl vinyl ether-: Alt -maleic anhydride) mixtures for wound care applications. RSC Adv. 2016;6(60):55211–9.

41. Boateng JS, Pawar H V., Tetteh J. Polyox and carrageenan based composite film dressing containing anti-microbial and anti-inflammatory drugs for effective wound healing. Int J Pharm. 2013;441(1–2):181–91.

42. Khutoryanskiy V V. Advances in Mucoadhesion and Mucoadhesive Polymers. Macromol Biosci. 2011;11(6):748–64.

43. Khutoryanskiy V V. Mucoadhesive Materials and Drug Delivery Systems. John Wiley & Sons; 2014:33.

44. Ways T, Lau W, Khutoryanskiy V. Chitosan and Its Derivatives for Application in Mucoadhesive Drug Delivery Systems. Polymers (Basel). 2018;10(3):267.

45. Deshayes S, Cabral H, Ishii T, Miura Y, Kobayashi S, Yamashita T, Matsumoto A, Miyahara Y, Nishiyama N, Kataoka K. Phenylboronic acid-installed polymeric micelles for targeting sialylated epitopes in solid tumors. J Am Chem Soc. 2013;135(41):15501–7.

46. Fischer MJ. Amine Coupling Through EDC/NHS: A Practical Approach. Methods Mol Biol. 2010; 627:55-73.

47. Gohel V, Vyas P, Chhatpar HS, Zitouni M, Fortin M, Thibeault J-S, Brzezinski R, Muzzarelli RA, Larionova NI, Zubaerova DK, Guranda DT, Pechyonkin MA, Balabushevich NG, Prochazkova S, Vårum KM, Ostgaard K, Wischke C, Borchert HH. Quantitative determination of chitosans by ninhydrin. Carbohydr Polym. 2006;38(2):255–7.

48. Ince BA, Anderson EJ, Neer RM. Lowering dietary protein to U.S. recommended dietary allowance levels reduces urinary calcium excretion and bone resorption in young women. J Clin Endocrinol Metab. 2004;89(8):3801–7.

49. GuhaSarkar S, Banerjee R. Intravesical drug delivery: Challenges, current status, opportunities and novel strategies. J Control Release 2010;148(2):147–59.

50. Alguacil J, Kogevinas M, Silverman DT, Malats N, Real FX, García-Closas M, Tardón A, Rivas M, Torà M, García-Closas R, Serra C, Carrato A, Pfeiffer RM, Fortuny J, Samanic C, Rothman N. Urinary pH, cigarette smoking and bladder cancer risk. Carcinogenesis 2011;32(6):843–7.

51. Yin J, Luo K, Chen X, Khutoryanskiy V V. Miscibility studies of the blends of chitosan with some cellulose ethers. Carbohydr Polym. 2006;63(2):238–44.

52. Luo K, Yin J, Khutoryanskaya O V., Khutoryanskiy V V. Mucoadhesive and elastic films based on blends of chitosan and hydroxyethylcellulose. Macromol Biosci. 2008;8(2):184–92.

53. Sogias IA, Williams AC, Khutoryanskiy V V. Why is chitosan mucoadhesive? Biomacromolecules 2008;9(7):1837–42.

54. Štorha A, Mun E a., Khutoryanskiy V V. Synthesis of thiolated and acrylated nanoparticles using thiol-ene click chemistry: towards novel mucoadhesive materials for drug delivery. RSC Adv. 2013;3(30):12275.

55. Matsumoto A, Cabral H, Sato N, Kataoka K, Miyahara Y. Assessment of Tumor Metastasis by the Direct Determination of Cell-Membrane Sialic Acid Expression. Angew Chemie Int Ed. 2010;49(32):5494–7.

56. Liu A, Peng S, Soo JC, Kuang M, Chen P, Duan H. Quantum dots with phenylboronic acid tags for specific labeling of sialic acids on living cells. Anal Chem. 2011;83(3):1124–30.

5. Conclusions / Future studies

The key findings of the PhD project as well as potential future work are detailed in this concluding chapter

5.1. General conclusions

Charitable Organisations (e.g. Action on Bladder Cancer, Fight Bladder Cancer and The Urology Foundation) that emphasise bladder cancer prevention and treatment, launched a "Shout Out About Bladder Cancer" campaign to raise awareness of bladder cancer and its symptoms to both the public and health professionals [1]. Also, current bladder cancer related clinical trials in the UK focus on bladder cancer diagnosis and treatment. Out of the current 13 clinical trials on the UK bladder cancer clinical trial database, 4 (31%) focused on disease diagnosis, 3 (23%) investigated surgical and radiation therapy, while 6 (46%) explored biologics and chemotherapeutic agents for bladder cancer treatment [2]. Surprisingly, improved formulations or methods for the intravesical delivery of Mitomycin-C are not currently studied in the UK bladder cancer related clinical trials [2]. Nevertheless, Mitomycin-C (with antimitotic and cytotoxic effects) is still the gold-standard for the treatment of superficial / non-invasive bladder cancer in the UK [3] and effective dosage forms for delivering chemotherapeutic agents to the bladder still occupies an integral component for the successful management of the disease to prevent metastasis and progression to muscle invasive forms. Moreover, there is a strong need to develop improved intravesical dosage forms that will be retained in the bladder for an extended period of time.

This PhD project focused on monotherapy which is typically used for superficial/non-muscle invasive bladder cancer treatment. Moreover, combination therapy through the systemic route of administration becomes critical for more advanced stages of the disease, though plagued by its therapy associated side effects and adverse reaction [4]. The first chapter provided an overview of various formulations that have been explored to improve drug residence time in the bladder. They include amphiphilic copolymers, biorecognitive drug carriers, mucoadhesive micro- and nanoparticles, *in situ* gelling formulations, floating and liposomal delivery systems. Most of these studied formulations were promising in terms of their drug loading, tumour regression, biocompatibility and duration of action. Some of the issues that prevented clinical translation of these promising dosage forms were identified, which include disparity in the *in vitro* and *in vivo* experimental design as well as scale-up of excipients and chemotherapeutic agents that were effective in animal models for efficient treatment of human urinary bladder cancer. The harmonisation of relevant *in vitro* and *in vivo* models and methods of evaluating the physicochemical and biological properties of intravesical formulations may be a step closer to regulatory approval and commercialisation of novel intravesical dosage forms.

Therefore, in the second chapter, mitomycin-C loaded chitosan/β-glycerophosphate (CHIGP) *in situ* thermosensitive gelling systems were formulated using three chitosan grades (with different molecular weights) generating low- (MMC/LCHIGP), medium- (MMC/MCHIGP) and high-molecular weight based (MMC/HCHIGP) gels. Control chitosan formulations without β-glycerophosphate (MMC/LCHI, MMC/MCHI and MMC/HCHI) were also prepared for comparison of physicochemical and biological properties. The method of preparing these dosage forms was simple and efficient yet the ability of the CHIGP mixtures to form gels at physiological temperature (37°C) was dependent on the concentration and volume ratio between chitosan and β-glycerophosphate solution. The formation of the gels was reproducible and independent of the vessels used for their preparation. The samples presented in the order of increasing ease of gelation with or without mitomycin-C: MMC/LCHIGP < MMC/MCHIGP < MMC/HCHIGP, inferring that chitosan molecular weight modulated the *in situ* gelling properties of the CHIGP mixtures.

Gel strength is one of the critical parameters required for bladder cancer therapeutic drug carriers as *in situ* gelling formulations will be in constant contact with urine. At physiological temperature, urea, the major component of urine, disrupts the hydrogen bonds in the gel network of the formulations *in situ*, making the formulations remain as a liquid within the bladder thereby compromising interaction between the dosage form and the urothelial mucosa [5]. Stronger gels are more resistant to the gel network disruptive effect of urine than weaker types. Amongst the CHIGP *in situ* gelling systems, HCHIGP could be the most promising drug carrier for bladder cancer chemotherapeutics delivery in terms of their overall physicochemical and biological properties: ease of gelation (2-5 min), gelation temperature (31 ^{o}C), gel strength (G'/G" 16.7 fold), drug release (37±17% over 6 h), and porcine mucoadhesive profile (WO_{50} 9±1 mL). Using rheological methods, LCHIGP, MCHIGP and HCHIGP had a satisfactory gelation time (≈ 2 min) and gelation temperature (≈ 30°C), but LCHIGP and MCHIGP gels were weaker than that of HCHIGP in terms of gel strength.

Our major findings was that chitosan gels were more mucoadhesive than LCHIGP, MCHIGP and HCHIGP in terms of their bioadhesiveness and resistance to artificial urine wash-out from porcine bladder mucosa. The β-glycerophosphate was thought to reduce the overall cationic charge of the drug carriers, thereby decreasing the electrostatic interaction between the formulations and mucin glycoproteins present on urothelial cell membranes. The mucoadhesive profile of LCHIGP, MCHIGP and HCHIGP, defined in terms of their urine wash-out_{50} values was 6±1 mL, 8±1 mL and 9±1 mL, respectively, which may reduce drug residence

time in the bladder. Nevertheless, high molecular weight chitosan based drug delivery systems may still be a promising drug delivery system due to their ease of gelation, gel strength and mucoadhesiveness. Thus we synthesised more mucoadhesive derivatives of high molecular weight chitosan that may be more resistant to urine wash-out than the parent chitosan.

In the third chapter, we hypothesise that chemical conjugation of methacrylate groups to chitosan would facilitate covalent interaction of the drug delivery system with the urothelial mucosal surfaces, thereby exhibiting superior mucoadhesive features relative to parent chitosan. Methacrylated chitosan was synthesised by reaction of chitosan with methacrylic anhydride. The method of synthesis provided a quick reaction due to the reactivity of methacrylic anhydride and so a coupling agent was not required. Two types of the methacrylated chitosan were synthesised with low and high degree of methacrylate conjugation (LMeCHI and HMeCHI respectively) in order to study the influence of methacrylation on the mucoadhesiveness of the polymers. The extent of methacrylation influence the mucoadhesive properties where HMeCHI (with $55.4 \pm 1.0\%$ of methacrylation extent based on ninhydrin test) exhibited a superior urine wash-out$_{50}$ value relative to LMeCHI (with $34.3 \pm 2.0\%$ of methacrylation extent) and unmodified chitosan (48 ± 1 mL vs 24 ± 1 mL vs 15 ± 4 mL respectively). We established the safety of these polymers by incubating UMUC3 bladder cancer cells with growth medium containing polymer solutions/dispersions for 4 h at 37°C with 5% CO_2 atmosphere; and cell viability/recovery after 72 h incubation in fresh growth medium was evaluated using MTT assay. The methacrylated chitosans (LMeCHI and HMeCHI) had similar safety profile as the unmodified chitosan (HCHI) based on their IC_{50} values (polymer concentration that killed 50% of incubated UMUC3 cells).

Another group of chitosan derivatives, boronated chitosan, was also developed. Unlike the methacrylated chitosan synthesised by direct reaction of chitosan with methacrylic anhydride at 40°C for 12 h, the boronated chitosan (BCHI) required a coupling system (N-3-(dimethylaminopropyl)-N-ethylcarboiimide hydrochloride (EDC)/ N-hydroxysuccinimide (NHS)) for amide bond formation between the chitosan amino groups and the carboxyl groups of 4-carboxyphenylboronic acid (4-CPBA). Also, a longer reaction time (24 h) was required for the synthesis of BCHI though the reaction was carried out at room temperature. The synthesis also required DMSO in dissolving 4-CPBA, NHS and EDC. In contrast, DMSO was not required for the synthesis of methacrylated chitosan as methacrylic anhydride was presented as liquid samples.

Interestingly, there was no significant differences in the resistance to changes in the turbidity of HBCHI and LMeCHI (both prepared using 0.79 moles of 4-CPBA and MA per unit mole of chitosan, respectively) as the pH values of the polymer solutions were increased stepwise from 3 to 9. For instance, HBCHI and LMeCHI displayed similar absorbance values of 0.01 at pH 7 with rapid increase in their turbidity at pH 9 (0.16 and 0.18 respectively). Also, none of the boronated chitosan exhibited comparable turbidity profile with HMeCHI, which is expected as HMeCHI had more methacrylate groups conjugated to chitosan than the amount of boronate groups conjugated to chitosan in the case of HBCHI. Nevertheless, methacrylate and boronate groups displayed similar pH-turbidity profile as a function of chitosan hydrophobic modification. The physiological implication of this finding is that the ability of methacrylated and boronated chitosan to withstand pH fluctuations in the bladder will be dependent on the extent of chitosan conjugation with the hydrophobic groups (methacrylate or boronate).

Boronation modulated the mucoadhesiveness of LBCHI, MBCHI, and HBCHI (with boronation extent of 4.4%, 7.4% and 10.7%, respectively based on ninhydrin analysis): HBCHI exhibited a superior urine wash-out$_{50}$ value relative to MBCHI, LBCHI and unmodified chitosan (55 mL vs 48 mL vs 23 mL vs 15 mL). We did not carry out any biocompatibility or cytotoxicity testing of the boronated chitosans on UMUC3 cells due to time and money constraint, though a number of *in vitro* and *in vivo* studies have established the safety of phenylboronic molecules using mouse and mammalian cancer cell lines [6,7] as well as healthy rabbits [8]. Nevertheless, it is important to evaluate their safety in healthy bladder cell lines.

Figure 5.1 shows the porcine urine wash-out profile of the three groups of transmucosal drug delivery carriers. The WO$_{50}$ values of methacrylated and boronated chitosan may change after formulating them with other excipients and loading with drugs. For example, HCHIGP displayed similar WO$_{50}$ profile with MCHI, suggesting that addition of the β-glycerophosphate component reduced the mucoadhesive potential of HCHI resulting in the formulation displaying comparable mucoadhesiveness with MCHI. Thus, a future formulation development strategy will be aimed at improving physicochemical and mucoadhesive properties of the dosage forms without compromising their safety.
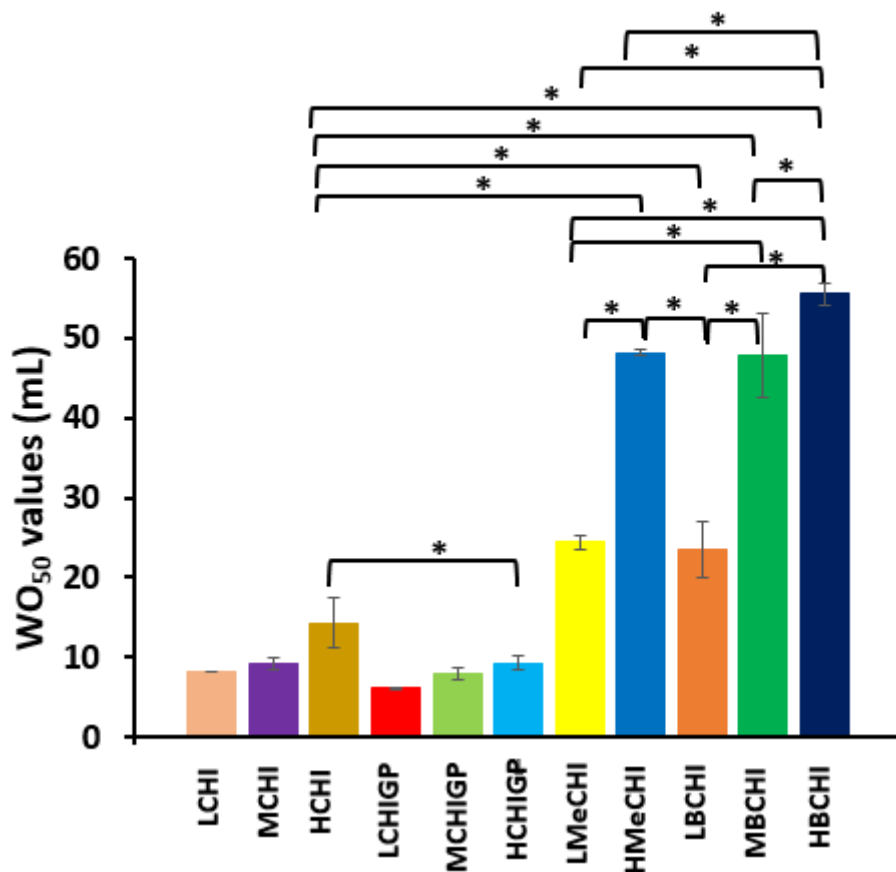
Fig. 5.1 WO$_{50}$ profile of chitosan related drug carriers: CHIGP *in situ* gelling systems, methacrylated chitosan and boronated chitosan. Results are presented as bars indicating mean WO$_{50}$ values ± S.D, n=3, Asterisk (*) depicted statistically significant differences between groups of samples.

Interestingly, HMeCHI synthesised using 4.65 moles per unit mole of chitosan exhibited WO$_{50}$ values of 48 mL which is comparable (p > 0.05) to that observed for MBCHI (WO$_{50}$ values 46 mL) synthesised using 0.39 moles of 4-CPBA per unit mole of chitosan (Fig 5.1). This finding suggested that boronate conjugated chitosan was more mucoadhesive than methacrylate derivatised chitosan because the carbonyl groups of methacrylated chitosan interact with urothelial cysteine groups of the mucin glycoproteins via Michael addition reaction to establish C-S covalent linkage [9] while phenylboronic acid groups of boronated chitosan could form cyclic ester bond with the sialic acid component of the mucin [10], which is a superior covalent linkage.

CHIGP *in situ* gelling systems (LCHIGP, MCHIGP and HCHIGP) exhibited lower urine WO$_{50}$ values (6-9 mL) than methacrylated (24-48 mL) and boronated chitosan (23-55 mL). FS/LCHI, FS/LCHIGP and FS/MCHIGP displayed similar WO$_{50}$ values with FITC-dextran (p > 0.05), whose

limited mucoadhesiveness has been well-established [11–13]. On the other hand, FS/MCHI, FS/HCHI and FS/HCHIGP formulations were more mucoadhesive than FITC-dextran based on their WO_{50} values (Fig. 5.1) ($p < 0.05$). This finding demonstrated that high molecular weight chitosan may be more efficient in formulating CHIGP delivery systems for intravesical administration.

A tensile test was conducted for CHIGP *in situ* gelling systems, methacrylated chitosans and boronated chitosans. This test provides complementary information to the urine wash-out$_{50}$ profile of the studied delivery systems. The flow-through mucoadhesion test (where urine was used to wash-out applied fluorescein-sodium/polymer mixture from porcine bladder mucosal surfaces) is more physiologically relevant as it simulates the *in vivo* bladder environment that is constantly in contact with urine. So, the urine flow-through/fluorescent microscopy technique may be a more reliable technique in evaluating the mucoadhesiveness of a potential drug carrier. Nevertheless, it is still desirable to conduct a tensile test in addition to the urine wash-out test. There is a similar trend from the mucoadhesive patterns for all the studied drug carriers, obtained with both tests (Table 5.1). In other words, the highly methacrylated or boronated chitosan was shown to be the most mucoadhesive amongst the evaluated chitosan derivatives using the urine wash-out and tensile test. Also, the high molecular weight chitosan/β-glycerophosphate *in situ* gelling systems was also the most mucoadhesive and resistant to urine wash-out from the bladder.

Table 5.1.

Tensile test parameters and WO_{50} values of CHIGP mixtures, methacrylated and boronated chitosan

Samples	Urine WO_{50} (mL)	Force of adhesion (N)	Work of Adhesion (N·mm)
LCHIGP	6.1 ± 0.1	0.03 ± 0.01	0.07 ± 0.03
MCHIGP	7.9 ± 0.7	0.06 ± 0.01	0.13 ± 0.03
HCHIGP	9.3 ± 0.9	0.13 ± 0.01	0.35 ± 0.02
LMeCHI	24.4 ± 0.8	0.10 ± 0.02	0.16 ± 0.02
HMeCHI	48.2 ± 0.4	0.11 ± 0.01	0.22 ± 0.02
LBCHI	23.4 ± 3.5	0.08 ± 0.01	0.16 ± 0.01
MBCHI	47.8 ± 5.3	0.11 ± 0.01	0.20 ± 0.01
HBCHI	55.5 ± 1.5	0.32 ± 0.02	0.39 ± 0.02

The use of methacrylated chitosan and boronated chitosan is not restricted for intravesical application. In fact, it is useful for all transmucosal routes of administration where drug formulations need to come in contact with mucosal surfaces. Thus there is a strong need to develop dosage forms using these chitosan derivatives as polymeric excipients as well as evaluate their safety, efficacy and pharmacokinetic profile *in vitro* and *in vivo*.

The aims of the project has been achieved as three types of chitosan/β-glycerophosphate *in situ* gelling systems were developed using different chitosan grades. The method of preparing the CHIGP formulations was optimised so that they displayed reproducible physicochemical characteristics such as gelation temperature and time as well as drug release profile. This is particularly important for drug carriers that would be moved forward to clinical trials in the coming years. To date, no chitosan/β-glycerophosphate formulations have made it to clinical trials or market, especially for bladder cancer treatment. Thus the development of optimised CHIGP *in situ* gelling systems is particularly timely and important. Moreover, their formulation process does not require any costly equipment as it only required vessels and stirrers. With its optimisation to generate more mucoadhesive drug carriers, they will be affordable for bladder cancer patients when they are eventually launched to the market after clinical trials and regulatory approval. However, more *in vitro* and *in vivo* studies definitely need to be carried out before the CHIGP products could be commercialised. Nevertheless, step has been taken to develop affordable drug carriers for the treatment of bladder cancer since it is one of the most expensive cancers to treat [14–17]. Moreover, mitomycin-C loaded chitosan formulations entrapped the drug limiting its release to a maximum of 25% over the 6 h release period, inferring the use of CHIGP formulations for intravesical drug delivery is valuable as such drug carriers (e.g. LCHIGP) facilitated controlled drug release of up to 63% within 6 h.

Secondly, the chitosan derivatives (two types of methacrylated chitosan and three type of boronated chitosan) have proven to be mucoadhesive materials that will be widely explored in the coming decades for transmucosal application based on their superior mucoadhesive profile relative to unmodified chitosan and CHIGP formulations. . The zeta potential analysis of boronated chitosan was not carried out as its mode of interaction of boronated chitosan with the urothelial mucosal surfaces was predominantly via covalent linkage with sialic acid group on the bladder mucosa. Moreover, earlier studies have shown that positive zeta potential values of chitosan was reduced after boronation [6], implying that there may be diminished electrostatic interactions between the drug carrier and the urothelium. Their biocompatibility is also good and comparable to that of the parent chitosan.

There is a strong need to use organs from animal models that are physiologically related to that of humans for the clinical testing of the drug loaded transmucosal dosage forms as the most commonly used animals for intravesical drug delivery studies are rats and mice [18]. This is because lots of experiments using extracted bladder of rodents maintained in artificial urine cannot simulate the physiological situation in the human bladder as issues such as differences in the physiology of human and murine bladder; sufficient tissue perfusion and environmental control [19] may make it difficult to scale-up excipients appropriately to prepare effective dosage forms for humans.

5.2. Future work

The study could not cover all the aspects that must be considered when translating the drug carriers further towards its regulatory approval and marketing authorisation. For example, the cytotoxicity testing as well as cellular uptake studies of the drug loaded CHIGP *in situ* gelling systems need to be carried out on UMUC3 cells. This is to evaluate whether the drug containing dosage form will be readily taken up into malignant tissues as well as demonstrate antitumour activity on bladder cancer cells. It would be important to carry out SV-HUC-1 cell viability studies of boronated chitosan using MTT assay to evaluate their biocompatibility with bladder cells before they are further developed into intravesical dosage forms for bladder cancer treatment. Dosage forms such as composite systems of nanoparticles and hydrogels could be developed from methacrylated (MeCHI) and boronated chitosan (BCHI). MeCHI and BCHI could be formulated using β-glycerophosphate or Pluronic F-127 to generate *in situ* gelling dosage forms. Then, mitomycin-C loaded nanoparticles can be incorporated into the MeCHI and BCHI hydrogels. These delivery systems may display superior mucoadhesive profile relative to chitosan/β-glycerophosphate systems as the more mucoadhesive chitosan derivatives may enable the drug carrier to adhere onto the urothelial mucosal surfaces for prolonged period of time by interacting through stronger covalent bonds as in the case of boronated chitosan. Another possible dosage form to be developed may be methacrylated chitosan nanoparticles coated with boronated chitosan to improve its tumour targeting potential. Thus boronated chitosan could enhance covalent interaction with mucosal surfaces and targeted intratumour delivery while core methacrylated chitosan nanoparticles would sustain and prolong the covalent interaction between the drug carrier and the urothelial malignant tissues.

Orthotopic mice models (implanted with human bladder tumours), established models in the cancer research field due to their ability to mimic disease processes in humans, and can be

used to study the *in vivo* antitumor effect of drug loaded MeCHI and BCHI based dosage forms [20,21].

It will be interesting to perform *in vivo* biocompatibility tests for the methacrylated chitosan and boronated chitosan using pig models as their bladder has similar structure [19,22,23] and urodynamic [19,24–27] features to that of humans, to ascertain their feasibility for the development of dosage forms for the treatment of various grades of bladder cancer.

Another innovative dosage form such as the use of nanocapsules to deliver two anticancer agents for the treatment of advanced stages of bladder cancer [28] is desirable as synergism may prevent drug resistance possible with monotherapy.

Concluding remark

Out of the studied drug delivery systems, boronated chitosan appeared to be the most promising in terms of its mucoadhesive profile for intravesical application. The UMUC3 cell cytotoxicity test of the chitosan derivative was not carried out due to time constraint. Nevertheless, all the studied methacrylated chitosan and CHIGP systems are still useful for various drug delivery applications depending on the onset and duration of action required.

This work is indeed a valuable contribution to the plethora of advanced mucoadhesive drug carriers administered through the transmucosal route. Since most diseases originate from the mucosal surfaces of tissues and organs, these new groups of materials may be able to reduce the overall global disease burden.

References

1. Quale, D.Z., Bangs, ., Smith, M., Guttman, D., Northam, T., Winterbottom, A., Necchi, A., Fiorini, E., Demkiw S. Bladder Cancer Patient Advocacy: A Global Perspective. Bl Cancer I. 2015;117–22.

2. Cancer Research UK. Trial Search Results - Bladder cancer (Recruiting) [Internet]. Clinical Trials Information. 2018 [cited 2018 Sep 26]. p. 1–9. Available from: https://www.cancerresearchuk.org/about-cancer/find-a-clinical-trial/clinical-trials-search?populate=Bladder cancer&f%255B0%255D=field_trial_status%3A4386&cancertype=157%236%23Bladder cancer&AdvancedSearchFormType=research_and_trials_adv_search_form&stillr.

3. NICE. NICE Guidelines, Bladder cancer: diagnosis and management. NICE guidelines. 2015 [cited 2018 Oct 21]. Available from: https://www.nice.org.uk/guidance/ng2/chapter/recommendations-diagnosing-and-staging-bladder-cancer-2.

4. NICE. Managing muscle-invasive bladder cancer: The role of chemotherapy in treatment of organ-confined muscle-invasive urothelial carcinoma of the bladder. Bladder Cancer: Diagnosis and Management. 2015, National Collaborating Centre for Cancer (UK), London: NICE guideline No. 2 [cited 2018 Oct 21]. Available from: https://www.ncbi.nlm.nih.gov/books/NBK356308/.

5. Cho J, Heuzey MC, Bégin A, Carreau PJ. Effect of urea on solution behavior and heat-induced gelationof chitosan-β-glycerophosphate. Carbohydr Polym. 2006;63(4):507–18.

6. Wang X, Tang H, Wang C, Zhang J, Wu W, Jiang X. Phenylboronic acid-mediated tumor targeting of chitosan nanoparticles. Theranostics. 2016;6(9):1378–92.

7. Wang X, Wei B, Cheng X, Wang J, Tang R. 3-Carboxyphenylboronic acid-modified carboxymethyl chitosan nanoparticles for improved tumor targeting and inhibitory. Eur J Pharm Biopharm. 2017;113:168–77.

8. Liu S, Chang CN, Verma MS, Hileeto D, Muntz A, Stahl U, Woods J, Jones LW, Gu FX. Phenylboronic acid modified mucoadhesive nanoparticle drug carriers facilitate weekly treatment of experimentallyinduced dry eye syndrome. Nano Res. 2015;8(2):621–35.

9.   Shitrit Y, Bianco-Peled H. Acrylated chitosan for mucoadhesive drug delivery systems. Int J Pharm. 2017;517(1–2):247–55.

10.   Cambre JN, Sumerlin BS. Biomedical applications of boronic acid polymers. Polymer (Guildf). 2011;52(21):4631–43.

11.   Štorha A, Mun E a., Khutoryanskiy V V. Synthesis of thiolated and acrylated nanoparticles using thiol-ene click chemistry: towards novel mucoadhesive materials for drug delivery. RSC Adv. 2013;3(30):12275.

12.   Mun EA, Williams AC, Khutoryanskiy V V. Adhesion of thiolated silica nanoparticles to urinary bladder mucosa: Effects of PEGylation, thiol content and particle size. Int J Pharm. 2016;512(1):32–8.

13.   Kolawole OM, Lau WM, Khutoryanskiy V V. Methacrylated chitosan as a polymer with enhanced mucoadhesive properties for transmucosal drug delivery. Int J Pharm. 2018;550(1–2):123–9.

14.   Sievert KD, Amend B, Nagele U, Schilling D, Bedke J, Horstmann M, Hennenlotter J, Kruck S, Stenzl A. Economic aspects of bladder cancer: What are the benefits and costs? World J Urol. 2009;27(3):295–300.

15.   Barocas DA, Globe DR, Colayco DC, Onyenwenyi A, Bruno AS, Bramley TJ, Spear RJ. Surveillance and treatment of non-muscle-invasive bladder cancer in the USA. Adv Urol. 2012;2012:19–24.

16.   Yeung C, Dinh T, Lee J. The Health Economics of Bladder Cancer: An Updated Review of the Published Literature. Pharmacoeconomics. 2014;32(11):1093–104.

17.   Svatek RS, Hollenbeck BK, Holmäng S, Lee R, Kim SP, Stenzl A, Lotan Y. The economics of bladder cancer: Costs and considerations of caring for this disease. Eur Urol. 2014;66(2):253–62.

18.   Kolawole OM, Lau WM, Mostafid H, Khutoryanskiy V V. Advances in intravesical drug delivery systems to treat bladder cancer. Int J Pharm. 2017;532(1):105–17.

19.   Parsons BA, Drake MJ, Gammie A, Fry CH, Vahabi B. The validation of a functional, isolated pig bladder model for physiological experimentation. Front Pharmacol. 2012;3:1–8.

20.   Martin DT, Hoimes CJ, Kaimakliotis HZ, Cheng CJ, Zhang K, Liu J, Wheeler MA, Kelly WK, Tew GN, Saltzman WM, Weiss RM. Nanoparticles for urothelium penetration and delivery of the histone deacetylase inhibitor belinostat for treatment of bladder cancer. Nanomedicine. 2013;9(8):1124–34.

21.   Tamura K, Kikuchi E, Konno T, Ishihara K, Matsumoto K, Miyajima A, Oya M. Therapeutic effect of intravesical administration of paclitaxel solubilized with poly(2-methacryloyloxyethyl phosphorylcholine-co-n-butyl methacrylate) in an orthotopic bladder cancer model. BMC Cancer. 2015;15(1):317.

22.   Dixon JS, Gosling JA. Histology and fine structure of the muscularis mucosae of the human urinary bladder. J Anat. 1983;136(2):265–71.

23.   Teufl, F.; Dammann, F.; Wehrmann M. In vitro study of morphology of the bladder wall using MR tomography at 1.0 Tesla: correlation with histology. Rofo. 1997;166:406–10.

24.   Sibley BYGNA. A comparison of spontaneous and nerve-mediated activity in bladder muscle from man, pig and rabbit. J Physiol. 1984;431–43.

25.   Crowe, R.; Burnstock G. A Histochemical and Immunohistochemical Study of the Autonomic Innervation of the Lower Urinary Tract of the Female Pig. Is The Pig a Good Model for the Human Bladder and Urethra? J Urol. 1989;141:414–22.

26.   Mills, I.W.; Noble, J.G.; Brading AF. Radiotelemetered cystometry in pigs: validation and comparison of natural filling versus diuresis cystometry. J Urol. 2000;164:1745–50.

27.   Shaw MB, Herndon CD, Cain MP, Rink RC, Kaefer M. A porcine model of bladder outlet obstruction incorporating radio-telemetered cystometry. BJU Int. 2007;100(1):170–4.

28.   Lu S, Xu L, Kang ET, Mahendran R, Chiong E, Neoh KG. Co-delivery of peptide-modified cisplatin and doxorubicin via mucoadhesive nanocapsules for potential synergistic intravesical chemotherapy of non-muscle-invasive bladder cancer. Eur J Pharm Sci. 2016;84:103–15.
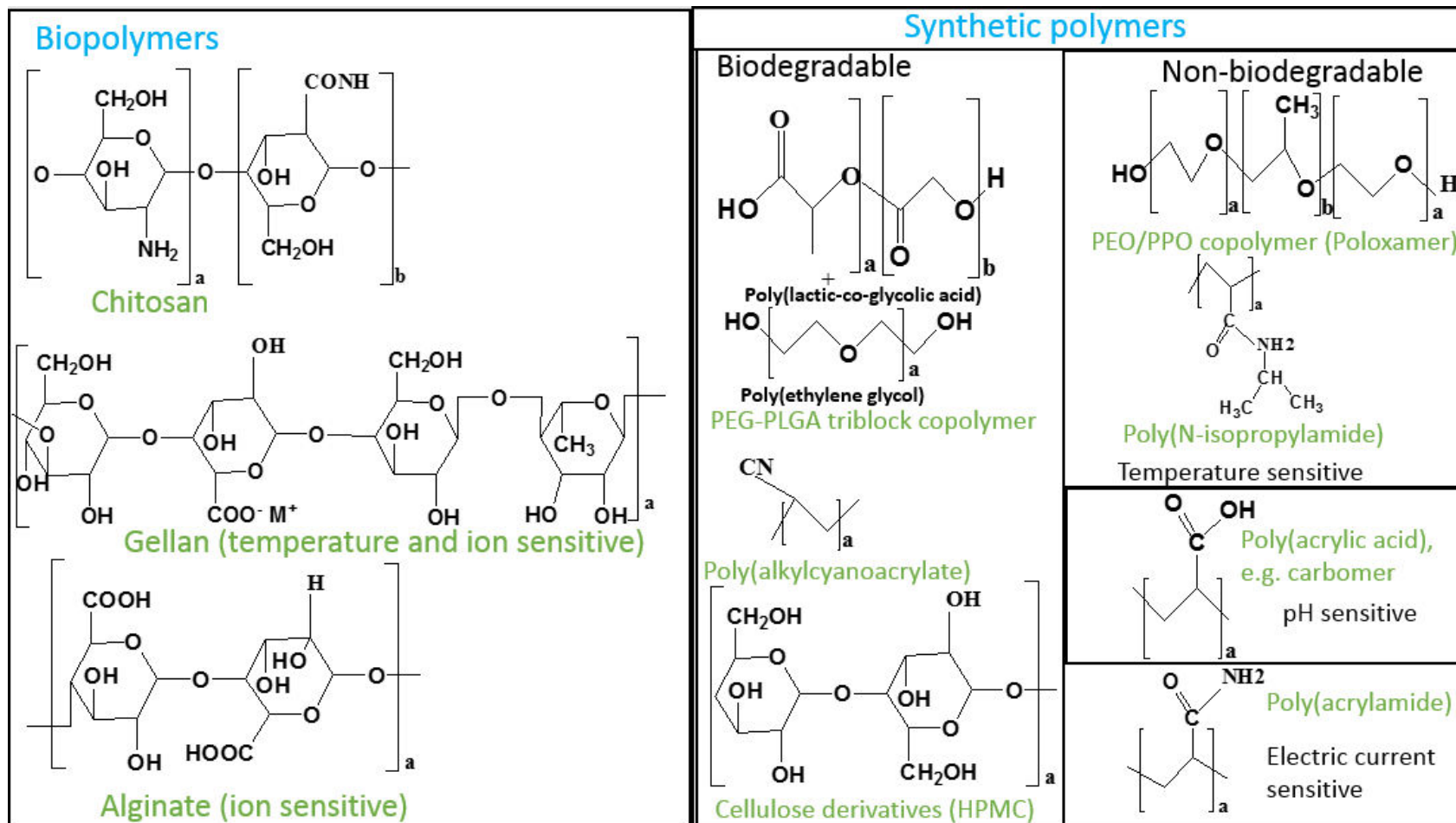
Appendix 1: Chemical structures of mucoadhesive polymers: (PEO: poly(ethylene oxide), PPO: poly(propylene oxide), HPMC: hydroxypropyl methylcellulose. Biodegradable and synthetic (biodegradable and non-biodegradable) polymers can be used to form temperature, pH or ion sensitive gels.
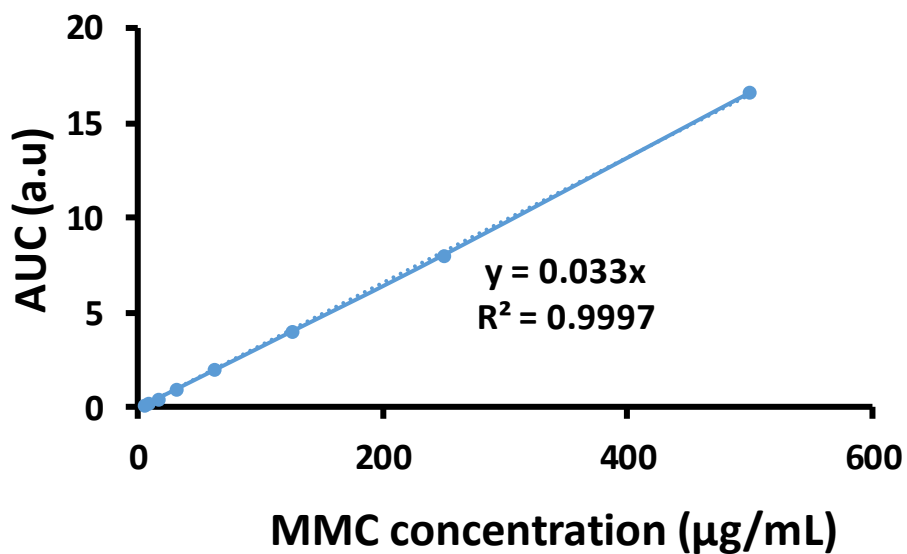
Appendix 2: Calibration curve of standard solutions of mitomycin-C (3.9 to 500 µg/mL) used to evaluate extent of drug release from chitosan and CHIGP samples during *in vitro* drug release experiment.

Appendix 3: Gel permeation data for the three chitosan grades depicting their average molecular weight estimated using pullulan as standard.

Parameters	Low MW chitosan	Medium MW chitosan	High MW chitosan
Number-average MW (Mn)	18196	35088	53038
Weight Average MW (Mw)	**62343**	**124072**	**370006**
Polydispersity (Mw/Mn)	3.4262	3.536	6.9762
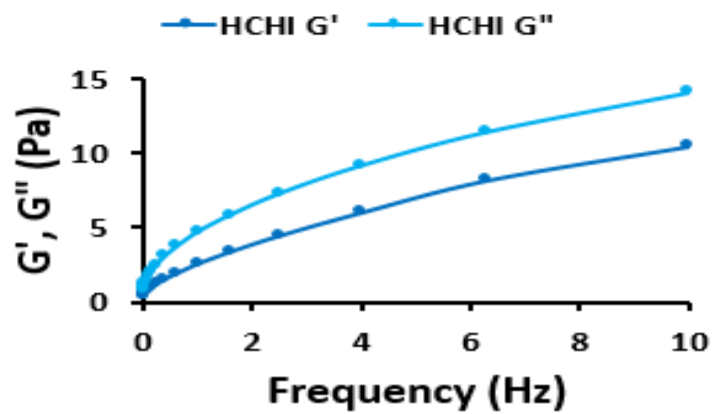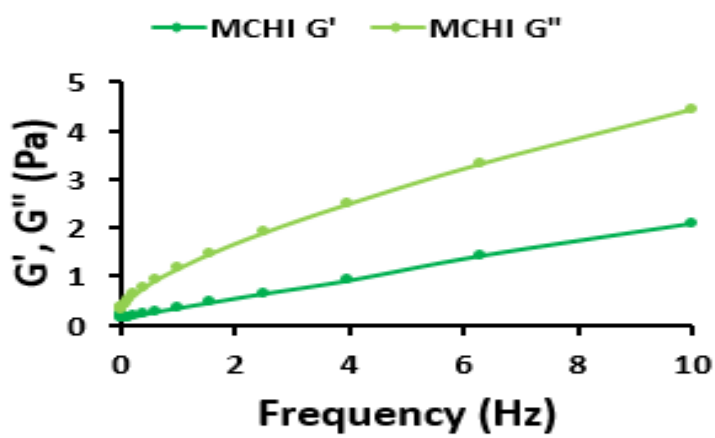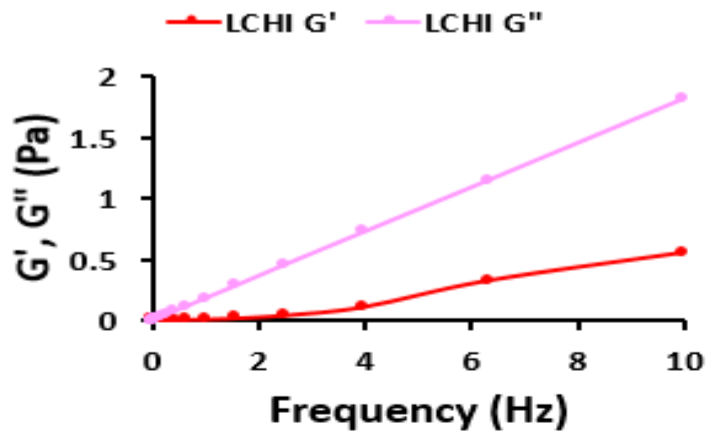
Appendix 4: Exemplar rheological profile of LCHI (red), MCHI (green) and HCHI (blue) showing the frequency-dependent changes in the viscoelastic properties of samples maintained at 37°C and subjected to frequency ranges from 0.1 to 10 Hz, with G" consistently greater than G' for all the studied chitosan solutions, though HCHI exhibited the greatest magnitude of G' and G" values.